1999

Sediment Transport in the Swash-Zone of Natural Beaches

Butt, Tony

Sediment Transport in the Swash-Zone of Natural Beaches

by

Tony Butt

A thesis submitted to the University of Plymouth
in partial fulfilment for the degree of

Doctor of Philosophy

Institute of Marine Studies
Faculty of Science

September 1999

Tony Butt

Sediment Transport in the Swash-Zone of Natural Beaches.

Abstract

Concurrent measurements of velocity, water depth, sub-surface pore-pressure and suspended sediment concentration (SSC) were obtained from the swash-zone of a macrotidal, dissipative ($\tan\beta \approx 0.014$), fine to medium grained ($d_{50} \approx 0.24$mm) beach at Perranporth, Cornwall, UK, in low ($H_s \approx 0.8$m) to high ($H_s \approx 2.2$m) energy conditions. Velocity, pressure and SSC were measured using electromagnetic current meters, pressure transducers and a four-level array of miniature optical backscatter sensors respectively. Results show an infragravity dominated wave field in the swash-zone in both high and low energy conditions. In low energy conditions, the ratio between low ($f < 0.05$Hz) and high ($f > 0.05$Hz) frequency variance increased from 0.6 to 2.3 for both cross-shore velocity and surface elevation, and SSC at $z = 1$cm increased by a factor of about 5, between just shoreward of the breakpoint ($h/h_b = 0.6$) and the swash-zone ($h/h_b = 0.2$). Swash-zone suspended sediment fluxes at $z = 5$ to 6cm increased by a factor of about 2 from low to high energy conditions. Low frequency cross-shore velocity skewness values for low and high energy conditions were 0.04 and –0.81 respectively, suggesting an important contribution to offshore transport in high energy conditions, from large, low frequency backwashes manifest in the velocity time-series as low frequency negative skewness. Using 3D velocities from a similar experiment at Muriwai, New Zealand, it is found that TKE/velocity ratios in the uprush were about 1.7 times larger than in the backwash, suggesting greater turbulence in the uprush. Turbulence and rapid flow reversal are important onshore transport mechanisms, manifest as high frequency negative asymmetry in the velocity time-series. Values for high frequency negative asymmetry at Perranporth were 1.8 times larger in low than in high energy conditions. The influence of in-exfiltration is investigated using velocity and sub-surface pore-pressure measurements, and a modified Shields parameter, which includes terms to account for the competing effects of stabilisation-destabilisation and boundary layer modification. It is found that there is dominance of stabilisation-destabilisation, resulting in a 4.5% increase in backwash transport and a 10.5% decrease in uprush transport, integrated over a swash cycle. Sensitivity tests show a reversal in this dominance if the median grain size is increased above about 0.55mm, suggesting the transport influence is onshore on coarser grained beaches and offshore on finer grained beaches. Calculations show that hydraulic jumps due to uprush-backwash interaction were about 2.1 times as likely to occur during high than during low energy conditions. Visual observations suggest that more sediment is advected offshore from these jumps in high energy conditions. An antidune ripple field, which enhances transport through increased bed roughness, may also form beneath hydraulic jumps, but this is shown to influence the total dimensionless transport over a 17-min. time-series by less than 5%. Overall results suggest that swash-zone erosion occurs more readily on relatively fine-grained beaches in storms, and accretion occurs more readily on relatively coarse-grained beaches in calm conditions, which is consistent with observations in nature. Large infragravity frequency backwashes manifest as negative infragravity skewness appear to be a key factor in linking enhanced offshore transport in the swash-zone with high energy conditions.

Contents

Figures and tables

List of abbreviations

The following is a list of symbols used in the thesis. Symbols are also always locally identified within each section of the thesis.

ADV	Acoustic Döppler velocimeter.
BLW	Bound long wave.
EMCM	Electromagnetic current meter.
FFT	Fast Fourier transform.
FOBS	Fibre-optic backscatter sensor.
LDV	Laser Döppler velocimeter.
MOBS	Miniature optical backscatter sensor.
OBS	Optical backscatter sensor.
PT	Pressure transducer.
SSC	Suspended sediment concentration.
TKE	Turbulent kinetic energy.

A	Asymmetry.
a	Wave amplitude.
a_b	Breaker amplitude.
a_p	Primary, or fundamental, amplitude.
c	Constant relating to the non-linear relation between shear stress and velocity.
C_b	Absolute velocity of a bore.
C_g	Group celerity.
C^2	Coherence-squared.
d	Grain size.
$\bar{d}$	Mean grain size.
d_{50}	Median grain size.
d_{Q0}	Grain size at which the influence of in-exfiltration changes direction.
E	Energy.
f	Frequency.
f_p	Primary, or fundamental, frequency.
Δf	Bandwidth.
f'	Friction factor.
f'_0	Friction factor not considering the effects of backwash ripples.
f'_R	Friction factor considering the effects of backwash ripples.
F_b	Buoyancy force per unit volume.
F_g	Gravity force per unit volume.
Fr	Froude number.

h	Water depth.
H_0	Deep-water wave height.
H_b	Breaker height.
h_b	Breaker depth.
I_b	Total immersed weight of sediment transported during backwash.
I_u	Total immersed weight of sediment transported during uprush.
I_0	Dimensionless transport integrated over a swash cycle not considering backwash ripples or in-exfiltration.
I_R	Dimensionless transport integrated over a swash cycle including the effects of backwash ripples.
I_{rip}	Dimensionless transport integrated over a swash cycle specifically due to backwash ripples.
I_w	Dimensionless transport integrated over a swash cycle including in-exfiltration.
K	Hydraulic conductivity.
K_b	Backwash calibration constant.
K_u	Uprush calibration constant.
k	Bed roughness.
k_g	Bed roughness for grains only.
k_R	Bed roughness for ripples only.
L_0	Deep water wavelength.
m	Calibration constant.
N	Arbitrary number.
N_w	Number of non-overlapping windows in spectral estimates.
n	Porosity.
Ny	Nyquist frequency.
p	Pressure.
p_{atm}	Atmospheric pressure.
P_j	Likelihood of formation of a hydraulic jump.
P_{XX}	Un-normalised power spectrum (autospectrum) of sequence X.
P_{XY}	Un-normalised co-spectrum between sequences X and Y.
Q	Dimensionless sediment transport.
Q_0	Dimensionless sediment transport with no in-exfiltration or backwash ripples.
Q_{infilt}	Dimensionless sediment transport solely due to the effects of in-exfiltration.
Q_j	Resultant sediment transport from hydraulic jumps over a time-series.
Q_R	Dimensionless sediment transport including backwash ripples.
Q_{rip}	Dimensionless sediment transport solely due to the effects of backwash ripples.
Q_w	Dimensionless sediment transport including the effects of in-exfiltration.
q_u	Uprush sediment advection from hydraulic jump.
q_b	Backwash sediment advection from hydraulic jump.
R	Run-up height.
R_F	Frequency resolution.
$R_{2\%}$	2% run-up height exceedance value.
Re	Reynolds number.

R_{IG} Infragravity run-up height.
R_{max} Maximum run-up height.
s Specific gravity.
S Velocity skewness.
Sk Grain size skewness.
S_{xx} Radiation stress.
S_{XX} Normalised power spectrum (autospectrum) of sequence X.
S_{XY} Normalised co-spectrum between sequences X and Y.
S_W Window size in spectral analysis.
t Time.
T Wave period.
T_s Significant period.
T_b Backwash duration.
T_u Uprush duration.
u Cross-shore velocity.
u* Friction velocity.
v Longshore velocity.
V Voltage.
V_{out} Output voltage.
V_{off} Offset voltage.
w Vertically upwards velocity.
w_c Critical fluidising velocity.
W Immersed sediment weight per unit area.
W_0 Immersed sediment weight per unit area with no in-exfiltration.
W_w Immersed sediment weight per unit area including the effects of in-exfiltration.
x Cross-shore distance; horizontal distance.
y Longshore distance.
z Vertically upwards distance.
z_0 Roughness length.

α Constant relating to Nielsen's (1998) linear relation between shear stress and velocity.
β Beach slope.
δ Boundary layer thickness.
Δ Ripple height.
ε Surf scaling parameter.
ϕ Angle; Phase.
ϕ_f Friction angle of sediment.
ϕ_p Primary, or fundamental, phase.
ϕ_{50} Median grain size on Udden-Wentworth scale.
γ Degrees of freedom.

η Surface elevation.

φ Acceleration.

ϑ Significance level in spectral estimates.

κ Von Karman constant.

λ Ripple length.

θ Shields parameter.

Θ Volume.

ρ Fluid density.

ρ_s Sediment density.

σ Standard deviation.

σ^2 Variance.

τ Shear stress.

τ_0 Shear stress with no in-exfiltration.

τ_w Shear stress including the effects of in-exfiltration.

υ Kinematic viscosity.

ω Angular frequency.

Ψ Ratio of TKE to cross-shore velocity.

ξ_0 Irribarren number.

ζ Specific yield or drainable porosity.

Acknowledgements

For their generosity in allowing us to use their clubhouse during the data collection, I would like to thank Nick Berringer and the Perranporth Surf Life Saving Club. Andy Baird is also gratefully acknowledged for kindly lending us the pressure transducers, as is the kind assistance of Peter Ganderton, Sam Lamiroy, Andy Manning and Jon Miles during the field deployments.

Throughout the data analysis many consultations were made, internally and externally. External help is gratefully acknowledged from Phil Osborne (for supplying the Muriwai data), Troels Aagaard, Michael Hughes, Peter Nielsen, Gerben Ruessink and Ian Turner. Within the University I would like to acknowledge the help of Mark Davidson, Keith Dyer, David Huntley, Travis Mason, and last, but not least, my supervisor, Paul Russell.

Author's declaration

At no time during the registration for the degree of Doctor of Philosophy has the author been registered for any other University award.

Relevant scientific seminars and conferences were regularly attended at which work was often presented; external institutions were visited for consultation and several papers prepared for publication.

Relevant publications:

Butt, T., Russell, P. and Turner, I. (in review). The influence of swash infiltration-exfiltration on beach face sediment transport: onshore or offshore? Submitted to *Coastal Engineering.*

Butt, T. and Russell, P. (in press). Suspended sediment transport processes in high energy swash. *Marine Geology.*

Butt, T. and Russell, P. (in press). Hydrodynamics and sediment transport in the swash-zone of natural beaches: a review. *J. Coastal Research.*

Butt, T., Davidson, M. and Russell, P. 1998. *Erosion and Accretion Processes on the North Cornish Coast.* Abstract. The Cornish Coast. Falmouth, Cornwall. Oct. 1998.

Butt, T., Russell, P. and Huntley, D. 1998. *Time-series measurements of sediment transport in the swash-zone of a natural beach.* Abstract. Oceanography '98. Southampton University. Sept. 1998.

Signed: 

Date: 26 oct 99

1. Introduction

1.1 The importance of the swash-zone

The swash-zone is defined as the region where the uprush-backwash cycle occurs on the beach face, i.e. between the uprush limit (the peak of the uprush) and the backwash limit (the lowest part of the backwash). The uprush-backwash cycle is an oscillation superimposed on the maximum surf-zone mean water level or set-up (Gourlay, 1992).

The morphological behaviour of the coastline is important for a great number of reasons. There has been much recent concern about the effects of global warming, one of which may be the possibility for increased shoreline erosion due to more frequent storms, caused partly by a rise in sea surface temperature. To allow predictions to be made of the erosion and accretion of the shoreline in response to dynamic wave conditions, the cross-shore (on-offshore) movement of sediment on the beach needs to be quantified. Cross-shore sediment transport data is required to validate models of shoreline evolution, and it has been established for some time (e.g. Sunamara, 1984), that the inclusion of the swash-zone in these studies, is vital. The net cross-shore direction and magnitude of the sediment transport in the swash-zone provides a significant contribution to the overall erosion and accretion of the beach-face, therefore the hydrodynamic processes which control this sediment flux must be investigated. However, despite the importance of this area, the swash-zone has been largely neglected, especially with regard to sediment transport studies.

Models of shoreline evolution have so far made slow progress in dealing with the swash-zone. Out of the six short-term coastal profile models evaluated by Brøker-Hedegaard *et al* (1992), none of them was capable of describing swash-zone processes. Recent attempts at including the swash-zone in morphodynamic models have used only very simple parameterisations (e.g. Holland *et al*, 1998).

One factor which shows the swash-zone to be very important, especially on dissipative beaches, is the fact that infragravity waves, which have already been shown to be important sediment transporting mechanisms in the surf-zone (e.g. Russell, 1993), tend to grow shorewards. Hence infragravity energy would be high in the swash-zone, especially during high energy conditions. A schematic illustration of the cross-shore change in incident and infragravity wave height is illustrated in figure 1.1. The height of

the incident waves is limited by breaking, and between the breakpoint and the shore, the height is roughly proportional to the depth. In higher energy conditions, the incident waves simply break further seawards. In contrast, infragravity waves are considered to be unaffected by breaking (due to their length), and therefore continue to increase in height as far as the shoreline.

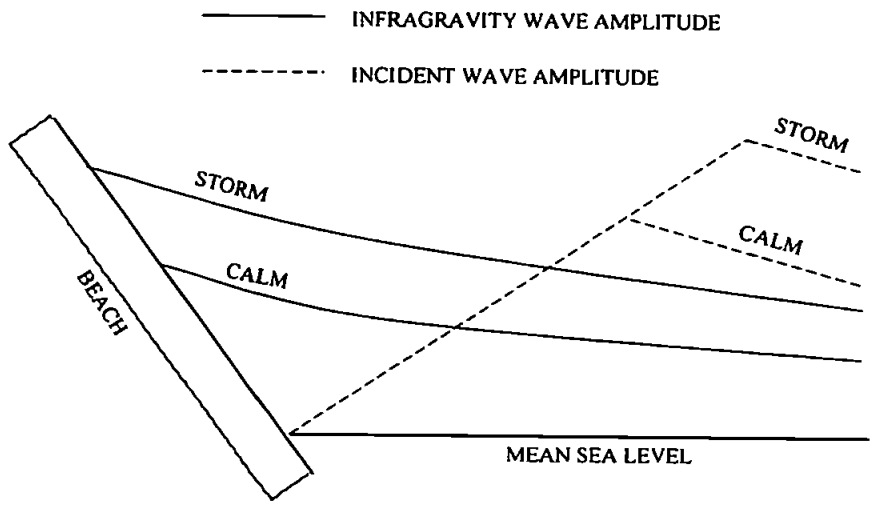

Figure 1.1: cross-shore variation in incident and infragravity wave amplitude during 'storm' and 'calm' conditions on a dissipative beach (adapted from Holman, 1983).

The processes acting in the swash-zone are different from and more complex than those acting in deeper water. Complications arise from factors such as the following:

- The water in the uprush and backwash phases does not behave in the same way. For example during the uprush the flow is decelerating, whilst in the backwash it is accelerating.
- It is still a matter of controversy whether the flows in the swash-zone should be treated as quasi-steady or oscillatory (*c.f.* Turner and Masselink, 1998)
- Near-bed suspended sediment concentrations in the swash-zone are much higher than those found in the inner surf-zone. Beach and Sternberg (1991) found them to be 3 to 9 times greater.
- Some processes which may not exist in the surf-zone (e.g. infiltration-exfiltration) could contribute significantly to the sediment transport in the swash-zone (e.g. Baird *et al*, 1996; Turner and Nielsen, 1997; Turner and Masselink, 1998).

1.2 The swash-zone and the coastal morphodynamic system

The study of coastline morphology generally uses the approach of considering the shoreline as a series of compartments, each having its own particular spatial and temporal scale (Ruessink, 1998). Each compartment may be considered as a simple system in which the water motion drives the sediment transport, and gradients in sediment transport cause morphological change, which, in turn, alters the water motion. For example, Wright and Thom (1977) define coastal morphodynamics as the 'mutual adjustment of topography and fluid dynamics involving sediment transport'.

Figure 1.2 shows a simplified schematic representation of such a system. For the purposes of the present study it is sufficient to consider only one input (the dynamic characteristics of the offshore wave field) and one output (the eroding or accreting shoreline), although in reality the situation is much more complex. Each stage in the flowchart of figure 1.2 is explained as follows:

1) Dynamic characteristics of the fluid. This refers to the characteristics of the wave field seaward of the break point.
2) Surf-zone processes. The processes which cause onshore or offshore transport of sediment in the surf-zone have been studied much more extensively than those in the swash-zone. The most important mechanisms appear to be positive (onshore) skewness at incident frequencies in low energy conditions causing onshore transport, and offshore-directed mean flows (undertow) coupled with infragravity oscillations in high energy conditions causing offshore transport (Russell and Huntley 1999).
3) Swash-zone processes. In the swash-zone the processes which transport the sediment are very poorly understood, and some mechanisms still need to be identified before this gap in the system can be closed.
4) Shoreline erosion or accretion. It is widely accepted that beaches generally tend to erode in high-energy conditions and accrete in low-energy conditions. In the swash-zone, the balance between processes must also be examined to determine what contribution the swash-zone makes to this generally observed result.
5) Feedback. Once the shoreline has begun to change, then this will affect the fluid motions themselves within the system, and hence the manner in which they subsequently affect the shoreline. The closure of the system through this feedback loop provides a temporal link between present and past states of the system. Some workers (e.g. Cowell and Thom, 1995) assert that the feedback loop is of paramount importance in controlling the morphodynamics. The treatment of coastal morphodynamics as a

dynamical system in which the beach topography is dependent upon its own past, and may be self-organising, is an approach which appears to be gaining popularity (e.g. Werner and Fink, 1993; Jaffe et al, 1994; Southgate and Capobianco, 1998)

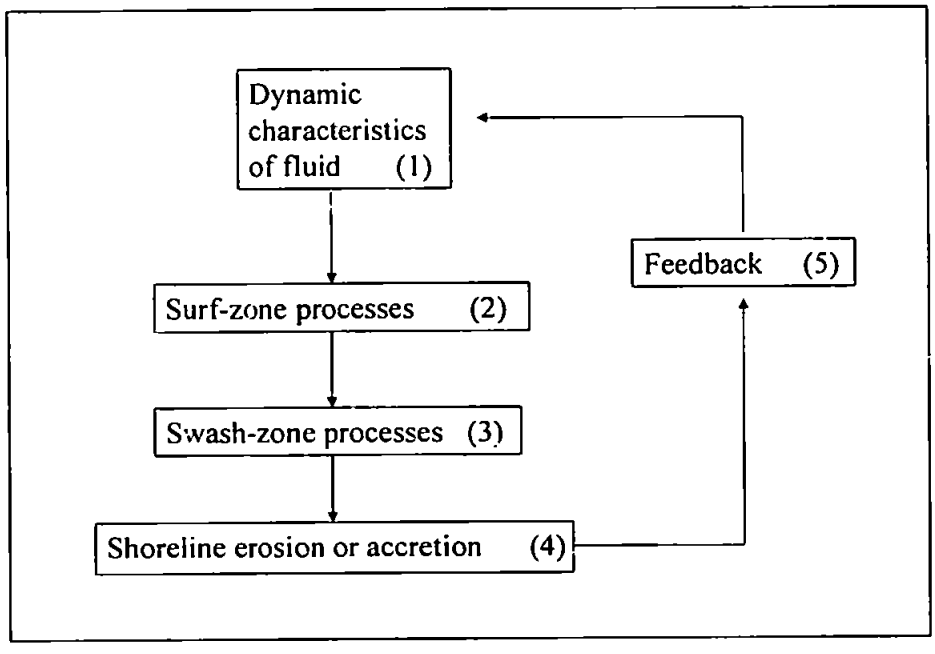

Figure 1.2: simplified schematic representation of shoreline. Numbers refer to notes in the text.

1.3 State of the art

There has been considerable pessimism about the swash-zone in the literature, up until very recently. For example "...Too little is known at present to even attempt a description of the basic sediment transport mechanisms in this area..." (Nielsen, 1992); and "...The physical description of fundamental sediment transport mechanisms operating within the swash-zone is presently beyond the state of the art..." (Turner, 1995). There has been an overall perception that field measurements in the swash-zone are prohibitively difficult to obtain, especially during times of significant morphological change (Hughes *et al*, 1997).

However, between about 1997 and the time of writing, the swash-zone has started to regain popularity. So far, however, various aspects of swash-zone sediment transport have been addressed only in isolation. The present study combines cross-shore velocity and SSC measurements with those of sub-surface pore-pressures, and also repeats a set of the same measurements in a variety of different conditions. Both these aspects have not previously been reported in the literature.

Most very recent studies have concentrated on relatively low-energy conditions (e.g. Hughes *et al*, 1997, 1998; Holland *et al*, 1998; Masselink and Hughes, 1998) on steep beaches, where incident wave fluctuations are more directly related to swash. Since the work of Beach and Sternberg (1991), the only study that has been published from a dissipative beach in high-energy conditions (where the incident waves are saturated and infragravity waves dominate in the swash-zone) is that of Osborne and Rooker (1998, 1999). The measurements undertaken in the present study are from a dissipative site in both high and low energy conditions, providing a much-needed contribution to this type of work.

The importance of new processes which appear to be unique to the swash-zone, has been identified in the most recent studies, but little work has been done in measuring and parameterising them. For example:

- The importance of higher velocity moments has been established for some time in the surf-zone (e.g. Nairn and Southgate, 1993), but this, together with acceleration (e.g. King, 1991), has not yet been applied in any detail in the swash-zone, although its importance is established beyond doubt in the present study.
- Turner and Nielsen (1997), Nielsen (1998) and Turner and Masselink (1998) acknowledge that infiltration-exfiltration may be important on sand beaches for different reasons from those pointed out in early studies on shingle beaches (e.g. Grant, 1946, 1948, where percolation and loss of backwash volume was thought to decrease offshore transport). It has not been clear in which direction infiltration-exfiltration biases the transport. The present study considerably improves the understanding of this.
- Hughes *et al* (1998) and Osborne and Rooker (1998, 1999) identify the existence of hydraulic jumps as significant sediment suspending mechanisms, but go no further. The present study makes a start at quantifying the transport due to these mechanisms.

It is therefore evident that a gap exists in the knowledge regarding the identification and assessment of the relative importance of various new, swash-zone-unique, processes. Moreover, because of the considerable lack of data from high energy conditions, this is

where more effort should be directed. To improve the understanding of how sediment moves in the swash-zone, the above points are therefore addressed in the present study.

1.4 Initial motivation for the research

After considering the results of various surf-zone studies, it began to emerge that there was an urgent need for swash-zone data. The initial conception of the project resulted from the studies of Foote *et al* (1994), Russell *et al* (1996), Fisher and O'Hare (1997, 1998), and Russell and Huntley (1999).

Field data from a variety of British beaches was used to highlight cross-shore variations in sediment transport (Russell *et al*, 1996; Russell and Huntley, 1999). Results showed that, seaward of the breakpoint, the transport was predominantly onshore in direction, and decreased in magnitude towards the breakpoint. Shoreward of the breakpoint the transport was predominantly offshore, increasing in magnitude towards the shore (see figure 1.3). Although the shallowest measurements were from the inner surf-zone, this potentially implied a large amount of sediment transport in the swash-zone.

Fisher and O'Hare (1997, 1998) tidally advected this 'shape function' to produce characteristic beach profiles. Since there was no data from the swash-zone, the shape function had to be extrapolated from the inner surf-zone to the shoreline. To obtain physically realistic profiles this extrapolation had to be based upon an assumed net onshore transport in the swash-zone. This, together with the already observed shoreward increase in sediment flux and long wave magnitude, highlighted the need for *in-situ* swash-zone sediment transport measurements.

Obviously a great deal more research had to be done after the initial conception of the project, to identify the gaps in knowledge and determine the direction which the study would follow. Based on this initial research, the problem definition and consequent aims of the present study could be drawn up, and are developed below. See also the literature review (chapter 2).

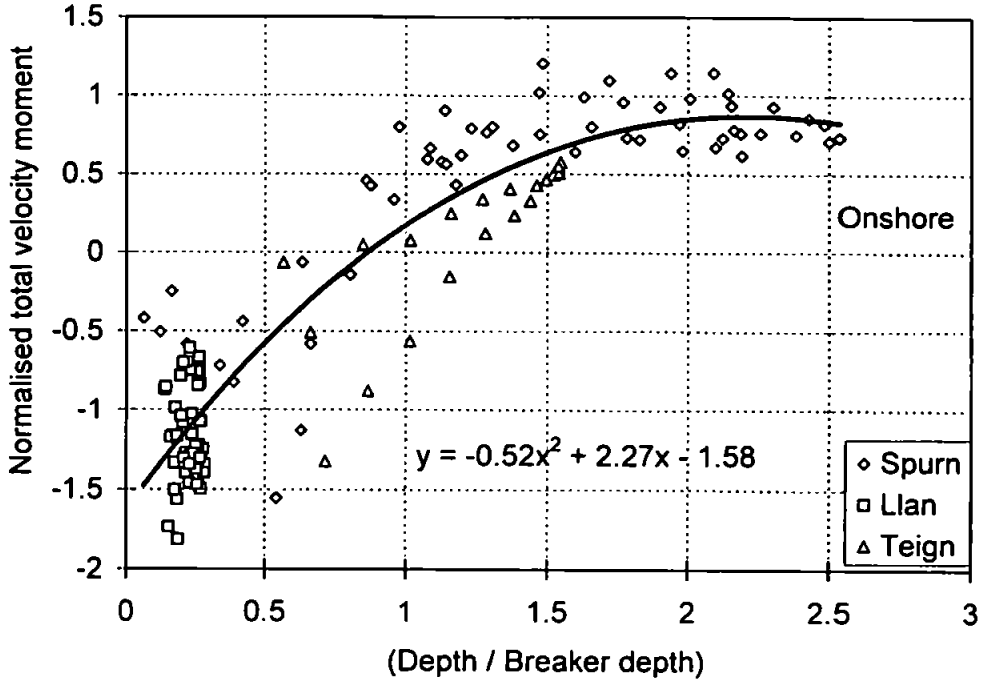

Figure 1.3: shape function from Russell and Huntley (1999): normalised total velocity moment term against normalised depth. 'Spurn', 'Llan' and 'Teign' refer to data from Spurn Head, Llangennith and Teignmouth respectively.

1.5 Aims and objectives of the present study

1.5.1 Theory-measurement interactions

Before knowledge can be improved about the dynamical processes which control the movement of sediment in the coastal zone, there must be certain interaction between theory and measurement. Three basic forms of interaction identified by Peregrine (1990) as being relevant to oceanographic studies are (a) observations in nature or in the laboratory lead to new theories being developed; (b) new phenomena are predicted by theory, which leads to experiments being designed to verify that theory; and (c) discrepancies are found between theory and measurements, which stimulates further development of both.

The general aim of the present study is to improve the understanding of the processes which control sediment transport in the swash-zone, in an attempt to fill the gap in knowledge which exists. This is principally achieved through the collection and analysis of field data, which initially requires the selection of the specific parameters to measure.

Deciding which parameters to measure is paradoxical, since the relative importance of the processes involved will not have been established until measurements are obtained of the parameters which control those processes. Therefore, the approach is to pick up on *potentially* important processes which have been identified in previous studies, but which obviously require further investigation. The relevant parameters to measure are then chosen in association with these processes. After the data has been gathered, it might turn out that further new processes are identified which, themselves, need different instrumentation or measurement techniques to be verified.

A study such as the present one should therefore be thought of as not an end in itself, but as a single step in a continuous iteration between the theory-measurement interactions described above.

1.5.2 Specific processes studied

The identification of processes and the selection of which parameters to measure are mutually dependent. Potentially important processes were identified before the measurements were undertaken, mainly from acknowledgements in the recent literature that they exist, and indications that further study was required. The following processes are addressed in detail in this thesis:

- Non-linearities in the cross-shore velocity field in the swash-zone manifest as large, infragravity frequency backwashes and high onshore accelerations at incident frequencies. These processes are directly applied after several workers have identified them as being important in deeper water (e.g. Elgar *et al*, 1988; King, 1991).
- Infiltration-exfiltration, and the opposing effects of boundary-layer modification and stabilisation-destabilisation. The importance of in-exfiltration has been highlighted recently (e.g. Baird *et al*, 1996; Turner and Masselink, 1998), and it has emerged that the net sediment transport direction and relative significance of these processes need to be resolved.

- Hydraulic jumps, and under what circumstances sediment is either advected shoreward or seaward of the jump. The existence of hydraulic jumps and their importance has been hinted upon (e.g. Osborne and Rooker, 1998), but very little analysis has been performed.
- Backwash ripples, their generation and subsequent effect on the flow. These were studied some time ago by Broome and Komar (1979), but their significance has not been determined in conjunction with that of other processes.

1.5.3 Specific parameters measured

The following is a list of the principal field measurements made for the present study at Perranporth, Cornwall, U.K., a high energy, macrotidal, dissipative beach:

- Cross-shore velocity using miniature electromagnetic current meters (EMCMs), mounted at 5-6cm from the bed.
- Suspended sediment concentration (SSC) using four specifically designed miniature optical backscatter sensors (MOBS), at heights of 2-11cm from the bed.
- Water depth and sub-surface pore-pressure gradients using pressure transducers (PTs).

Several aspects of this arrangement are either totally new, or have been addressed very little in the past. For example, concurrent measurements of SSC and cross-shore velocity from the swash-zone of a dissipative beach using fast response sensors has only been reported in the literature from two experiments (i.e. Beach and Sternberg, 1991; Osborne and Rooker, 1998, 1999). The simultaneous measurement of cross-shore velocity and sub-surface pore-pressure in the swash-zone has not yet been reported.

All these measurements are made as close as possible to a single point, and are therefore, necessarily, Eulerian. These kinds of measurements have been extremely useful so far in elucidating important sediment transport processes inside and outside the surf-zone. For the kind of analysis undertaken in the present study, the best kind of measurements are those of many parameters simultaneously, logged at a relatively high frequency, so that short-term temporal changes in these, and other inferred, parameters may be resolved. Note that temporal variations in, for example, suspended sediment flux are considered of primary importance, whereas absolute values are secondary.

The present study does not attempt to go into great detail about the longshore transport of sediment in the swash-zone, although a brief examination of longshore

velocities are presented in section 6.3, where the longshore velocities are found to be an order of magnitude smaller than the cross-shore velocities. For the beach under study, the waves tend to approach the beach shore-normal. For obliquely incident waves, longshore transport in the swash-zone is important, and has been studied by a few workers (e.g. Thornton and Abdelrahman, 1991).

1.5.4 Summary of specific aims

The following is a simplified list of the specific aims of the project:

- Identify from the literature potentially important processes in the swash-zone which require further study.
- Obtain concurrent high frequency measurements of the parameters which control the above processes.
- Perform basic inspection and analysis of the above data to obtain a picture of the flow characteristics in the swash-zone during the experiment, and to confirm the existence of the processes which will be studied in greater detail.
- Ascertain the relative importance of the key processes, and the direction (i.e. onshore or offshore) towards which each process influences the transport under particular conditions.
- Point the way forward for parameterisation of the processes and for eventual incorporation of the parameterisations into models of shoreline morphology.
- Identify aspects which require further study preceded by development of new measurement techniques.
- Generally fill the gap in knowledge which exists and improve the understanding of how sediment is transported in the swash-zone.

1.6 Structure of the thesis

A comprehensive review of the recent literature is given in **Chapter 2**, where gaps in the knowledge of sediment transport in the swash-zone are identified. **Chapter 3** describes the instrumentation, including in-house design and development of the MOBS sensors. **Chapter 4** gives chronological and logistical details of the field experiment. **Chapter 5** describes how the raw data is converted into a form suitable for subsequent

analysis. **Chapter 6** presents the time series extracted from the raw data, upon which all the subsequent analysis is performed.

Chapter 7 encompasses various preliminary studies, as a foundation for the more specific study detailed below. Firstly the hydrodynamics are examined, based upon frequency-dependent variations of velocity and surface elevation. Then the SSC flux time-series and spectra are inspected and a preliminary description of the temporal behaviour of SSC is given. Next, some three-dimensional velocity data from another field experiment at Muriwai Beach, New Zealand, which will be used later in the thesis, is introduced, and briefly compared with the Perranporth data. Lastly, an examination is made of the characteristics of SSC events within a single representative swash cycle.

The next three Chapters represent the central focus of the thesis. Each Chapter relates to a single process, or closely related set of processes, which are analysed in detail, providing new information on the relative importance of each, and the direction of transport influence under various conditions. **Chapter 8** is concerned with nonlinearities in the velocity field, causing onshore or offshore transport through asymmetry and skewness respectively. **Chapter 9** discusses the implications of infiltration-exfiltration in the swash-zone. **Chapter 10** focuses on higher order processes (namely hydraulic jumps and backwash ripples), which require the existence of other sediment-moving processes as pre-requisites.

The results of the study, particularly the processes identified in the last three Chapters and their interconnectedness, are drawn together and discussed as a whole in **Chapter 11**. Suggestions for further work are also given here. Finally, a list of conclusions is given in **Chapter 12**.

2. Literature review

2.1 Introduction

In this chapter is presented a review of the recent literature concerning studies of the hydrodynamics and sediment transport in the swash-zone. Many of the studies mentioned herein are not directly linked with the work undertaken in the present study, but nevertheless were included to provide a comprehensive background to the subject. Likewise, some aspects of the present work do not appear in the literature review because no comprehensive studies have been made on these subjects so far.

Special consideration is given to field studies of swash-zone sediment transport, and less emphasis is placed on laboratory work. A brief section on swash-zone hydrodynamics is presented, indicating the importance of infragravity motions at the shoreline. Recent groundwater studies are also reviewed, relevant to movements of the water-table in response to swash motions, and effects caused by infiltration and exfiltration.

2.2 Swash-zone hydrodynamics

2.2.1 The importance of long waves

The existence of long-period ocean waves has been acknowledged for some time, and their importance for sediment transport in the surf-zone has been recognised (e.g. Russell, 1993). It is also logical to assume that they must play an important role in transporting sediment in the swash-zone, since they generally grow in amplitude towards the shoreline, whilst breaking tends to reduce incident energy levels towards the shoreline (e.g. Huntley, 1976; Huntley *et al*, 1981; Holman, 1981; Guza and Thornton, 1982; Holman and Sallenger, 1985; Sallenger and Holman, 1987). Guza and Thornton (1985) observed an increase in infragravity cross-shore velocity variance of between 10 and 100 times, between 5m depth and the shoreline, and Masselink (1995) found a four to five-fold increase in infragravity surface elevation variance from a depth of 4m down to 1m.

Munk (1949) was one of the first to observe long period (30-300s) sea surface fluctuations in the nearshore. Tucker (1950) concluded that the amplitude of these oscillations was shown to have a quasi-linear relationship with the groups of incident waves seaward of the surf-zone, and the long-wave was thought to be primarily seaward propagating. However, Meadows *et al* (1982) suggested from observations that the long-wave was shoreward-propagating, and it was in antiphase with the incident wave envelope.

An explanation of the formation of long-waves was proposed by Longuet-Higgins and Stewart (1964), in terms of radiation stress. Since large waves have a greater mass transport than small waves, then the difference in momentum flux causes water to be expelled from regions of larger waves to regions of smaller waves; this in turn causes a 'set-down wave' which is 180^0 out of phase with the envelope of the wave-group, but has the same wavelength and period. The model of Longuet-Higgins and Stewart (1964), showed that a group-forced long-wave could be described by:

$$\eta(t) = -\frac{1}{\rho}\left[\frac{S_{xx}(t)}{gh - C_g^2}\right] \tag{2.1}$$

where $\eta(t)$ is the time-varying sea surface elevation averaged over the incident wave period, ρ is the water density, S_{xx} (t) is the time varying cross-shore radiation stress, h is the incident-period averaged water depth, and C_g is the group speed. The theory predicts a bound long wave (BLW) travelling at C_g . The hypothesis states that the BLW is then released at the breakpoint of the incident waves, and travels shorewards as a free wave.

An alternative explanation for the formation of low frequency oscillations in the surf-zone was proposed by Symonds *et al* (1982). Here the long-wave motion is driven by the cross-shore variation in the position of the breakpoint due to the variation in height of the incident waves. A time-varying wave set-up is created, which generates long waves propagating in the shoreward and seaward directions.

After propagation to the shoreline, the long wave is reflected and may either remain trapped to the shore as an edge wave (e.g. Huntley, 1976), or leak out into deeper water. A standing wave may be produced from the interaction between the shoreward-propagating wave and its reflection from the beach-face. The standing waves have a particular cross-shore structure, depending on the mode (Holman, 1981).

There has been a recent resurgence into the investigation of the source of long-waves in the nearshore, and whether they are, in fact, correlated with the incoming incident wave envelope. Observations well seaward of the surf-zone have indicated that surface fluctuations in the infragravity band contain both free and bound waves (e.g. Elgar *et al*, 1992) and it has been shown that the bound waves are in near antiphase with the incident wave groups (e.g. Herbers *et al*, 1994). Masselink (1995) actually related the free-propagating long-wave in the surf-zone with the incident wave envelope, and found that 40% of the incoming infragravity energy could be explained by incident wave group forcing.

Infragravity frequency oscillations have been established as one of the most important mechanisms contributing to the transport of sediment in the surf-zone, and, infragravity frequency variations of sediment flux have been found to increase shoreward (e.g. Beach and Sternberg 1988; Russell, 1993). Hydrodynamic studies have indicated that, in dissipative conditions, infragravity waves tend not to become saturated, and their energy is carried through to the shoreline (e.g. Guza and Thornton, 1982). Therefore, infragravity fluctuations not only generally increase shoreward but, in incident-saturated conditions, the shoreline becomes increasingly long-wave dominated with increasing offshore wave height. Sediment transport in the swash-zone in high-energy dissipative conditions has actually been found to be highly infragravity-dominated (Beach and Sternberg, 1991), although very few studies of this type have been made.

2.2.2 Field studies of swash-zone hydrodynamics

Field studies of the hydrodynamic processes in the swash-zone have normally been performed using offshore wave-gauges in association with various different types of device to measure either the run-up height (i.e. how deep the water is at any given time in a fixed position in the swash-zone), or the run-up distance (i.e. the instantaneous cross-shore displacement of the shoreline). It has been pointed out that the difference in reference frame (Eularian or Lagrangian) between these methods may have an important effect on the results (Longuet-Higgins, 1986; Baldock *et al* , 1997).

A study of swash hydrodynamics was performed by Guza and Thornton (1981, 1982), as part of the National Sediment Transport Study (NSTS), using run-up wires and pressure sensors on a gently sloping beach. When a large number of run-up heights was

compared with the corresponding incident wave heights, and the run-up variance was split into high and low frequency bands, it was found that the incident band energy levels appeared to be independent of incident wave height, (suggesting saturation). However, infragravity band swash oscillations were shown to increase approximately linearly with incident wave height (see Figure 2.1).

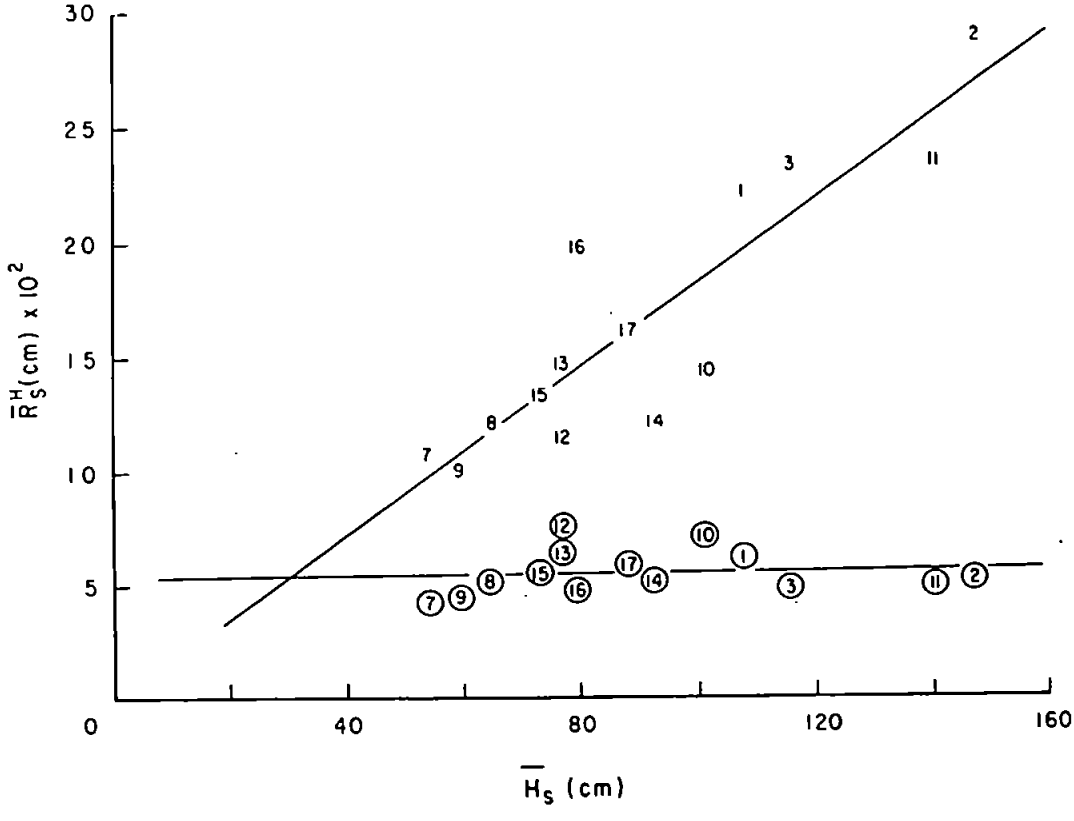

Figure 2.1. Run-up height obtained from low (<0.05Hz) and high (>0.05Hz) frequency swash variances, v. incident wave height. Each number corresponds to a different run, with different offshore wave conditions. Circled numbers represent the high frequencies. (after Guza and Thornton, 1982)

A method using time lapse photography with a super-8 movie camera, to measure shoreline position, was reported by Holman and Guza (1984). Using this technique, Holman and Sallenger (1985) obtained a large data set of shoreline positions on a steep beach, with incident wave heights varying between 0.4m and 4m. However, they experienced difficulty determining the backwash position due to the effects of infiltration. The connection between swash oscillations and offshore wave heights was investigated by using a surf-similarity parameter. In this way, the dependency of this relationship upon the degree of surf-zone saturation could be quantified. The dimensionless surf-similarity parameter, the Iribarren number, ξ_0, (Battjes, 1974) is defined as follows:

$$\xi_0 = \beta\left[\frac{H_0}{L_0}\right]^{-1/2} \tag{2.2}$$

where β is beach slope, and H_0 and L_0 are the deep-water significant wave height and length respectively. It was found that, for small values of ξ_0 the results were consistent with those of Guza and Thornton (1982), but for larger values of ξ_0 (i.e. no saturation), the incident frequency swash oscillations were actually related to offshore wave heights.

The data of Guza and Thornton were reanalysed by Holman (1986) to derive statistical relationships for extreme values of run-up, which were then normalised by H_0 and plotted against ξ_0. For example, regression analysis yielded $R_{max} = 0.55H_0\xi_0$ and $R_{2\%} = 0.45H_0\xi_0$, where R_{max} is the maximum run-up elevation and $R_{2\%}$ is the 2% exceedence elevation. The plots could then be used in conjunction with a storm value of ξ_0 and a design wave height, to estimate a design run-up height.

Sensitivity of run-up measurements to run-up wire elevation was also investigated by Holland *et al* (1995). Run-up wires at five elevations were used in conjunction with a modified video technique based on the method outlined by Aagaard and Holm (1989), whereby the most landward identifiable edge of the swash tongue was digitised to provide a time-series of shoreline location. It was apparent that the video observations were most consistent with those of the lowest wires, and therefore corresponded with a very near-bed measurement. The significant horizontal run-up excursion and the mean superelevation (set-up) were found to increase with decreasing height above the bed, with maximum values being produced by the video, and the greatest variation within 10cm of the bed. At low infragravity frequencies cross-shore standing wave patterns were observed, but there

appeared to be some overamplification of the swash magnitudes relative to a linear standing wave model. The maximum overamplifications occurred at the lowest elevations and at the lowest resolvable frequency (0.005Hz).

The work by Ruessink *et al* (1998) was done using a video camera to measure shoreline location, during highly dissipative conditions. They confirmed that a relationship exists between ξ_0 and R_{ig}/H_0 (where R_{ig} is infragravity swash height). They also found the saturated tails in their spectra to decay approximately as f^{-3} (see Figure 2.2).

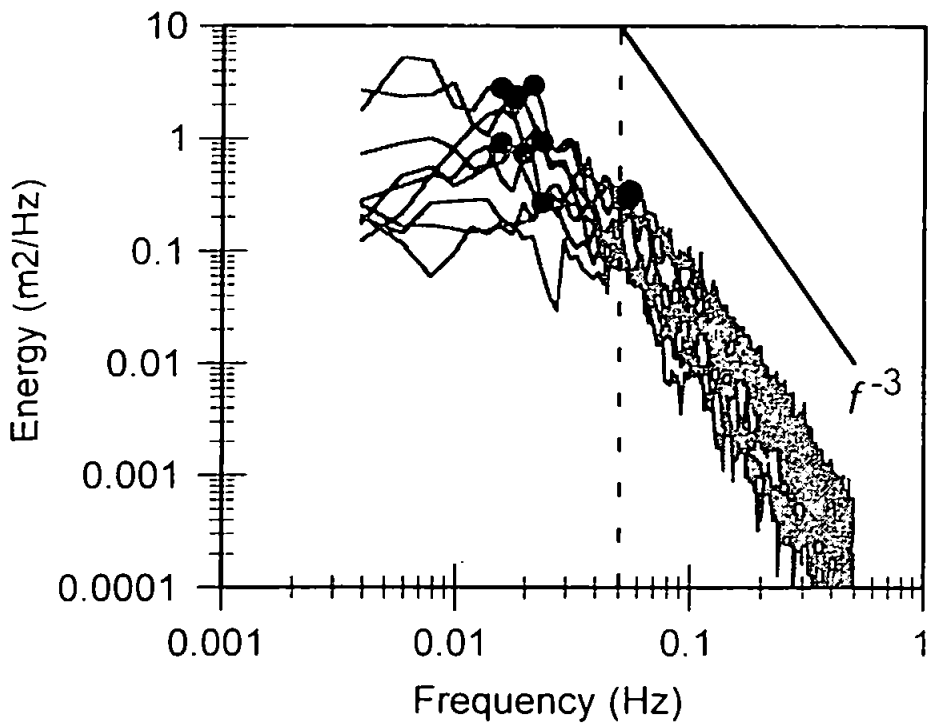

Figure 2.2. Energy spectra of run-up height, showing how saturation occurs at higher frequencies. The vertical dashed line is the division between the infragravity and incident bands (after Ruessink et al, *1998).*

The results of the above studies generally indicate that, if the beach is sufficiently dissipative to allow the incident waves to become saturated, then the incident frequency fluctuations at the shoreline will not increase with increasing offshore wave height. However, infragravity waves do not break due to their long wavelength and low steepness, and their amplitude at the shoreline will continue to be related to increases in the offshore incident wave height. This concept was recognised by Huntley *et al* (1977), whereby it was suggested that swash motions consist of a saturated incident-frequency component and a non-saturated long-wave component.

Figure 2.3 summarises from the literature how the relation between infragravity swash motions and offshore wave height changes according to the Iribarren number (indicating the degree of saturation). Instrumental differences and different methods of calculation may partly explain the variation between different workers (see Ruessink *et al*, 1998).

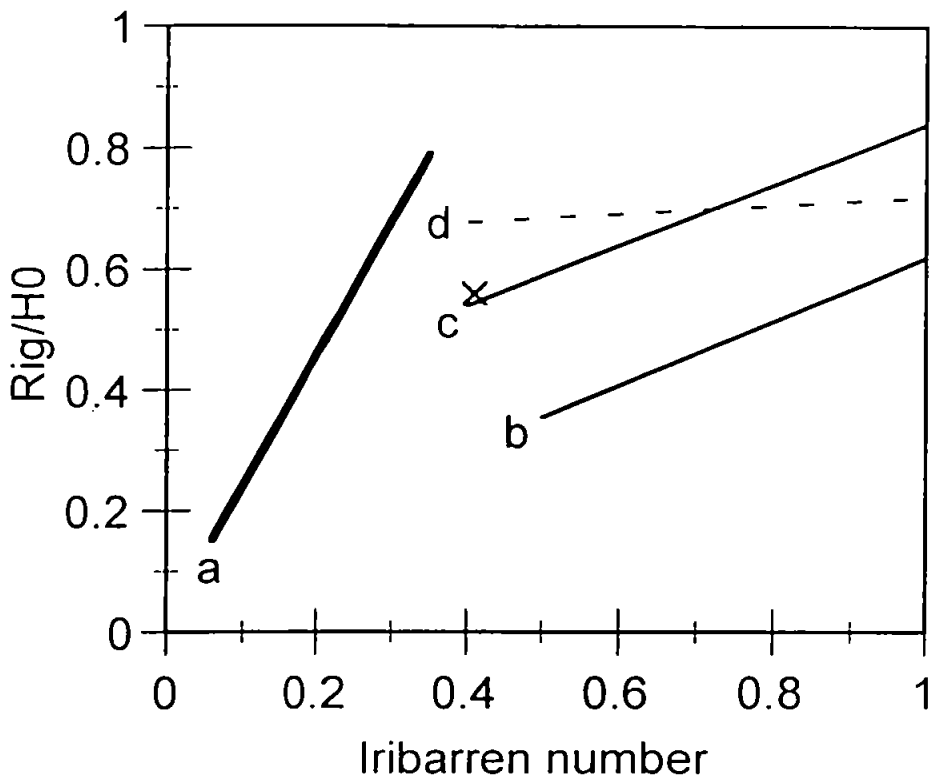

Figure 2.3: Overview of published ξ_0 dependencies of R_{ig} / H_0. Line (a) is Ruessink et al *(1998); line (b) is Holman and Sallenger (1985); line (c) is Holland (1995), and line (d) is Raubenheimer and Guza (1996). The single cross is from Holman and Bowen (1984). (after Ruessink* et al, *1998)*

However, many studies have also taken place in conditions which are not dissipative enough to allow all the incident waves to become saturated (e.g. Waddell, 1973; Sonu *et al*, 1976; Bradshaw, 1980, 1982; Mizuguchi, 1984). In these types of conditions the incident waves break close to the shore and are transmitted directly to swash motions. Therefore, the existence of two different types of kinematic behaviour of the shoreline has been acknowledged, which has led to difficulty in identifying the approach required for modelling. Furthermore, the existence of long waves at the shoreline directly derived from locally forced grouping has also been recognised, although mainly from the results of laboratory studies (Mase, 1988; Baldock *et al*, 1997).

2.2.3 Modelling swash-zone hydrodynamics

This section describes some of the attempts which have been made to develop models of run-up elevations and spectra. The theoretical description of run-up has been divided between (a): the standing wave hypothesis first proposed by Miche (1951), where the shoreline location is dependent upon the reflection of wave energy, with incoming energy above a particular threshold having been dissipated by breaking; and (b): the non-linear shallow water theory following bore collapse proposed by Ho *et al* (1962), and Shen and Meyer (1963). The latter theory was examined using numerical techniques by Freeman and LeMehaute (1964), and Amein (1966). The depth-integrated non-linear shallow water equations for motion and continuity are:

$$\frac{\partial u}{\partial t} + u\frac{\partial u}{\partial x} + g\frac{\partial \eta}{\partial x} = 0 \qquad (2.3)$$

and

$$\frac{\partial\left[u(\eta + h)\right]}{\partial x} + \frac{\partial \eta}{\partial t} = 0 \qquad (2.4)$$

where u is the cross-shore velocity, η is the surface elevation, h is average water depth, x is cross-shore distance, g is gravitational acceleration and t is time. These equations were solved numerically by Hibberd and Peregrine (1979) to describe the uprush and backwash of a bore climbing a beach. Many models have subsequently been developed based on this work (e.g. Kobayashi *et al*, 1987, 1989, 1990; Kobayashi and Karjadi, 1994, 1996), with

good success at describing the shoreline motion, but still not suitable for further application to sediment transport modelling (Horn, 1997).

A comprehensive study, including field measurements using a cross-shore transect of capacitance probes on a steep beach, was made by Hughes (1992), to examine the applicability of a model based on the shallow water theory to swash hydrodynamics on a natural beach. It was concluded that the model consistently over-predicted the maximum swash height, shoreline displacement and swash depth, which was thought to be due to the combined effects of friction and infiltration which were not originally considered in the model. It was also shown that the backwash was less well predicted than the uprush, and the behaviour of the backwash 'bore' needed to be studied further, together with the behaviour of granular fluids in the backwash. The non-linear shallow water equations have been used to model the swash height and shoreline position on the uprush only, with the addition of a friction factor (Hughes, 1995; Turner, 1995).

Raubenheimer *et al* (1995) measured the run-up characteristics on a fine-grained, gently sloping beach, using pressure sensors and a series of five run-up wires, stacked vertically. Results showed that (a): wave reflection at the shoreline was greater in the infragravity band than the incident band; and (b): reflection at incident wave frequencies increased with beach slope. There was found to be a predominance of standing wave energy in the infragravity band, and of progressive energy in the incident band. The non-linear shallow water equations were used to model run-up and surf-zone pressure and velocity fluctuations. The model was shown to predict well the shoreward increase of infragravity energy and decrease of incident wave energy. The observed transformation of wave shape (i.e. skewness and asymmetry) was also well predicted.

The above study was extended by Raubenheimer and Guza (1996), who compared results from a model and observations of run-up using vertically stacked run-up wires, from both a gently sloping beach and a steep concave beach, with semiempirical saturation formulae, e.g:

$$\frac{R_v}{H_o} = \left(\frac{\pi}{2\beta}\right)^{1/2} \qquad :\xi_0 \geq \xi_c \quad : \text{reflective} \qquad (2.5)$$

$$\frac{R_v}{H_o} = \frac{\xi_0^{\,2}}{\pi} \qquad :\xi_0 < \xi_c \quad : \text{saturated} \qquad (2.6)$$

where β is the beach slope, R_v is the run-up height, normalised by H_0, the deep water wave height, L_0 is the deep water wavelength, and $\xi_c = |\pi^3 / 2\beta|^{1/4}$. The run-up height becomes independent of offshore wave height in saturated conditions. The above formulae, and others, were found to be consistent with the model predictions and observations. The model also predicted well the relative increase of reflected energy with increasing distance shoreward, and increasing ξ_0. Considerable differences were found in the run-up excursions measured by the wires of different heights, owing to the shape of the leading edge of the run-up tongue. The measured run-up excursions and mean superelevation were found to increase with decreasing wire elevation, and flow divergence caused by continuous thinning of the run-up tongue sometimes resulted in onshore-directed near-bed velocities but offshore-directed velocities at 25cm above the bed.

Johnson and Kobayashi (1998) have developed a nonlinear time-averaged model of surf and swash-zone hydrodynamics which is more computationally efficient than traditional time-dependent models, and therefore more practical for studies of long term coastal morphology. The model extends the applicability of previous time-averaged models (e.g. Battjes and Stive, 1985; Dally and Dean, 1986) to the swash-zone. Various tests (Kobayashi *et al*, 1997, 1998) have shown a considerable improvement over the earlier time-averaged models, especially in the inner surf and swash-zones.

2.3 Sediment transport in the swash-zone

2.3.1 Modes of transport

The separation of sediment transport into bedload and suspended load has long been a source of difficulty in measuring cross-shore sediment transport in the surf-zone, due to the lack of suitable instrumentation for measuring bedload transport, poor theoretical knowledge and general observation difficulties. It is also a matter of some controversy whether the movement of sediment in the swash-zone should indeed be separated into these two modes (Masselink and Hughes, 1998).

The distinction between bedload and suspended load has been defined in various different ways depending on the context. Bagnold (1956) defined bedload as that part which is supported by intergranular forces, and suspended load that part which is supported

by fluid drag. However, a given grain may be supported by both mechanisms, which obviously creates measuring difficulties (Nielsen, 1992).

The difficulty in measuring bedload transport has hampered the process of model development (Huntley *et al* 1993), and, at the time of writing, a suitable standard high frequency measuring device for bedload is not yet in existence. Most attempts at measuring bedload have been made using traps (e.g. Hardisty *et al*, 1984; Kawata *et al*, 1990), although Hardisty (1991) used hydrophones to monitor the self-generated noise produced by inter-particle collisions to estimate bedload transport. This technique is described in detail in Jagger and Hardisty (1991), and based on previous work by Millard (1976), Thorne *et al* (1983, 1984, 1989), Heathershaw and Thorne (1985) and Thorne (1985, 1986). The experiment was carried out on a beach containing gravel of about 10-12mm diameter.

The relative importance of bedload transport compared with suspended load in the swash-zone was examined by Horn and Mason (1994). They used a trap containing compartments for bedload and suspended load. The division between the compartments was 1cm above the bed, which effectively meant that their definition of bedload was sediment moving below a height of 1cm. Suspended load was therefore defined as any sediment moving above 1cm. The traps were installed in the mid-point of the swash-zone, and retained in place throughout half a wave cycle (uprush or backwash). The relative weights of sediment caught in the traps were used to infer the relative importance of the two modes of transport. They concluded that, out of the four beaches studied, bedload transport was greater than suspended load on the backwash of three, and on both the uprush and backwash of two.

2.3.2 Laboratory measurements of sediment transport relevant to the swash-zone

Studies of sediment transport in tanks and wave flumes have the advantage of repeatability and much greater control over conditions compared with field studies. It is accepted that real wave characteristics are often difficult to mimic in the tank, and models developed for, say, monochromatic waves can be oversimplistic and inapplicable in the field, but laboratory tests do have a degree of usefulness. The nature of sheet-flow and the processes acting in the boundary layer are extremely difficult to observe in the field, and it

is here where laboratory tests come in useful. They also have the advantage of being able to employ instrumentation which would be impractical (e.g. not sturdy enough) to use in the field. This section describes some laboratory tests whose results could be useful in helping to describe the sediment transport processes in the swash-zone, although the tests themselves have not necessarily been performed in simulated swash-zones. Because the swash-zone is characterised by highly asymmetrical flow regimes, and the mode of sediment transport appears to be similar to sheet-flow (Hughes *et al*, 1997) then studies which concentrate on these aspects will be of greatest interest.

The phenomenon of sheet-flow was observed at high stresses by Yalin and Karahan (1979), who studied the inception of grain movement. The particles were seen to be dragged into motion in the form of a continuous layer, several grain diameters thick, which they termed a "grain carpet". This phenomenon was recognised by Wilson (1987, 1989) for unidirectional and oscillatory flow respectively. Sheet-flow in skewed (Stokes) waves was studied extensively in a large oscillating water-tunnel by Ribberink and Al-Salem (1990, 1992). A velocity-cubed relation was suggested for the net transport produced by these flows (Ribberink and Al-Salem, 1994, 1995; Wilson *et al*, 1995).

Although attention has recently been drawn towards using wave-flumes to study the sediment transport under irregular oscillatory flows, most studies have concentrated on skewed, or Stokes waves (symmetrical about the vertical but not the horizontal axis). Although this type of irregularity exists in the swash-zone, what is also very important is sawtooth asymmetry (characterised by a vertical rather than horizontal asymmetry), which has rarely been studied. Important implications exist concerning the net sediment flux which might result from the directional differences in acceleration (Hanes and Huntley, 1986; Elgar *et al*, 1988). Using a pair of mirror-imaged sawtooth waves, King (1991) was able to show that greater sediment transport could be produced by the sawtooth in the 'steep fronted' direction.

2.3.3 Field measurements of swash-zone sediment transport: general

Although there has been considerable investigation into swash-zone hydrodynamics, field studies of swash sediment transport have been relatively few in number. Only very recently have advances in instrumentation allowed more promising measurements to be made.

Early field studies of swash-zone sediment transport concentrated on measuring changes in bed elevation of the foreshore during uprush-backwash cycles (e.g. Duncan, 1964; Strahler, 1966; Waddel, 1973, 1976). Also, Howd and Holman (1984) have suggested that sediment level oscillations in the foreshore may be related to infragravity motions.

Field measurements of sediment transport in the swash-zone might be divided into two separate schools.

(a) Low energy conditions, with steep beaches in the reflective end of the continuum. Here, incident waves tend to break very close to the shoreline, and transform directly into swash motions, i.e. incident frequency oscillations in shoreline position are directly related to wave heights beyond the break-point.

(b) High energy conditions on relatively flat, dissipative beaches, where there is a wide surf-zone, and incident waves become saturated. Here there is a predominance of infragravity energy at the shoreline, and continuous measurements of suspended sediment concentration have been made using instruments such as the optical backscatter sensor (Downing *et al*, 1981).

2.3.4 Field measurements on steep, reflective beaches

In most of the studies described in this section, individual swash events have been monitored separately, and the sediment has been collected in traps. As opposed to measuring the instantaneous sediment flux, the total amount of sediment transported up or down the beach on the uprush or backwash respectively has been measured.

Hardisty *et al* (1984) measured uprush and backwash sediment load and cross-shore velocity on two relatively steep beaches in the UK. The velocity was estimated using the deflection of a 'swinging vane', and the sediment was collected in two bedload traps, one for uprush and one for backwash. The experiment was designed to calibrate a modified version of the Bagnold beach equations (Bagnold, 1963, 1966); i.e.

$$I_u = \frac{K_u u_u^3 T_u}{\tan\phi_f + \tan\beta} \qquad (2.7)$$

$$I_b = \frac{K_b u_b^3 T_b}{\tan\phi_f - \tan\beta} \tag{2.8}$$

where the subscripts 'u' and 'b' are for uprush and backwash respectively, I is the total immersed weight of sediment transported during either the uprush or backwash phase of the swash cycle, u is the flow velocity, T is the uprush or backwash duration, ϕ_f is the angle of internal friction of the sediment (also known as the angle of repose or shear), β is the beach slope, and K_u and K_b are the calibration constants. There appeared to be little difference in the derived values for the calibration constant for uprush and backwash, which seemed to suggest the denominator in equations 2.7 and 2.8 was compensating for the differences in upslope and downslope transport in the correct way. They also suggested that the value of K_u and K_b was likely to vary from beach to beach, with a possible dependence upon grain size.

The results of the above study were also used to examine a very simple equilibrium model, in which the ratio between the uprush and backwash transport was used to determine whether the beach was eroding or accreting. It was found that the transport was uprush dominated, indicating overall accretion throughout the experiment, and this was confirmed by comparing beach slopes.

Yu *et al.* (1990) performed an experiment in the swash-zone in fairly low-energy conditions, on a beach in Norderney, Germany, to observe the characteristics of sheet-flow in the field. Sediment concentration changes in the sheet-flow layer were measured using a resistance type sheet-flow probe (Ribberink and Al-salem, 1992, 1995), and concentration changes were compared with flow velocities measured higher in the water-column. The intrusion depth of the sheet-flow layer itself was also measured, together with the local morphological changes throughout the experiment. A moving layer of sediment up to 8mm deep was found, which could be observed during periods of increased velocity, especially during the final stages of the backwash.

A recent field study in the swash-zone was carried out by Hughes *et al.* (1997), on a steep beach with wave heights of about 0.5m. It was noted that the swash oscillations were occurring principally at incident wave frequencies. Measurements were taken on the uprush only, of (a) 'total' (bedload and suspended) sediment load using a sediment trap with an opening 50cm high by 10cm wide; (b) flow velocity using ducted-impeller type current meters, and (c) water level using a capacitance probe. It was acknowledged that certain errors would be inevitable from the flow meters, especially in shallow depths due to the

water not completely covering the impeller. It was also pointed out that care must be taken to avoid fouling due to seaweed and other debris, and also the tendency of the impeller to continue revolving after it dries out.

The total load of sediment transported during the uprush was noted for 35 swash 'events', and this was compared with the average total transport of sediment per uprush-backwash cycle, calculated from the morphological change of the beach throughout the experiment. It was found that the amount of sediment moved during each uprush was far greater than net movement during the whole uprush-backwash cycle, implying that the net transport per swash cycle is the relatively small difference between two large quantities.

The applicability of the modified Bagnold bedload equations (2.7 and 2.8) was also investigated for use in the swash-zone. The K_u value in equation 2.7 (uprush only) was found by regression analysis against the data. The value of K_u seemed to be much smaller than that obtained by Hardisty *et al.* (1984), and this was attributed to either differences in grain size, or the inability of the swinging vane instrument used by Hardisty *et al.* to respond to rapid changes in velocity (which would tend to underestimate the time-averaged velocity, and hence overestimate K_u). A calculation was also made based on the sheetflow criterion suggested by Wilson (1987) to confirm that sheetflow conditions were, in fact, predominant in this experiment.

A very similar experiment was performed by Masselink and Hughes (1998), who monitored 27 swash events, with the sediment load of each event being correlated with both the uprush and backwash velocities. The sediment transport was found to display a strong relationship with the velocity cubed. The constant of proportionality in both Bagnold and Shields type sediment transport models on the uprush was found to differ from that on the backwash. This was attributed to inherent differences between uprush and backwash processes such as accelerating versus decelerating flows, groundwater effects, and excess suspended sediment on the uprush due to bore collapse.

The results of the above studies highlight the importance of high concentrations of sediment moving low in the water column, which are still extremely difficult to measure. Uncertainties and sometimes conflicting results appear due to the different measurement techniques used. Further difficulties would also arise in deploying fragile instruments such as the sheet-flow probe of Yu *et al* (1990) in high-energy conditions (see below).

2.3.5 Field measurements on dissipative beaches

Advances in the design of non-obtrusive instrumentation which can be used very close to the bed have allowed measurements of instantaneous near-bed velocity and suspended sediment in the swash-zone to be made. These instruments have been developed directly from those used in the surf-zone. However, very few measurements of this kind in the swash-zone have been made so far.

The optical backscatter sensor (OBS), originally designed for measuring suspended sediment in the surf-zone (Downing *et al*, 1981) may also be used in its original, or modified forms, to measure sediment concentrations in the swash-zone. This instrument consists of an infra-red emitting diode and a silicon photo-voltaic cell (light detector). The OBS has been used successfully in the inner and outer surf-zone at vertical elevations as low as 5cm above the bed (e.g. Downing, 1984; Jaffe *et al*, 1984; Sternberg *et al*, 1984, 1989; Beach and Sternberg, 1988; Greenwood *et al*, 1990; Black and Rosenberg, 1991; Russell *et al*, 1991; van Hardenberg *et al*, 1991; Davidson *et al*, 1993). Note also that, using estuarine muds, Kineke and Sternberg (1992) have used the OBS to measure concentrations of up to 320g/l. To measure suspended sediment concentration close to the bed, attention has been paid to developing miniaturised versions of the OBS, to avoid the relatively large vertical cross-section of the probe causing scour from flow redirection. Sternberg *et al* (1984) used a miniature version of the optical backscatter sensor, at 3.5cm above the bed. The FOBS, fibre-optic backscatter sensor (Beach *et al*, 1992) has a very small diameter and a vertical orientation which ensure that the flow around the instrument is minimally disturbed.

The acoustic Döppler velocimeter (ADV) is a state-of-the-art instrument which is becoming available in miniature form, suitable for measuring flow velocities in environments such as the swash-zone (Kraus *et al*, 1994). It can simultaneously measure all three components of flow at sampling rates of up to 25Hz, thereby making it suitable for turbulence measurements. Recent tests have been carried out to evaluate the accuracy of this instrument (Voulgaris and Trowbridge, 1998), whereby simultaneous measurements were carried out using the ADV together with an LDV (laser Döppler velocimeter), in the same sampling volume. Using this technique, the measured values from the ADV could be compared with 'true' values of flow characteristics. It was found that the ADV could measure the mean velocity to within 1% of the (much more accurate) LDV values.

If measurements of suspended sediment concentration are combined with those of cross-shore velocity in a similar way to the techniques used in the inner and outer surf-zone

(e.g. Huntley and Hanes, 1987), then values of cross-shore suspended sediment fluxes may be obtained in the swash-zone.

Beach and Sternberg (1991) used the FOBS to measure suspended sediment concentration in the swash-zone of a highly dissipative beach in very high energy conditions, with offshore wave heights of several metres. An array of FOBS sensors was placed between 0.5cm and 5cm above the bed. Measurements of flow velocity were also taken using a single 4cm diameter impeller-type current meter. The sediment transport in the swash-zone was found to be highly infragravity dominated, with the largest sediment suspension 'events' at frequencies of 0.01 to 0.02Hz (50 to 100s period).

The vertical array of sensors in the above experiment also allowed the time-dependent vertical distribution of sediment to be analysed. It was found that, at the start of the uprush, the sediment concentrations were at a maximum, then tended to decrease rapidly as the uprush decelerated. On flow reversal to backwash, when the flow was accelerating, the sediment was suspended progressively higher in the water column and overall concentrations increased. Co-spectral analysis of the cross-shore velocity and sediment concentration measured by FOBS sensors at 2.8cm and 5cm, revealed considerable differences between the infragravity transport at the two different heights. At 5cm, the co-spectrum showed two large infragravity peaks of opposite sign, but similar magnitude, with the onshore-directed peak of a slightly higher frequency. At 2.8cm there was a single, very large infragravity peak, directed offshore. These transport differences between the two heights were attributed to a frequency-dependent velocity-concentration phase reversal (causing the transport to change direction), being associated with a time lag due to the vertical diffusion of sediment.

Osborne and Rooker (1998, 1999) examined the hydrodynamics and sediment transport in the swash-zone and inner surf-zone of a high-energy dissipative beach. Near-bed velocities and turbulence were measured using an ADV, and suspended sediment concentration was measured using the OBS. In addition to findings which confirm those of previous workers (e.g. Beach and Sternberg, 1991), that concentrations of suspended sediment may be much higher in the swash-zone than those in the inner surf-zone, and that the temporal structure of the velocity and concentration was infragravity-dominated, it was also observed that very high suspended sediment concentrations were present in association with hydraulic jumps generated by the uprush interacting with the previous backwash.

Holland *et al* (1998) made a comprehensive set of measurements during the DUCK94 and SANDYDUCK experiments on a dissipative beach. Swash-zone

measurements included cross-shore velocity using an ADV, suspended sediment concentrations using optical backscatter sensors, and swash edge velocity and displacement together with 3D foreshore topography using the video method of Holland and Holman (1997). Their observations were used to develop and validate a very simple model of swash-zone sediment transport, using the measured shoreline change in conjunction with the hydrodynamic measurements. The model was found to be successful in making qualitative predictions of the shoreline morphodynamic evolution.

Note that, in high-energy conditions where the surf-zone is saturated, the division between the swash-zone and the surf-zone is somewhat arbitrary. Measurements such as those of Beach and Sternberg can be seen to be continuous, i.e. the instruments were continually covered with water, which shows them to have been deployed slightly seaward of the 'true' swash-zone, i.e. seaward of the run-down limit (Gourlay, 1992).

2.4 Groundwater

2.4.1 General

One of the difficulties of describing and modelling the hydrodynamics and sediment transport in the swash-zone comes from the added complication of the flow of water into and out of the beach face, and the shape and position of the water-table relative to the swash-zone. A recent review of coastal groundwater dynamics were given by Nielsen (1998) and an overview of measurement techniques and recent results is given by Turner (1998).

2.4.2 The water-table

The uprush-backwash cycle has been found to have direct effects upon the shape and position of the groundwater table, which could affect the hydrodynamics and sediment transport in the swash-zone by altering the degree of saturation of the beach face. This section describes studies relating to the dynamics of the water-table and how it is linked with the swash cycle.

There has been much interest in improving the understanding of the behaviour of the beach water-table in terms of relatively long-period oscillations ranging from

infragravity-frequency to seasonal fluctuations (e.g. Ericksen, 1970; Harrison, 1971; Lewandowski and Zeidler, 1978; Nielsen *et al.*, 1988; Nielsen, 1990; Nielsen and Kang, 1995; Turner *et al.*, 1997). Somewhat fewer measurements have been made of incident frequency groundwater level (e.g. Waddell, 1973, 1976, 1980; Bradshaw, 1974, 1980; Turner, 1995; Turner and Nielsen, 1997; Li *et al*, 1997). It was generally found that standing waves produced by reflection on a steep beach could translate low frequency motions to the water table, whereas the water table was less likely to respond directly to the incident waves. Hence it was suggested that the beach matrix acted as a low pass filter. Hegge and Masselink (1991) compared run-up measurements taken using a run-up wire, with the time-varying response of the groundwater level measured with a piezometer, on a steep beach during incident-wave periods of between 10 and 20s (0.05-0.1Hz). It was found that the water-table seemed to act as a band pass filter, responding more readily to oscillations with frequencies around 0.013Hz (77s), than to those either side. Despite this, incident frequency oscillations in the water table were detectable, and were closely related to swash oscillations. The response of the water-table also appeared to be asymmetrical, exhibiting a rapid-rise and slow fall, comparable with the observations of Nielsen *et al* (1988) at tidal frequencies.

A study of the moisture content below the bed of sandy beaches was performed on two contrasting beaches (a coarse grained, steep beach and a fine grained, dissipative beach) by Turner (1993a). A neutron probe was used to measure shore-normal profiles of the moisture content between the water-table and the surface. The presence of a previously hypothesised saturated capillary fringe above the water-table was confirmed, which could explain the ability of the water-table to rise almost instantaneously upon addition of a thin layer of surface water such as that produced by a swash uprush (this is a well-known hydrological phenomenon known as the reverse Wieringermeer effect).

A model was developed by Baird and Horn (1996) to predict tide-induced variations in water-table elevations in sandy beaches, based on a one-dimensional form of the Boussinesq equation, i.e:

$$\frac{\partial h}{\partial t} = \frac{K}{\zeta}\frac{\partial}{\partial x}\left(h\frac{\partial h}{\partial x}\right) \tag{2.9}$$

where h is the elevation of the water-table, t is time, K is the hydraulic conductivity of the beach sediment, ζ is the specific yield or drainable porosity, and x is the horizontal

distance. This model was field tested on a relatively low energy microtidal beach, using a shore normal transect of screened wells containing pressure transducers. It was found that the model was able to predict with some accuracy the changes in shore-normal profile of the water-table elevation over time, therefore providing a suitable boundary condition for swash infiltration and pressure propagation models (see also Baird *et al*, 1998).

2.4.3 Infiltration-exfiltration

Most of the studies described in this section suggest that sediment transport on the backwash is enhanced by the process of infiltration-exfiltration, but it is still unclear whether this is always the case.

A few theoretical studies have been performed in the past, going back to Grant (1946, 1948) who was one of the first to suggest a relation between groundwater and sediment movement in the foreshore. The following mechanism was proposed: (a): On the uprush, if the beach is dry (i.e. the watertable is low), the uprush will infiltrate into the sand and hence slow down, causing greater deposition of the sediment suspended in the uprush. If the beach is wet (a high watertable), there will be less infiltration, hence less deceleration and therefore less deposition. (b): On the backwash, the outflow of groundwater causes fluidisation of the upper layer of sand, and hence augments offshore transport of sediment.

A model was developed by Packwood (1983), based on the assumption that one of the major contributing factors to sediment transport on the foreshore is infiltration-exfiltration. The model was used to predict runup due to a single bore incident on an initially dry beach. He found that the amount of water percolating into the beach face increased with grain size, and for fine sand, the runup was almost the same as that on an impermeable slope. However, with medium sand, the greater porosity meant that there was a large amount of infiltration. This was seen to cause significant thinning of the swash 'lens' on the backwash, which would alter the ability of the flow to transport sediment. Packwood's conclusions were that, not only did grain size greatly affect the amount of infiltration, but that this effect was seen much more on the backwash than the uprush.

The effect of the permeability of a beach on the uprush-backwash cycle is illustrated in Figure 2.4. On a relatively impermeable beach (a) the sediment remains saturated throughout the uprush-backwash cycle and there is little infiltration. This effect

would be enhanced by a previously elevated water table (from, say, a high tide). On a relatively permeable beach (b), water will sink into the beach face on the uprush, then flow seawards to eventually emerge at a point below the mean water surface.

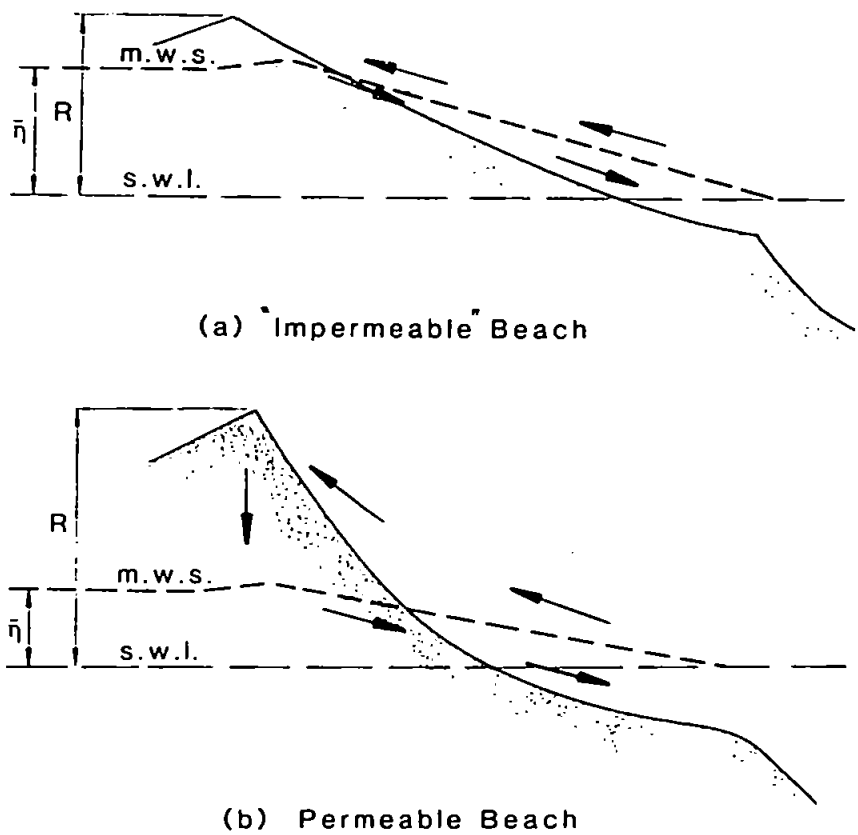

Figure. 2.4. Swash cycle on permeable and impermeable beaches. R = run-up, η = wave set-up. (after Gourlay, 1992)

Turner (1995) developed a model to simulate the influence of groundwater seepage on the swash-zone sediment transport of macro-tidal beaches. The water-table exits the beach face at some point in the inter-tidal zone. As the swash-zone moves up and down the beach with the tide, the sediment transport will be influenced by the relative position of

the water-table exit point. The model simulates the hydrodynamics in the uprush using the non-linear shallow water theory, and couples this to a Bagnold-type sediment transport model (Bagnold, 1963, 1966). However, due to difficulties in modelling the backwash, the beach slope was then used to parameterise the net transport of sediment over the whole uprush-backwash cycle. A possible explanation is also included of the slope break found in the intertidal zone of some macrotidal beaches. On the 'dry' upper portion of the zone, there is a greater degree of infiltration than on the 'wet' lower part. Hence on the upper part, the backwash is weakened, due to some of the water having been lost during the uprush. This suggests that net onshore transport is favoured in this region, causing the equilibrium beach-slope to be steeper. On the lower part, less water is lost from infiltration in the uprush, eventually leading to a less-steep equilibrium profile.

The equilibrium beach profile model of Quick (1991) includes the effects of infiltration on the stresses imparted on the beach face sediment. During the uprush, the stresses in the sediment increase due to the effects of infiltration; whilst on the backwash the hydraulic gradient associated with infiltration collapses and reverses, causing exfiltration. As the water emerges from the surface, the sediment is dragged into motion by the backrushing water.

A similar hypothesis was investigated by Baird *et al* (1996, 1998). On the uprush the water pressure will propagate rapidly into the upper layers of the sediment; then on flow reversal to backwash, there will be a rapid decrease of pressure, producing forces acting vertically upwards just below the surface. This may lead to rapid groundwater outflow and hence fluidisation. They developed a model based on the three-dimensional form of equation 2.9, governing water movement through an isotropic and homogeneous saturated sediment; i.e:

$$\nabla^2 h = \frac{\zeta}{K}\frac{\partial h}{\partial t} \tag{2.10}$$

where h is the hydraulic head, ζ is the specific yield, t is time, and K is the hydraulic conductivity of the sediment. This model was then initially tested using a one-dimensional column of saturated sand, and some of the field data collected by Hughes (1992). It was concluded that fluidisation is indeed likely to occur, especially in the latter stages of the backwash. The model also suggests that fluidisation of the bed occurs before the beach

surface is exposed, increasing the likelihood of entrainment and seaward advection of sediment on the backwash.

Determining the magnitude of the pressure gradients just below the surface is critically important if the through-bed flow behaviour is to be studied. Horn *et al* (1998) conducted experiments to measure sub-surface pressure gradients in the swash-zone of a fine-grained microtidal beach using a method developed by Baldock and Holmes (1996). They concluded that the pressure gradients are somewhat dependent upon the tidal stage. For example, on a rising tide they observed small positive pressure gradients on the uprush and large negative pressure gradients on the backwash; but on a falling tide, these differences did not occur.

Turner and Nielsen (1997) measured pore-pressure at three heights below the bed, using a vertical array of pressure sensors, in the swash-zone of a relatively flat beach, with wave heights of about 0.5m. By careful consideration of the groundwater dynamics in conjunction with their field results, they showed that rapid and relatively large upward fluctuations in the water table, due to the 'reverse Wieringermeer effect', can be caused by small amounts of downwards infiltration caused by swash uprush. They pointed out that these fluctuations are not actually associated with vertical flows of water into and out of the beach face, rather simply the displacement of a constant pressure surface. Therefore, only the physical movement of water due to pressure gradients beneath the bed can cause fluidisation.

If laminar flow is assumed, it is possible to calculate w, the instantaneous vertical flow of water through the beach face, from Darcy's law, i.e:

$$w = K\left(\frac{1}{\rho g}\frac{\partial p}{\partial z} - 1\right) \tag{2.11}$$

where K is the hydraulic conductivity, ρ is the fluid density, and $\partial p/\partial z$ is the vertical pressure gradient. The *critical fluidising velocity*, w_c i.e. the vertically-upwards velocity at which bed fluidisation is possible, is also calculable if the weight of the sediment is balanced against the upward buoyancy force due to the pressure gradient, i.e:

$$\rho_s g\Theta = \frac{w_c}{K}\rho\Theta \tag{2.12}$$

where Θ is volume and ρ_s is the sediment density. Hence,

$$w_c = K\left(\frac{\rho_s}{\rho} - 1\right) \tag{2.13}$$

Turner and Nielsen (1997) found that, on their beach under study, vertical flow magnitudes were of the order of 10^{-4} m/s, whereas w_c for the grain size at their site was about 10^{-2} m/s, meaning fluidisation was unlikely. They illustrated that, if the velocity of water-table rise were (mistakenly) taken to be associated with upwards flow of water, then this would have easily exceeded w_c and hence fluidisation might have been expected.

Nielsen (1998) derived a modified version of the Shields parameter to account for the effects of infiltration-exfiltration on sediment transport in the swash-zone. The two opposing effects are boundary layer modification (Martin, 1970) and stabilising-destabilising (Nielsen, 1992). The former is parameterised in the numerator, and the latter in the denominator, therefore, the overall effect on the Shields parameter will depend on which process dominates, i.e.

$$\theta = \frac{u_*^2\left(1 - \alpha\frac{w}{u_*}\right)}{gd_{50}\left(s - 1 - 0.5\frac{w}{K}\right)} \tag{2.14}$$

where u_* is the friction velocity, α is an empirical constant, and d_{50} is the median grain size. Nielsen hypothesised that quartz sands with $d_{50} < 0.58$mm are likely to be stabilised by infiltration (i.e. decreased transport on the uprush), whereas with larger grain sizes the boundary layer effects may start to become dominant, effectively increasing uprush transport.

Turner and Masselink (1998) derived an alternative form for the modified numerator, which has been derived from work by Mickley *et al* (1954), and Conley and Inman (1994). The numerator, unlike Nielsen's, does not assume a linear relation between shear stress and infiltration velocity. The parameter was tested using pore-pressure data from a beach with a median grain size of 0.5mm, and simulated cross-shore velocities. It was found that the effect of boundary layer modification appeared to dominate, with the

simulated peak transport rates increased by up to 40% on the uprush and reduced by 10% on the backwash.

2.5 Summary

This review has summarised the recent literature on the hydrodynamics and sediment transport in the swash-zone of natural beaches, and identified important aspects and gaps in the knowledge which will be addressed in this thesis. The main points covered are as follows:

- The importance of long wave motions in the inner surf-zone is well established, and recent work has also highlighted its importance in the swash-zone.
- The hydrodynamics of the swash-zone has been studied fairly comprehensively, and has been modelled with reasonable success in the uprush, using modified forms of the non-linear shallow water equations.
- Sediment transport measurements in the swash-zone have been relatively few in number, and this has been due to the lack of progress in developing suitable instrumentation which can measure sediment concentrations and flow velocities close to the bed in shallow water, in an area which is likely to be wetting and drying.
- There is a general lack of data from dissipative beaches in high-energy conditions, during which the practicalities of data collection in the swash-zone are particularly challenging.
- There is also the added complication of groundwater influx and outflux. Attempts are being made to measure pore-pressure below the bed to investigate hypotheses that infiltration-exfiltration modifies the sediment transport one way or the other according to the dominance of one process over another.

This chapter of the thesis was based on *Hydrodynamics and Sediment Transport in the Swash-Zone of Natural Beaches: a Review* by T. Butt and P. Russell, accepted for publication in the *Journal of Coastal Research.*

3. Instrumentation

3.1 Overview

In this chapter a description is given of the measuring instruments used in the present study. The three basic parameters measured were velocity, suspended sediment concentration (SSC) and pressure. The latter is translated to either water depth or sub-surface pore-pressure, depending on the deployment of the instrument. Each parameter is measured using a transducer whose electrical output varies according to the variation in the value of that parameter. The 'real' value of each parameter is then inferred from the size of the electrical signal, through a previously determined calibration relationship. To measure velocity, SSC and pressure, electromagnetic current meters (EMCMs), miniature optical backscatter sensors (MOBS) and pressure transducers (PTs) were used.

Special emphasis is given to the MOBS sensors as these were developed in-house. Development procedures and various pre-deployment tests are described. Also the calibration procedure for this type of instrument is not standardised, and calibration to high concentrations of suspended sediment is very difficult.

Less details are given on the EMCMs and PTs as these were already in existence. However they were used in a somewhat non-standard manner, therefore various techniques are described to ensure their suitability in the swash-zone.

3.2 MOBS sensors

3.2.1 Initial specification

The principle of operation of the optical backscatter sensor is based on the variation of the amount of light reflected from particles in suspension, according to their concentration. The sensor comprises a light emitting diode and a phototransistor, mounted side by side. The amount of light received by the phototransistor depends upon the proportion of emitted light backscattered by the suspended sediment. Hence the voltage output of the phototransistor may be directly related to the concentration, through laboratory calibration.

Commercially available sensors such as the Downing OBS3 were considered too bulky to obtain measurements at multiple heights above the bed in the swash-zone. If, say, four of these sensors were mounted in a vertical array, the bodies of the instruments would present a large surface area to the flow. It would also be physically difficult to mount the lowest one at the desired height of 1cm. The only sensor known to be potentially suitable for the work proposed in the present study was the FOBS unit developed by Beach *et al* (1992). Since these turned out to be unavailable, it was decided to develop an array of MOBS specific to this project.

Christie (1997) successfully developed and used a system employing MOBS sensors for measuring the turbidity of estuarine muds (see also Christie and Dyer, 1998). These sensors were mounted individually on the end of 6mm diameter mounting tubes, and up to eight units were deployed simultaneously. The transducers used were Honeywell HOA 1397 reflective sensors. These operate at a wavelength of 960nm, which is strongly attenuated by water, e.g. 63% for every 5cm in clear water (D & A Instruments, 1991). The optical and electrical specifications of these transducers (RS Components, 1997), and their small size (approximately 4mm by 6mm by 6mm) meant they might be suitable for measuring multiple heights of suspended sediment in the swash-zone.

It was proposed to mount the transducers in a suitable container, such that SSC could be measured at four heights, with the lowest sensor about 1cm above the bed. The main design criteria were that the system be as unobtrusive to the fluid flow as possible, to avoid flow re-direction and hence altered velocity and sediment suspension characteristics, and also that the mounting system be robust enough to survive the high velocities encountered in the swash-zone (*c.f.* Hughes *et al*, 1997).

Ideally the sensors should be in a vertical line to avoid horizontal heterogeneities in the SSC, but they should not be so close to each other as to cause cross-talk. Visual observations suggest that most backwash sediment movement is below 5cm, and uprush sediment movement extends above this height. Therefore, to be able to measure at least some SSC on the backwash (it is acknowledged that this method will not be able to measure 'bedload'), together with uprush SSC, the sensors must be deployed above and below 5cm. Since higher concentrations are found nearer the bed, then it is logical to assume that the vertical SSC gradients will also be higher, which suggests that the near-bed sensors should be closer together.

Based on these observations, it was decided to mount the sensors in a vertical tube, at nominal heights of 1, 2, 5 and 10cm above the bed. Inspection of tubes mounted in the

bed (see subsequent section on scour tests) showed that significant amounts of sand were 'splashed' up the side of the tube in the direction of the flow, therefore the preferred circumferential orientation of the sensors is 'looking' alongshore, all on the same side of the tube. It was also recommended by Ludwig and Hanes (1990) that optical backscatter sensors deployed in environments where the flow direction is constantly changing, be orientated at right angles to the flow, since the response of the sensor changes with orientation to the flow.

The following three sections contain details of preliminary trials which were carried out on prototypes, between July 1997 and March 1998, before the design of the MOBS tube was finalised. Examples of important aspects of the design which required practical trials are: (a) how a sensor mounted at a particular height in the water-column responds to light backscattered from another height, and whether one sensor is picking up backscattered radiation which was emitted from another sensor; (b) implications of the intrusiveness of the instruments themselves in the fluid flow; and (c) the effects of ambient light on the sensors.

3.2.2 Angular response tests

Ideally, the MOBS sensors should be able to measure the sediment concentration at the same height as the sensor, and should not be affected by any changes in concentration above or below the sensors, i.e. the sensing volume should not intrude above or below the sensor. Therefore, the aims of this test were to determine the response characteristics of the MOBS to a reflective object not placed directly in front of the sensor, i.e. the magnitude of the output voltage using a reflective object placed at various angles around the periphery of the sensor. This would then give some indication of the potential problems which might be encountered due to (a) cross-talk between two adjacent sensors placed vertically very close to each other, (b) internal reflection from the water surface when the sensors are very close to the surface, and (c) the unit responding to changes in sediment concentration not at the height of the sensor.

The circuit used by Christie (1997) for signal conditioning of the same MOBS units, included a clocking facility, whereby the transmitter and receiver were switched on and off synchronously at 1kHz. Each sensor was clocked at a different phase from the others, in an attempt to eliminate cross-talk between sensors, i.e. the light source of one

sensor being picked up by the other. One of the aims of this test is to determine whether it is necessary to incorporate a circuit of this type, or use a much simpler circuit. Disadvantages of this circuit reported by Christie (1997) included internally generated noise in the form of spurious negative voltages. The circuit is also bulky and expensive.

It must be born in mind that the variation in concentration of suspended sediment in water is not quite the same as the variation in distance of a fixed object. At high sediment concentrations, any photon emitted from the sensor will be reflected by a particle relatively close to the sensor, whereas, at low concentrations, the photon will travel further away from the sensor before encountering a particle from which it will be reflected (see figure 3.1).

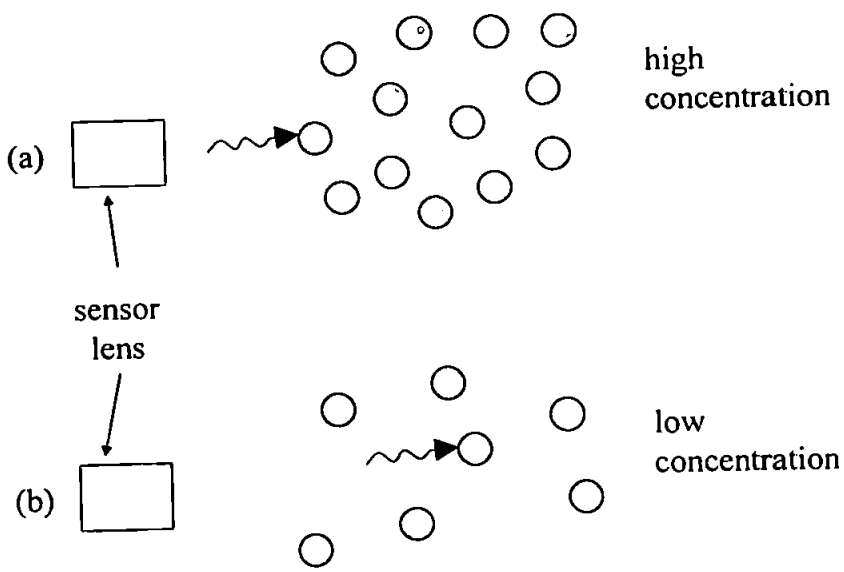

Figure 3.1: at high concentrations (a), the photon encounters a particle close to the sensor, and at low concentrations (b) it travels a greater distance before encountering a particle.

A single transducer of the type used by Christie (1997), already mounted in a waterproof housing, was connected to the simple test circuit shown in figure 3.2. The sensor was then placed in water, and a reflective object was placed at a distance of 5mm

from the sensor. Readings of the output voltage were taken whilst the object was moved around the sensor in increments of 10^0. This procedure was repeated with the object being placed at distances of 2.5, 5, 10, 15 and 20mm from the sensor. The voltages from each 10^0 angle increment were averaged over the various distances from the sensor, and then the data were normalised by dividing each result by the voltage obtained when the object was placed directly in front of the sensor, i.e.

$$V_{norm}(\phi) = \frac{V(\phi) - V_0}{V_{max} - V_0} \tag{3.1}$$

where $V_{norm}(\phi)$ is the normalised voltage, $V(\phi)$ is the average voltage obtained at angle ϕ, V_{max} is the average voltage directly in front of the sensor ($\phi = 0$), and V_0 is the offset voltage, obtained with the sensor free from any reflective objects.

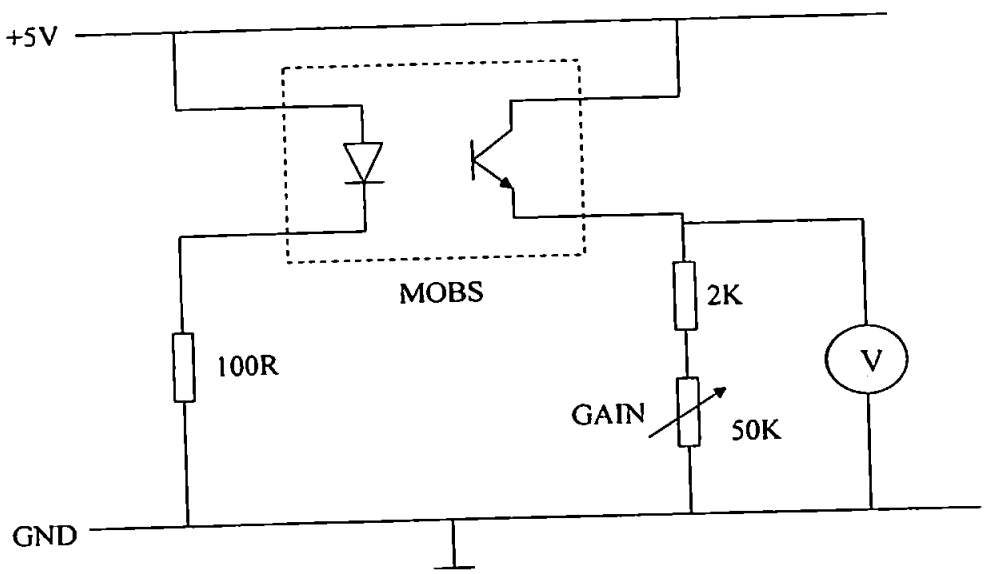

Figure 3.2: test circuit for MOBS.

The results are shown plotted in figure 3.3. The large numbers refer to values of V_{norm} and the angular grid spacing is 10^0. From figure 3.3 it can clearly be seen that the output of the MOBS reduces to zero at about 60^0 either side.

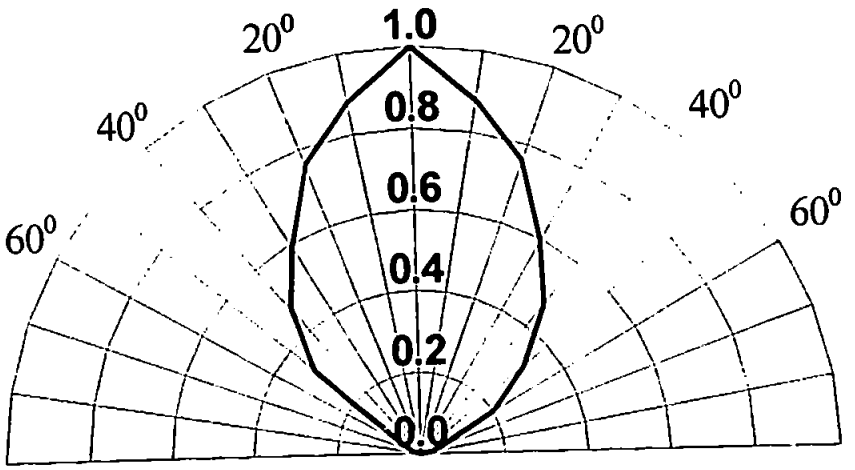

Figure 3.3: angular response of MOBS unit. Large numbers refer to normalised voltage output.

From the results presented here it can be seen that care must be taken when interpreting the results of sediment concentrations from the MOBS sensors, with regard to changes in concentration picked up by one sensor which may actually be occurring at the height of the other sensor. Since the response drops to zero at about 60^0, from simple geometry it may be deduced that the above effect will not be apparent if the reflective object is placed at a distance of less than 2.5mm from the sensor (see figure 3.4).

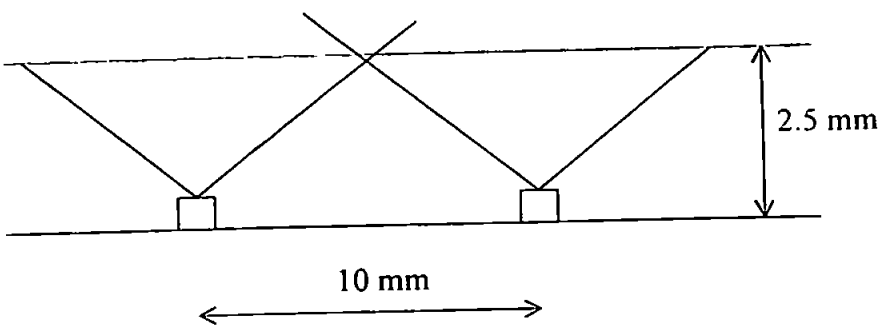

Figure 3.4: maximum distance from the sensor a reflective object may be placed outside which backscattered light from the object may be detected by both sensors.

Figure 3.5 shows the variation in response as a reflective object is moved to one side of the sensor, at a distance 2.5mm away from the sensor. The angle ϕ is converted to a distance either side of the sensor (Δz) at distance x, by the relation $\Delta z = x \tan\phi$.

Here it can be seen that the output reduces exponentially with distance either side of the sensor.

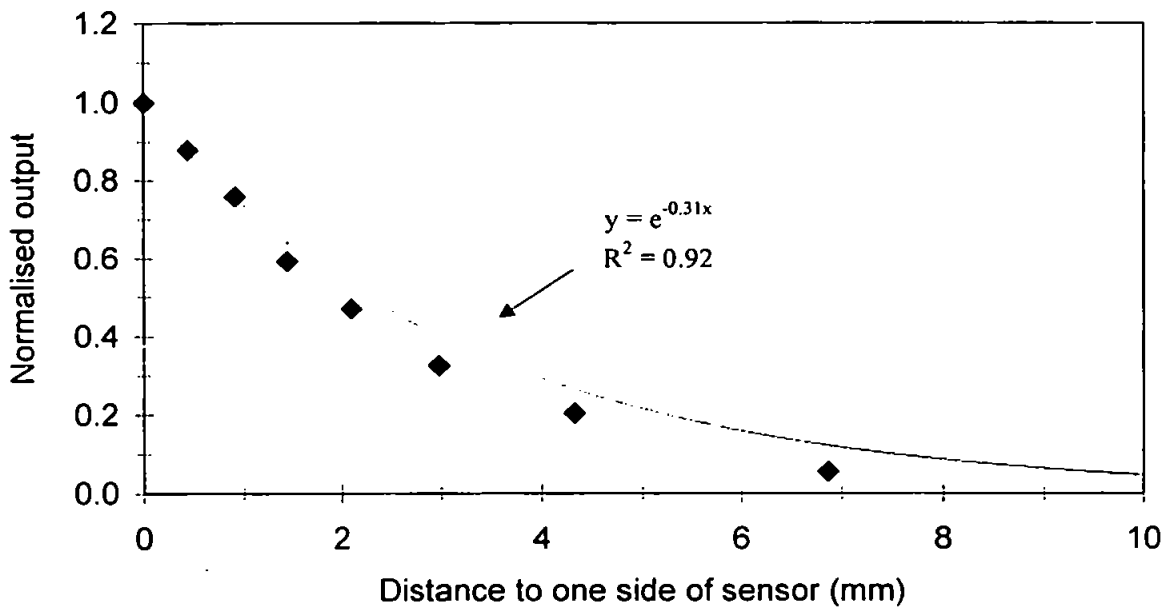

Figure 3.5. Variation in output when a reflective object placed 2.5mm away from the sensor, is moved various distances either side of the sensor.

At distances greater than 2.5mm from the sensor (figure 3.4), the output will be less than 50% of that at 1.27mm (RS Components, 1997), when an object is placed directly opposite the sensor. From figure 3.5 it can be seen that, at a lateral distance half way between the two sensors placed 10mm apart (i.e. 5mm), there is a further reduction factor of about 0.2. Hence the maximum response of each sensor from particles existing in any volume which is common to the two sensors, will be about 0.1 times the maximum available response.

From figure 3.5 it can also be seen that a sensor would have to be placed at a distance of about 0.75mm from the water surface to obtain a response of at least 50% of the maximum available, from internal reflection. Since this distance is relatively small, problems from internal reflection will be likely to occur only on very short time scales, as the sensor will be within this distance from the surface for extremely short periods only.

3.2.3 Scour tests

It is a basic physical concept that the observation of any physical process alters, to a certain extent, the process itself. The presence of a measuring instrument in a moving fluid will alter the flow characteristics of that fluid. This effect can never be removed completely, but it can be minimised.

In an area such as the swash-zone where measurements are taking place very close to the bed, flow redirection due to the presence of the instruments themselves is a potential problem. One consequence of flow re-direction is localised erosion (known as scour) due to increased shear-stress around the instrument. Figure 3.6 illustrates flow re-direction around a cylinder placed in a moving fluid, analogous to that which occurs around a tube protruding from the bed in the swash-zone. The streamlines become 'crowded' as the flow is re-directed around the cylinder. Due to the principle of continuity of discharge (e.g. Williams and Elder, 1989), the flow velocity will increase, producing a corresponding increase in bed shear-stress.

Once a 'scour hole' is present, this will add uncertainties to the measurements being made. For example, the height above the bed at which the instruments are measuring will immediately change. Also, the scour hole will itself produce vortices causing further flow redirection, and unpredictable fluid movements. Measured velocities and sediment concentrations in the presence of a scour hole may be different from that which would occur with no scour.

Scour has been recognised as a problem when making measurements in high-energy swash, and efforts have been made to reduce the size of the instruments to make them as unobtrusive as possible. The flow redirection, hence the amount of scour produced, increases with the surface area presented to the flow. Typically, instruments used in this environment would be mounted vertically, therefore the amount of scour would tend to increase with the diameter of the instrument. Beach *et al* (1992) developed the fibre-optic backscatter sensor (FOBS) with a very small (2.5mm) diameter, designed to

be mounted in a 'pipe-organ' array, hanging down towards the bed, with the lowest sensor about 5mm from the bed.

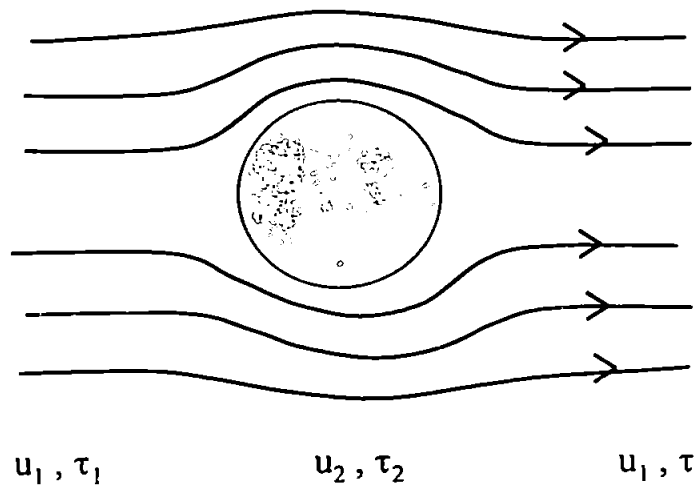

Figure 3.6: view from above of the streamlines around a pole mounted vertically protruding from the bed. The velocity (u) and hence bed shear-stress (τ) increase near to the pole due to flow constriction.

Most workers in high-energy swash have mounted their instruments vertically hanging down (e.g. Beach and Sternberg, 1991; Osborne and Rooker, 1998, 1999; Puleo, 1998). However, observations during the present study suggest that burying the instruments, with the part containing the transducer protruding from the bed, produces very little scour provided the diameter of the tube protruding from the bed is below about 20mm. There are considerable advantages in putting the main body of the instruments below the bed. The instruments are completely 'hidden' from the flow apart from the protruding section containing the transducers. Deployment is much more straight-forward, and there is no need for a bulky and expensive structure above the bed, which could also be potentially unstable. The structure itself could also cause considerable flow re-direction. Therefore, if the scour can be reduced to an acceptable level with the instruments mounted below the bed, then there are no advantages in mounting them above the bed.

Moreover, if the instruments were mounted hanging down from above the bed, then the container in which the transducers would have to be mounted would extend a few

millimetres below the height of the lowest sensor. Therefore, if it is required to measure say, SSC, at 1cm above the bed, then this would result in the container having to be mounted extremely close to the bed. The flow around the bottom of the container would be redirected vertically, causing increased shear stress directly below the container, and hence scour.

The aims of this test are to examine the relationship between the amount of scour and the diameter of a tube placed sticking out of the bed. In this way, a maximum size of tube can be decided upon which will produce an acceptable amount of scour. These results can then be used as a contribution to the general design of the instrument layout.

Nine poles of various diameters between 8mm and 65mm were chosen for this test. It was considered that anything outside this range would not normally be used in swash-zone studies. For example a standard scaffolding pole, which is often used for instrument mounting, is 50mm in diameter; and the proposed tube containing the miniature optical backscatter sensors (MOBS) has a minimum diameter of 12mm to accommodate the wiring and the sensors themselves.

The experiment was conducted during a 1 hour period over high water. The poles were inserted into the sand in a longshore transect, approximately 1m apart, and the tide was allowed to advect over them. The poles remained in the swash-zone throughout the duration of the experiment. Once the tide had receded far enough for the poles to be permanently uncovered, then the diameter and depth of each scour hole could be carefully measured. Significant wave height and period observed by eye were 0.8m and 7s respectively.

The relationship between the pole diameter and the size of the scour hole (diameter and depth shown separately) is shown in figure 3.7.

The relationship appears to be non-linear, i.e. there is a sharper increase in both diameter and depth of the scour hole, with larger pole sizes. The regression lines plotted through the data are second order polynomials, and these are simply intended to provide a visual indication of the non-linear nature of the relationship. Note that no attempt is made here to describe mathematically the fluid flow around the pole, but one factor which might suggest this result to be logical is the quadratic relationship between shear-stress and velocity.

No scour was detectable around the 8mm pole, and the scour hole around the 18mm pole measured 50mm by 10mm. The MOBS sensors are to be mounted in a tube of

diameter 12mm, so the likely size of scour hole would be somewhat smaller than 50mm by 10mm. The other instruments to be mounted below the bed are the current meter, whose 'stem' is smaller than 12mm diameter, and the pressure transducers, which do not necessarily have to have any parts protruding from the bed.

The main conclusion of this test is that providing the part of the instrument protruding from the bed has a diameter of less than about 18mm, the advantages of below-bed deployment outweigh the disadvantages of scour, which is relatively small at these diameters. It is recommended in any deployment in the swash or surf-zones that any object protruding from the bed have as small a diameter as is practical. The use of scaffolding poles, although convenient, is not recommended because a considerable amount of scour is produced at diameters around 50mm.

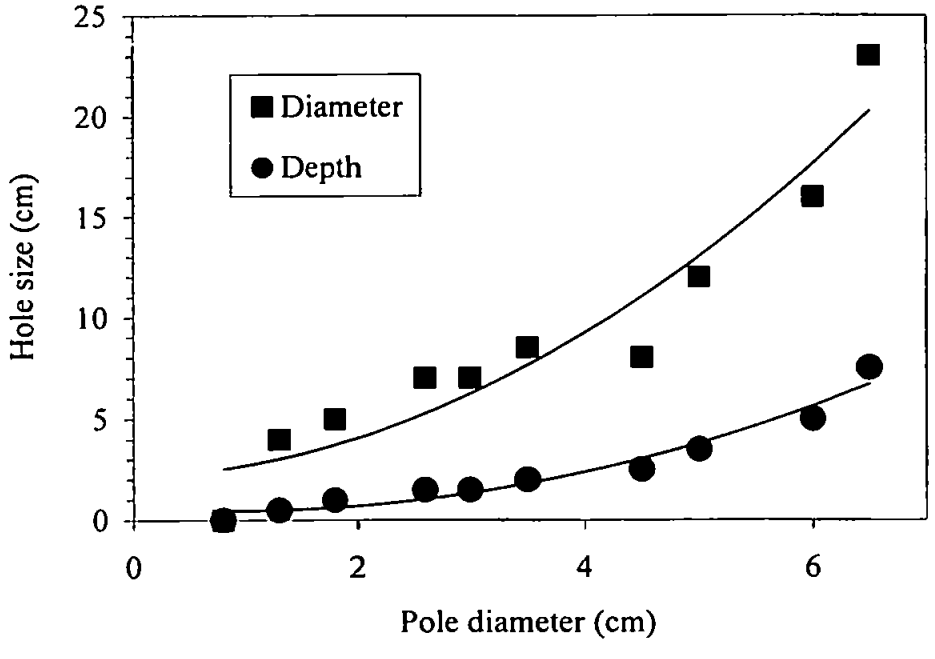

Figure 3.7: Increase of diameter and depth of scour hole with increasing pole diameter.

3.2.4 Preliminary trial of prototype

The aims of this simple test were to deploy a prototype design containing four MOBS sensors, in an environment similar to that which will be encountered in subsequent

experiments, in a simple and repeatable fashion, so that any practical deployment problems could be identified, and the physical performance of the unit could be assessed.

The equipment consisted of a vertical tube containing four MOBS sensors (see figure 3.8). The tube was placed so that the sensors were at heights of 1, 2, 5 and 10cm from the bed, with the lower part of the tube buried in the sand, and the section containing the sensors sticking out of the sand vertically. The top and bottom sensors only were connected, through two circuits as shown in figure 3.2, to simple hand-held l.e.d. voltmeters. Therefore, the outputs of the upper and lower sensors could be monitored in real time, but at this stage there was no facility for recording the outputs.

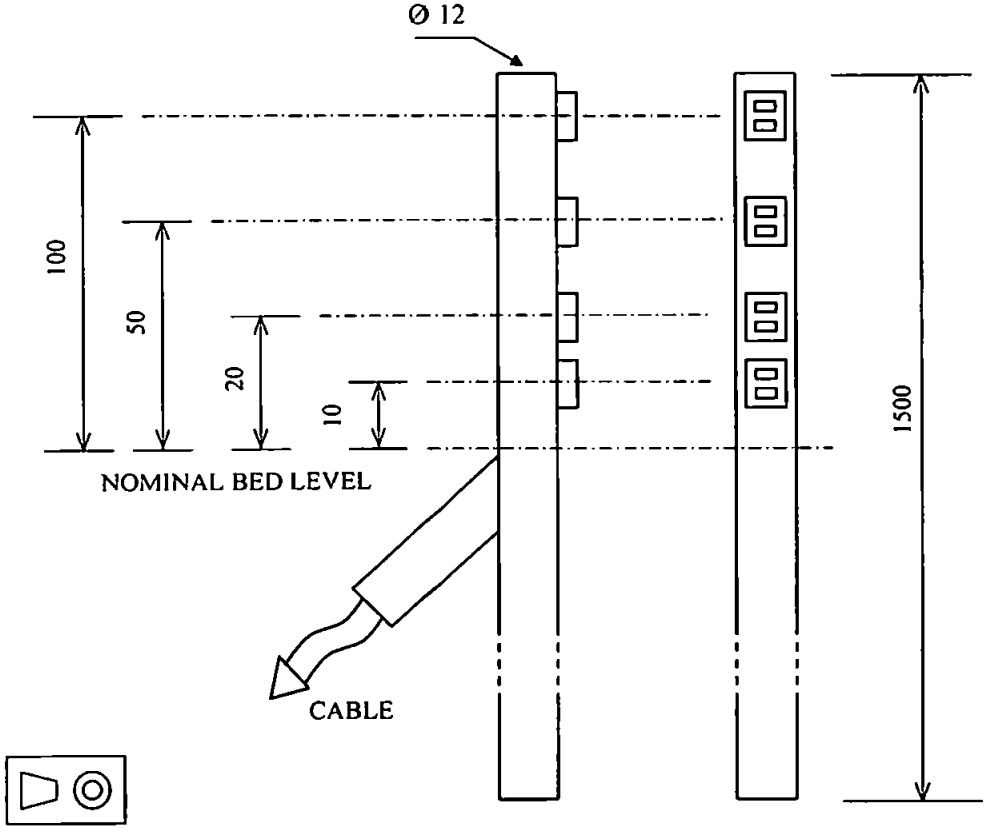

Figure 3.8: MOBS tube. Dimensions in millimetres.

The trial was conducted during observed significant wave heights and periods of about 1.0m and about 10s respectively, swell-dominated. The breakpoint was about 30m from the shoreline.

The experiment itself consisted of placing the tube in the sand, burying the cables, and monitoring the response of the top and bottom sensors on the uprush and backwash, for a period of about 1 hour over high tide. The MOBS sensors were orientated looking alongshore, to avoid any affects from sediment 'splashing' up the sides of the tube in the direction of the flow.

The physical deployment of the instrument in the bed was relatively straightforward. Consistent with previous trials, the tube appeared to be of a small enough diameter to avoid any significant scour affects. In this particular case, the bed level did not change over the deployment period.

During the uprush, increased sediment concentration could be seen at both sensors, indicating the presence of suspended sediment high in the water-column. During the backwash, the output was generally lower from the top sensor than that from the bottom sensor, confirming visual observations that sediment tends to move low in the water-column on the backwash, but at all levels on the uprush.

Much of the time the top sensor became uncovered on the backwash. Here it was found that the output of the top sensor suddenly rose to a maximum upon uncovering. Further investigation revealed that this was due to a bead of water remaining over the lens of the sensor, causing internal reflection and hence a high reading. This effect is essentially the same as if the unit were exposed to ambient light when out of the water. The application of a hydrophobic substance on the sensor lenses might avoid this problem. However, a more reliable solution would be to filter the SSC time-series, so that when each sensor was out of the water its output would be forced to zero. An accurate measure of the instantaneous depth at the same horizontal position as the MOBS sensors is available from the pressure transducers (see section 5.2.3).

3.2.5 Final design and recommendations

As a result of the above tests, a final design for the MOBS tube, and recommendations for its deployment, may be drawn up.

Mounting the instruments in a 12mm pole, sticking out of the bed, appears to be a robust and relatively unobtrusive method. The deployment of the instrument was straightforward, and once deployed, a very small amount of scour was generated around the tube. Therefore the physical design in figure 3.8 will be adhered to, and it is recommended that the other instruments used in this study be mounted in a similar way, provided the diameter of the protruding part is less than about 15mm. The design, fabrication, and deployment of a complicated rig above the bed, is therefore avoided.

Since there is a chance of saturated readings due to water remaining on the lens when the unit is out of the water, then data reduction of the time-series must include an algorithm which forces the SSC to zero when that particular sensor goes dry. Note that a similar problem exists with the acoustic Döppler velocimeter, in that the signal to noise ratio decreases significantly when the instrument is out of the water (e.g. Osborne and Rooker, 1998. 1999).

The fact that sediment moving on the backwash has been observed principally at low levels in the water-column, means that the proposed vertical logarithmic spacing of the transducers is useful to resolve the vertical variations in SSC near the bed.

3.2.6 Calibration

An optical backscatter sensor is designed to produce a voltage output according to the concentration of sediment. The response will be affected by the optical characteristics of the sediment itself, and the grain size distribution (Gordon *et al*, 1984). Therefore, the instrument must be calibrated using samples of sediment found at the field site.

Calibration of the MOBS sensors consists of obtaining an empirical relationship between the voltage output of the sensor and the 'real' suspended sediment concentration. Normally, the instrument is placed in some controlled environment in a laboratory, and is exposed to various known concentrations of suspended sediment, whilst the voltage output is noted. The 'real' concentrations are usually measured by gravimetric methods, i.e. drying and weighing the sediment.

Recent studies using this type of instrument (e.g. Beach *et al*, 1992) have used a large recirculating tank for calibration (Downing and Beach, 1989; Green and Boon, 1993). This apparatus is able to produce continuous stable concentrations of up to around

$100gl^{-1}$. Such equipment was not available for this study, so simpler methods of obtaining homogeneous high concentrations had to be developed.

Concentrations expected in the swash-zone were much higher (> 80 gl^{-1}) than typical measurements in the inner surf-zone (~ $30gl^{-1}$, e.g. Miles, 1997). Hence the best method of calibration was developed through a process of trial and error. The following describes three different methods, each one an improvement on the previous. The third and final method was used for the field data.

For the first method, a number of samples of sediment were dried and weighed beforehand, and these were then placed one by one in a container of water, together with the MOBS tube, so that, effectively, the SSC was incrementally increased. At each increment the sediment was suspended by a rotary stirring device placed in the water. The voltage readings of the sensors were recorded for about 1 minute for each increment, and the average voltage over that time was taken.

It was found that this method worked satisfactorily below concentrations of about 30 gl^{-1}, but above this, the sediment rapidly began to suspend in 'clouds', making it impossible to obtain a temporally and spatially homogeneous suspension. Moreover, at very high concentrations, not all of the sediment was able to be suspended by the stirring device, so there was a false 'levelling off' of the voltage output. This effect was initially thought to be caused by grain shielding (Kineke and Sternberg, 1992).

The second method was similar to the first, but instead of having *a priori* knowledge of the incremental concentrations, arbitrary amounts of sediment were placed in the container, and samples were taken from as near as possible to each sensor, using a pipette. These samples were then dried and weighed, to obtain the 'true' concentrations, which could be compared with the average voltage outputs of the sensors for each increment. In this way, the fact that all the sediment in the container might not be suspended ceased to be a problem because the 'real' concentrations were measured from a very small sample near the sensor.

However, two problems were still apparent with this method. Firstly, it was impossible to obtain suspended sediment concentrations above about $65gl^{-1}$ using the stirring device. Secondly, the fact that the sediment tended to suspend in 'clouds' made it very difficult to know when to take a sample; i.e. the suspension was still spatially heterogeneous even very near to the sensors. Note that Christie (1997) reports that using estuarine muds (which are less dense than quartz sand), the sediment stays in suspension

for much longer periods of time, and so these problems are much less significant. The reason why sand does not suspend homogeneously is because there is always a distribution of grain sizes and densities, so each grain will respond differently to the turbulence which is suspending it. Sand is also much less buoyant than mud, therefore it will settle out much quicker.

The third method employed a water jet instead of a rotary stirring device, to suspend the sediment. This was found to be much more controllable. The concentration did not need to be incremented by adding more sediment to the container, rather the water jet could simply be adjusted to produce higher suspended concentrations near the sensors. The suspension could be made to be somewhat more temporally and spatially homogeneous than the previous methods. Samples were taken very close to each sensor, using a 3mm pipette. Instead of performing separate runs on the recording equipment for each concentration increment, a single run was performed for each of the four sensors, with a sample taken at regular time intervals. The concentration was incrementally increased, to coincide with the sample taking. Note that it was possible to monitor the voltage readout on the logging computer in real time to obtain a rough idea of how the concentration was changing. The logging files were then inspected, and the average voltage output was noted from 2s either side of each time increment (when the sample was taken).

To obtain the suspended sediment concentration (SSC) in terms of the output voltage the following equation is used:

$$SSC = m(V_{out} - V_{off}) \tag{3.2}$$

where SSC is expressed in gl^{-1}, V_{out} is the output voltage of each sensor [V], m is the calibration coefficient [$gl^{-1}V^{-1}$], and V_{off} is the offset voltage. The voltage outputs corresponding to zero suspended sediment concentration (the offsets) were noted for each MOBS sensor during the experimental runs themselves. The offsets showed negligible drifting from one data run to the next. The values for V_{off} are as follows:

MOBS 1: $V_{off} = 0.005V$
MOBS 3: $V_{off} = 0.003V$
MOBS 4: $V_{off} = 0.011V$
MOBS 7: $V_{off} = 0.225V$

The calibration curves using the third method above are shown in figure 3.9. Note that the regression coefficient displayed on the graph must be inverted to obtain a value for m. The intercept in the regression equation is replaced by the offsets measured during the experiment. A summary of the results is also shown in table 3.1.

Using the third method above, it was possible to obtain concentrations up to about 92 gl^{-1}, and acceptable scatter on the regression plots. Other typical maximum concentrations in the swash and surf-zones in high energy conditions are $40gl^{-1}$ (Beach and Sternberg, 1988), $70gl^{-1}$ (Russell, 1993), and over $100gl^{-1}$ at z = 2.8cm (Beach and Sternberg, 1991). Beach *et al* (1992) and Osborne and Rooker (1998, 1999) show concentrations up to $200gl^{-1}$ in their data, but it is not known whether the instruments were calibrated up to this level, or the calibration curves were somehow extrapolated. The average R^2 correlation coefficient in the present study was about 91%. For comparison, Downing *et al* (1981) obtained an R^2 value of 99% for the OBS, and Beach *et al* (1992) obtained R^2 = 98-99% for the FOBS.

Table 3.1: summary of regression data for calibration of MOBS sensors. SSC is expressed in gl^{-1}, and V_{out} and V_{off} are in volts. The calibration equations correspond with equation 3.2 (above).

MOBS	Calibration equation		R^2 (%)
1 (top)	$SSC = 15.15(V_{out} - 0.005)$	(3.3)	94
3	$SSC = 16.39(V_{out} - 0.003)$	(3.4)	92
4	$SSC = 17.15(V_{out} - 0.011)$	(3.5)	90
7 (bottom)	$SSC = 19.23(V_{out} - 0.225)$	(3.6)	91

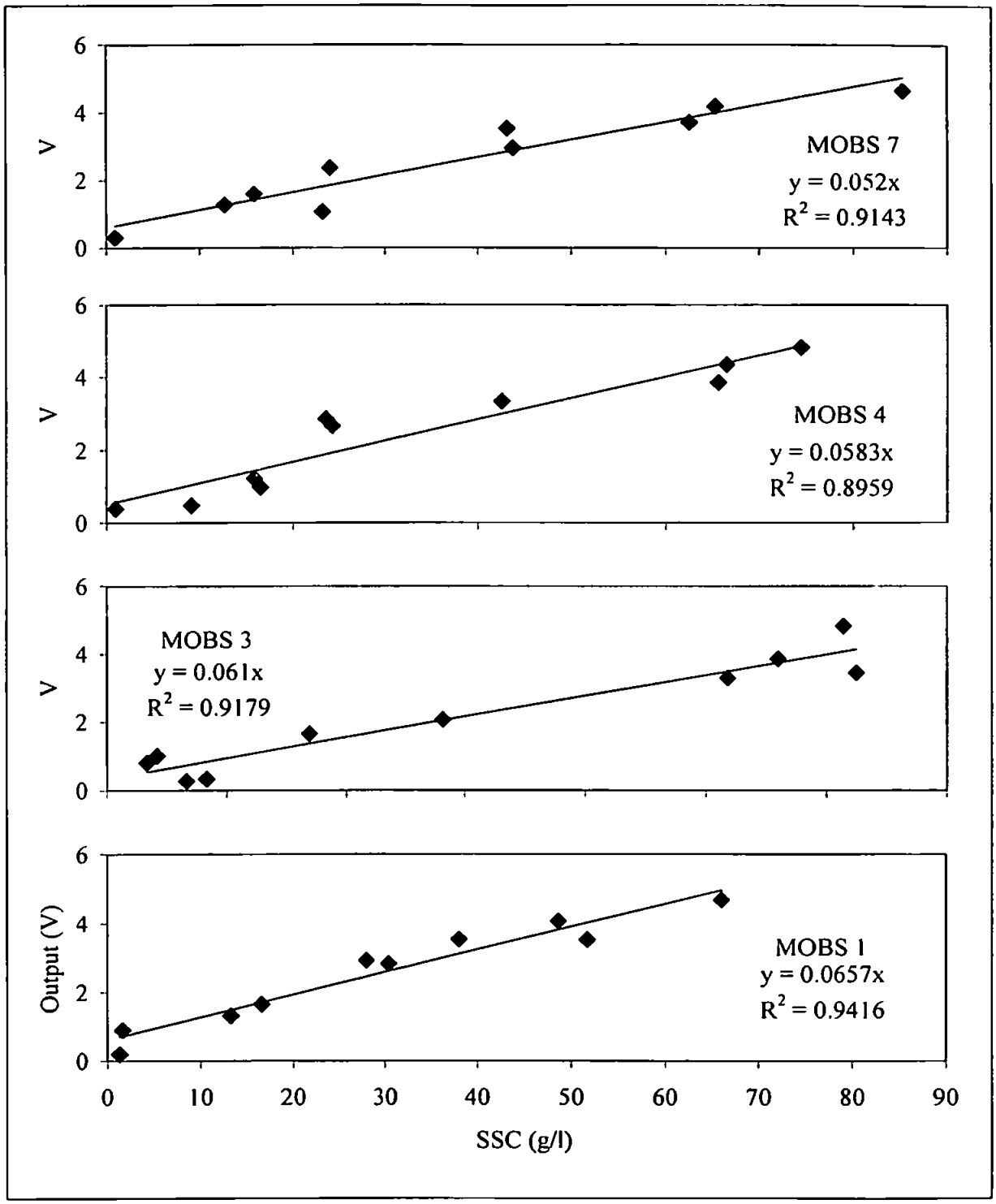

Figure 3.9: calibration curves for MOBS sensors.

3.2.7 Accuracy

To obtain an idea of the difference between the 'real' SSC and the SSC values obtained after the regression equation has been applied to the voltages measured in the field, several sources of error must be taken into account. The flowchart in figure 3.10 shows a schematic representation of the calibration procedure. Errors will be introduced at each stage in the 'pathway'.

Firstly, errors introduced during the calibration procedure will be inevitable, resulting in the SSC determined by the gravimetric method being different from the 'real' concentration. Possible sources of error using the third calibration method (above) are as follows.

- The pipette samples were as large as possible so that weighing inaccuracies were minimised. However, the samples were inherently small with this method, so weighing errors cannot be ruled out.
- Slight timing inaccuracies when taking the samples were possible.
- It was impossible to obtain a sample directly in front of the sensor, as the pipette would get in the way of the sensor, therefore the samples were taken about 1cm to the side of the sensor face. This may have had a slight effect on the results with regard to spatial heterogeneity of the suspension.

Great care was exercised in the calibration procedure to minimise these errors. It was found that the technique of physically increasing the concentration with the water jet, and of obtaining the sample with the pipette, required a certain amount of practice and co-ordination between the two 'team' members. After a few 'dry runs' the technique was considerably improved. Great care was also taken when drying and weighing the samples.

Further errors are then introduced by assuming the regression model (the straight line which has been fitted using least-squares regression) fits the data. This is reflected in the correlation coefficient (R^2), which effectively quantifies the variance explained by the regression model divided by the total variance in the data. For example, $R^2 = 50\%$ means that the regression model only explains half the variance in the data. Here the average R^2 of 91% roughly means that an error of 9% is introduced by the regression model.

Combining the errors above, an estimate for the approximate accuracy of the MOBS sensors might be about ± 15%. However, a very important point is that temporal variations in SSC are of more importance in the present study than absolute magnitudes. As already mentioned in the introduction, the most important conclusions drawn later in

the thesis are based on the temporal structure of sediment suspension and velocity events, and not absolute values of SSC.

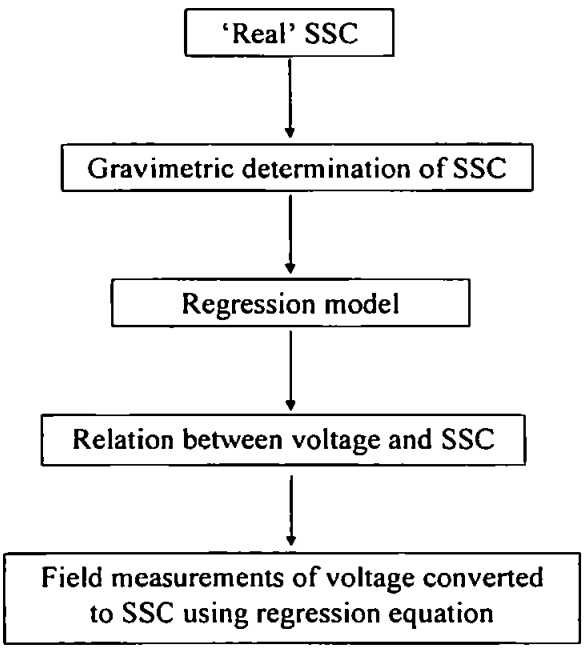

Figure 3.10: flow chart showing the general calibration procedure.

3.3 Electromagnetic current meters

3.3.1 General description

The miniature EMCMs used were Valeport series 800, with 2cm diameter discus heads. The principle of operation is based on Faraday's law which states that a voltage will be induced by a conductor moving in a magnetic field. In this case the conductor is the water, and the magnetic field is produced by a coil inside the sensing head. The voltage is measured by two orthogonal pairs of electrodes, so that flow measurements in two axes may be made. Due to the very low voltages induced by the water flow, each unit has a built-in preamplifier which provides an output of ±5V.

The minimum sensing volume of the discus type head is recommended as being a cylinder of the same diameter as the sensor, projecting from its face by half its diameter; in other words, the sensing face of the 2cm head must be placed at least 1cm from any solid object (in this case, the sea bed). The head must also be fully immersed before the signal is reliable.

The EMCM was originally designed to be used in environments where the head is fully immersed all the time. The kind of deployment in the present study is one where the sensors are continually being covered and uncovered. Initial laboratory trials carried out in May 1997 revealed that the output tends to be noisy upon wetting and drying, and with sudden velocity changes. This was also confirmed to occur with Marsh Mc.Birney EMCMs commonly used in many surf-zone studies (B. Raubenheimer, pers. comm., 1997). Therefore, the reduction of this noise had to be carefully considered if these instruments were to be suitable for swash-zone deployment. The discus shape and vertical orientation of the head means that the time during which the sensor is partly immersed is minimised. By monitoring the depth with one of the PTs, the signal was able to be set to zero when the water level was below the height of the sensor, and once the data had been re-sampled from 18Hz down to 2Hz, the noise levels were negligible. Details and justification of the filtering techniques are given in section 5.2.

The large EMCM was also Valeport series 800, but with a 5.5cm diameter spherical head. The sensing volume of this instrument is a sphere of approximately three head diameters ($\approx$ 16.5cm), therefore the sensor must be placed at least 5.5cm from any boundary. Note that, although this instrument was deployed in the field experiment, it malfunctioned rendering the data unusable.

3.3.2 Calibration

The voltage output of the these instruments is recorded as a number between +2048 and -2048 by the logging equipment, and the response to flow velocity is quasi-linear.

To obtain the velocity from the sensor output the following general form of the calibration equation is used:

$$u = m(N_{out} - N_{off}) \tag{3.7}$$

where u is flow velocity [ms^{-1}], m is the calibration coefficient [ms^{-1}], N_{out} is the output of the sensor [dimensionless], and N_{off} is the offset, i.e. the output of the sensor in calm water. The unknowns are N_{off} and m. For the present study, values for N_{off} are found as part of the field experiment (see below). Values for m are taken from a previous calibration of the instruments performed in an annular flume at the manufacturer's premises (Christie, 1997), i.e.

EMCM1: $m = 0.000577\ ms^{-1}$
EMCM2: $m = 0.000496\ ms^{-1}$

One of the disadvantages of the design of this instrument is a slow, unpredictable variation in N_{off} known as 'zero drift' or 'offset drift'. The effect of this can be partly compensated for if N_{off} for each instrument is measured before and after each data run, by performing a short offset run with the instrument placed in calm water. For the present study, to obtain the most realistic value of N_{off} to insert into the calibration equations, the output value during each offset run was averaged, then these values were linearly interpolated over time, i.e.

$$N_{off} = \overline{N}_B + \frac{t_R}{t_A - t_B}\left(\overline{N}_A - \overline{N}_B\right) \tag{3.8}$$

where suffix A and B mean 'after' and 'before' each data run or series of runs, and t_R is the time in the centre of the data run for which N_{off} is required.

Offset runs were performed during the field experiment by inserting the EMCMs in a bucket of still water for approximately five minutes, or until the visual indication of the output on the logging computer had become steady. This could only be done each time the instruments were re-deployed, i.e. before run W1, at between runs W3 and TH1, and after run FR1. (The timing and explanation of the data runs is fully detailed in section 4.2).

The results of the offset interpolation are shown in table 3.2. The second column shows the times of each offset run together with the times corresponding to the centre of each data run. The mean output values for each offset run are shown in the third and fourth columns together with the interpolated values corresponding to the centre of each data run.

Hence a different calibration equation must be applied for each EMCM for each data run. For example, for EMCM1 on run W1, the calibration equation to be used is:

$$u = 0.000577(N_{out} - 0.45)$$

Table 3.2: average output values [dimensionless] of EMCMs for the three different offset runs, with interpolated offset values corresponding to each data run (in bold).

Run	Day/time	Output EMCM 1	Output EMCM 2
Offset 1	Tue 1912	-4.21	-90.2
Data: W1	Wed 0240	**0.45**	**-45.2**
Data: W2/3	Wed 1505	**8.19**	**29.8**
Offset 2	Wed 1919	10.7	53.2
Data: TH1	Thu 0330	**3.26**	**53.6**
Data: TH2	Thu 1600	**-8.42**	**54.1**
Data: FR1	Fri 0430	**-20.1**	**54.7**
Offset 3	Fri 0821	-23.6	54.9

3.3.3 Accuracy

Overall accuracy of the EMCMs for instantaneous flow is a combination of gain accuracy, zero drift, hydrodynamic noise and electronic noise.

Accuracy figures were obtained as part of the present study, to compare with those published by the manufacturer. The average of the standard deviation of the offset values in table 3.2 was taken for zero drift, and typical hydrodynamic and electronic noise levels (rms) were obtained by Christie (1997). Gain accuracy, being a function of the electronics, was unable to be assessed independently.

Table 3.3 shows a summary of values obtained herein compared with published values. A rough idea of the overall accuracy was obtained by adding the last three

parameters and then calculating a percentage error for $1ms^{-1}$, which was then combined with the ±1% gain accuracy.

Table 3.3: EMCM accuracy specifications.

Parameter	Valeport spec.	Present study
Gain accuracy	± 1%	± 1%
Zero drift	$0.005ms^{-1}$	$0.020ms^{-1}$
Hydrodynamic noise at $1ms^{-1}$	$0.002ms^{-1}$	$0.047ms^{-1}$
Electronic noise	$0.003ms^{-1}$	$0.001ms^{-1}$
Approx. total accuracy at $1ms^{-1}$	± 2%	± 7.8%

A number of tests in the past have been performed on EMCMs to assess possible measurement errors both in the laboratory (e.g. Aubrey and Trowbridge, 1985; Aubrey *et al*, 1984) and in the field (e.g. Guza *et al*, 1988). Aubrey (1989) asserted that the sensor is generally accurate to within 10% for both steady and oscillatory flows. (Whether the flow in the swash-zone should be considered oscillatory or quasi-steady is still under debate: this is discussed later in the thesis).

In the present study, the absolute magnitudes of the velocities are of lesser importance than the time-varying characteristics of the flows and, the EMCM still remains the best choice within the limited set of alternatives. For example, the ducted impeller flowmeter (Beach and Sternberg, 1991; Hughes *et al*, 1997; Puleo, 1998), is partly covered (and hence unreliable) for a larger proportion of the time than the EMCM. The three-dimensional ADV (Osborne and Rooker, 1998, 1999), cannot be mounted as close to the bed as the EMCM due to the probe configuration and the sensing volume needing to be covered.

3.4 Pressure transducers

3.4.1 General description

The large pressure transducer was a Druck PTX164, which had also been used previously for nearshore work by Miles (1997). The sensor output is a constant current from 4 to 20mA ('current loop'), corresponding to a pressure of 0 to 2000hPa absolute. When put through a 250Ω resistor, this gave a voltage of between 1 and 5V. Therefore zero output corresponds with zero pressure and the output for atmospheric pressure would be about half way between 1 and 5V, depending on the atmospheric conditions.

The miniature pressure transducers were Druck PDCR1830. These instruments had also been used for previous measurements of pore-pressure in the swash-zone (Baird *et al*, 1998). The direct output from the transducer is 0 to 100mV corresponding to 0 to 700hPa gauge pressure (i.e. zero output corresponds to atmospheric pressure, apart from the offset). This voltage was found to be inadequate to provide the resolution required, therefore an amplifier circuit was added, whose output was 0 to 1V for 0 to 700hPa gauge. The transducers were covered in a Terram geotextile shroud to prevent the impingement of sand grains which could alter the output (*c.f.* Turner and Nielsen, 1997).

3.4.2 Calibration

The PT used to measure water depth for the runs W1, W2 and W3 was the PTX164, which had previously been calibrated in the department. The absolute water depth, i.e. the head of water above the sensor plus the height of the sensor above the bed, may be expressed in terms of the voltage output using the following equation:

$$h = mV_{out} - mV_{atm} + z \tag{3.9}$$

where h is the water depth [m], m is the calibration coefficient [$V^{-1}m$], V_{out} is the output voltage, V_{atm} is the voltage output for atmospheric pressure (the offset) and z [m] is the height of the sensor above the bed. The first term on the right-hand-side represents the head of water corresponding to the total pressure (including atmospheric), and the second term is that corresponding to atmospheric pressure alone. The value of V_{atm} depends on

the atmospheric pressure on the day of the experiment, and this was obtained by noting the dry readings of the transducer.

Offset runs were performed before and after each data run with the instrument out of the water, noting the average voltage output. There was some drift in offset values between the start of run W1 and the end of W3. These values are shown in the calibration equations in table 3.4, together with the previously derived value for m of 5.18 $V^{-1}m$.

Table 3.4: Calibration equations for pressure transducer measuring water depth during runs W1, W2 and W3. h is expressed in metres and V_{out} in volts.

Run	Calibration equation	
W1	$h = 5.18(V_{out} - 3.030) + z$	(3.10)
W2	$h = 5.18(V_{out} - 3.020) + z$	(3.11)
W3	$h = 5.18(V_{out} - 3.015) + z$	(3.12)

Of the five PDCR1830 miniature pressure transducers deployed on runs TH1, TH2 and FR1, water depth was measured by PT1, while the other 4 sensors (PTs 2, 3, 7 and 8) were deployed below the bed to measure pore pressure.

The following general equation may used to express pressure in terms of output voltage for these sensors:

$$p - p_{atm} = m(V_{out} - V_{off}) \tag{3.13}$$

where p is absolute pressure [hPa], m is the calibration coefficient [$hPaV^{-1}$], V_{out} is the output voltage, and p_{atm} is the atmospheric pressure. V_{off} is the offset voltage, i.e. the voltage corresponding to atmospheric pressure.

Calibration was achieved by lowering each sensor into a tube filled with water to a height of 20cm, and noting the voltage output at 2cm increments. Calibration curves were then drawn up, see figure 3.11. Note that 1cm head of water is equivalent to 1hPa. Since the pore pressure gradients between sensors is of interest rather than the pressures themselves, the value of p_{atm} need not be known. The values for V_{off} were obtained by

noting the reading of the sensors when exposed to the air before deployment. This is better than taking the intercept of the calibration curves because there is no guarantee that the atmospheric pressure was the same on the days of the experiment as it was during calibration. Values of V_{off} were as follows:

PT2: 0.0059V
PT3: 0.0054V
PT7: 0.0165V
PT8: 0.0036V

The calibration equations for the sub-surface PTs are shown in table 3.5. The calibration coefficients have been derived from the regression coefficients of the calibration curves.

For the miniature PT used above the surface (PT1), the absolute depth of water, h, may be expressed as

$$h = m(V_{out} - V_{off}) + z \tag{3.14}$$

where m is the calibration coefficient [$V^{-1}m$] and z is the height of the sensor above the bed. Offset runs were performed before and after each data run and the drift in offset values was negligible. The value of V_{off} was found to be 0.003V. Therefore the calibration equation for the above-surface PT for runs TH1, TH2 and FRI is

$$h = 608.4(V_{out} - 0.003) + z \tag{3.15}$$

where h is expressed in cm and V_{out} in volts.

It is noteworthy that the PTs have a remarkably linear response, with average R^2 values of 99.9%.

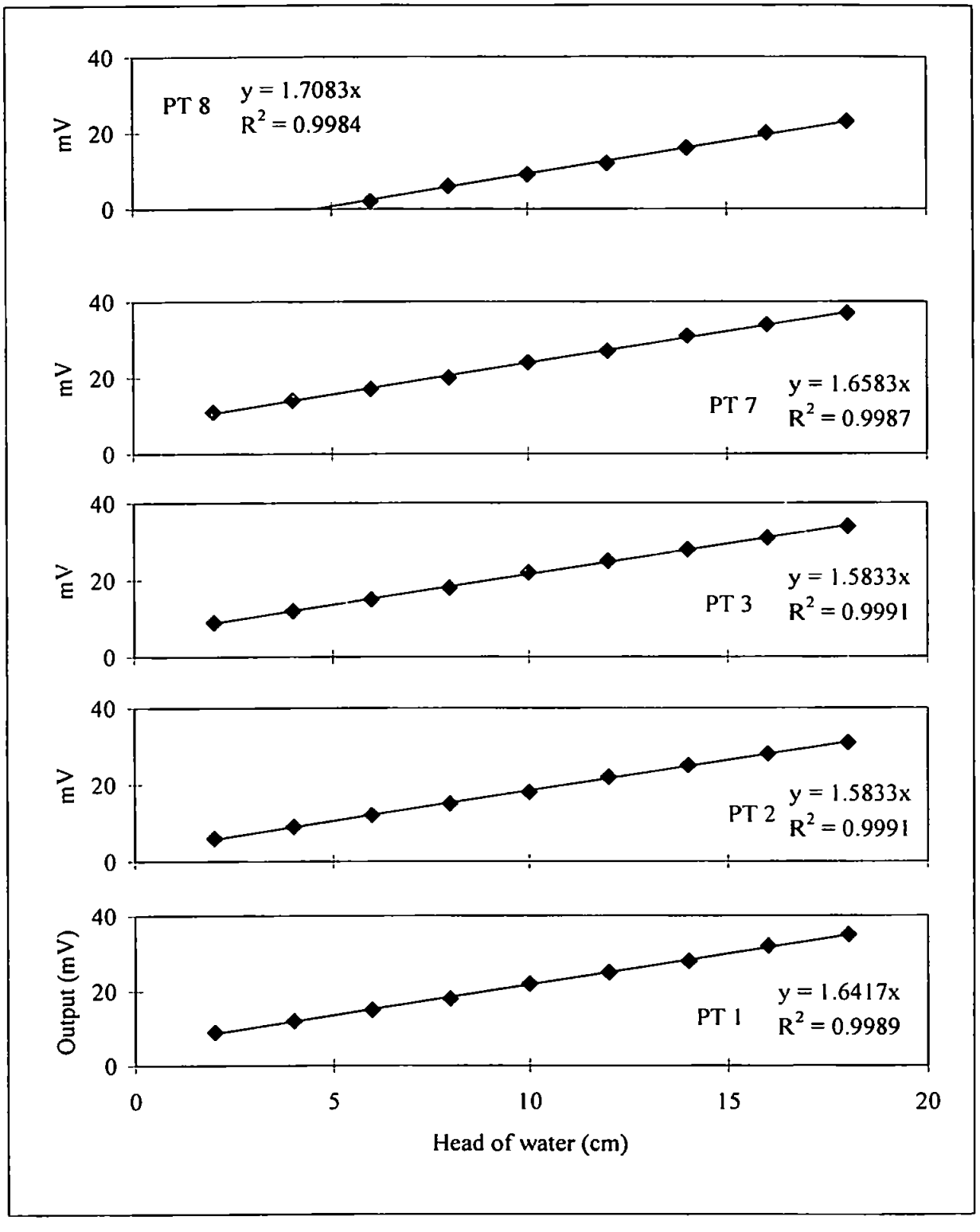

Figure 3.11: calibration curves for miniature pressure transducers.

Table 3.5: Calibration equations for miniature pressure transducers measuring below-bed pore pressure. ($p - p_{atm}$) is expressed in hPa and V_{out} in volts. Note that 1hPa ≡ 1cm head of water.

PT	Calibration equation		R^2 (%)
7 (top)	$p - p_{atm} = 602.2(V_{out} - 0.0165)$	(3.16)	99.9
2	$p - p_{atm} = 631.0(V_{out} - 0.0059)$	(3.17)	99.9
8	$p - p_{atm} = 584.4(V_{out} - 0.0036)$	(3.18)	99.9
3 (bottom)	$p - p_{atm} = 631.0(V_{out} - 0.0054)$	(3.19)	99.9

3.4.3 Accuracy

Published accuracy of both the above PTs (combined non-linearity, hysteresis and repeatability) is ±0.1%.

4. Field experiment

4.1 The field site

4.1.2 Selection of field site

The data used in this study was obtained from a field experiment performed at Perranporth Beach, on the North Cornish Coast, U.K. (see figure 4.1). Several factors contributed to the suitability of this beach.

(a) The beach is extremely flat ($\tan\beta \approx 0.014$), allowing conditions to be highly dissipative, with mostly spilling breakers and a surf-zone which can easily become saturated.

(b) Considerable wave activity is received, both from local storms and Atlantic swell. The mean significant wave height is 1.4m (Davidson *et al,* 1998).

(c) The mean tidal range is 5.25m. The large tidal range of this beach means that a single instrument rig can be used to measure at various different positions in the cross-shore direction, as the tide advects over the rig.

(d) The beach contains fine to medium sand, but very few stones. (Adjacent beaches in the area appear to contain fine to medium sand, mixed with stones of about 5cm diameter). This is important to minimise the chances of instrument damage.

(e) The Perranporth Surf Life Saving Club was able to be used as a 'base' throughout the experiment. The logging equipment, tools and spare instrumentation were housed in the building, and the electricity was supplied by the club.

Perranporth has been used for oceanographic observations dating back many years. For example, Barber and Ursell (1948) measured the spectra at Perranporth of swells originating up to 6000 miles away; Tucker (1950) made some of the first observations of infragravity waves; and Darbyshire (1952) used wave observations at Perranporth to investigate empirical methods of wave forecasting. Work is also presently underway at Perranporth to investigate long-term trends in beach morphology using video cameras, as part of the world-wide ARGUS program (Davidson *et al*, 1998).

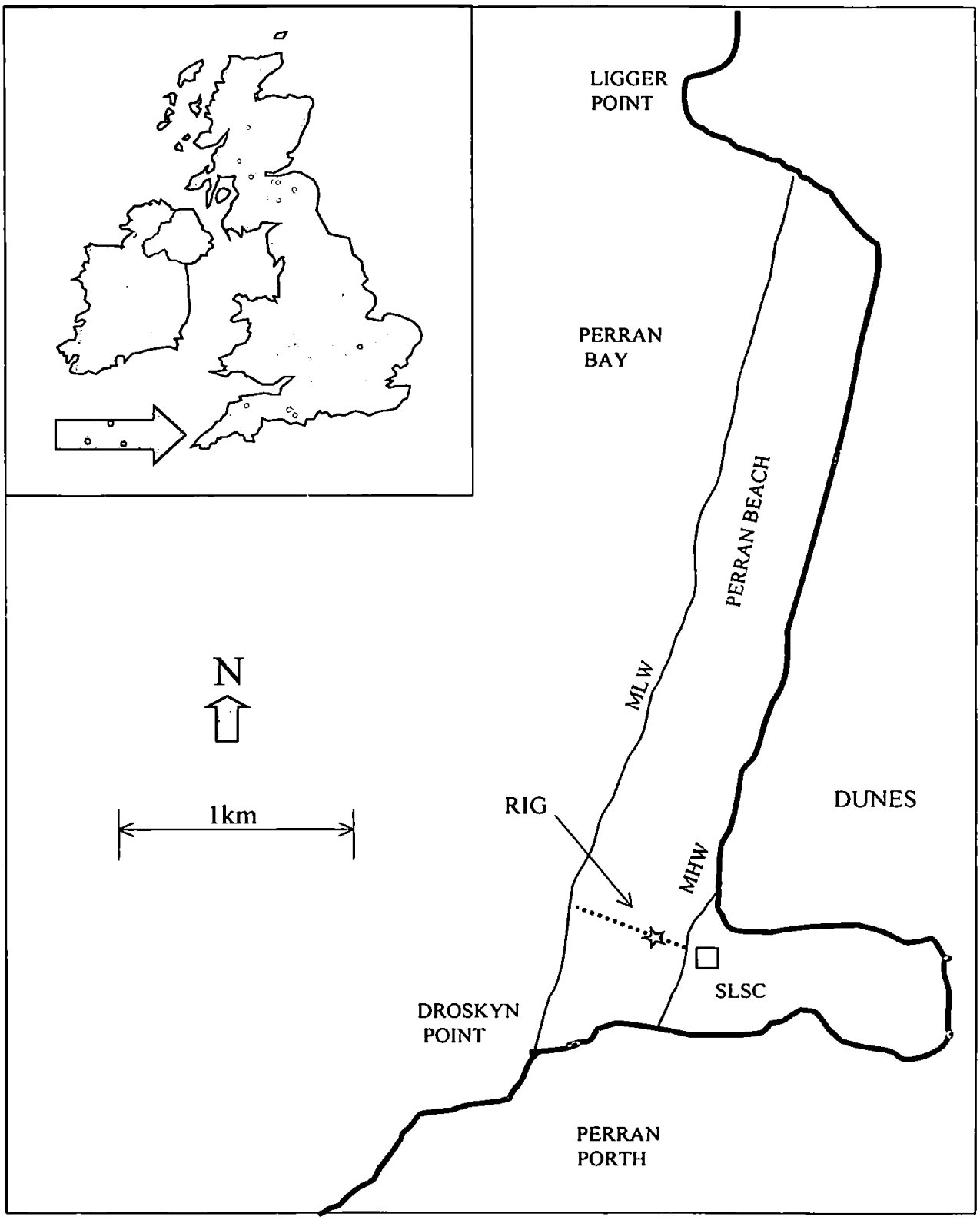

Figure 4.1: measurement location. MLW = mean low water; MHW = mean high water; SLSC = surf life saving club.

4.1.3 Beach profile

To provide an estimation of the beach slope in the region where the measurements were taken, and to confirm the dissipative nature of this beach, a cross-shore profile was taken. A diagram of the beach profile is shown in figure 4.2, showing the two rig positions. Two sets of three data runs were taken at each position (see section 4.2.3).

The method used was as follows. A known benchmark exists at the top of the beach, which was used as a starting point. Sights were taken at 5m increments to about 250m from the top of the beach, increasing to 2m increments about 5m either side of each instrument rig position.

The average beach slope (β) 20m either side of the instrument rig positions was 0.79^0 for the more seaward position and 0.82^0 for the more landward position (i.e. $\tan\beta$ = 0.0137 to 0.0143).

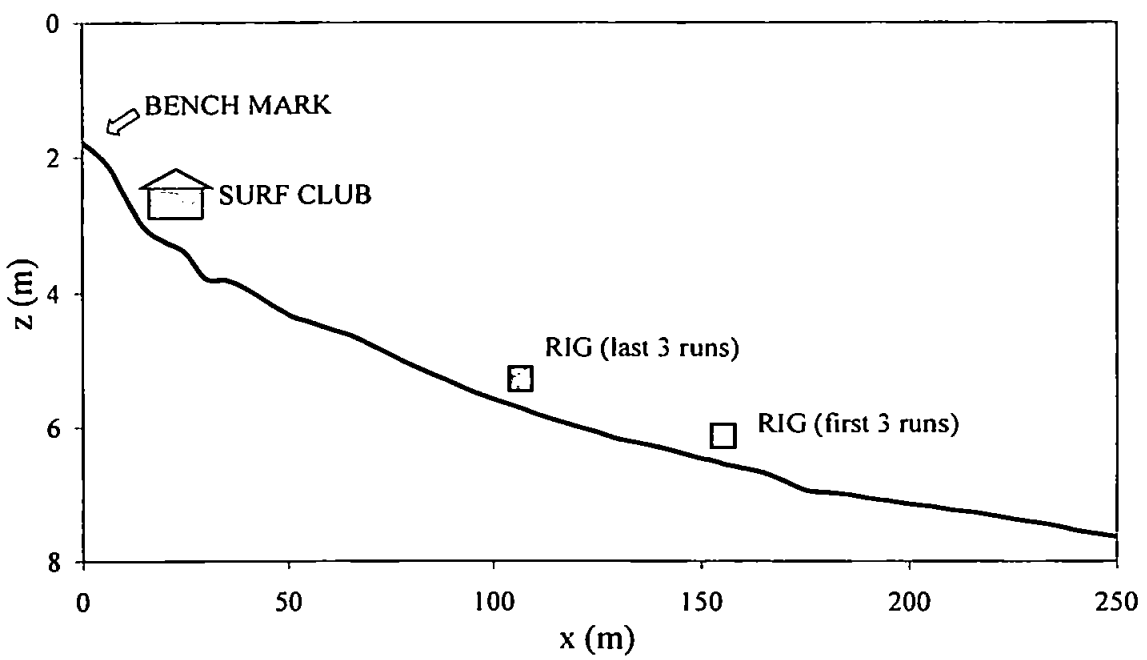

Figure 4.2: beach profile showing the two cross-shore positions of the instrument rig (a 'run' refers to data collected over a tide).

4.1.4 Beach classification

Wright and Short (1984) explain how beaches may be classified within a continuum from reflective to dissipative using a surf-scaling parameter, ε (Guza and Inman, 1975), where

$$\varepsilon = a_b \omega^2 / g \tan^2 \beta \qquad (4.1)$$

where a_b is the breaker amplitude (≈ half breaker height H_b), $\omega = 2\pi / T$ is the radian frequency, T is the wave period, and tan β is the beach slope. The classification is summarised in table 4.1.

Using H_b = 0.8 to 2.2m and T = 8s, values of ε for the conditions in this study varied from 164 to 452, thus indicating the conditions to be highly dissipative.

Table 4.1: Beach types.

ε	Beach	Waves
< 2.5	reflective	surging
2.5 to 20	intermediate	plunging
> 20	dissipative	spilling

4.1.5 Grain size analysis

The grain size distribution of a sample of sediment taken from the average position of the instrument rig was found using standard dry sieving techniques, at half-phi intervals. Results are shown in table 4.2 and figure 4.3. The cumulative distribution function was also calculated, and this is shown in figure 4.4.

Note that to convert from any grain size (d) in mm to grain size in phi, the Udden-Wentworth scale is used (Wentworth, 1922; Krumbein, 1934), i.e.

$$d(\phi) = -3.32 \log_{10} d\,(\text{mm}) \qquad (4.2)$$

Table 4.2: dry sieving results.

Sieve size (ϕ)	Range in sieve (ϕ)	Mean size in sieve (ϕ)	Weight (g)
0	< 0	0	0.1
0.5	0 to 0.5	0.25	0.6
1	0.5 to 1	0.75	5.5
1.5	1 to 1.5	1.25	32
2	1.5 to 2	1.75	270
2.5	2 to 2.5	2.25	77
3	2.5 to 3	2.75	11
3.5	3 to 3.5	3.25	0.6
4	> 3.5	3.75	0

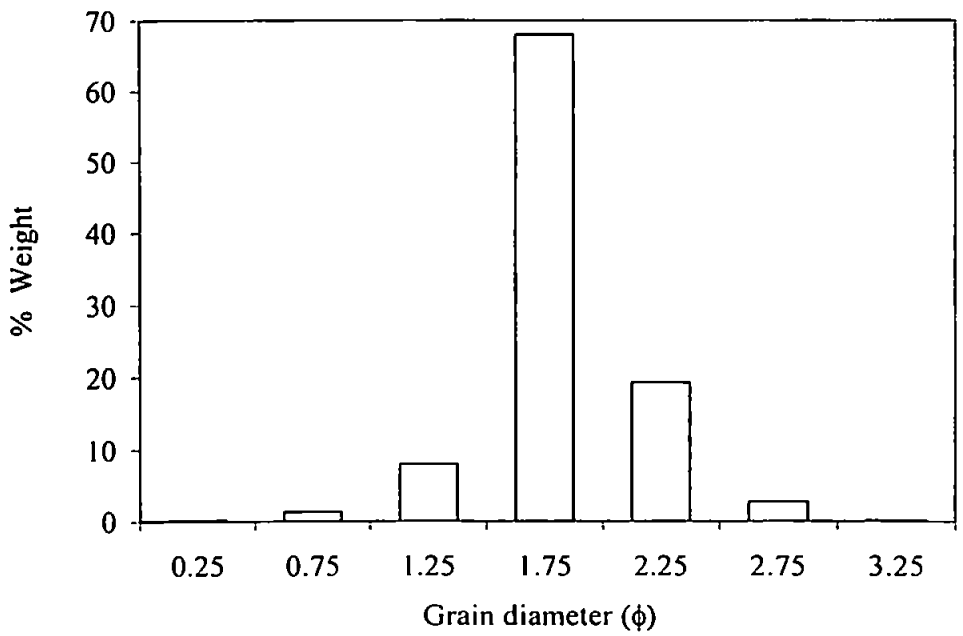

Figure 4.3: grain size distribution histogram.

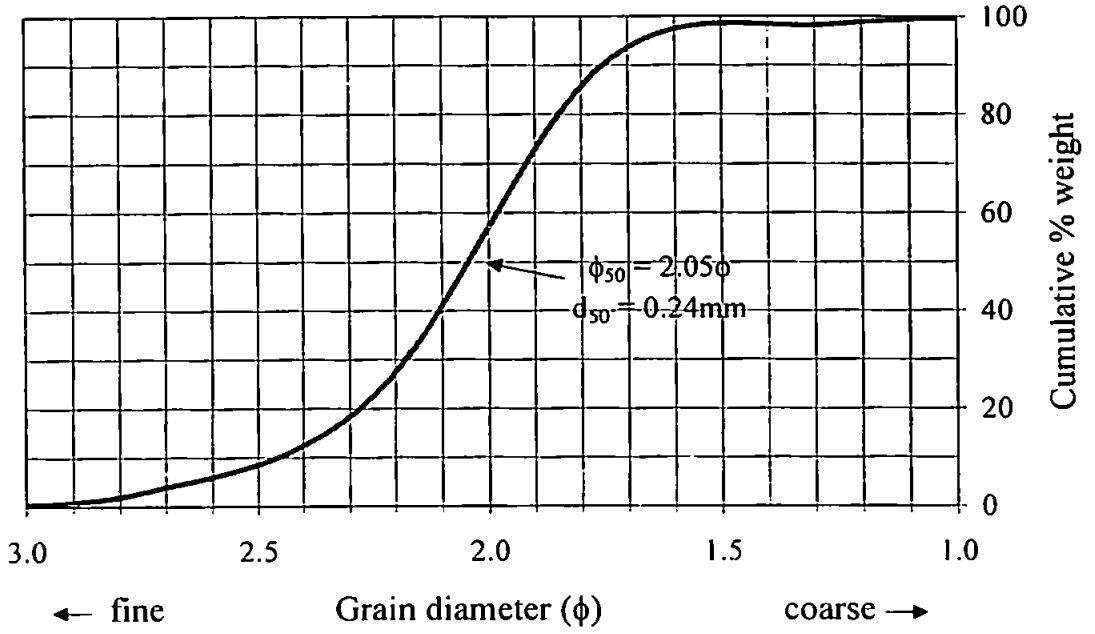

Figure 4.4: cumulative percentage weight distribution of grain size.

From figure 4.4, the median grain size (d_{50}) is 2.05ϕ, (0.24mm). The mean grain size ($\bar{d}$), the standard deviation (σ) and the skewness (Sk) may also be found from the cumulative distribution curve using formulae devised by Folk and Ward (1957), i.e.

$$\bar{d} = \frac{\phi_{84} + \phi_{50} + \phi_{16}}{3} \tag{4.3}$$

$$\sigma = \frac{\phi_{84} + \phi_{16}}{4} + \frac{\phi_{95} + \phi_{5}}{6.6} \tag{4.4}$$

$$Sk = \frac{\phi_{84} + \phi_{16} - 2\phi_{50}}{2(\phi_{84} - \phi_{16})} + \frac{\phi_{95} + \phi_{5} - 2\phi_{50}}{2(\phi_{95} - \phi_{5})} \tag{4.5}$$

A summary of the grain statistics is shown in table 4.3, which shows that the sediment is very well sorted and slightly negatively skewed on the phi scale. Note also that the mean grain size ($\bar{d}$) is very close to the median grain size (d_{50}). This value will be used for further analysis in subsequent sections of the thesis.

It has been pointed out by Jaffe *et al* (1984) that optical backscatter sensors are less reliable in concentrations containing a wide range of grain sizes, therefore it is an advantage for the sediment to be well-sorted.

The negative skewness means that sediment has been removed at the fine end of the scale. The tail of fine sediment has been truncated, shifting the peak slightly towards the fine end and leaving a longer tail of coarse sediment. This is a common characteristic for beach sands (e.g. Friedman, 1961; Folk, 1966).

Table 4.3: summary of grain statistics.

Parameter	Value	Description
d_{50}	2.05ϕ (0.24mm)	
$\bar{d}$	2.06ϕ (0.24mm)	fine to medium sand
σ	0.28ϕ (0.82mm)	very well sorted
Sk	– 0.16	slightly negatively skewed

4.2 Experimental procedure

4.2.1 Introduction

Instrument development and preliminary trials were carried out between April 1997 and March 1998, including a two-day preliminary field deployment at Perranporth between 24 and 25 July 1997. The experiment described in the present study was performed over a four-day period between Tuesday 24 March and Friday 27 March, 1998.

Six data runs of approximately two hours duration were recorded in total, with a re-arrangement of the instrument set-up and position after the first three. Each run was performed over high-water, with the intention of allowing the tide to advect over the rig. The parameters measured were cross-shore velocity, longshore velocity, suspended sediment concentration at four heights above the bed, pressure above the bed and pressure at four levels below the bed. This section gives chronological details of the experiment and describes the physical layout of the instruments, during both sets of data runs.

4.2.2 Physical conditions during the experiment

A summary of the weather conditions for each day, estimated by eye, is shown in table 4.4, and a summary of the wave conditions, also estimated visually, is shown in table 4.5, where H_b is breaker height, and T_S is significant period. These were the average conditions throughout the day, estimated at two-hourly intervals during daylight.

The wave conditions on the Thursday were those of a local storm, with strong onshore winds and increasing wave height, but a broad spectrum with a relatively short significant period. On the Friday, the wind was less strong, but the wave height and significant period had increased, and there were visual indications of the presence of swell together with the localised windsea.

Table 4.4: meteorological conditions

Day	Wind direction	Windspeed (Beaufort scale)	Weather	Cloud cover
Tue 25	SW	2 - 3	Light rain	4 / 8
Wed 26	SW	3 - 4	Light to mod rain	6 / 8
Thu 27	W	6 - 8	Heavy rain	8 / 8
Fri 28	SW	3 - 5	Moderate rain	8 / 8

Table 4.5: wave conditions

Day	H_b (m)	T_S (s)	Width of surf-zone (m)	Width of swash-zone (m)
Tue 24	0.8	7	40	15
Wed 25	1.0	8	60	20
Thu 26	2.0	7	80	25
Fri 27	2.3	10	120	30

4.2.3 Timing of data runs

Details of the timing of each data run are shown in table 4.6, together with the times and heights of high-water. Previous tests of the MOBS sensors revealed that they might suffer from interference caused by ambient light. However both daylight and night runs were performed, as (a) it was envisaged that some analysis might be performed without the SSC data, (b) it might turn out that the effect of ambient light on the SSC data is small enough to allow some analysis to be done, and (c) the extra effort required to perform day runs was minimal once the equipment had already been set up

Table 4.6: timing of data runs

Day	Run	Start time (GMT)	End time (GMT)	Time of high-water (GMT)	Height above chart datum (m)
Wed	W1 (night)	0100	0420	0239	6.2
Wed	W2 (day)	1310	1530	1507	6.2
Wed	W3 (day)	1550	1700	1507	6.2
Thu	TH1 (night)	0230	0430	0330	6.7
Thu	TH2 (day)	1445	1715	1556	6.8
Fri	FR1 (night)	0220	0640	0418	7.2

4.2.4 Instruments deployed on each run

Due to cable length restrictions, the miniature pressure transducers were not able to be deployed on all the runs. For the first three runs, the larger pressure transducer was deployed to measure water depth, and below-bed pore pressure was not measured. Table 4.7 shows a list of the instruments deployed on each run, and the parameters each one was measuring.

Table 4.7: instruments deployed on each run

Runs	Equipment	Measuring
W1, W2, W3	MOBS tube	SSC at four heights above the bed.
	Spherical EMCM	cross-shore velocity
	Miniature EMCM (#1)	cross-shore velocity
	Miniature EMCM (#2)	longshore velocity
	'Large' PT	Water depth
TH1, TH2, FR1	MOBS tube	SSC at four heights above the bed.
	Spherical EMCM	cross-shore velocity
	Miniature EMCM (#1)	cross-shore velocity
	Miniature EMCM (#2)	longshore velocity
	Miniature PT	Water depth
	4 Miniature PTs	Pore pressure at four heights below the bed.

4.2.5 Instrument set-up

As shown in table 4.7, the instruments were deployed in two different configurations. These are illustrated in figures 4.5 and 4.6, for the first and second configuration respectively. Since the instruments were not re-deployed after each run, the instrument heights at the beginning of each run differed slightly due to bed level changes. The heights above the bed for each instrument at the beginning of each run are shown in table 4.8. The EMCMs were measured to the position of the sensing electrodes.

The four below-bed pressure transducers were mounted on the MOBS tube itself, with the highest pressure transducer remaining 3cm below the lowest MOBS sensor. To avoid preferential flow of groundwater up and down the mounting tube, the transducers were mounted horizontally, protruding out from the tube so that the sensing heads were 6cm away from the tube. The intakes were covered with a permeable cloth filter, to prevent additional pressure due the grains themselves impinging on the diaphragm of the transducer.

Ideally, all the instruments will obtain measurements from the same point in space, (the sensing volume), but clearly this is impractical due to one instrument interfering with another. However, certain steps may be taken to allow the sensing volumes to be as close as possible. The miniature EMCM measuring cross-shore flow, and the MOBS sensors, were positioned so that their sensing volumes were as near as possible to being vertically aligned, without causing any backscatter from the body of the EMCM. The sub-surface pressure transducers were also positioned so that their sensing volumes were directly below those of the MOBS.

Previous tests during the development of the MOBS tube revealed that sediment tends to splash up the sides of the tube, in the direction of strongest flow, which is expected, in this case, to be cross-shore. Therefore, the MOBS tube was mounted with its sensors 'looking' in a longshore direction, to avoid this form of instrument intrusion (see also Ludwig and Hanes, 1990).

All the instruments were positioned in such a way as to avoid flow disturbance caused by one sensor being upstream of another (assuming the principal flow is cross-shore).

It was decided to mount the instruments protruding from the bed, with the diameter of the protrusion as small as possible to minimise scour. Previous trials with the MOBS tube showed that minimal scour was evident using a tube diameter of 12mm, although, with 50cm tubes, an unacceptable level of scour was produced (see section 3.2.3). Therefore, the stems of EMCMs, the surface pressure transducer, and the MOBS tube

itself, were of a diameter of less than 15mm. The most important area to avoid scour is around the base MOBS tube, since it must be known at what height above the bed the lowest sensor will be measuring suspended sediment. Scour will produce a 'false' bed level, and therefore could reduce locally suspended sediment. Scour around the other instruments is relatively unimportant for their own function, but could still affect the MOBS. The only protrusion of a diameter of more that 15mm was a scaffolding pole, used for anchoring purposes, and this was always at least 80cm away from the MOBS.

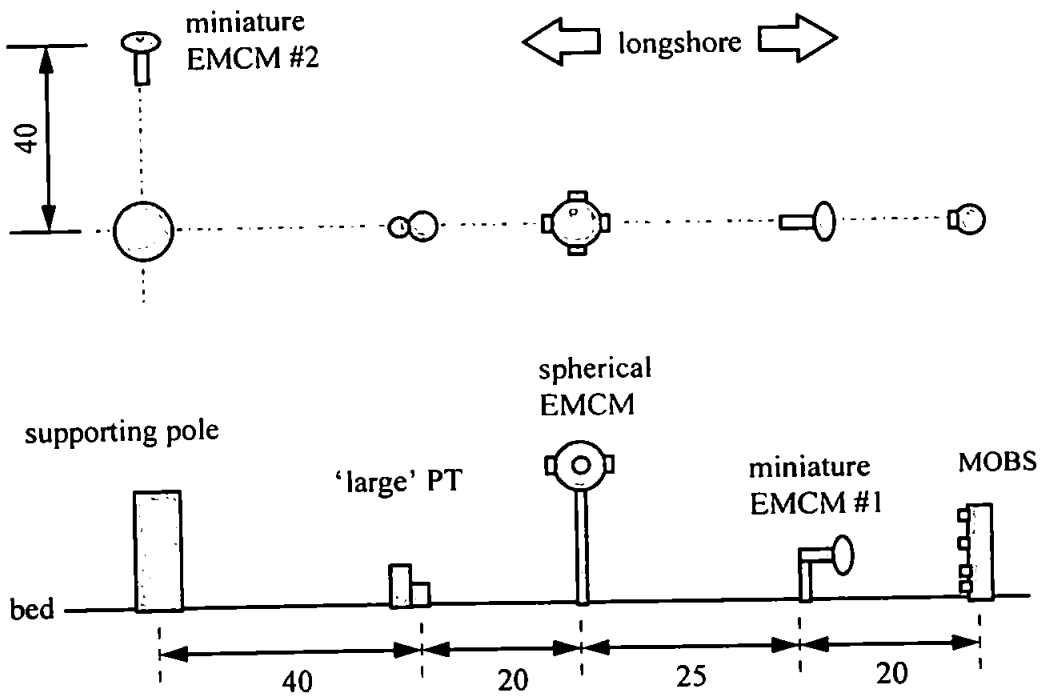

Figure 4.5: Instrument set-up for runs W1, W2 and W3. Plan view (top) and side view (bottom). Dimensions in cm.

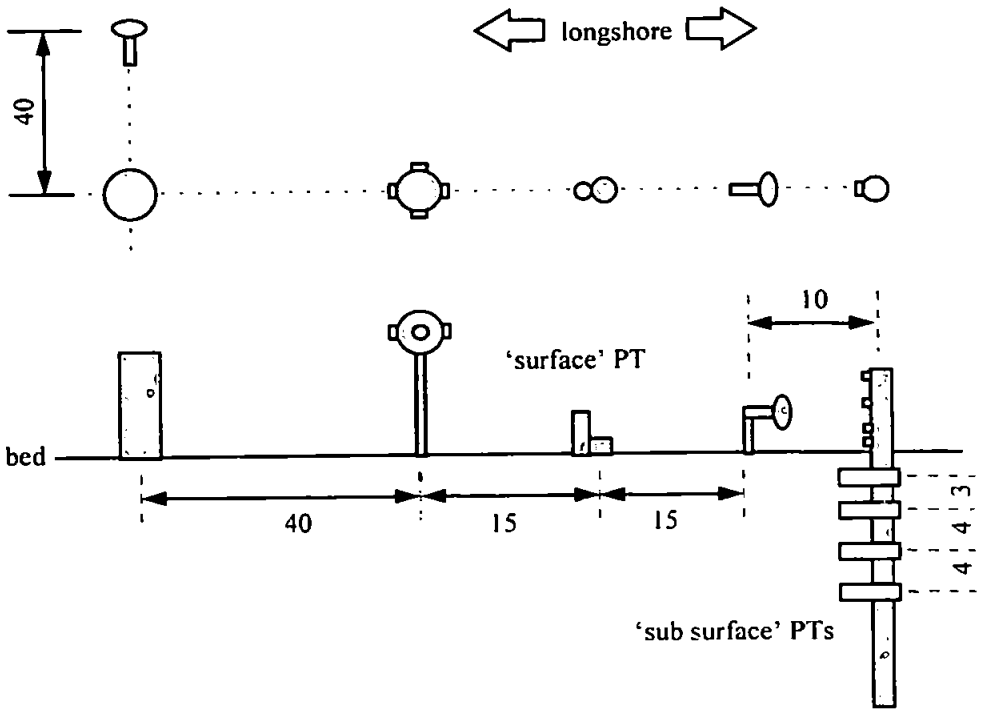

Figure 4.6: Instrument set-up for runs TH1, TH2 and FR1. Dimensions in cm.

Table 4.8: heights (cm) of instruments above the bed at the beginning of each run.

Run	MOBS sensors	Spherical EMCM	Miniature EMCMs	'Large' PT	Miniature PT (surface)	Sub-surface PTs
W1	1, 2, 5, 10	15	5	1	-	-
W2	1, 2, 5, 10	15	5	1	-	-
W3	1, 2, 5, 10	15	5	1	-	-
TH1	1, 2, 5, 10	6	4	-	1	-2, -5, -9, -13
TH2	1, 2, 5, 10	6	4	-	1	-2, -5, -9, -13
FR1	2, 3, 6, 11	7	5	-	2	-1, -4, -10, -14

A simplified schematic illustration of the physical layout of the instrument rig, the electronics modules, and the logging equipment is shown in figure 4.7. The diagram is common to both instrument set-ups. Note that (a) the instrument rig was 140m from the surf club for the first configuration and 90m from the surf club for the second, and (b) for the first configuration the 'large' PT only required a single cable, whereas, for the second configuration there were five cables, one for each miniature PT. See figure 4.2 for the two positions of the rig relative to the beach profile. The *in situ* interface units, containing the analogue to digital converters and anti-aliasing filters for the MOBS and the EMCMs, were buried under the bed about 5m from the instrument rig, in a longshore direction. These units are designed to have negative buoyancy, and are therefore particularly heavy. The advantage of having these units near to the instruments is that all the data for seven instruments is taken up the beach using two RS232 cables. Power was supplied using a separate cable. The PTs, on the other hand, required a single data/power cable for each instrument. The analogue to digital converters and anti-aliasing filters for the PTs, together with further interfacing circuitry, were housed in the surf club, along with the logging computer.

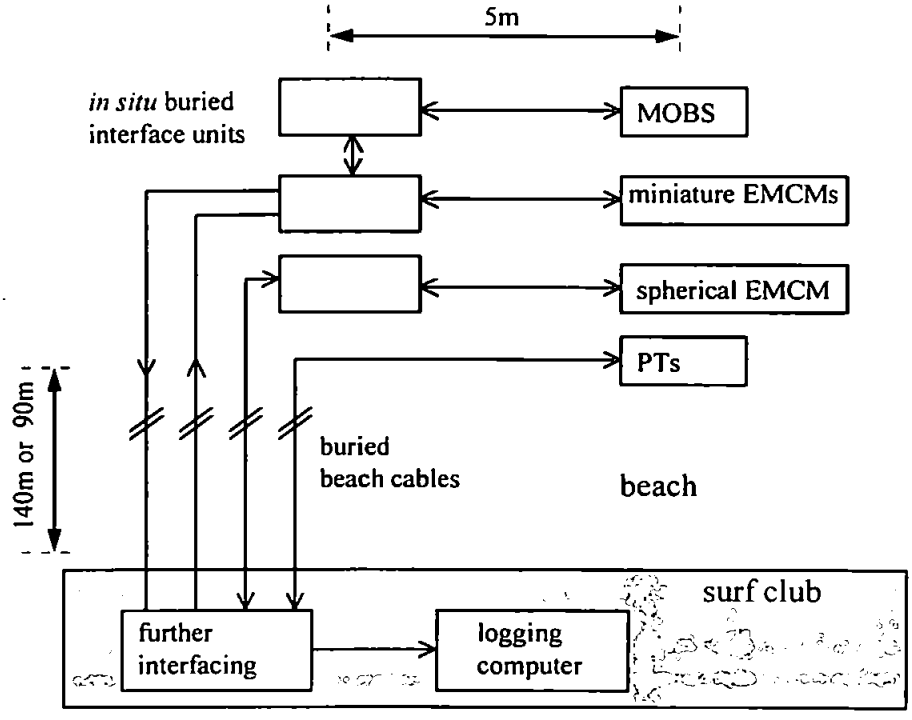

Figure 4.7: simplified schematic illustration of relative positions of rig, electronics modules and logging equipment, common to both the first and second configurations.

4.2.6 Deployment: general notes

Offset runs were performed by inserting the EMCMs in a bucket of still water for approximately five minutes, or until the visual indication of output had become steady. This could be done each time the instruments were re-deployed, i.e. before run W1, between runs W3 and TH1, and after run FR1.

Changes in bed level throughout each run were estimated by measurement of instrument heights before and after the runs. Any scour around each instrument was also noted.

Visual observations of hydraulic jumps were performed during the experiment. Details of this are given in chapter 10.

The spherical EMCM malfunctioned, therefore no data from this instrument was usable.

5. Data reduction

5.1 Introduction

5.1.2 General

The first part of this chapter describes how the data were arranged into a suitable format for subsequent analysis. The data were re-sampled at 2Hz to provide more manageable files, and also to filter out high frequency noise in the EMCM outputs. Each data run was divided into a number of 17-minute 'data bursts', which was considered the maximum length to preserve stationarity (see below). The data were then inspected to allow any time-series which contained no useful information for analysis to be rejected.

Because of potential problems with spurious signals arising from exposure of the MOBS sensors to either ambient light or bubbles, a filtering technique was applied to the data to reject any signals which appeared when the pressure at the height of that sensor dropped below a certain value. Also, since the EMCMs were factory set to read a maximum velocity of $1.2ms^{-1}$, then an extrapolation algorithm was applied to the high-energy backwashes which exceeded this value.

The second part of this chapter gives a brief introduction to the spectral analysis techniques necessary for application in certain parts of the analysis. Successful analysis in the frequency domain is dependent upon the three-way compromise between stationarity, spectral resolution and confidence, and this is clearly explained.

5.1.3 Stationarity

The statistical properties of a time-series which has reached the equilibrium state of stationarity are independent of absolute time (e.g. Emery and Thomson, 1998). For example, a truly stationary time-series will have a constant mean and variance, and so to obtain these quantities it would not be necessary to average over the whole time-series.

The time-series in the present study are considered short enough to maintain a reasonable approximation to stationarity so that slowly varying quantities such as the tides have negligible affects on the results (e.g. an anomalous low-frequency peak appearing on the spectra). On the other hand, the time-series is sufficiently long to provide enough

repeat cycles for accurate resolution of the periodic behaviour (e.g. infragravity waves). This is explained in more detail below in section 5.3.

5.1.4 Aliasing

To preserve all the information in a signal, the sample rate must be at least twice that of the highest frequency of interest. The frequency of half the sampling rate is known as the Nyquist frequency, Ny. If signals are present above the Nyquist frequency (i.e. these signals will be sampled at a rate less than twice their frequency), then there will be a danger that these will be 'folded back' to appear as lower frequencies indistinguishable from the useful data. This is known as aliasing, (see figure 5.1).

The outputs of the sensors may contain unwanted spurious signals of a frequency more than half the sampling rate, and so these should be filtered out using a low-pass filter (anti-aliasing filter), set at a frequency just above the highest frequency of interest.

In the present study, a hardware anti-aliasing filter was already fitted to the signal processing electronics, which was adequate to avoid any aliasing errors with the original 18Hz sampling rate. However, since the data were re-sampled at 2Hz, care had to be taken to ensure that the re-sampling software also contained an anti-aliasing filter (see below).

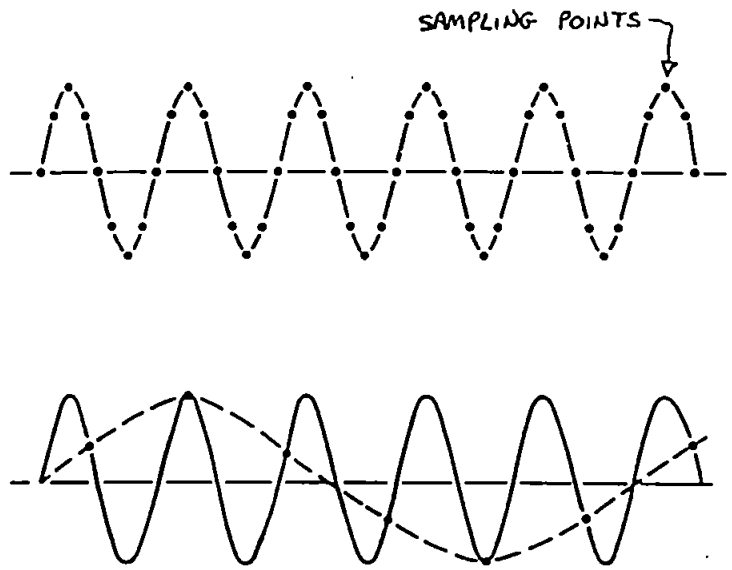

Figure 5.1: aliasing: the sampling rate is much lower that the signal frequency, so all the fluctuations are not seen by the sampler. If the values at the sampling points are simply joined together, then it will appear as a lower frequency. To avoid this, the sampling rate must be at least twice the signal frequency.

5.2 Time-series processing

5.2.1 Re-sampling

In the initial data collection, the sampling frequency was fixed at 18Hz. With the sampling frequency this high, it was found that the file length required to provide a reasonable number of repeat cycles of the infragravity oscillations contained too many samples for efficient data handling. Also, the EMCMs were found to be slightly noisy on sudden velocity changes, which is inherent in the design of these instruments, (B. Raubenheimer, pers. comm., 1997), therefore it was considered advisable to apply a low-pass filter.

After careful consideration, it was decided that the data could be re-sampled at 2Hz, thus giving a highest frequency of interest (Ny) of 1Hz. The number of data points in each time-series were reduced using the re-sampling routine available in Matlab. This program has an automatic anti-alias filter, which is necessary since there is a possibility for aliasing errors to occur due to spurious signals between 2Hz and 8Hz (the cut-off frequency of the hardware anti-alias filter fitted to the logging electronics).

The original file length in the data collection was 8192 samples, at 18Hz. This was then re-sampled at 2Hz so that the new file length was 910 samples. Note that, at this stage, it was not envisaged that the kind of problems might occur which would require subsequent re-sampling. To provide the maximum length of data burst for analysis, whilst still conserving stationarity, the original files were then joined together to make 2048 samples. For the FFT calculations it is always preferable that the file length be a power of 2 (note the original choice of 8192).

5.2.2 Time-series selection for subsequent analysis

The whole data set was examined initially, and various data were immediately eliminated for not containing any useful information. For example, sometimes the run continued after the tide had receded past the instrument rig, leaving all the instruments dry. In some cases, the length of cables available and the tidal height meant that usable data was available for quite short periods within a run (e.g. no useful data was available from the TH1 run, as the water never reached the instruments).

Further inspection of the data revealed that the following sets of time-series could be extracted and used for further analysis:

- A set of time-series could be taken from the earlier runs (where cable lengths allowed the instruments to be in the inner surf-zone for some of the time), whereby the velocity field could be compared at various cross-shore positions in the surf-zone through to the swash-zone, as the tide was allowed to advect over the instruments. Note that this was chosen on the incoming tide only, as little data were recorded into the surf-zone on the outgoing tide.
- Since the sea state increased throughout the measurement campaign, representative data bursts in high and low energy conditions could be used as the basis for examining how swash-zone sediment transport evolves as conditions change. Analysis is somewhat limited if the velocity time-series is not continuous (Osborne and Rooker, 1999), therefore it was decided to take these data from the seaward-most part of the swash-zone, where the instruments were at the threshold of wetting and drying.
- The velocity time-series from the 'mid' swash-zone (where the instruments were continually wetting and drying) in the lower energy ($H_b \approx 0.8$m) runs did not show any backwashes, due to the height of the EMCM above the bed. Also, due to the extra height of the tide, the instruments were in the mid swash-zone for a very short time during the FRI run. Therefore the only useable mid-swash data was from the TH2 run, which was taken during daylight. (Careful inspection of the SSC time-series suggested that noise from ambient light was not a problem once the sensors were fully immersed). This data would be useful for inspection of the velocity and SSC time-series during individual, isolated, swash events.
- Examination of how infiltration-exfiltration affects swash-zone sediment transport could be also be made from the above data burst. It was found that the clearest picture of changing pore-pressure gradients could be obtained from the data recorded in the mid swash-zone, where each swash cycle was separated from the next.

Table 5.1 lists the data bursts used for each part of the analysis, in chronological order. Note that for the 'mid-swash' data the tide only just reached the level where the instruments were in the middle of the swash-zone, but for the calm and storm data it rose high enough to allow the instruments to be at the seaward limit of the swash-zone. The mean depth was taken over the whole time-series, so for the discontinuous data (i.e. mid-swash) this must be interpreted carefully. A schematic illustration of the relative position of the instruments within the swash-zone is shown in figure 5.2.

Table 5.1: List of data bursts taken for analysis.

Burst	Run	H_b (m)	Mean depth (m)	Tide
Calm	W1	0.8	0.20	flood
Transect 1	W1	0.8	0.41	flood
Transect 2	W1	0.8	0.55	flood
Transect 3	W1	0.8	0.64	slack
Mid-swash	TH2	2.0	0.04	slack
Storm	FR1	2.2	0.23	slack

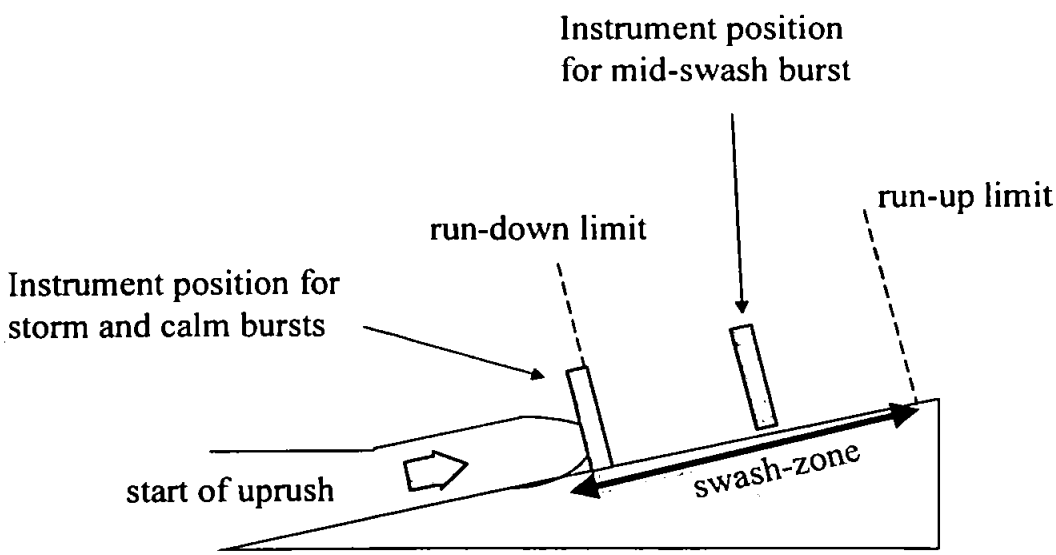

Figure 5.2: schematic representation of the relative position of the instruments within the swash-zone.

5.2.3 'Dry-out filtering'

Although Downing *et al* (1981) pointed out that the scattering angle from air bubbles is much less than that from sediment particles, it is now known that optical backscatter sensors are generally sensitive to bubbles, and care must be taken to avoid false SSC readings (T. Aagaard, pers. comm., 1999). As an incoming swash front hits the sensor array, before the array is completely immersed, high readings of apparent SSC may be seen. This may sometimes cause the vertical concentration profile to appear reversed, i.e. the top sensor shows a high reading before the lower ones. This problem was apparent for the latter, higher energy data (the 'mid-swash' and 'storm' data bursts).

Since it would be meaningless for the sensors to be measuring suspended sediment concentration when out of the water, it was decided to force the data to zero during periods when each sensor was uncovered. Hence a simple algorithm was written to force the SSC to zero if the depth of water was below the height of that particular sensor.

Note that the 'foam' which precedes a bore-front or swash-front is of a much lower density than water due to the presence of bubbles, therefore the pressure transducer will not measure any head of water until the sensors are completely immersed. This filtering should therefore contribute to the reduction of the effect of bubbles on the MOBS sensors (see schematic, figure 5.3), although it is acknowledged that a few bubbles will still exist in the water-column below the height which the PT considers to be the surface.

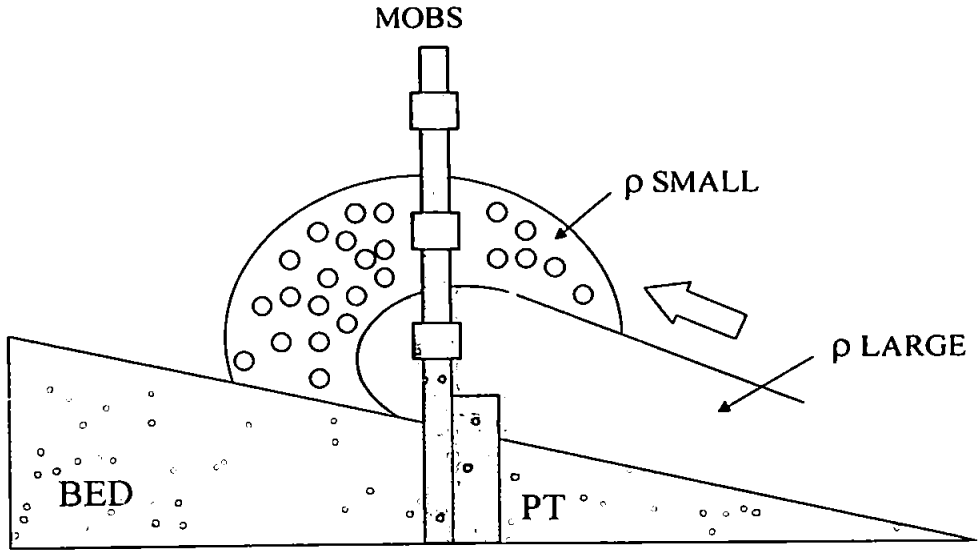

Figure 5.3: simplified schematic illustration of swash-front containing area of foam. ρ = density. The filtering algorithm will force the readings of the top two sensors to zero, as the PT considers the 'surface' to be below the middle sensor. Therefore, the possibility for false readings from the MOBS is reduced.

An example of a sediment suspension event before the algorithm was applied is shown in figure 5.4. Here it can be seen that, at t ≈ 177s the depth goes below the height of the top sensor, which starts to show a high reading. As the depth progressively becomes low enough to uncover each sensor in turn, each one starts to 'saturate'. The same event is shown in figure 5.5, but this time with the filtering applied. Here, at t ≈ 176 to 180s a backwash suspension event can be seen, where the sediment is seen suspended only at the lower levels in the water-column. Then at t ≈ 188s there is a suspension event associated with the arrival of the next uprush, where sediment is suspended to all heights in the water-column, but at the lower levels first.

A similar algorithm was also applied to the cross-shore velocity signal in the 'mid-swash' time-series, as here it was found that the EMCM tended to behave erratically when out of the water. Again, the signal was set to zero as soon as the water depth fell below the height of the sensor. Figure 5.6 shows a section of the time-series with and without the filtering. It can be seen how, after filtering, the velocity is only non-zero at depths greater than 5cm, for example between t ≈ 263s to t ≈ 275s.

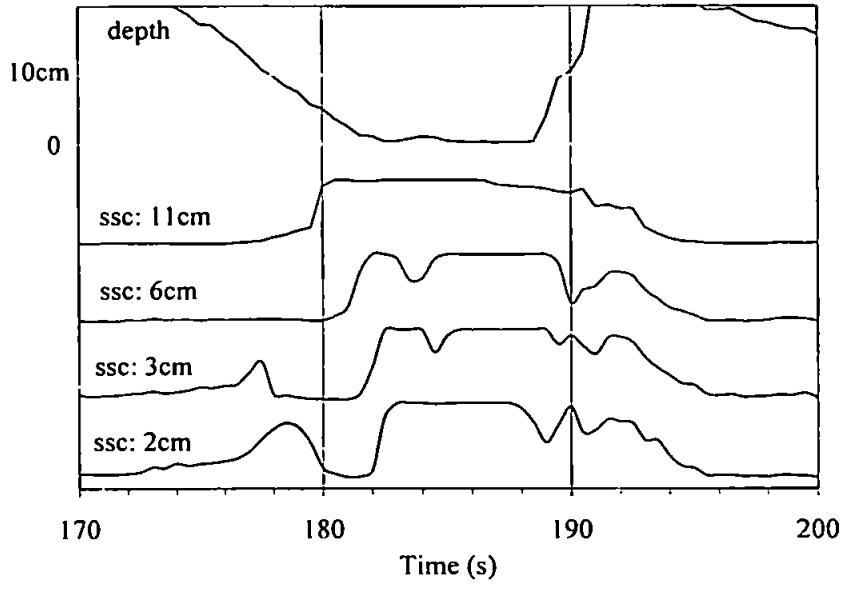

Figure 5.4: example of sediment suspension event with each MOBS sensors reaching saturated values upon drying out.

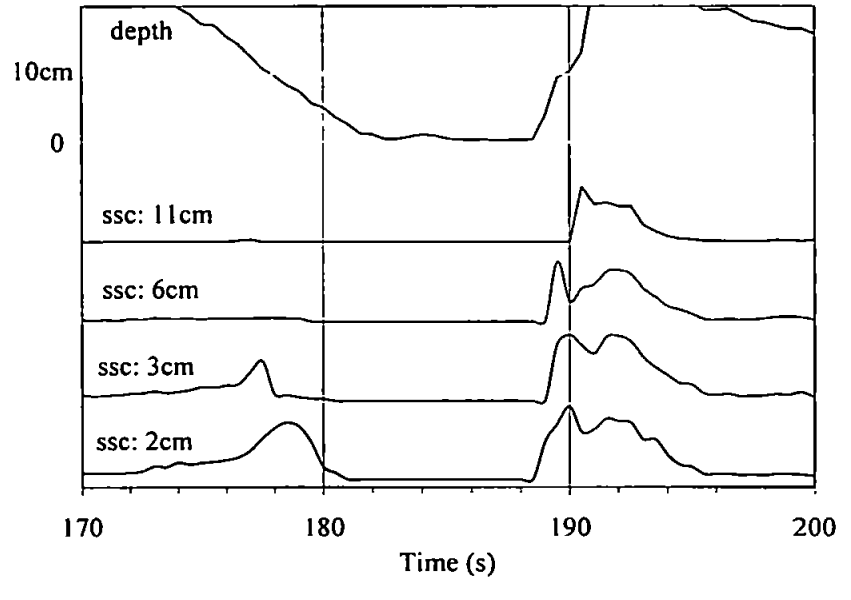

Figure 5.5: the same suspension event as that shown in figure 5.4, but this time after the MOBS outputs have been forced to zero when the sensor becomes dry.

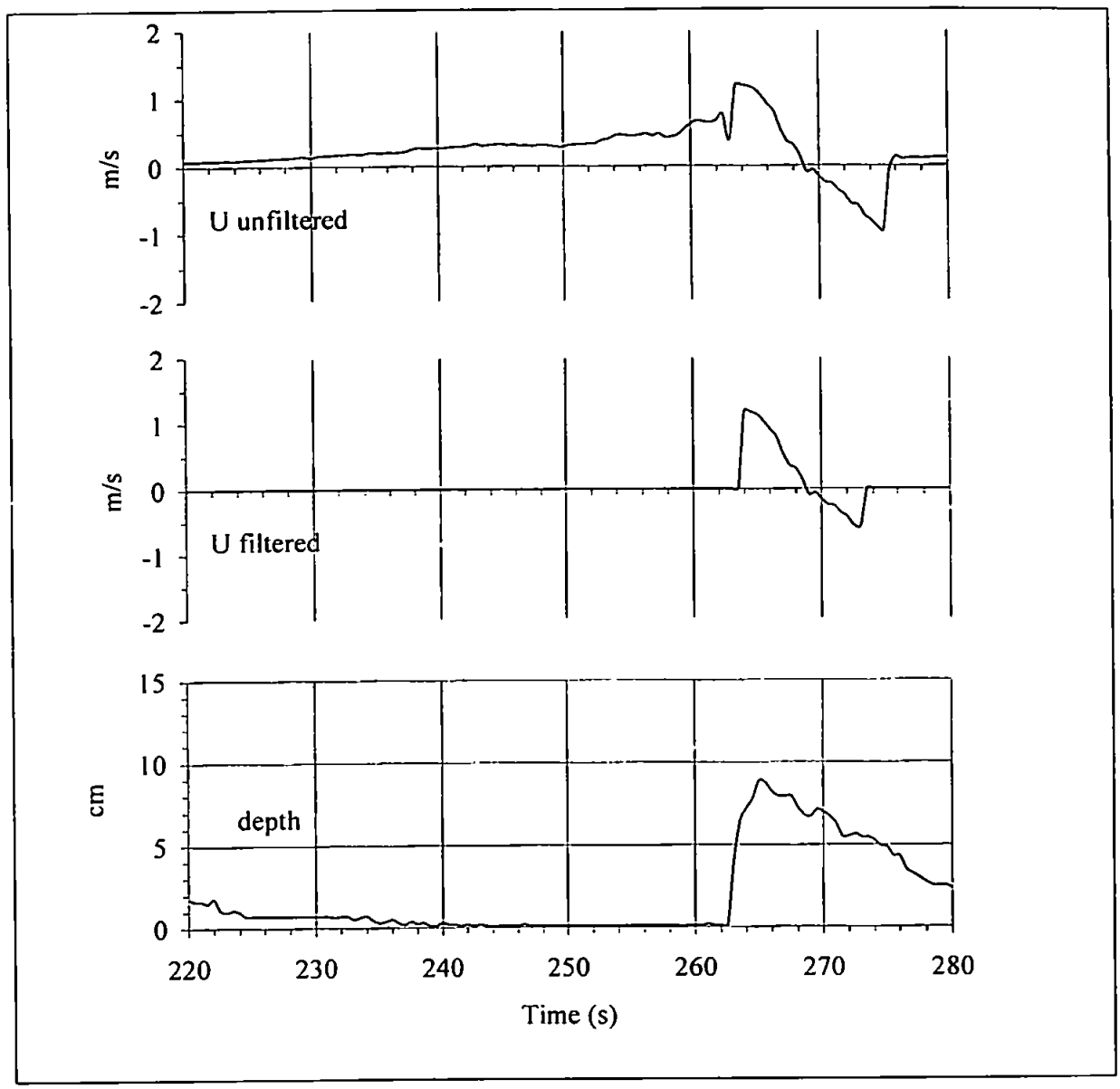

Figure 5.6: dryout filtering for the cross-shore velocity (u) from the mid swash-zone. The signal is forced to zero if the depth goes below the height of the EMCM (5cm).

5.2.4 EMCM signal clipping

The EMCMs available for the present study were factory-set to measure a maximum velocity of $1.2ms^{-1}$. For the work of Christie (1997), for which the system was originally designed, this was not a problem because the maximum velocities were less than this. However, in the swash-zone, maximum velocities up to $2ms^{-1}$ have previously been

measured in similar conditions (Beach and Sternberg, 1991; Osborne and Rooker, 1998, 1999).

The cross-shore velocities recorded as part of the present study on occasions reached values exceeding $1.2ms^{-1}$, particularly during certain large backwashes in the 'storm' time-series. At these times, the velocity trace appeared 'clipped' at $1.2ms^{-1}$, which is obviously unsatisfactory if calculations of spectra, sediment fluxes and higher-order velocity moments are to be made. Therefore, some sort of extrapolation had to be devised, which gave the best representation of the velocities expected during these backwashes, in the absence of any measured information.

A number of similar backwashes were inspected from the infragravity-dominated swash data of Beach and Sternberg (1991), and Osborne and Rooker (1999), and also from the data of Hughes *et al* (1997) and Masselink and Hughes (1998), to see if the velocity exhibited any regular features above $1.2ms^{-1}$. For example, it might be found that a regular feature of high-velocity backwashes is for the slope of the velocity to change above $1.2ms^{-1}$ (i.e. the acceleration may not be constant). Theoretical models (e.g. Shen and Meyer, 1963; Hibberd and Peregrine, 1979) suggest that the displacement of the shoreline is generally parabolic through time, hence having a constant offshore acceleration throughout the swash cycle. However, the measurement of cross-shore velocity in the mid or outer swash-zone in infragravity-dominated random wave conditions is somewhat more complicated.

For the backwashes inspected from the studies mentioned above, the average slope of the velocity above $1.2ms^{-1}$ tended to be about 20% less than that below $1.2ms^{-1}$. A few perturbations due to incident frequency oscillations embedded within the infragravity cycle were visible. However, these tended to be relatively small on the backwash compared with the uprush and their significance is probably minimal for the purposes of the proposed analyses mentioned above. Therefore, it was decided to extrapolate each 'clipped' backwash using a slope based on 80% of the average slope of the velocity during that particular backwash between zero and $1.2ms^{-1}$. An example from the 'storm' time-series is shown in figure 5.7. Note that the end of the backwash was determined by linearly back-extrapolating the backwash-uprush transition (e.g. $t \approx 964s$).

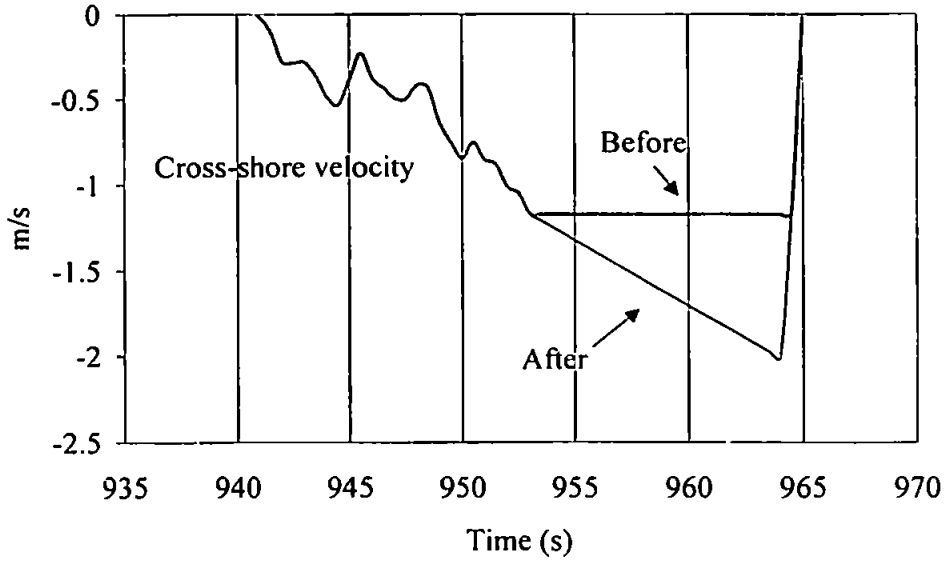

Figure 5.7: example of a large backwash 'clipped' at 1.2ms^{-1}, before and after extrapolation.

5.3 Spectral analysis

5.3.1 General

To estimate the relative contributions of the different frequency fluctuations in the measured parameters, it is necessary to shift the data from the time domain into the frequency domain. This is normally achieved using the fast Fourier transform (FFT) algorithm, which is a method of computing the discrete Fourier transform, details of which may be found in Oppenheim and Schafer (1975). The output of the FFT includes a series of sine waves up to a maximum of the Nyquist frequency (Ny). The Nyquist frequency divided by the number of estimates in the FFT is the bandwidth (Δf).

A particularly useful function is the power spectrum, which has the property that its integral over a frequency band is equal to the power of the signal in that band (Parseval's relation). The power spectrum (P_{XX}) of a signal is given by the magnitude squared of the FFT of that signal. The result is termed a periodogram.

However, without further modification, the periodogram has rather limited use, since its variance is inherently large, and this cannot be reduced by increasing the number of estimates in the FFT. The Welch method (Welch, 1967), may be used to reduce the variance of the periodogram. This is a nonparametric method, i.e. it makes no assumptions about the original data series. The data series is split into a number of equal-length segments, and the periodograms for each of these segments are computed, to provide a number of estimates of P_{XX}. The average is then taken of all the individual periodograms. Note that, to obtain the different segments, a tapered 'window' is applied to the data to ensure that the data at the ends of each segment reduce to zero. To compensate for any loss of data by the windows, they are allowed to overlap, typically by 50%.

The major disadvantage of this method is the loss of resolution, due to the reduced number of data points. The smaller the windows, the fewer data points in each, hence the lower the resolution. The frequency resolution R_F is given by:

$$R_F = 2Ny / S_W \tag{5.1}$$

where 2Ny is the sampling frequency, and S_W is the size of the window. The value of R_F must be lower than the lowest frequency of interest, e.g. if it is required to analyse infragravity waves of 100s period (0.01Hz) then R_F must be less than 0.01Hz.

To aid visual identification of any peaks on the graph, the number of data points can effectively be increased by zero padding, which interpolates between values on the graph but does not actually improve the frequency resolution in the spectral estimate.

The units of the y-axis of the periodogram are the units of the original sequence squared, for example, ms^{-1} would become m^2s^{-2}. To provide a meaningful comparison between plots obtained using different bandwidths (e.g. by different workers), the periodogram may be normalised by dividing by the bandwidth Δf. The normalised periodogram is denoted here as S_{XX}. The units in the example above would then become $m^2s^{-2}Hz^{-1}$ or m^2s^{-1}.

5.3.2 The co-spectrum

A useful function for estimating the contribution at different frequencies of the sediment transport due to the fluctuating components of velocity and SSC is the co-

spectrum, which has the property that its integral over a frequency band is equal to the total sediment transport due to fluctuating components of velocity and SSC, in that band. The co-spectrum and the quadrature spectrum are products of the cross-spectrum (P_{XY}), which is given by the product of the FFT of one signal and the complex conjugate of the other. The quadrature spectrum is the unreal part of the product, whereby the velocity and concentration are 90^0 out of phase. The co-spectrum is the real part, whereby their phase difference is 0^0 or 180^0 .

Huntley and Hanes (1987) pointed out that when large positive or negative velocity fluctuations coincide with fluctuations in SSC, the sediment is likely to be transported, whereas, if they are at different frequencies or at quadrature (when the largest suspended sediment concentrations correspond with zero velocity), then there will be no net transport since their product will average to zero over time. Therefore the appropriate function for estimating sediment flux in the frequency domain is the co-spectrum.

The units of the co-spectrum are the units of the two original sequences multiplied together, e.g. for sediment and velocity these would be (kgm^{-3}) x (ms^{-1}) = $kgm^{-2}s^{-1}$. A normalisation may be applied by dividing by Δf, the units now becoming $kgm^{-2}s^{-1}Hz^{-1}$ or kgm^{-2}.

5.3.3 Coherence-squared

This represents the fraction of the variance in one sequence ascribable to the other through a linear relationship between the first and second (Emery and Thomson, 1997). In simple terms it is a measure of how well correlated the two sequences are as a function of frequency. The coherence-squared, $C^2_{XY}(f)$, of two sequences 'X' and 'Y' at frequency f, is given by:

$$C^2_{XY}(f) = \frac{|P_{XY}(f)|^2}{P_{XX}(f)P_{YY}(f)} \qquad (5.2)$$

where $P_{XX}(f)$ and $P_{YY}(f)$ are the power spectral estimates of the two sequences, and $P_{XY}(f)$ is the co-spectral estimate, as described above.

5.3.4 Confidence

To measure the confidence in the estimate, a linear relationship exists between the number of degrees of freedom and the number of segments (windows) that the original sequence was split into, based on a 50% overlap, i.e:

$$\gamma = 3.82N_W - 3.24 \tag{5.3}$$

where γ is the number of degrees of freedom and N_W is the number of non-overlapping windows, (i.e: the length of the sequence divided by the size of the window). The number of degrees of freedom may then be related to the size of the error bars on the plot by a function such as that shown in figure 5.8. The smaller the windows, the fewer degrees of freedom, hence the larger the error bars. The size of the window must be chosen so that the best compromise is achieved between the confidence in any peaks observed, and the required frequency resolution.

A confidence limit (C^2_{lim}) must be set for the coherence-squared estimates. This is the limit below which the coherence-squared values can occur by chance. Therefore for frequencies at which the coherence-squared is below this limit, any co-spectral estimates would be unreliable. This may be computed from

$$C^2_{lim} = 1 - \vartheta^{1/(0.5\gamma-1)} \tag{5.4}$$

where ϑ is the significance level (e.g. for 95% confidence, $\vartheta = 0.05$) and γ is the number of degrees of freedom (Thompson, 1979). For example, with 27 degrees of freedom, the 95% coherence-squared confidence limit would be 0.2.

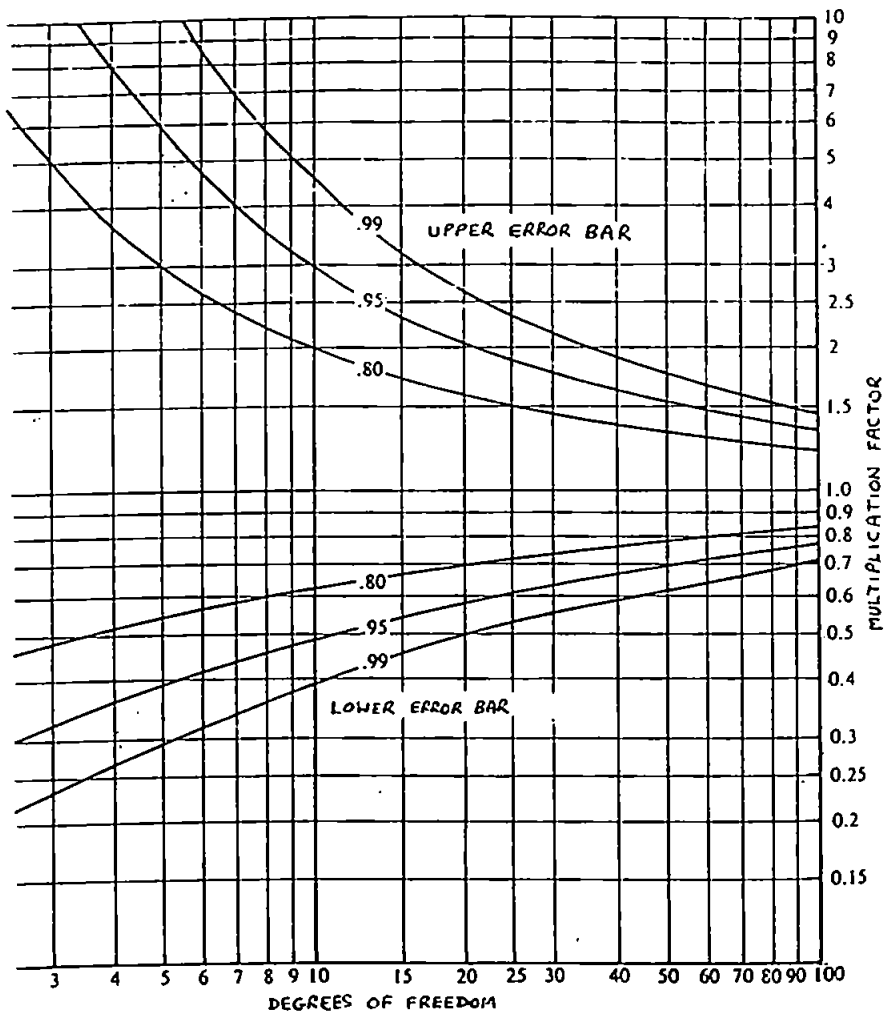

Figure 5.8: relationship between the peak spectral multiplication factors to obtain upper and lower limits of error bars, and the number of degrees of freedom for confidence limits 80% ,95% and 99%, which is in turn related to the size of the windows. (After Jenkins and Watts, 1968).

5.3.5 Obtaining the total variance

The total variance in a time-series may be computed in the frequency domain by summing the values in the periodogram (P_{XX}), which is equivalent to integrating under the normalised periodogram (S_{XX}). For example, the total variance (σ^2) for a velocity time-series [m^2s^{-2}] would be given by

$$\sigma^2 = \sum_{1}^{N} S_{XX}\Delta f \tag{5.5}$$

where Δf is the bandwidth, or frequency increment between estimates, and N is the number of estimates between zero and the Nyquist frequency. To obtain variance over a limited frequency range, then the integral is taken over that range. This is useful, for example, in discriminating between the transport associated with infragravity and incident band fluctuations.

5.3.6 Matlab

Available within Matlab is a program (called 'spectrum') which automatically plots the periodogram using the Welch method. A Hanning type window is used, whose length may be specified by the user, together with the number of data points per window (automatic zero padding is provided if this is longer than the window length). The user inputs the sampling rate, and the x-axis is scaled to real frequency. Note that the data is also automatically de-trended. Various outputs are available from 'spectrum' including autospectra, cross-spectra and coherence and phase.

To obtain the normalised periodogram (S_{XX}), 'spectrum' has been written such that its output (P_{XXM}) must be divided by the Nyquist frequency (Miles, 1997), i.e:

$$S_{XX} = P_{XXM} / Ny \tag{5.6}$$

However, since the bandwidth Δf may also be expressed as:

$$\Delta f = Ny / N \tag{5.7}$$

where N is the number of estimates from zero to Ny, then from (5.5),

$$\sigma^2 = \frac{1}{N}\sum_{1}^{N} P_{XXM} \tag{5.6}$$

5.3.7 Summary

The three-way compromise between stationarity, spectral resolution and confidence may be summarised by looking at the values in the present study as an example. Before any spectral analysis is applied, it is usually known how long the time-series can be before stationarity starts to become affected, and also the lowest frequency of interest which must be resolved.

- Let the lowest frequency of interest (R_F) be 0.01Hz, for infragravity waves of up to 100s to be resolved. Hence from equation (5.1), if Ny = 1Hz then the minimum window size (S_w) to resolve this frequency is 200 data points.
- The maximum length of time-series without affecting stationarity has already been fixed at 17 min. (= 2048 points at 2Hz).
- The maximum number of non-overlapping windows (N_w) of $S_w \geq 200$ which will fit into a series of length 2048 is 8 windows of 256 points.
- Using equation (5.3) and figure 5.8, with $N_w = 8$, the number of degrees of freedom is 27, giving upper and lower error bounds of 170% and 63% respectively at the 95% confidence level.
- With $S_w = 256$ the spectral resolution (from equation 5.1) is 0.0078Hz.
- Since overlapping windows are desirable, 16 Hanning windows with 50% overlap are used.
- To improve the appearance of the plots, zero padding is used to increase the number of points to four times the window length (i.e. 1024 points). This will have the effect of extending the lower end of the plots down to 0.002Hz.

Spectral analysis is performed at various stages throughout the thesis using the criteria specified above. The calculation of the co-spectrum, phase spectrum and coherence is similar to the autospectrum, and therefore only brief details are given here. A more comprehensive review of the theory behind these spectra, relevant to studies similar to the present one, is given by Miles (1997).

6. Results

6.1 Overview

In this chapter are presented the full 17-minute sets of time-series which will be used for subsequent detailed analysis. This data has already been pre-processed as detailed in section 5.2, which includes (a) re-sampling at 2Hz, (b) 'dryout filtering' for the velocity and SSC time-series, and (c) extrapolation above $1.2ms^{-1}$ for the velocities.

Note that, since detailed analysis is made of the cross-shore rather than longshore velocity, any reference to velocity in the thesis will be assumed cross-shore unless otherwise stated. A brief inspection of the longshore velocities is presented in section 6.3 .

The time-series shown for each data burst are water depth [cm], cross-shore velocity (u) [ms^{-1}], longshore velocity (v) [ms^{-1}] and SSC at four heights above the bed [gl^{-1}]. For the 'mid-swash' data burst, sub-surface pore-pressure (p) [hPa] is also shown at four levels below the bed. For the longshore velocity, north is positive. The data bursts shown are listed in table 6.1.

Table 6.1: data bursts shown herein.

Burst	Figure
Calm	6.1
Transect 1	6.2
Transect 2	6.3
Transect 3	6.4
Mid-swash	6.5
Storm	6.6

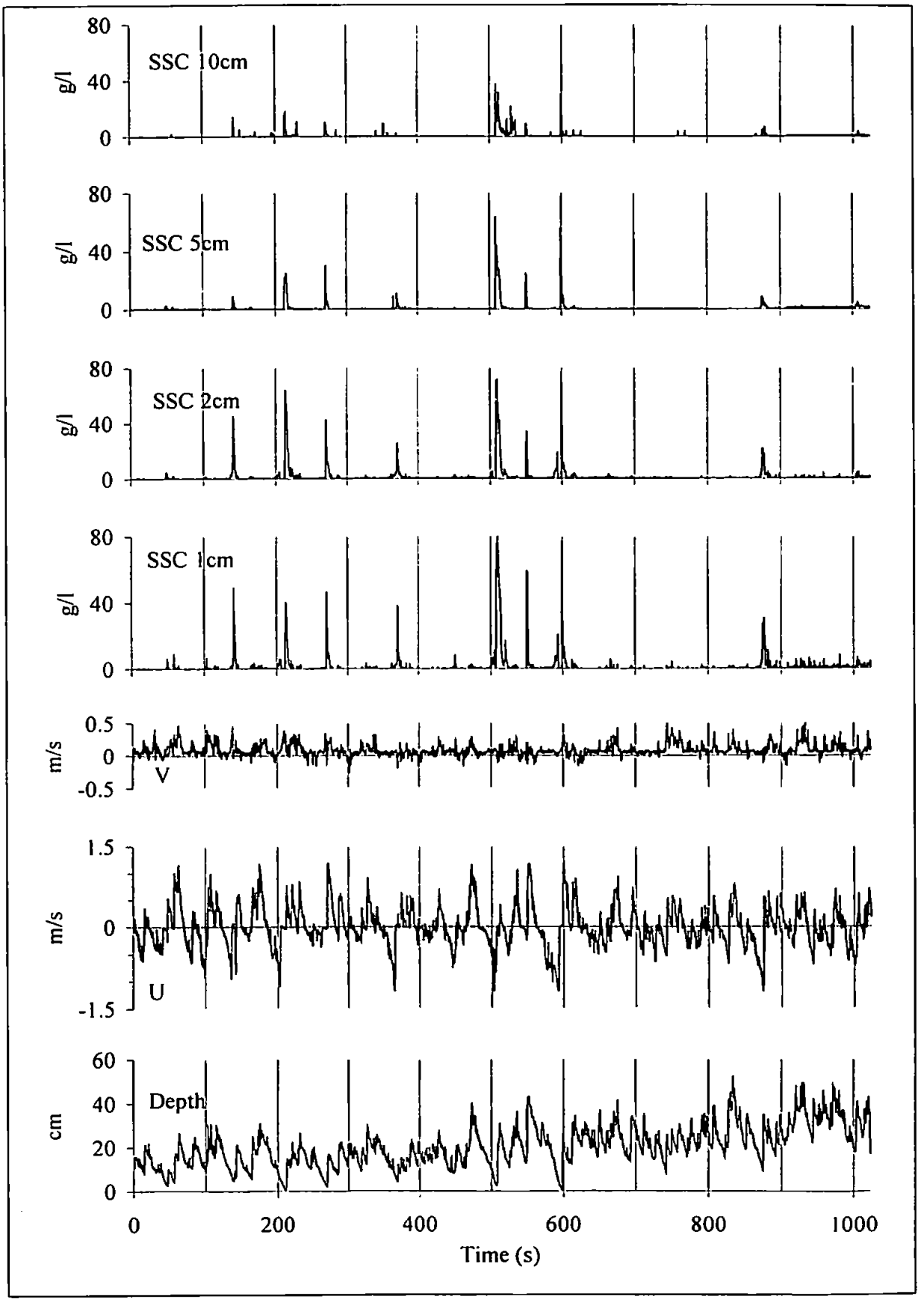

Figure 6.1: calm time-series.

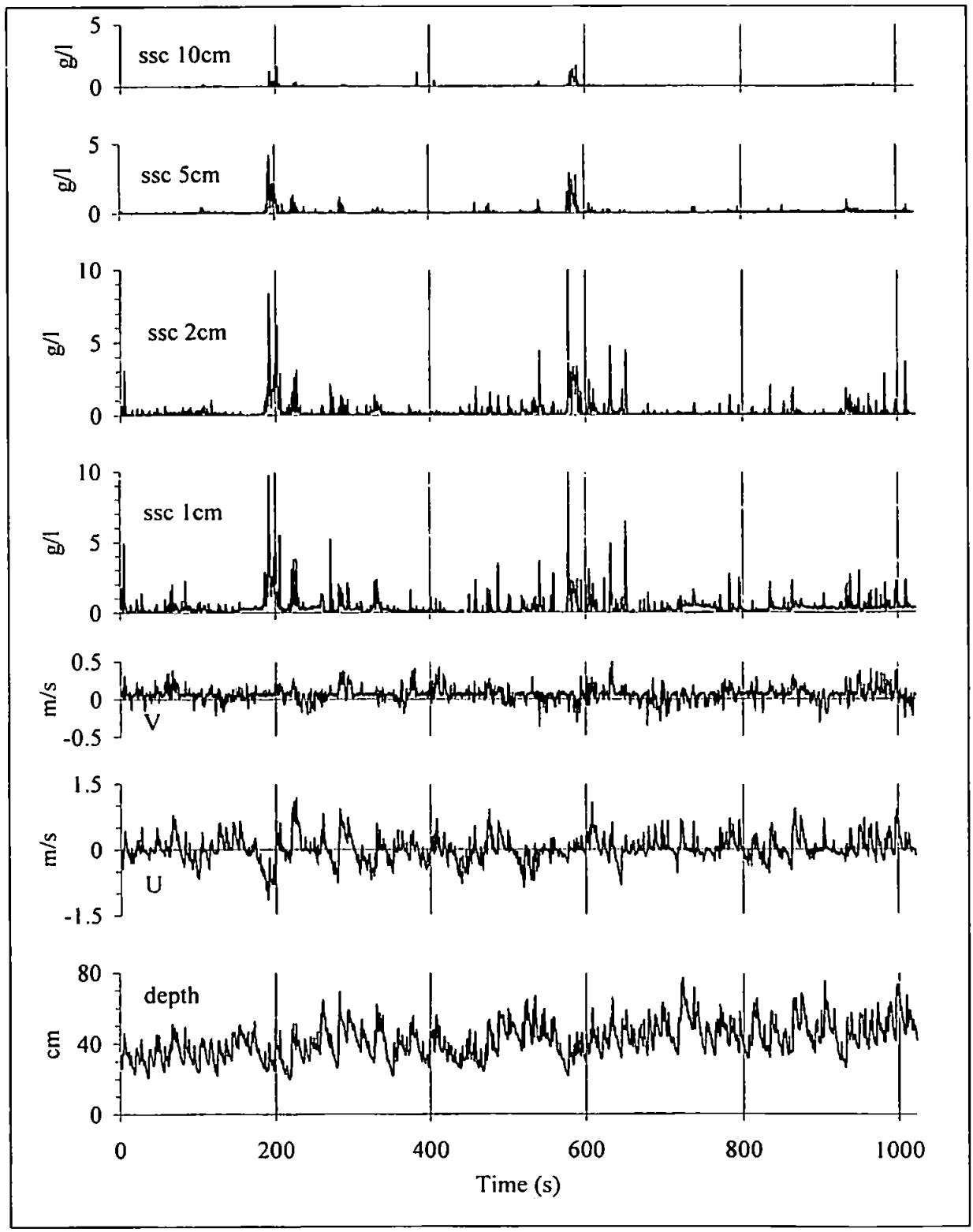

Figure 6.2: transect 1 time-series.

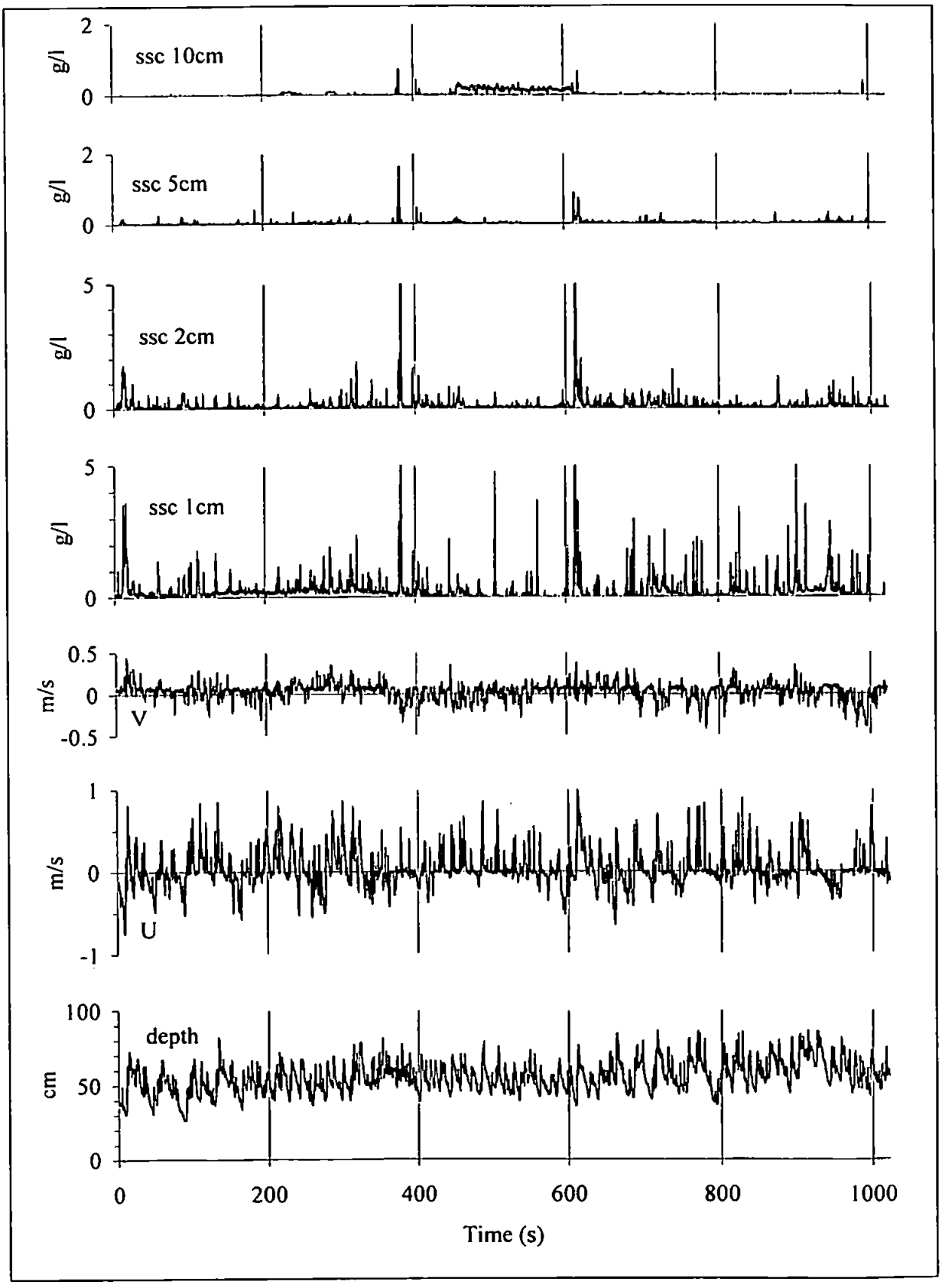

Figure 6.3: transect2 time-series.

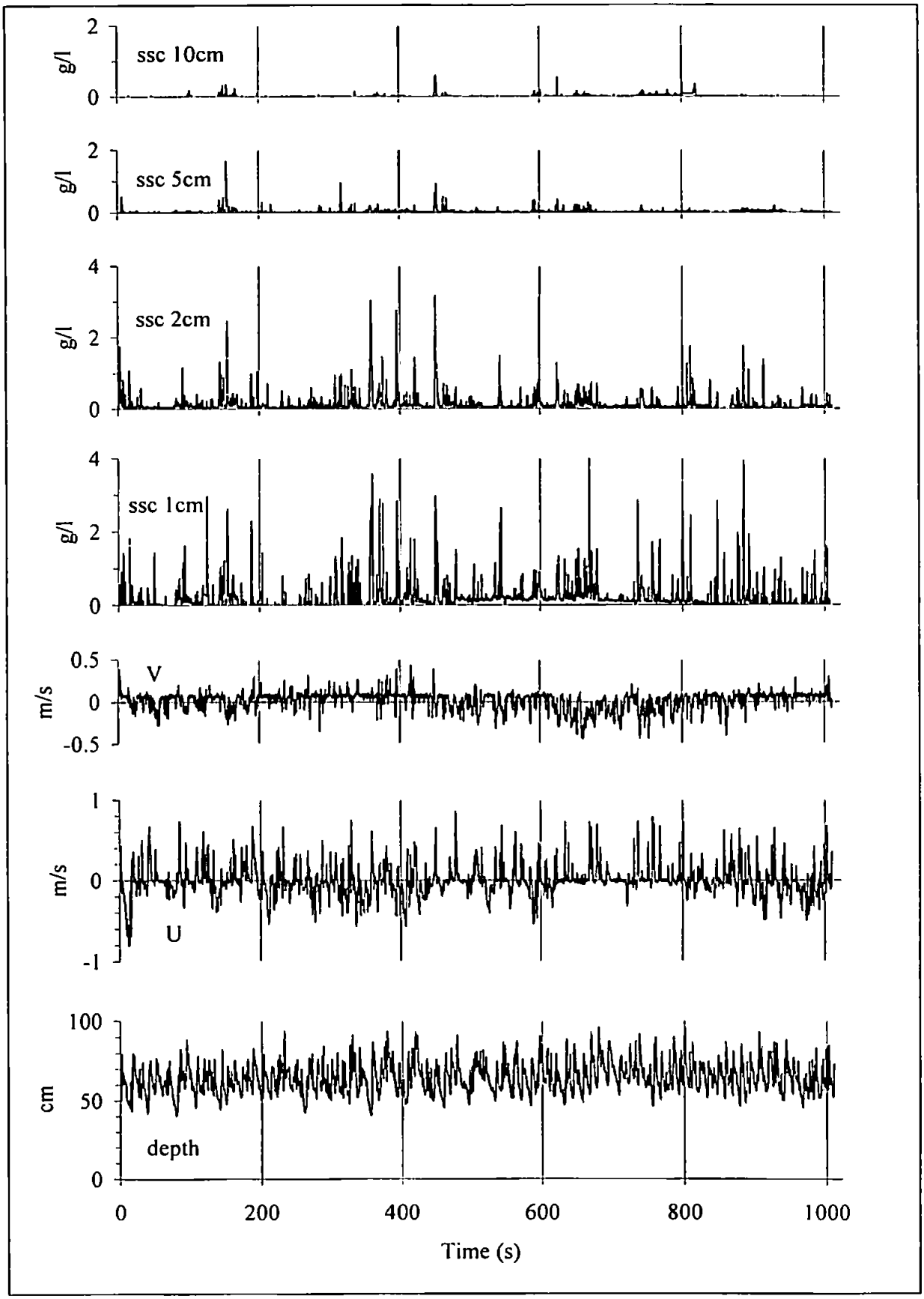

Figure 6.4: transect 3 time-series.

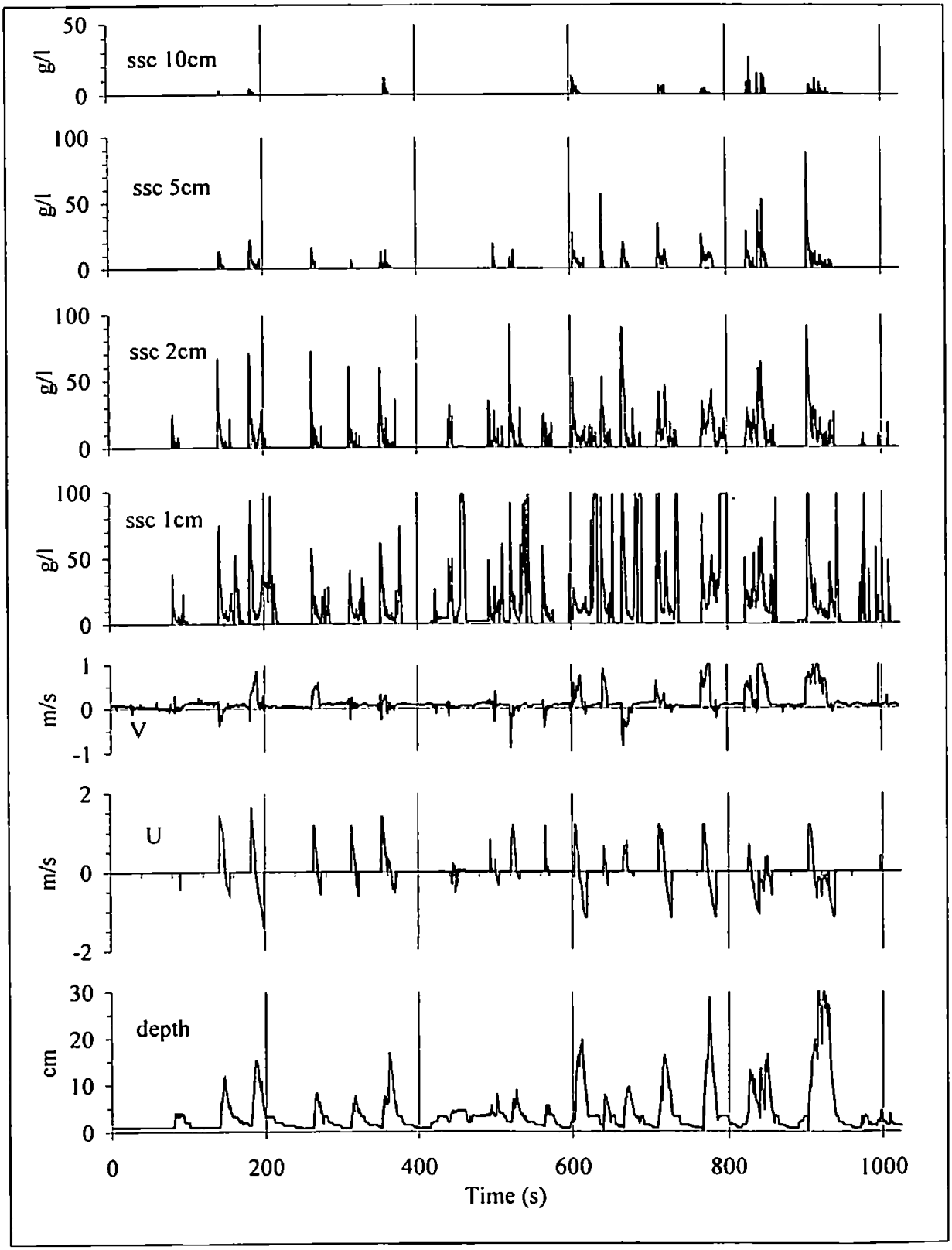

Figure 6.5a: mid-swash time series (1).

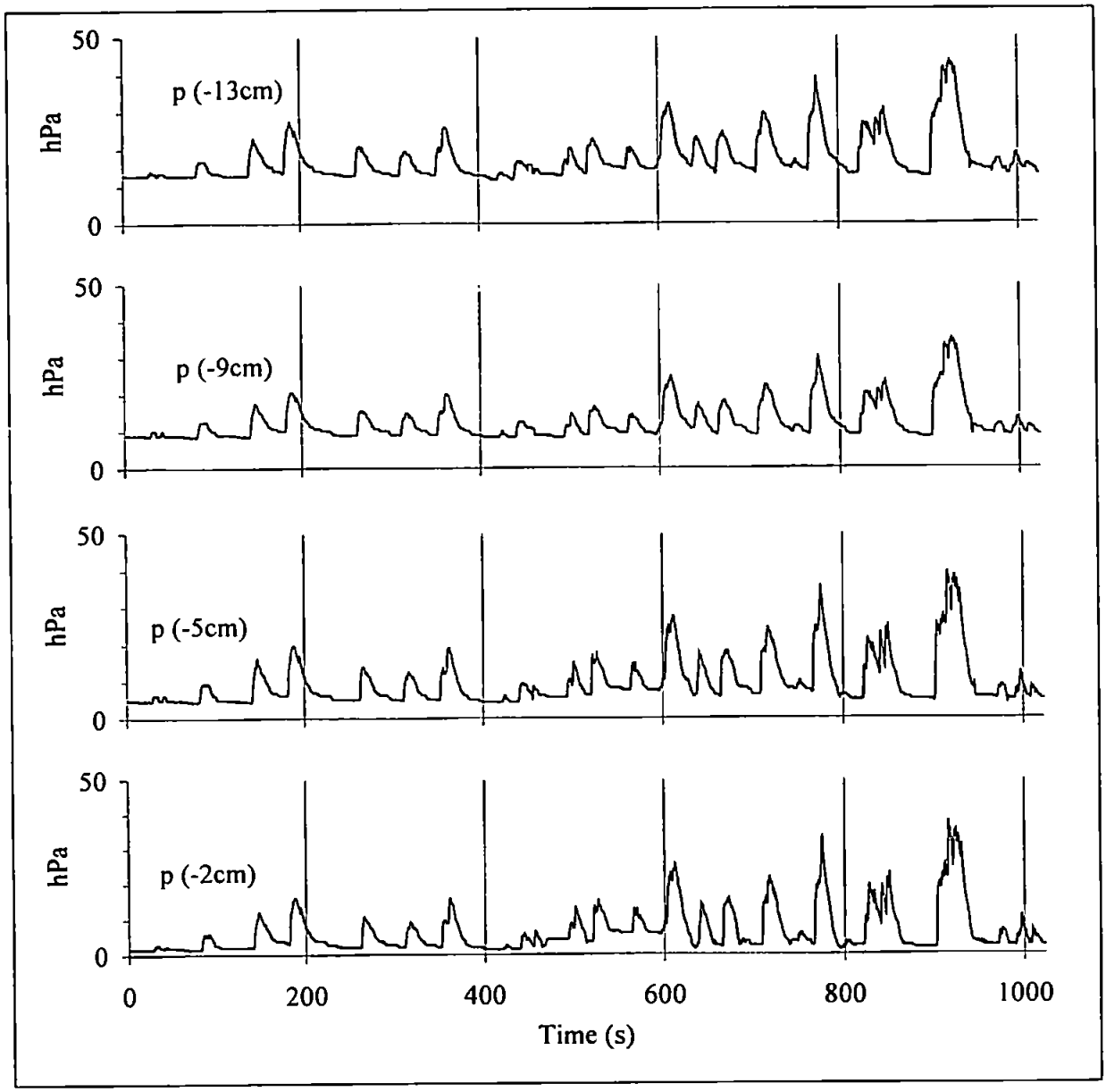

Figure 6.5b: mid-swash time-series (2).

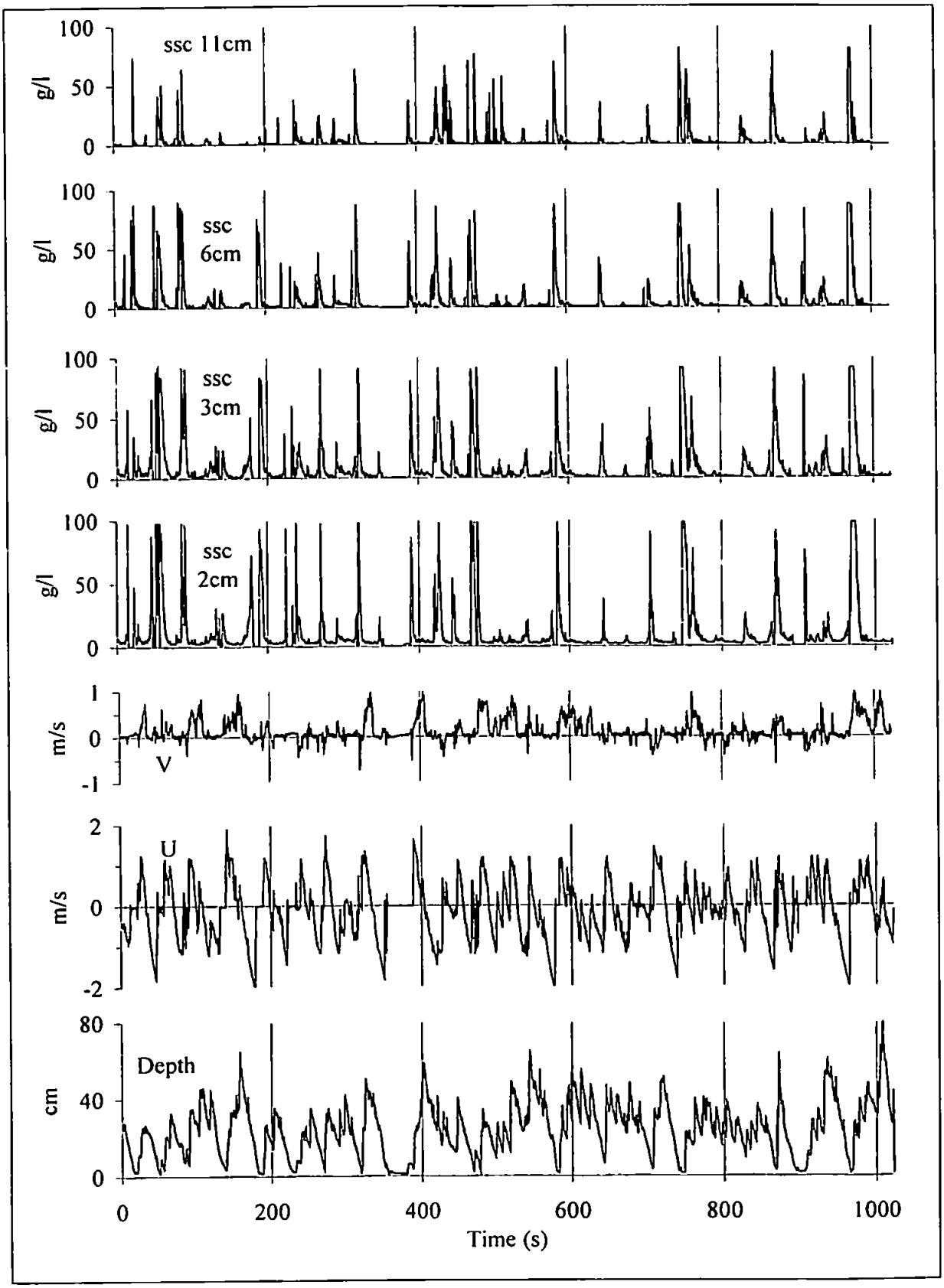

Figure 6.6: storm time-series.

6.2 Observations

The following basic observations may be made from preliminary inspection of the time-series in figures 6.1 to 6.6:

- There is a significant increase in energy for the storm day over the calm day.
- The velocity and depth time-series consist of short-period oscillations of about 6 to 8s period embedded within long-period (infragravity) oscillations of about 30 to 50s period.
- The velocity time-series exhibits a 'sawtooth' form, with high onshore and lower offshore accelerations. This effect increases towards the shore.
- Backwash velocities appear to be higher than uprush velocities, especially in storm time-series and at infragravity frequencies.
- Longshore velocities are generally less than half the magnitude of cross-shore velocities.
- Sediment suspension occurs in short 'events'. These were first observed by Sutherland (1967), and are now commonly observed in suspended sediment studies.
- The largest sediment suspension 'events' occur at infragravity frequencies.
- Suspended sediment concentrations are generally higher at lower levels in the water-column.
- Suspended sediment concentrations increase dramatically towards the shore.
- Sub-surface pore-pressures tend to follow the instantaneous water depth.

6.3 Note on longshore velocities

The present study is principally concerned with the cross-shore transport of sediment in the swash-zone, which requires measurements of cross-shore velocity. To assess whether the longshore velocities are of significant importance, a simple comparison of magnitudes can be made, and an assessment of how the relative magnitudes change from the calm to the storm days. However, it must be stressed that detailed analysis of longshore mechanisms are beyond the scope of the present study.

The time series in figures 6.1 and 6.6 show that the longshore velocities are generally lower than the cross-shore velocities. Also, for both the calm and storm data, there appear to be higher positive than negative longshore velocities. To highlight these

differences, the total variance for each time-series was computed (using the frequency domain method described in section 5.3.5), together with the average longshore current, results of which are shown in table 6.2.

The velocity variances in the cross-shore are roughly an order of magnitude larger than those in the longshore, for both the calm and the storm data. The average longshore velocities also confirm that the longshore velocities happened to be more northerly-directed on both days.

Another interesting point is that, especially for the storm data, the largest longshore velocities tend to occur at the run-up limit (when the cross-shore velocity is small). This can be observed visually in the swash-zone, where there appear to be larger amounts of longshore drifting at the 'slack' part of the uprush-backwash cycle.

Table 6.2: comparison of cross-shore (u) and longshore (v) velocities. Positive longshore velocities are towards the north.

	u variance [m^2s^{-2}]	v variance [m^2s^{-2}]	Variance ratio	$\langle v \rangle$ [ms^{-1}]
Calm	77.2	8.2	9.4	+ 0.081
Storm	233	22.5	10.4	+ 0.102

7. Preliminary analysis

7.1 Overview

This chapter is concerned with performing certain 'standard' analyses on the data as a basis for the more advanced study, relating to specific sediment transport processes, undertaken in chapters 8, 9 and 10. In the first two sections, the hydrodynamics and SSC data are inspected and compared with results from other workers. The third section introduces velocity data from another, similar, experiment, where 3D velocities were obtained using an ADV, as a basis for useful comparisons made between results of the two studies. The fourth section is concerned with examining the characteristics of a single, representative, swash cycle using the method of ensembles. This is useful for comparing velocity-SSC phase relationships within the swash cycle (*c.f.* Osborne and Rooker, 1999).

7.2 Preliminary analysis of hydrodynamics

7.2.1 Introduction

In this section is presented a preliminary look at the hydrodynamic behaviour in the swash-zone, based around the variation of velocity and surface elevation with frequency. Surface elevation, in this context, is the de-meaned instantaneous depth. Note that the mid-swash data burst was not included in this analysis due to the discontinuous nature of the time-series.

The first part compares the velocity and surface elevation autospectra in low and high energy conditions (from the calm and storm data bursts), and looks at how the infragravity and incident band variance change with changing conditions. The autospectra are plotted on a log-log scale so that the high frequency saturated roll-off can be compared with theoretical values and that obtained by other workers.

A series of spectra is then presented from the 'transect' data bursts, to compare the behaviour of velocity and surface elevation from just shoreward of the break point, to the outer part of the swash-zone, in low energy conditions. The variation of incident and infragravity variance with depth (i.e. distance from the shoreline) is examined.

Lastly, a comparison of the phase between velocity and surface elevation at infragravity frequencies and that at incident frequencies, is made, in the time and frequency domains, using data from the storm burst. It has been suggested that the infragravity wave-field should be near standing due to reflection and subsequent interaction with the incoming waves, but the incident wave-field mostly progressive due to dissipation through breaking.

7.2.2 Comparison of spectra for calm and storm days

Autospectral curves for the calm and storm swash-zone velocity and surface elevation time-series are shown in figure 7.1. The total variance for frequencies either side of 0.05Hz (20s period), was calculated by integrating under the spectral curve (see section 5.3.5). These variances are shown in table 7.1. To obtain the frequency division, no obvious spectral valley was visible on the autospectra due to the broad-banded nature of the incident wave field (see below). The main infragravity peak appeared to be at about 40 to 50s and the visually observed incident wave period about 8s, therefore a frequency division of 20s was considered reasonable.

Comparing the calm and storm autospectra, the following points may be noted:

- There is a large infragravity peak at around 0.02Hz (50s period) on all the curves. Interestingly, the infragravity peak for the calm time-series is at a slightly lower frequency than that for the storm time-series.
- There is a second peak at the first harmonic of the main infragravity peak, although the confidence limits mean that the existence of this peak cannot be certain. Energy in the harmonics is associated with nonlinearities of the waveform generated through the shoaling process, and it appears that the first harmonic is making a major contribution. This peak appears to be larger for the calm data than for the storm data, relative to the main peak.
- The velocity and surface elevation spectra show saturation at incident frequencies, with a region above about 0.2Hz where energy decreases with frequency. The velocity shows an approximate $f^{5/3}$ roll-off (i.e. $E \alpha f^{5/3}$) which is consistent with theory relating to the turbulent dissipation of energy at high frequencies (e.g. Stapleton, 1996). The surface elevation shows a roll-off of $f^{5/2}$, which differs from that obtained by other workers who measured shoreline run-up height using photographic methods, video and

run-up wires. For example Huntley *et al* (1977), Mase (1988) and Raubenheimer and Guza, (1996) obtained f^{-4}; whereas Guza and Thornton (1982) and Ruessink (1998) obtained f^{-3}. It must be borne in mind that these time-series were necessarily taken from the outer part of the swash-zone using a pressure transducer, and therefore are likely to be different from those taken at the shoreline.

- The variance around the visually observed incident wave period ($\approx$ 8s), is rather broad-banded, confirming the presence of a large amount of locally generated windsea. This is in contrast to many previous studies where the wave field is largely bi-modal, and a distinct spectral valley can be seen (e.g. Holland *et al*, 1995; Raubenheimer *et al*, 1995).
- The variance calculations for both velocity and surface elevation show that, from the calm day to the storm day, there is an approximate three-fold increase in the total energy and an approximate four-fold increase in the infragravity band energy. For the calm day there is approximately 2.3 times as much energy in the low frequency than the high frequency band, and for the storm day, this ratio increases to about 3.5.

Table 7.1: total variances computed from the velocity and surface elevation autospectra. High and low frequency variances are $f > 0.05$Hz and $f < 0.05$Hz respectively.

		Total variance	High freq. variance	Low freq. variance
Velocity [m^2s^{-2}]	calm	77.3	23.5	53.8
	storm	262.1	63.5	198.6
	ratio	3.39	2.71	3.88
Surface elevation [m^2]	calm	2.31	0.69	1.62
	storm	8.3	1.86	6.74
	ratio	3.59	2.68	4.17

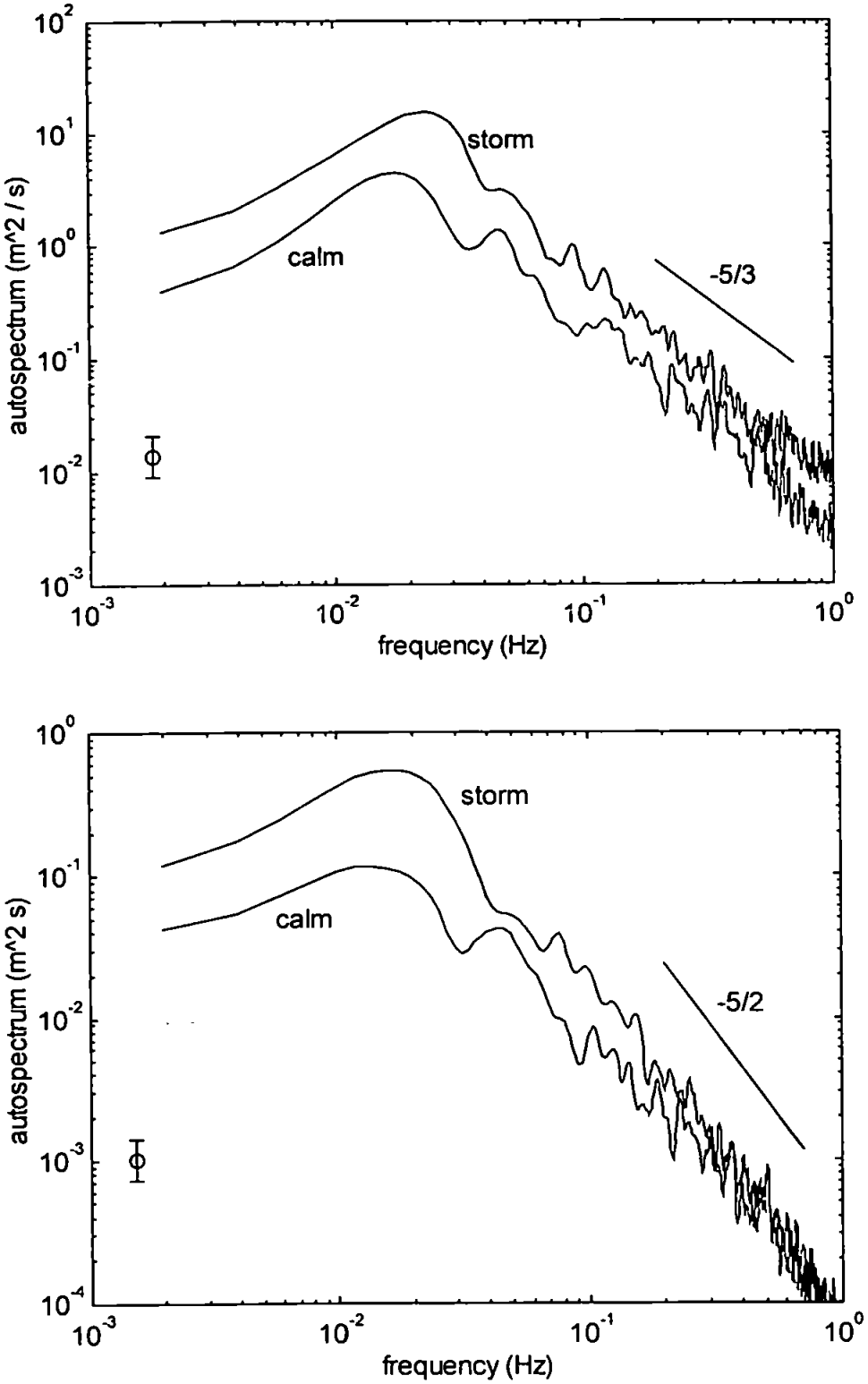

Figure 7.1: normalised velocity (top panel) and surface elevation (bottom panel) autospectra for calm and storm days. The error bar represents 27 degrees of freedom at the 95% confidence level.

7.2.3 Comparison of spectra from cross-shore transect

Velocity and surface elevation autospectra for a cross-shore transect of four data bursts are shown in figure 7.2. The most shoreward data burst in the transect was that used for the calm data, and the other three were recorded in progressively deeper water as the tide advected over the instrument site.

Each spectrum has a particular value of mean depth over breaker depth (h/h_b), associated with it, which gives an indication of the cross-shore position within the surf-zone. Mean depth for each data burst was calculated from the pressure records, and the breaker depth was approximated using $H_b/h_b = 0.78$, (where H_b is breaker height), which is commonly thought to be adequate for dissipative surf-zones containing spilling breakers (e.g. Bowen *et al*, 1968; Longuet-Higgins, 1970). For all data bursts in the transect, $H_b \approx$ 0.8m, therefore $h_b \approx$ 1m. Therefore, all the data were taken from inside the breakpoint. Unfortunately no data were available between $h/h_b = 0.64$ and the breakpoint.

From figure 7.2 it can be seen that all spectra are dominated by an infragravity peak at about 0.02Hz (50s period). This peak generally grows towards the shoreline. Also visible is a peak at the first harmonic, whose size relative to the main peak increases shoreward. The ratio between the approximate size of the main and first harmonic peaks increases from 1.2 at the most seaward location to 2.0 at the most shoreward location for the surface elevation. Similarly, for the velocity, this ratio goes from 1.5 to 3.4. The increased generation of harmonics with decreasing depth is due to the increasing nonlinearity of the waveform through shoaling (e.g. Elgar and Guza, 1985; Elgar *et al*, 1988). Note that most of the harmonic energy appears to be in the first harmonic. Nonlinearites of the wave-field are discussed more fully in chapter 8.

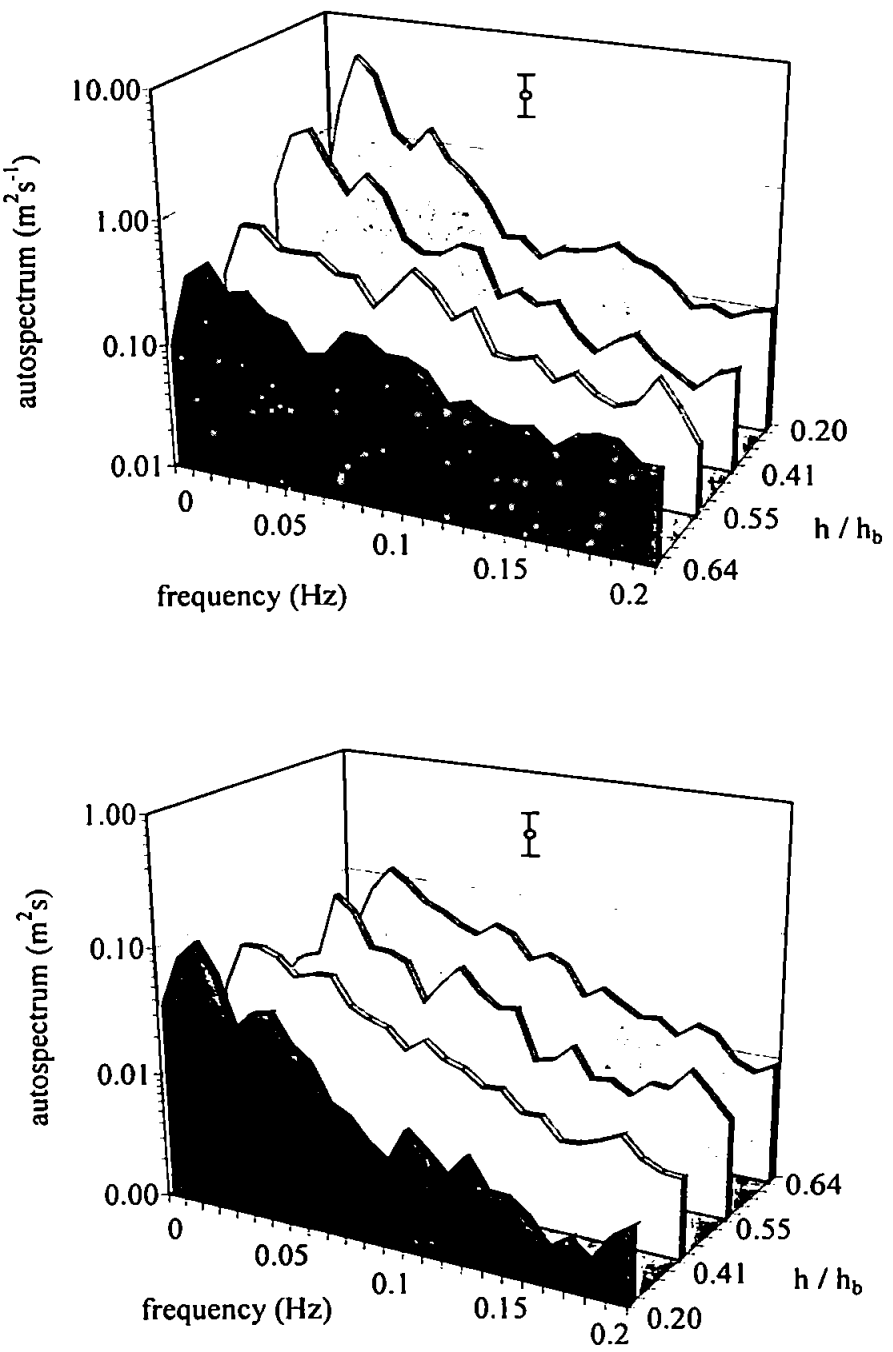

Figure 7.2: cross-shore profile of normalised velocity (top panel) and surface elevation (bottom panel) autospectra. The error bar represents 27 degrees of freedom at the 95% confidence level.

The total variance for frequencies lower than 0.05Hz and for frequencies between 0.05Hz and 0.5Hz, was calculated by integrating under the spectral curve in the same way as that above for the calm and storm spectra comparison. These variances were then plotted against h/h_b for the velocity and surface elevation (see figure 7.3).

From figure 7.3 it can be seen that the low frequency energy tends to increase shoreward, especially from $h/h_b = 0.41$. More importantly, it can be seen that the wave field becomes increasingly infragravity dominated towards the shoreline, with the ratio between low and high frequency energy increasing from about 0.6 at the most seaward location to about 2.3 at the most shoreward location, for both velocity and surface elevation. The incident waves are dissipated through breaking, but the infragravity waves continue through to the shoreline (e.g. Huntley and Bowen, 1973; Huntley, 1976; Huntley *et al*, 1981; Oltman-shay and Guza, 1987, and many others).

The infragravity waves may become trapped as edge waves, but the 'leaky' (untrapped) waves interact with the incoming waves to produce a complex structure of nodes and antinodes (e.g. Suhayda, 1972, 1974; Sasaki and Horikawa, 1978; Guza and Thornton, 1985, and others). On a beach of linear slope, the offshore location of nodes and antinodes of a purely standing wave field varies as the inverse square of the frequency (Huntley *et al*, 1993). Note that this complex structure may affect the exact ratios between infragravity variances at each cross-shore location. However, the main purpose of this section is merely to show that the wave-field becomes increasingly infragravity dominated towards the shore. It must be remembered that the cross-shore transect of measurements was obtained by allowing the tide to advect over the instruments. To describe the cross-shore nodal structure would require a stationary set of concurrent velocity and pressure measurements from a cross-shore array of instruments.

It can also be seen that the ratio between velocity variance and surface elevation variance increases towards the shore. This is consistent with the results of Guza and Thornton (1985) who found a more rapid seaward decay of the infragravity velocity field, compared with the surface elevation field.

This may also be explained simply using the relationship between velocity and surface elevation derived from linear theory (see e.g. Miles, 1997 for a full derivation). The instantaneous surface elevation (η) may be expressed as

$$\eta = u\sqrt{\frac{h}{g}} \tag{7.1}$$

where u is the instantaneous cross-shore velocity, g is gravity and h is the average water depth. Re-arranging:

$$\frac{u}{\eta} = \sqrt{g}\frac{1}{\sqrt{h}} \tag{7.2}$$

Therefore it is easy to see that the ratio between velocity and surface elevation increases with decreasing average water depth (i.e. towards the shore):

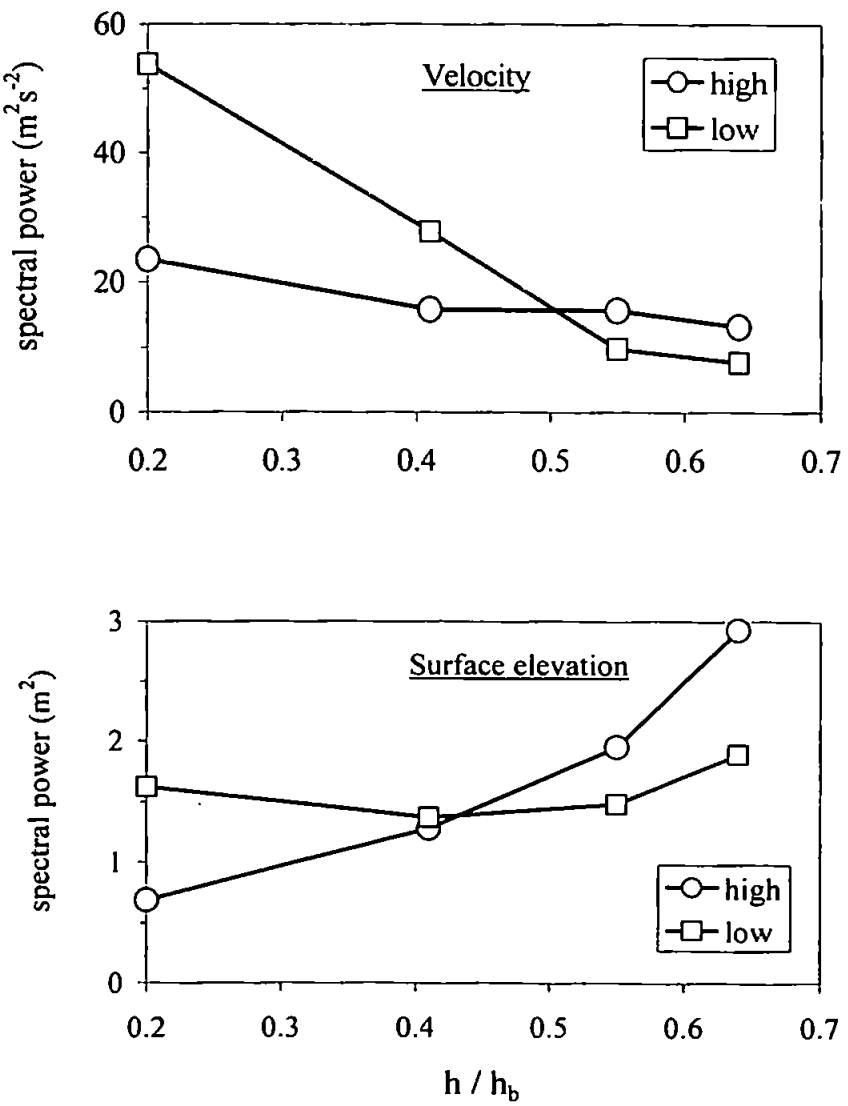

Figure 7.3: cross-shore profile of total high and low frequency variance for velocity (top panel) and surface elevation (bottom panel). High and low frequency bands are f > 0.05Hz and f < 0.05Hz respectively.

7.2.4 Frequency dependent velocity and surface elevation phase difference

In infragravity dominated conditions, the infragravity wave field in the inner surf zone is often standing, with the surface elevation and cross-shore velocity exhibiting a 90^0 phase difference (Suhayda, 1972, 1974), due to interaction between the reflected and incoming components of the infragravity wave. On the other hand, the incident waves dissipate through breaking, and do not get reflected from the shoreline. Therefore the incident wave field should be progressive.

To investigate the above hypothesis using the data available in the present study, the storm time-series of velocity and instantaneous depth are shown, together with the same time-series filtered to include frequencies above 0.05Hz only (figure 7.4). Various zero down-crossings of the velocity, (where the swash cycle is at the end of the uprush and the start of the backwash), are used as reference points to visualise the velocity-surface elevation phase relationship.

Inspection of the infragravity-scale swash cycles ($T \approx 40s$) in the non-filtered time-series shows that, at $t \approx 35$, 70, 110, 160, 205, 255 and 280s, the depth is near a maximum at or just before the run-up limit, i.e. when the velocity goes from uprush to backwash. In other words the velocity is leading the surface elevation by just under a quarter of a cycle (90^0). On the other hand, the high-pass filtered time-series shows the velocity and surface elevations to be mostly in phase. However, due to the broad-banded nature of the incident wave field during the present study, this interpretation is somewhat less certain.

To investigate further the above observations, the velocity-surface elevation phase spectrum has also been plotted, together with the surface elevation autospectrum and the coherence spectrum (figure 7.5). The spectral computations were made so that a positive phase indicates velocity leading surface elevation.

It can be seen that the velocity and surface elevation are highly coherent in the infragravity band. The phase is $+70^0$ at the frequency of the main infragravity peak, which suggests that, at that frequency, the velocity is leading the surface elevation by 70^0. Therefore the infragravity wave field must be near standing, although still partly progressive with a small onshore component (if, for example, the phase were between 90^0 and 180^0 then the wave field would be partly standing and partly offshore-directed). At the observed incident wave period of 8s (0.125hz), the phase is near-zero, suggesting that the incident waves are progressive at this frequency.

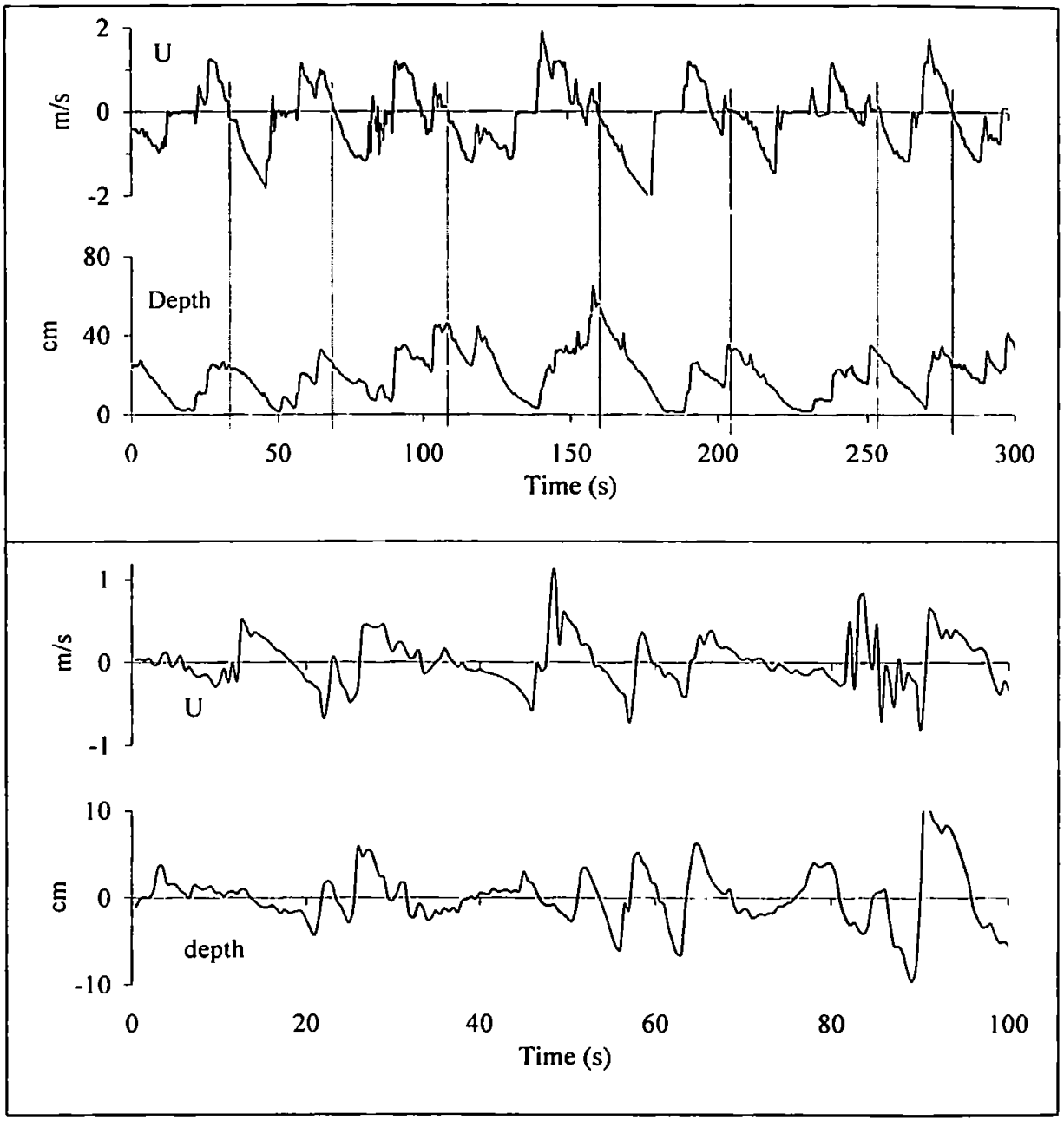

Figure 7.4: section of velocity and depth time-series from storm data to illustrate phase difference. Top panel is unfiltered and bottom panel is high-pass filtered at 0.05Hz. Note different time scales.

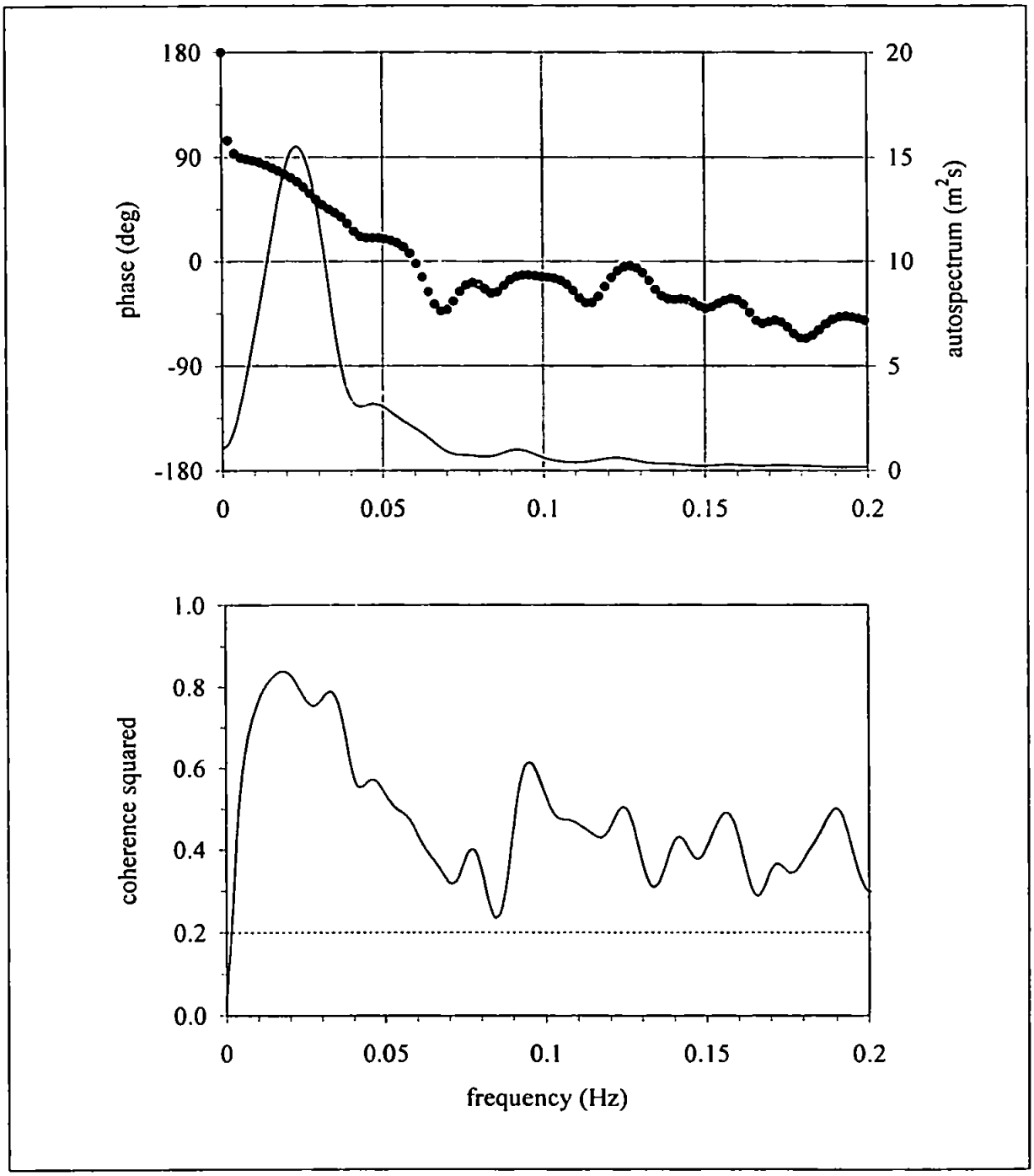

Figure 7.5: upper panel: normalised surface elevation autospectrum (solid line) and velocity-surface elevation phase spectrum (dots) for storm data. Lower panel: velocity and surface elevation coherence spectrum. The dotted line on the coherence plot is the 95% confidence limit.

7.2.5 Summary

Important points observed in this section from preliminary analysis of the hydrodynamics are as follows:

- The spectra show that the wave field is infragravity dominated for all data bursts, with a large peak at about 0.02 to 0.025Hz (40 to 50s).
- The incident wave-field was broad-banded throughout the experiment, with no distinct peaks, although visual observations indicated the approximate incident period to be 7 to 8s.
- The region above about 0.2Hz (5s) is saturated, with the spectra showing a decrease in energy with frequency.
- Variance calculations show that the increase in energy from calm to storm conditions is greater at infragravity frequencies.
- Variance calculations for the cross-shore transect of measurements show that the wave field becomes increasingly infragravity dominated towards the shore.
- A peak visible on the spectrum at about 0.05Hz (the first harmonic of the main infragravity peak) appears to grow in relative size towards the shore. This is likely to be due to harmonic growth caused by wave nonlinearities through shoaling.
- Phase analysis between velocity and surface elevation confirms previous suggestions that the infragravity waves are near standing and the incident waves are near progressive.

7.3 Preliminary analysis of SSC data

7.3.1 Introduction

In this section a preliminary look at the behaviour of the suspended sediment is presented, through inspection of sediment flux time-series and spectra. Note that more detailed analysis of the sediment fluxes are performed in section 8.5.

Sediment flux time-series are compared for the storm and calm data, and plots of velocity and SSC autospectra, co-spectra, phase and coherence spectra are examined, mainly from the storm data at z = 6cm.

Then, time-averaged SSC values are compared for the different positions in the cross-shore transect, to investigate how these change between the inner surf-zone and the swash-zone, albeit in low energy conditions only (because a cross-shore transect of data was only able to be obtained on the 'calm' day).

7.3.2 Comparison between calm and storm data

Suspended sediment flux time-series were calculated for the calm and storm data in the time domain by multiplying the velocity time-series by the SSC time-series at z = 5cm (calm) and z = 6cm (storm). These are shown in figure 7.6. The following observations may be made from initial inspection of figure 7.6:

- The sediment flux 'events' for the storm data are between two and three times as large as those for the calm data. Interestingly, the breaker height was about 2.75 times as large on the storm day than on the calm day. However, the r.m.s. fluxes were also calculated, and these differed by a factor of about 5.5.
- The calm time-series is more 'spiky' in nature, the large peaks being fewer in number, and shorter in duration.
- For both time-series the offshore flux 'events' are about half the size of the onshore fluxes. Especially for the calm time-series, there are a number of occasions when there is a large onshore flux of sediment, presumably from an uprush, but no corresponding backwash flux event.

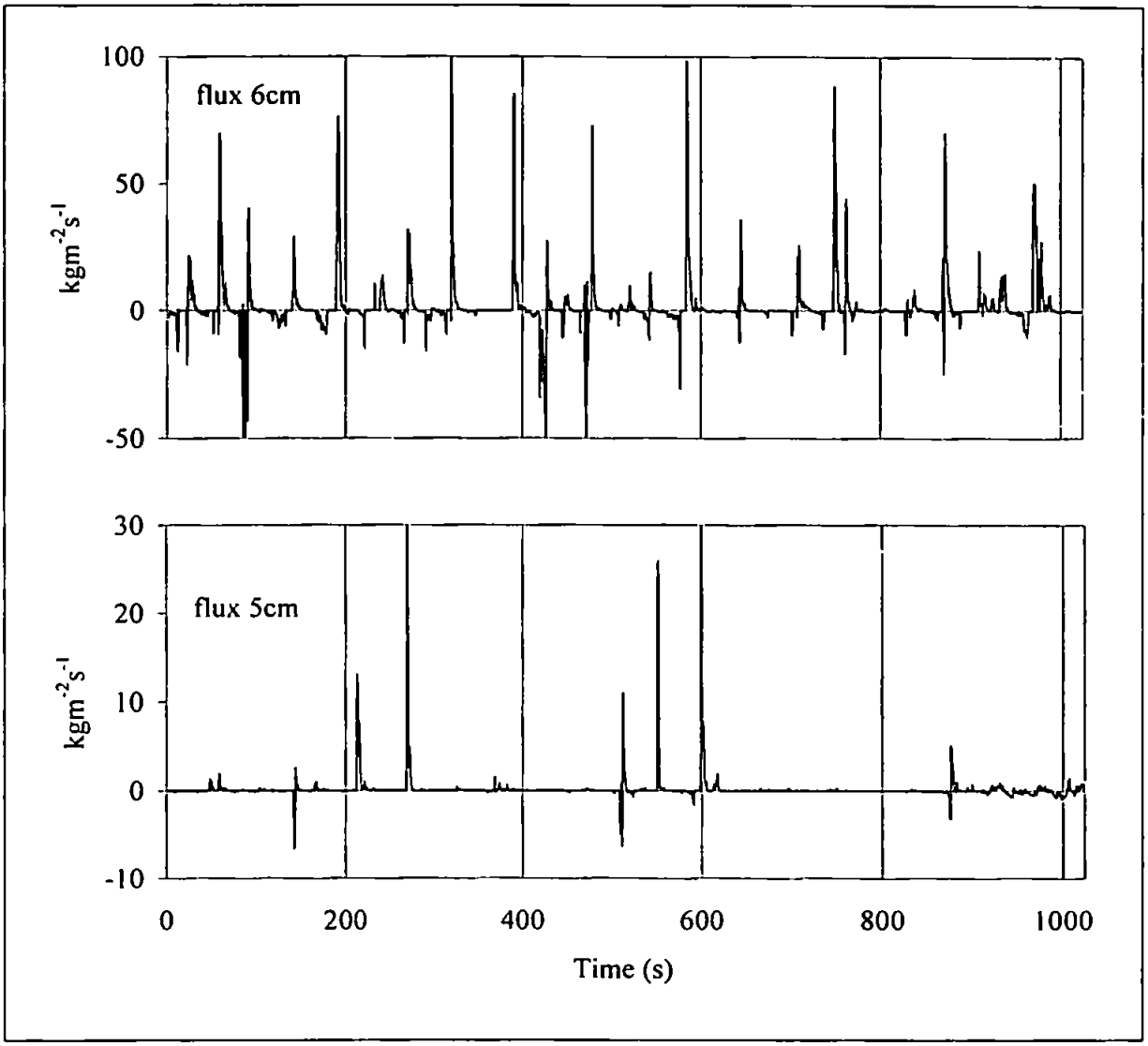

Figure 7.6: time-series of suspended sediment flux for storm data (upper panel) and calm data (lower panel).

Figures 7.7 to 7.10 show, for the calm and storm data, velocity and SSC autospectra, coherence-squared, phase spectra and co-spectra. Inspection of the coherence-squared plot for the calm data shows that coherence-squared between velocity and SSC is very poor, except for a small region around what may be the first harmonic of the infragravity peak. This, together with the 'spikiness' of the time-series, casts doubt on the validity of any interpretations made from the spectral plots of the calm data. Therefore, most of the observations in this section are from the storm spectra, but the calm spectra are nevertheless shown for comparison.

The velocity and SSC for the storm data are highly coherent around the infragravity peak (≈ 0.025Hz) and also in the incident band at about 0.1Hz. The co-spectrum is dominated by a large onshore-directed infragravity peak and a slightly lower frequency smaller offshore directed peak. The sediment flux at incident frequencies appears to be very small in comparison. There is also some energy in the first harmonic, which is connected with the nonlinearities generated in the shoaling process (see section 8.4).

The fact that the onshore flux appears to be larger than the offshore flux, (which can also be confirmed by inspection of the time-series), may be due either to the fact that most of the offshore transport is taking place below 6cm, or there is a true dominance of onshore transport.

The slightly lower frequency of the offshore peak may be due to large sediment flux events on the backwash occurring less frequently than those on the uprush, due to the difference in the way the sediment is suspended. The turbulence in the leading edge of the swash-front means that the uprush will nearly always contain suspended sediment high into the water-column, whereas on the backwash the velocity would have to reach some threshold before sediment starts to become suspended. Therefore not every backwash will contain a suspension event.

This result may be compared with other similar studies. For example, Beach and Sternberg (1991) obtained onshore and offshore peaks at similar frequencies to those in the present study, although the offshore peak for their data was of a larger magnitude. In contrast, Osborne and Rooker (1999) obtained an onshore peak of slightly lower frequency than the offshore peak. The flux time-series of Osborne and Rooker shows a dominance of offshore transport, with some backwash sediment events not having corresponding uprush events.

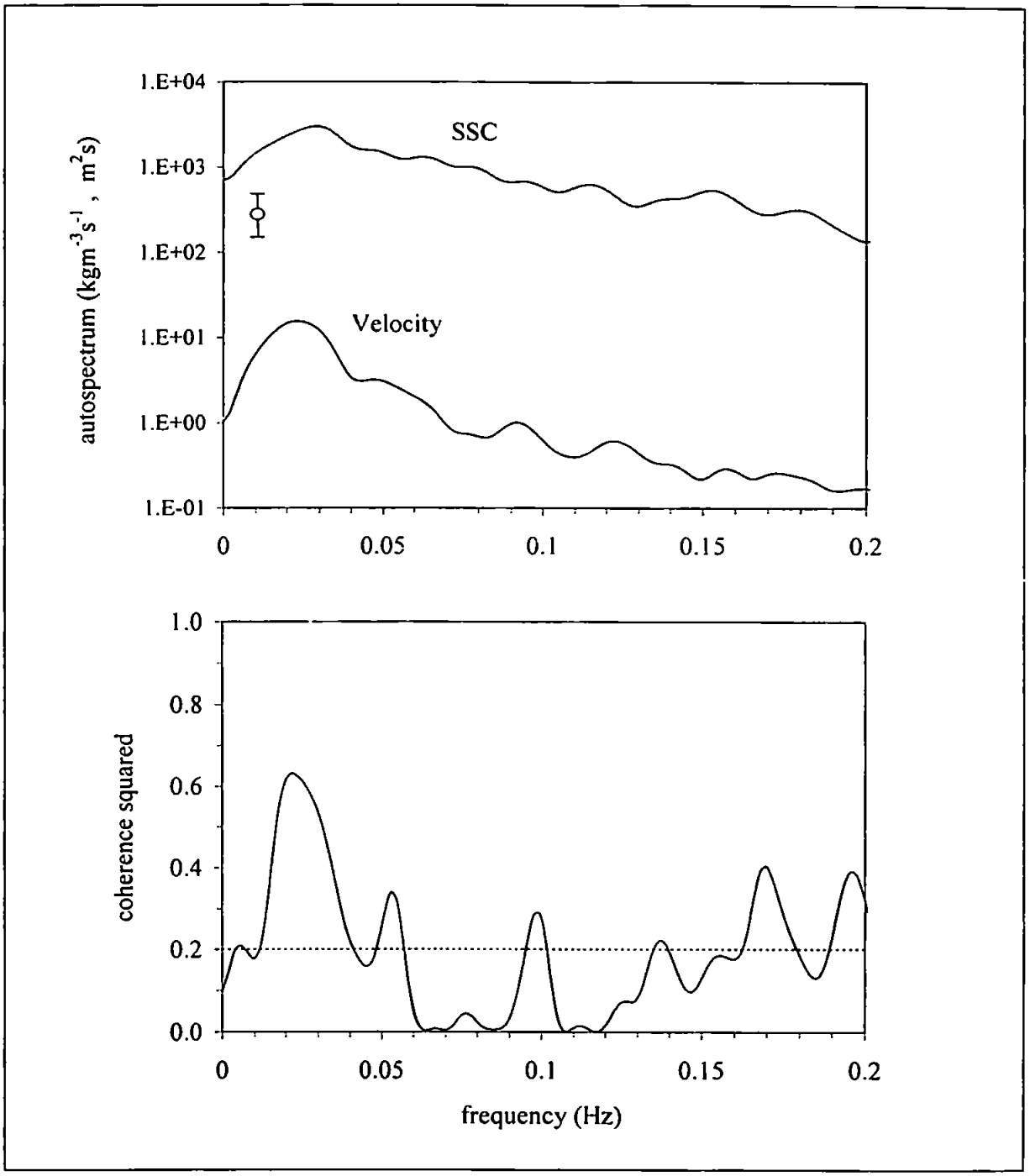

Figure 7.7: normalised velocity and SSC autospectra (top panel) and coherence spectrum (bottom panel) for storm data at z = 6cm. The error bar represents 27 degrees of freedom at the 95% confidence level. The dotted line on the coherence plot is the 95% confidence limit.

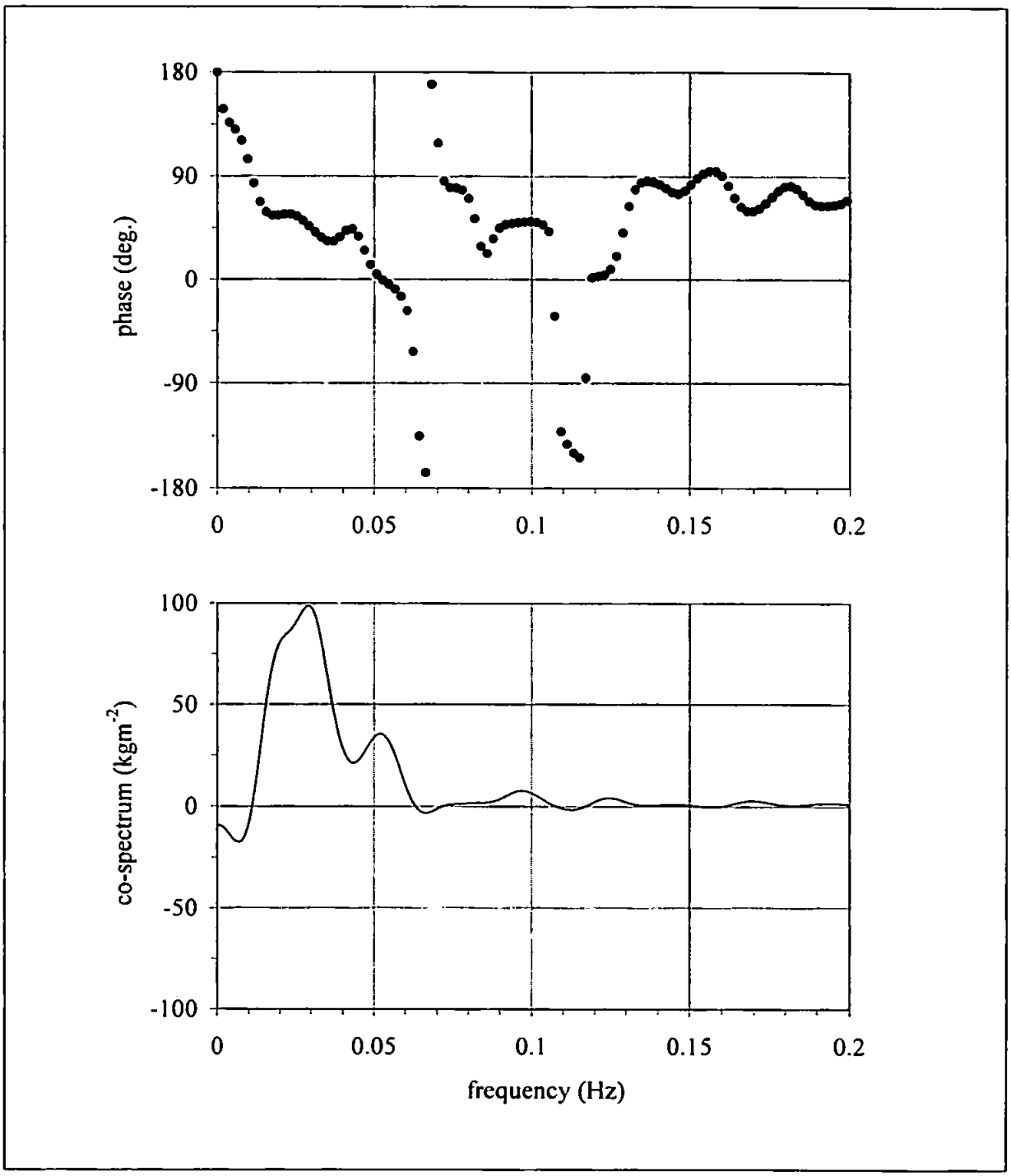

Figure 7.8: phase spectrum (top panel) and normalised velocity-SSC co-spectrum (bottom panel) for storm data at z = 6cm. Upper and lower error bounds are 170% and 63% respectively at the 95% confidence level.

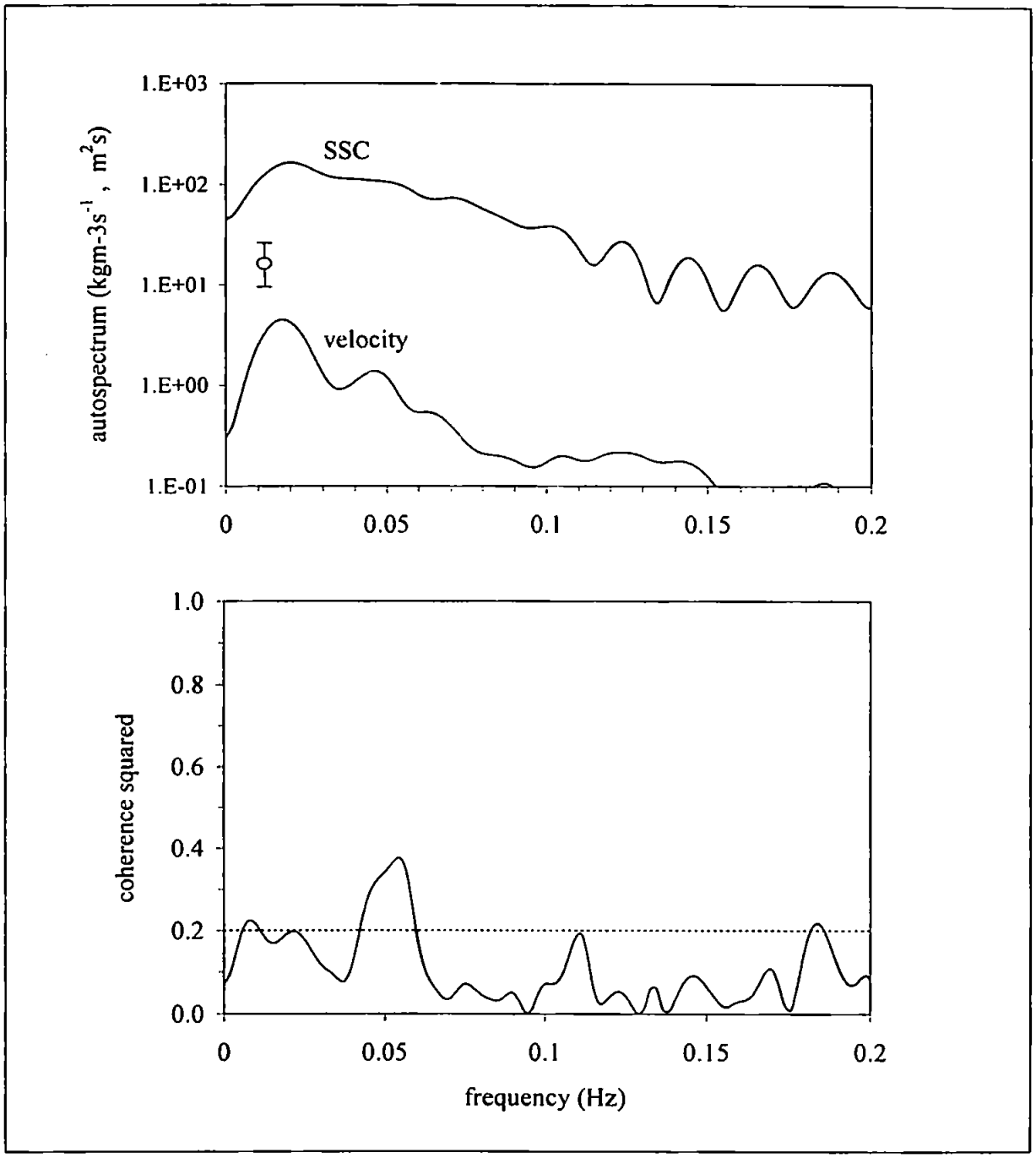

Figure 7.9: normalised velocity and SSC autospectra (top panel) and coherence spectrum (bottom panel) for calm data at z = 5cm. The error bar represents 27 degrees of freedom at the 95% confidence level. The dotted line on the coherence plot is the 95% confidence limit.

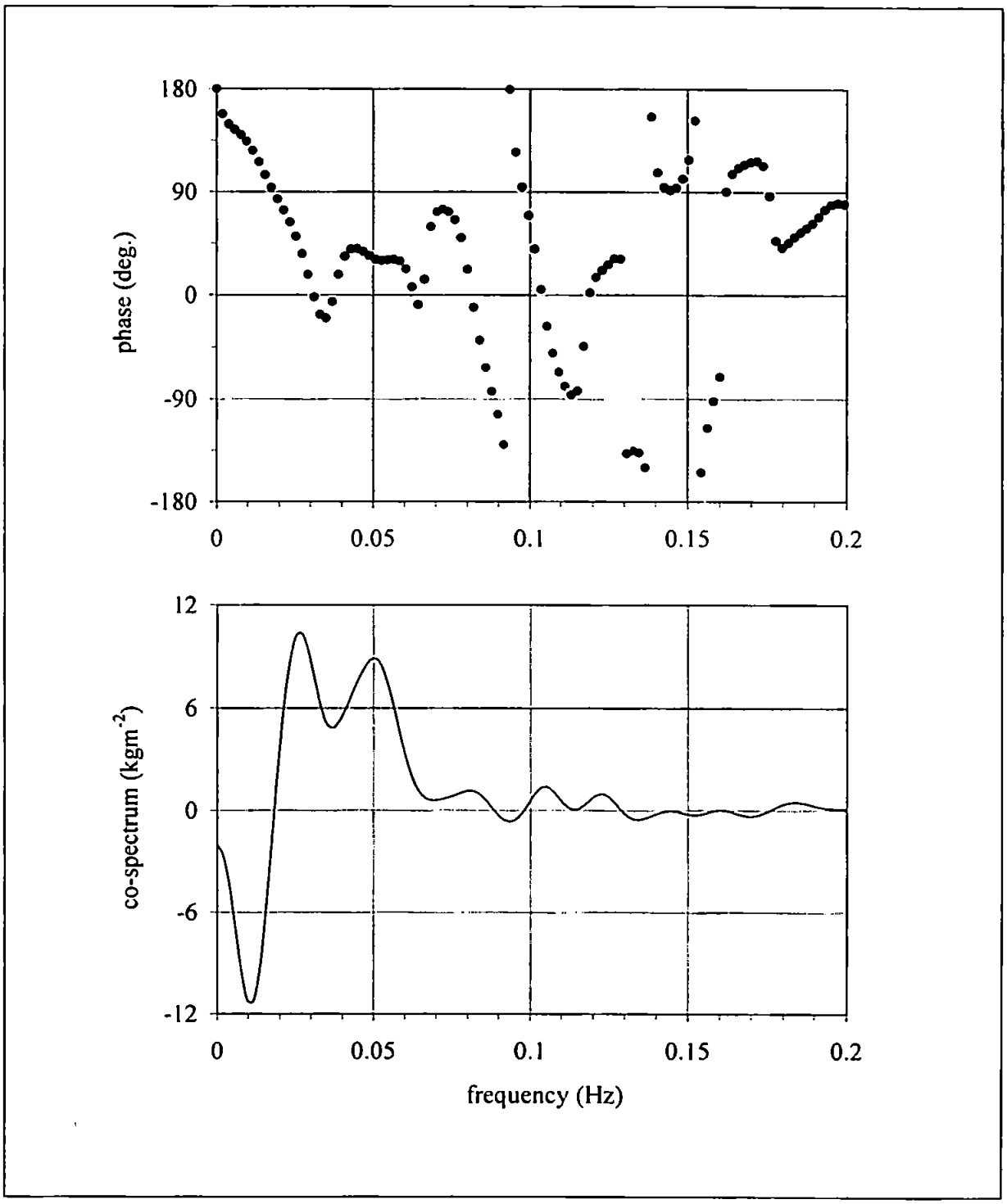

Figure 7.10: phase spectrum (top panel) and normalised velocity-SSC co-spectrum (bottom panel) for calm data at z = 5cm. Upper and lower error bounds are 170% and 63% respectively at the 95% confidence level.

7.3.3 Cross-shore transect

Figure 7.11 shows the SSC averaged over the time-series, at four heights above the bed, at each position in the cross-shore transect. Beach and Sternberg (1991) found mean concentrations in the swash-zone to be between three and nine times as large as those in the inner surf zone. Those findings are confirmed here, with the mean SSC at z = 1cm being about five times as large at $h/h_b = 0.2$ than at $h/h_b = 0.6$.

The other interesting thing to note is that the mean concentrations rapidly increase between $h/h_b = 0.4$ and $h/h_b = 0.2$, especially at very low levels in the water column. This might suggest a distinct swash-zone / surf-zone boundary, either side of which different sediment suspension mechanisms exist. It will be discussed later in the thesis that some sediment suspension processes which have been identified in the surf-zone cannot exist in the swash-zone and *vice-versa.*

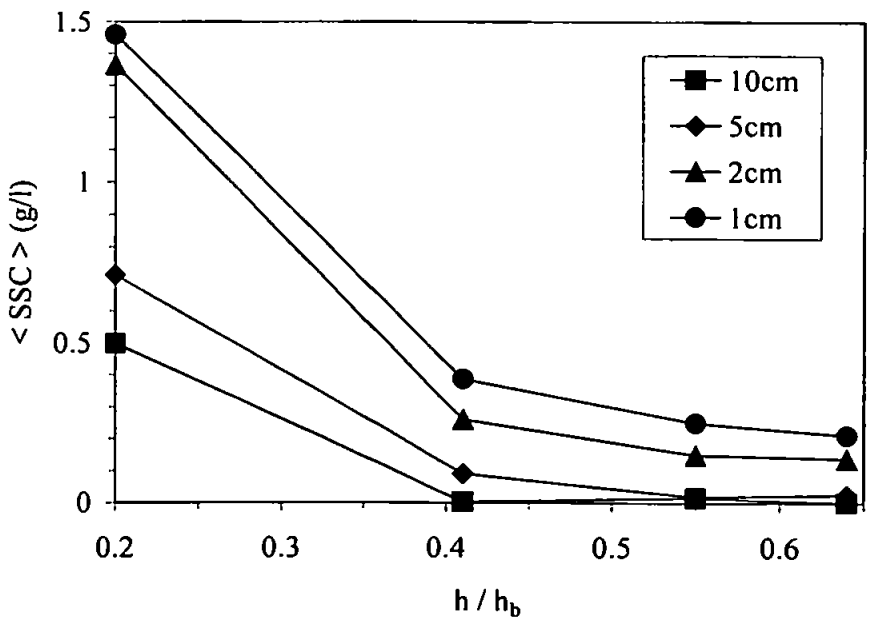

Figure 7.11: variation of time-averaged SSC with average depth / breaker dept (≅ normalised distance between shoreline and breakpoint).

7.3.4 Summary

In this section, preliminary observations were made of the behaviour of the suspended sediment, through examination of sediment flux time-series and spectra. The following important points summarise the findings:

- Suspended sediment fluxes were found to be more than twice as large for high energy conditions (storm data) compared with low energy conditions (calm data).
- From the sediment flux time-series, at z = 5cm and 6cm the onshore flux 'events' are about twice as large as the offshore 'events', for both high and low energy conditions.
- The velocity and SSC co-spectra are dominated by a large infragravity peak at about 0.025Hz.
- From the co-spectra, it appears that offshore transport is occurring at lower frequencies than onshore transport, which may be connected with the different sediment suspension processes on the uprush and backwash.
- Comparison of SSC figures from the cross-shore transect (in low energy conditions) shows about a five-fold increase in SSC from the inner surf-zone to the swash-zone.

7.4 Introduction of cross-shore velocity data from Muriwai, New Zealand

7.4.1 Introduction

This section is concerned with introducing some cross-shore velocity data, obtained from the swash-zone of a dissipative beach at Muriwai, New Zealand. A limited amount of data was made available from the swash-zone at Muriwai, for comparison with the data obtained in the present study. The velocity time-series available for comparison from the Muriwai data was one collected in the outer part of the swash-zone (i.e. just at the position where the instruments are beginning to wet and dry), which is similar to the storm and calm data bursts from Perranporth. Velocities collected at Muriwai were three-dimensional, using an ADV mounted with its sensing volume 5cm above the bed. Note that SSC measurements were also collected, but this data was unavailable for use in the present study.

Using the 3D velocities allows an estimate of the turbulence to be made (see section 8.2.2), which cannot be done from the velocity measurements at Perranporth, but which is suspected to be an important mechanism for sediment transport on the uprush. Another important reason for taking advantage of the availability of further data, is that the results and conclusions about the behaviour of the swash-zone, obtained from the Perranporth data, may be tested to see to what degree they might be applicable outside the constraints of a single site.

The section begins by comparing the morphological details of the two beaches, and assessing how 'dissipative' each beach is, at the time of each experiment. It is then described how the Muriwai data is processed into a format which is readily comparable with the storm and calm velocity time-series. All time-series are re-sampled at 2Hz, and are 17 min. long. Observations are then made from the velocity time-series and autospectra, and from high and low frequency variance calculations. Note that further analysis using this data is performed in chapter 8.

7.4.2 Classification of beaches

Muriwai, like Perranporth, is a highly dissipative beach, which also receives a considerable amount of mixed swell and windsea. Beach slopes are similar, and the wave conditions in the time-series presented here, appear to be somewhere in between the calm and storm data collected at Perranporth. The Muriwai data is from a day when breaker

heights were approximately 1.2m; at Perranporth the calm and storm days contained breaking wave heights of about 0.8m and 2.2m respectively.

Using the beach morphological classification of Wright and Short (1984), i.e.

$$\varepsilon = a_b \omega^2 / g \tan^2 \beta \qquad (4.1)$$

where a_b is the breaker amplitude ($\approx$ half breaker height H_b), $\omega = 2\pi / T$ is the radian frequency, T is the wave period, and tan β is the beach slope, both beaches may be seen to be highly dissipative (see also section 4.1.4). Table 7.2 shows a summary.

Table 7.2: morphological classification of the two beaches. T is significant period, H_b is breaking wave height, β is beach slope, and ε is the surf-scaling parameter, whereby the conditions are considered dissipative if ε exceeds 20.

Beach	H_b	T	tan β	ε
Perranporth	0.8 to 2.2m	8s	0.014	154 to 451
Muriwai	1.2m	8s	0.010	308

7.4.3 Data reduction

The Muriwai velocities were obtained using an ADV. When this instrument comes out of the water, a considerable amount of noise is generated. To remove this noise, the signal to noise ratio output of the instrument was utilised. Therefore a simple algorithm was written to set the velocity to zero if the signal to noise ratio fell below 20dB.

The data were sampled at 18Hz (Perranporth) and 10Hz (Muriwai), then re-sampled at 2Hz using the same technique as described in section 5.2.1. Autospectra were computed using Welch's averaged periodogram method, for both sets of data in the same way as that described in section 5.3 .

7.4.4 Time-series

Representative sections of the time-series are shown in figure 7.12.

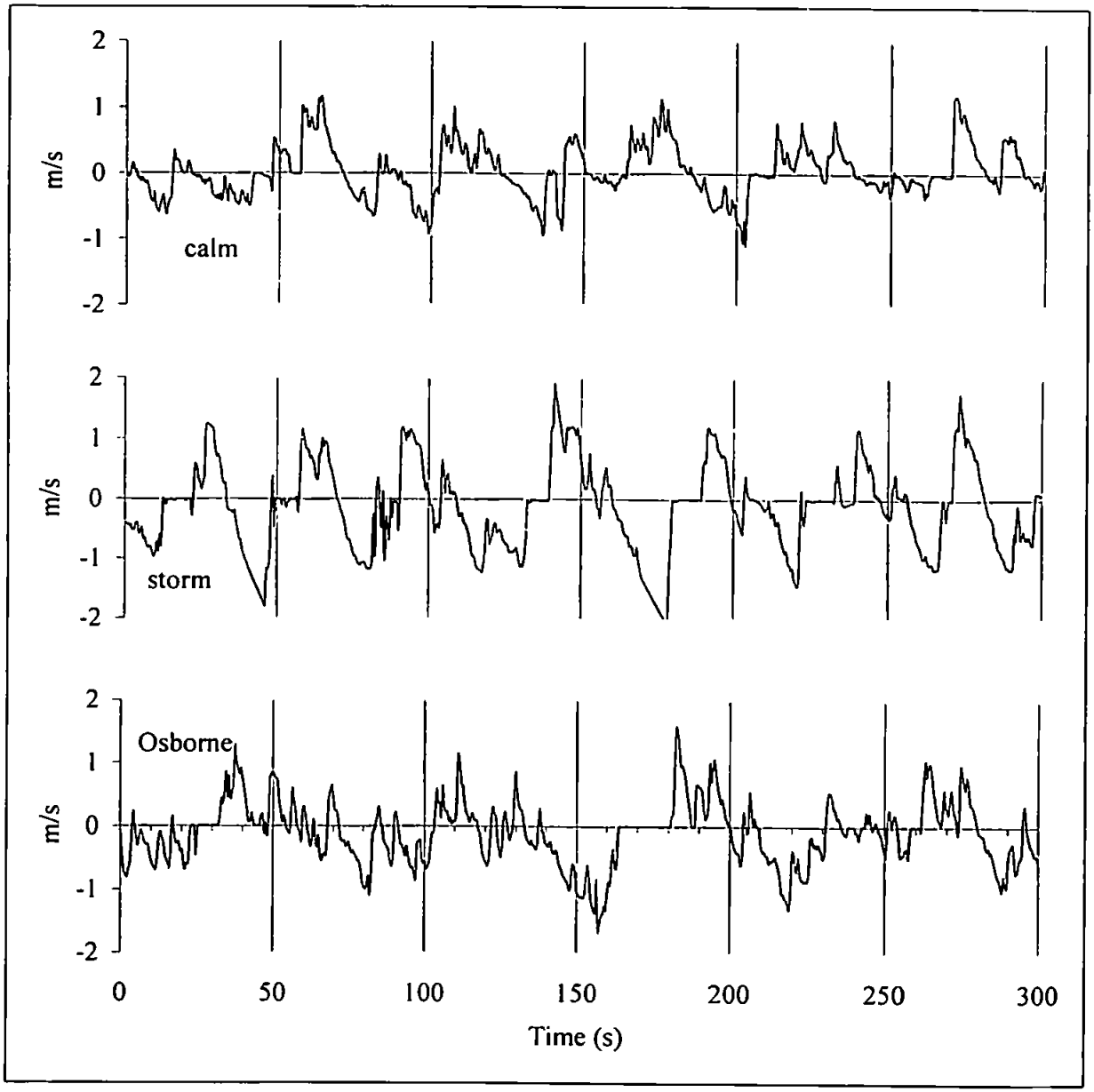

Figure 7.12: section of velocity time-series for calm and storm days compared with the Muriwai data. 'Osborne' refers to the Muriwai data, and 'calm' and 'storm' are the two Perranporth days.

Points of interest observable from initial inspection of the time-series are as follows:

- The Muriwai data contains incident frequency oscillations embedded within infragravity cycles of about 50s period, similar to the Perranporth data.
- The maximum onshore and offshore velocities for the Muriwai data are somewhere in between the calm and storm velocities, roughly corresponding to the difference in breaking wave height.
- For the Muriwai data, the size of the incident frequency oscillations appears to be larger relative to the infragravity oscillations, than both Perranporth time-series.

7.4.5 Autospectra

The velocity autospectra for the three time-series are shown in figure 7.13. The total low and high frequency ($f < 0.05$Hz and $f > 0.05$Hz) variances, together with the low / high frequency variance ratios and the position of the infragravity peak, are shown in table 7.3. The variances were computed by integrating under the autospectral curve, as described in section 5.3.5. Basic observations from figure 7.13 and table 7.3 are described below.

From the spectra it can be seen that the Muriwai velocity is dominated by a large infragravity peak at about 0.011Hz (90s). This is lower than on both the Perranporth curves. Waves that reach Muriwai are likely to have propagated much greater distances than those at Perranporth, resulting in a greater proportion of long-period swell. In this situation, longer infragravity waves might then be generated by the grouping of longer incident waves. It is also interesting to note that the infragravity peak for the calm data at Perranporth is at a lower frequency than for the storm data. The development of the grouping structure of waves as they propagate from various sources, through the surf-zone, and on to the shoreline, is highly complicated.

An important difference between the Muriwai spectrum and those from Perranporth, is that there appears to be relatively more energy in the lower incident band, around 0.05 to 0.1Hz (10 to 20s). This is also visible on the time-series, where the incident frequency oscillations are noticeably larger relative to the infragravity cycles, and also by the low / high frequency variance ratio (see table 7.3) which is much lower for the Muriwai data.

The above observation could be due to the presence of some long-travelled swell waves, in addition to the local windsea which is evident by the lack of any specific peak in

the incident band. Note that, above about 0.2Hz, all the spectra conform to an $f^{5/3}$ roll-off, which shows saturation at these frequencies, and is consistent with the energy transfer to higher frequencies due to turbulent dissipation (e.g. Stapleton, 1996).

From table 7.3 it can be seen that the total variance is greatest for the storm day and least for the calm day, with the Muriwai data lying somewhere in between. This shows an overall energy increase corresponding roughly with the increase in wave height. For example, if the variance and breaker height are normalised to the values for the calm data, the relative total variances are 1.5 and 3, and the relative values of H_b are 1.5 and 2.8, for the Muriwai and storm data respectively.

The low-frequency variance shows a three-fold increase from the calm to storm day, but the increase in high-frequency variance is not so great. This suggests some agreement with the hypothesis that offshore increases in wave height are manifest only in low-frequency energy increases at the shoreline (e.g. Guza and Thornton, 1982; Raubenheimer and Guza, 1996; Ruessink *et al*, 1998, and many others).

A plot is shown of low and high frequency variance v. breaker height (see figure 7.14), and it can be seen that the incident band energy in the swash-zone is less dependent on breaker height than infragravity band energy, suggesting a degree of saturation. It must be stressed however, with only three different days, and one of them being from a different beach, this theory cannot be properly tested on the data presented here. Moreover, the swash-zone data presented here are velocity data, collected in the outer part of the swash-zone, as opposed to run-up height at the shoreline.

Table 7.3: characteristics computed from the autospectrum. High and low frequency variances are $f > 0.05Hz$ and $f < 0.05Hz$ respectively. Units of variance are m^2s^{-1}.

Data	Position of I/G peak [Hz]	Total variance	High freq. variance	Low freq. variance	Low/High freq. variance ratio
calm	0.018	0.151	0.046	0.105	2.3
Muriwai	0.012	0.218	0.089	0.129	1.5
storm	0.025	0.455	0.116	0.339	2.8

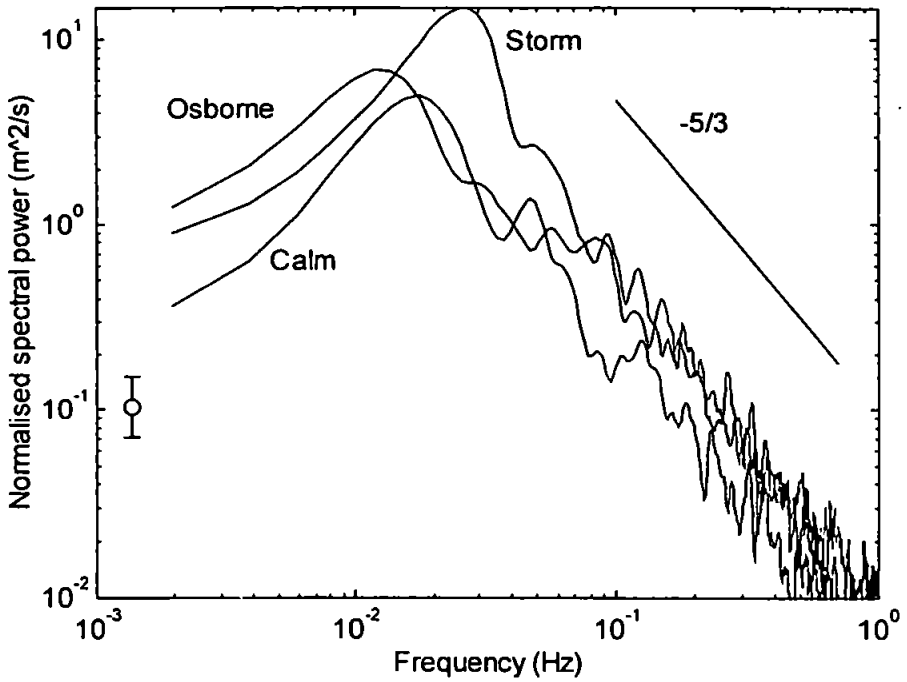

Figure 7.13: velocity autospectrum for calm, storm and Muriwai ('Osborne') data. The error bar represents 27 degrees of freedom at the 95% confidence level.

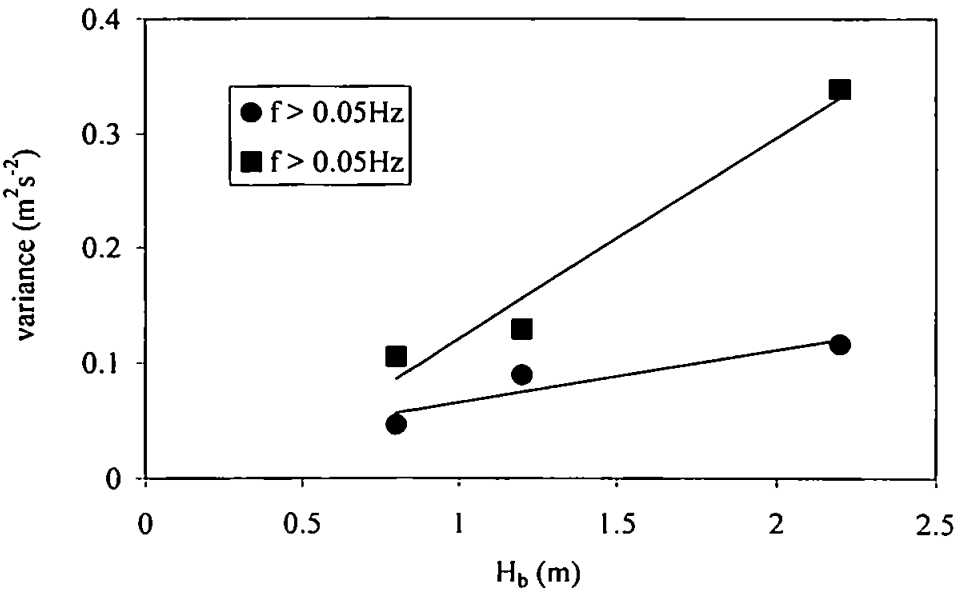

Figure 7.14: The variation of high and low frequency velocity variance with breaker height for different days.

7.4.6 Summary

Important points observed in this section from preliminary comparison of velocity data obtained from Muriwai Beach, New Zealand, with that obtained at Perranporth as part of the present study, are:

- Muriwai is a similar beach to Perranporth, with a slightly lower slope. Conditions for both experiments were highly dissipative, with the surf scaling parameter (Wright and Short, 1984) at 154 to 451 for Perranporth and 308 for Muriwai.
- Comparison of the velocity autospectra shows a large infragravity peak on all curves, but at a slightly lower frequency for the Muriwai data.
- Inspection of the velocity time-series, the autospectra, and variance calculations reveal that the incident band oscillations are larger relative to the infragravity band oscillations for the Muriwai data.
- The above observations suggest the possible presence of a long-travelled swell of period 10 to 15s, in addition to the local windsea, for the Muriwai data.
- Variance calculations show an increase in total energy roughly proportional to the increase in breaking wave height for the three data sets. A greater increase in low frequency ($f < 0.05$Hz) than high frequency ($f > 0.05$Hz) variance suggests some degree of saturation of the incident waves.

7.5 Individual swash cycle

7.5.1 Introduction

A useful preliminary step before detailed analysis is undertaken, is to look at a single uprush-backwash cycle, linking visual observations with time-series of an individual swash cycle taken from the data collected. A good description of the flow dynamics of a typical swash cycle on a steep reflective beach is given by Hughes *et al* (1998). However, the flow characteristics may not be exactly the same in infragravity dominated high-energy conditions on a dissipative beach.

In the first part of this section a simple description of the hydrodynamics in a typical swash cycle is given, using the ensembles of the velocity time-series together with a set of schematic illustrations. The illustrations are intended to show a highly simplified, idealised view of a swash cycle for visualisation purposes only. The ensembles are taken from infragravity-scale swash cycles, and no consideration is given at this stage to incident-frequency oscillations embedded within the infragravity cycles.

The second part of this section is concerned with investigating the temporal structure of SSC events within the swash cycle. It is not obvious that the maximum velocity always coincides with maximum SSC. Processes at the beginning of the uprush and the end of the backwash seem to complicate this, and Osborne and Rooker (1999) have pointed out that the balance between onshore and offshore transport in the swash-zone may be sensitive to small velocity-SSC phase differences. This subject is investigated in the time-domain using the ensembles of velocity and SSC time-series, and in the frequency domain using co-spectra and phase spectra.

Note that the mid-swash data burst, from which some of the SSC data is examined, was recorded during daylight. The SSC time-series were carefully checked for any anomalous saturated readings after the 'dryout filtering' was applied (see section 5.2.3). The absence of these readings indicated that the any interference from ambient light once the sensors were immersed was likely to be negligible.

7.5.2 Ensembles

The time-series of depth, velocity and SSC for a single infragravity swash cycle were obtained by taking an ensemble of seven swash 'events' from the mid-swash data burst (where individual 'events' are clearly isolated from each other). This is shown in figure 7.15, including the 'envelope' of the standard deviation between all the events.

Since each 'event' was not of the same duration, the time scale had to be normalised to the event duration. For example, 0.5 on the time-scale corresponds with the middle of the cycle.

The ensembles were obtained by interpolating each section of the time-series to an equal number of time steps, and then averaging the instantaneous values of depth, velocity and SSC at each time step. The average length of the cycle was 15.4s with a standard deviation of 3.3s. This cycle length is shorter than the infragravity period ($\approx$ 40s) because the sensors were out of the water for part of the time.

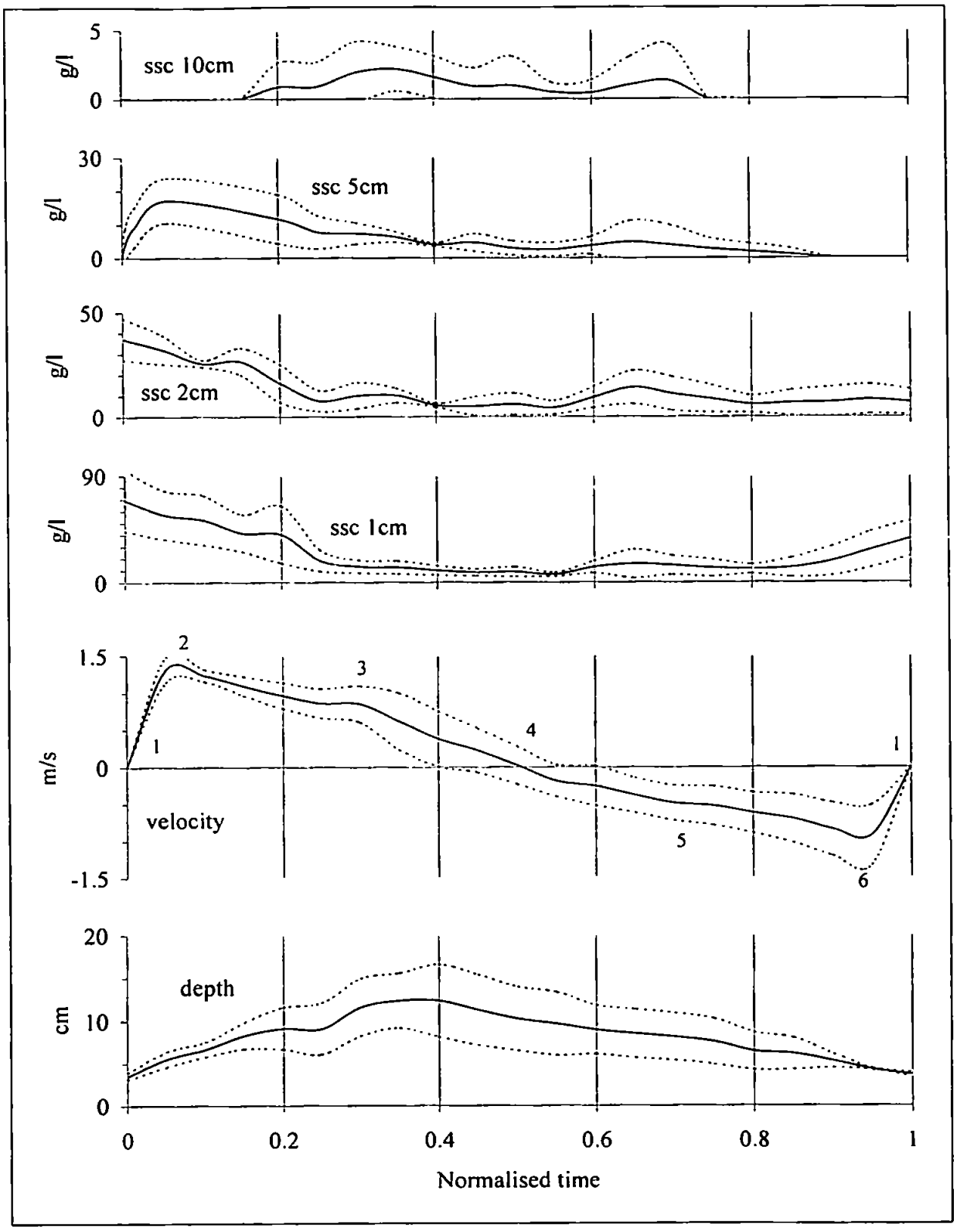

Figure 7.15: ensembles of depth, velocity and SSC time-series. The time-scale is normalised over the duration of the swash cycle. Numbers refer to stages in the swash cycle illustrated in figure 7.16. Dotted lines represent the mean plus or minus the standard deviation. Note different SSC scales for each height.

7.5.3 Hydrodynamics

Figure 7.16 shows a series of illustrations corresponding to the numbers in the velocity time-series in figure 7.15. The following description relates each illustration in figure 7.16 to the corresponding position in the velocity and depth time-series. Note that the current meter was 5cm above the bed, so the velocity was only measured when the depth was greater than 5cm. For the purposes of visualisation, in the hypothetical swash cycle shown, depth and velocity are assumed to be zero at the same time.

1) The velocity and depth are both zero since the instrument station is dry. An uprush bore is just about to arrive at the instruments.

2) The uprush bore arrives at the location of the instruments. The velocity increases to a maximum and the depth increases significantly.

3) In the middle of the uprush, the flow is decelerating in the onshore direction. The depth is close to its maximum value but still increasing.

4) The cycle is now at the top of the uprush, and the water is stationary at the instrument location. The depth already reached a maximum in the latter parts of the uprush, and is now decreasing. The fact that the maximum depth is reached before the end of the uprush is possibly due to the effects of flow divergence (Raubenheimer and Guza, 1996) and infiltration (see chapter 9). This was also observed by Hughes *et al* (1997).

5) The water has now started to accelerate offshore. The swash 'lens' is thinning considerably during the backwash. The next bore can be seen approaching the instrument site.

6) At the end of the backwash, the flow at the instruments is at a maximum offshore value. Just seaward of this point is the next uprush bore, whose large positive velocity is interacting with the seaward travelling backwash.

Eventually the backwash will thin enough so that the next bore is no longer considered to be travelling over water, and this is when 'bore collapse' occurs, from which point it is travelling over sand (as in illustration 1). On dissipative beaches, bore collapse may still cause some turbulence which may suspend extra sediment, but this is a much less prominent feature than on steep beaches (Hughes *et al*, 1997; G. Masselink, pers. comm., 1999; see also chapter 10).

The thinning of the swash lens between the start of the uprush and the end of the backwash has been attributed to velocity divergence in the cross-shore direction. This was first documented by Emery and Gale (1951) and more recently by Raubenheimer and Guza (1996). Careful visual observation confirms this divergence. For example, when the water is stationary in the middle of the swash lens (half way between the shoreline and the next incoming bore), the water at the shoreline is moving shorewards, and the water just in front of the next bore is moving seawards. This tends to stretch the swash lens horizontally, making it thinner vertically by the principle of continuity. It may also be observed that, on the backwash, the leading edge of the swash lens appears to remain stationary, with the rest of the lens moving offshore at this time. Therefore, if the convention for velocity is positive onshore, then the horizontal velocity gradient on both the uprush and backwash is positive, i.e.

$$\text{uprush:} \qquad \frac{\partial u}{\partial x} > 0 \tag{7.3}$$

$$\text{backwash:} \qquad \frac{\partial}{\partial x}(-u) < 0 \qquad \therefore \frac{\partial u}{\partial x} > 0 \tag{7.4}$$

A similar ensemble technique was used for an infragravity cycle ($T \approx 50s$) by Osborne and Rooker (1999). Also, non-ensembled individual swash events were examined by Hughes et al (1997, 1998) and Masselink and Hughes (1998). Even though the latter three studies were performed on a steep beach in incident-dominated conditions ($T \approx 6s$), results are very similar to those of the present study, and of Osborne and Rooker (1999). One notable difference is that, on the steep beach, the uprush duration appears to be consistently shorter than the backwash duration. Hughes *et al* (1997) attribute this to either minor flow convergence/divergence caused by some localised 3D topography, or to the effects of infiltration. They suggest that the 'infragravity swash' measured by Beach and Sternberg (1991) may be of a "fundamentally different nature".

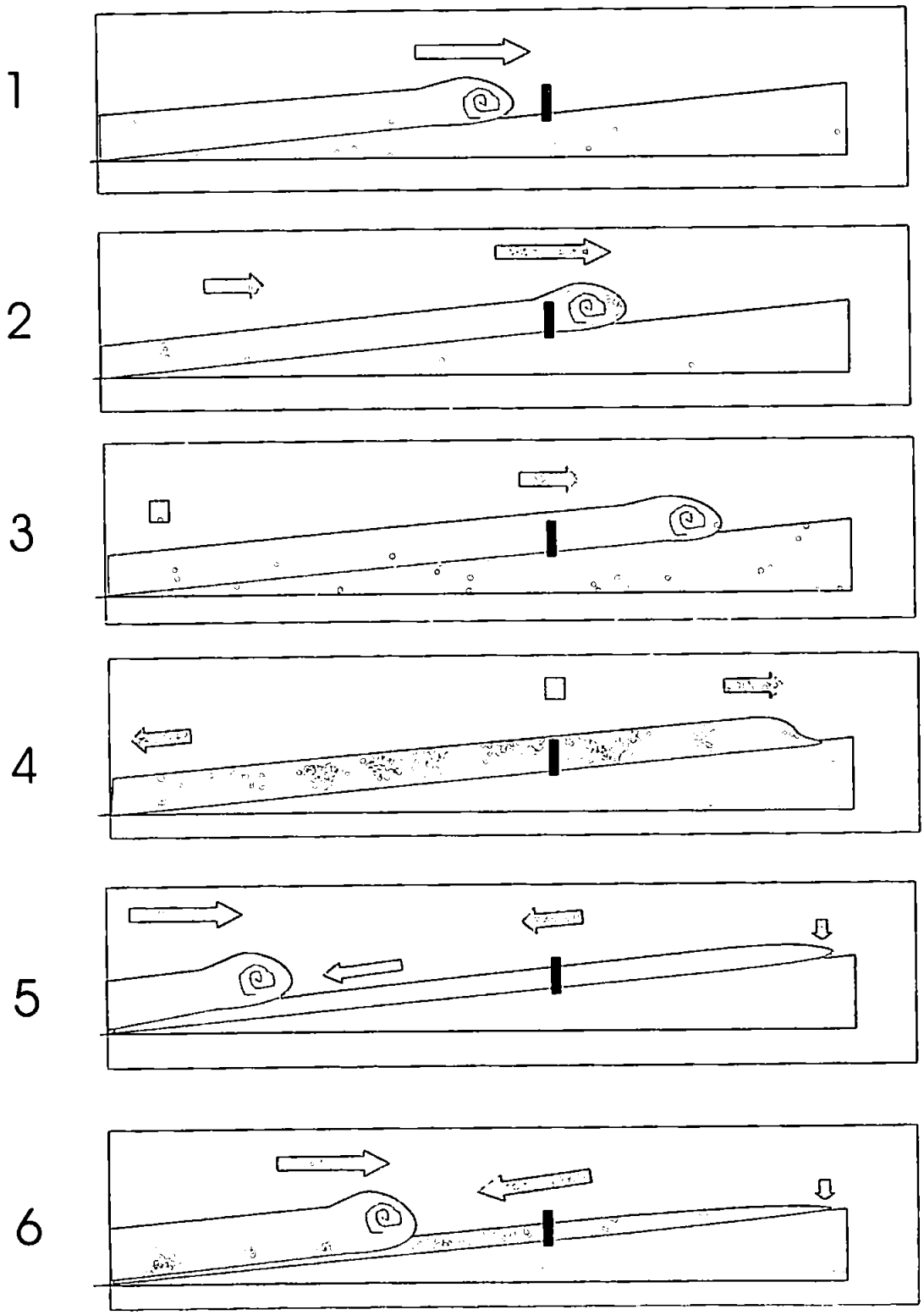

Figure 7.16: schematic illustration of an idealised swash cycle. The arrow length indicates velocity: the square referring to zero velocity. The instrument rig is shown by the small upright rectangle in the centre of each drawing.

7.5.4 Sediment behaviour: time domain

From the ensembles of SSC and velocity in figure 7.15, an insight may be gained as to when in the swash-cycle the sediment is actually being suspended. A SSC peak can be seen at the beginning of the uprush, principally due to the turbulence in the swash-front. As the uprush progresses the swash-front will move shoreward relative to the instrument station, and less sediment will be suspended as the local velocity decreases. The sediment that was suspended near the instrument site at the start of the uprush will have settled out when the flow reverses to backwash. On the backwash, the first part of the flow will be relatively clear of suspended sediment, but if the flow then reaches a threshold value for sediment suspension a second SSC peak will be seen.

The z = 1cm SSC trace in figure 7.15 clearly shows high values of SSC at the start and end of the swash-cycle. The upper sensors show progressively lower concentrations with height, but considerably less SSC on the backwash, which might suggest that either there is more sediment being suspended on the uprush than the backwash, or that sediment is moving lower in the water-column on the backwash than on the uprush. The 5cm and 10cm sensors go dry at $t \approx 0.9$ and 0.75 respectively, and the 10cm sensor was also dry for the first part of the uprush (before $t \approx 0.15$).

7.5.5 Sediment behaviour: frequency domain

The velocity-SSC co-spectrum and phase spectrum for the storm and calm data bursts were shown in section 7.3.2, figures 7.8 and 7.10, to investigate the phase shift between velocity and SSC. Plots of co-spectral density v. phase are also shown in figure 7.17 (below). The storm and calm data was used here rather than the mid-swash data, as these time-series consisted of continuous oscillations with very few breaks in the data where the water depth dropped below the height of the instruments. The SSC data used for the spectra were those recorded at the same height as the velocity (i.e. 5 and 6cm for calm and storm respectively).

The phase spectra for the both the storm and calm data show a shift of about 45^0 at the frequency of the main positive peak, and about 130^0 at the frequency of the negative

peak, confirmed by inspection of figures 7.8 and 7.10. Therefore, at the frequency at which the fluctuating sediment transport has the highest onshore (offshore) values the phase difference between SSC and velocity is 45^0 (135^0), i.e. the SSC is leading the velocity, which means that, on both the uprush and backwash, the SSC reaches a maximum before the velocity reaches a maximum. These phase shifts are consistent with results obtained by Beach and Sternberg (1991), but differ from Osborne and Rooker (1999), who obtained results suggesting a phase lead of SSC over velocity of 90^0 for both uprush and backwash.

Different results were obtained in the time-domain (above) for the mid-swash data, where the SSC and velocity both reached a maximum at the same time. The fact that there exist a greater number uncertainties in the frequency domain method suggests that these phase shifts might actually be an artefact of the confidence limits or the 'spikiness' of the time-series. The confidence limits imposed by the spectral analysis techniques mean that the position of the co-spectral peak could be shifted in frequency, which may in turn affect the phase. Beach and Sternberg (1991) specify "between 24 and 64 degrees of freedom", for their spectral analysis, which give average confidence limits of between 70% and 160% at the 95% confidence level (Jenkins and Watts, 1968). Osborne and Rooker (1999) give 16 to 36 degrees of freedom, leading to average confidence limits of between 60% and 200% at the 95% level. A 'spiky' time-series will also greatly reduce the reliability of any phase spectrum calculations.

However, if any phase shifts are present then these may significantly effect the overall sediment transport direction and magnitude. For example, if both velocity and SSC peaked simultaneously, then the instantaneous sediment flux would be greater than if they both peaked at slightly different times during either the uprush or backwash. The balance between the velocity-SSC phase shift on the uprush and that on the backwash may therefore be a significant contributing factor in the overall movement of sediment in the swash-zone.

The physical processes controlling these phase shifts are likely to be those which affect the nature of the flows at the start of the uprush and the end of the backwash, which are complicated. The uprush is characterised by turbulence, and the backwash by interaction with the next uprush (which may in turn cause second-order sediment suspension phenomena such as hydraulic jumps - see chapter 10). Therefore it is difficult to say under what circumstances the relationship between the timing of the SSC maximum and the velocity maximum will change.

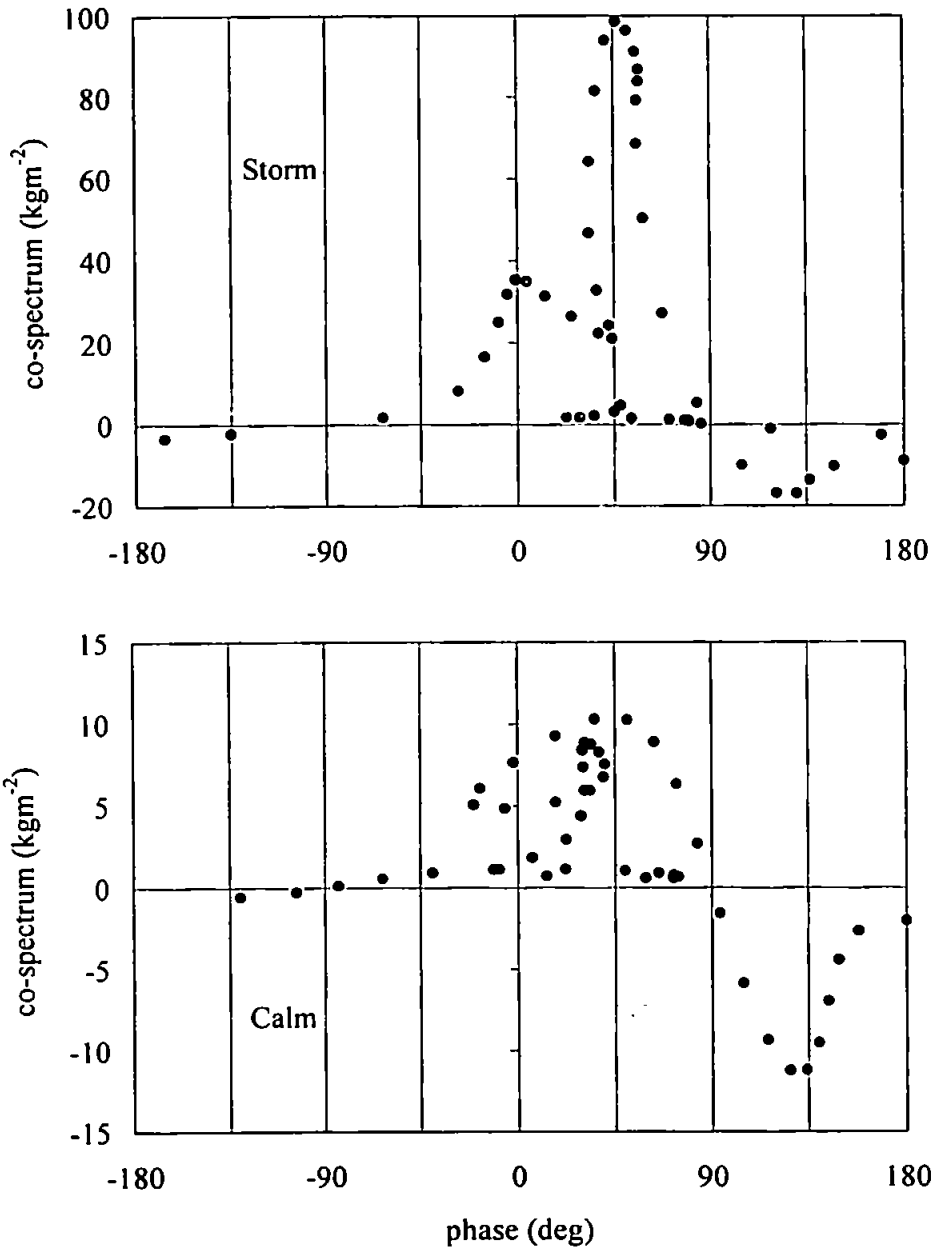

Figure 7.17: plots of co-spectral density v. phase for storm (upper panel) and calm (lower panel) data.

7.5.6 Summary

In this section, preliminary observations have been made of a typical individual swash cycle in infragravity dominated dissipative conditions. The following important points summarise the findings:

- The water depth tends to reach a maximum just before the zero down-crossing of the velocity at the end of the uprush. Maximum velocities occur close to the beginning and end of the swash cycle.
- On the backwash the leading edge of the swash 'lens' appears to remain stationary at the run-up limit, with the swash lens exhibiting a cross-shore spatial divergence.
- High values of SSC are generally found near the start of the uprush and the end of the backwash.
- Velocity and SSC maxima do not always occur synchronously within the swash cycle. This phase difference has important implications for the net magnitude and direction of sediment transport.
- Complications to the cross-shore flow such as turbulence and uprush-backwash interaction may be responsible for the above velocity-SSC phase differences.

8. Sediment transport from nonlinearities in the velocity field.

8.1 Introduction

Apart from the infragravity dominance, the velocity field in the swash-zone is highly irregular, containing a large amount of skewness and asymmetry generated during the shoaling process. The shoaling of surface gravity waves has been studied by many workers (e.g. Freilich and Guza, 1984; Elgar and Guza, 1985; Doering and Bowen, 1987), but, little attention has been paid to its relevance to sediment transport in the swash-zone.

The generation of harmonics during shoaling, and their interaction with the fundamental, and with themselves, causes the wave shape to contain skewness or asymmetry (or both), depending on the phase relationships between the harmonics.

Positive and negative skewness and asymmetry are illustrated schematically in figure 8.1, and the spectral composition and phase relationships are shown in figure 8.2. The velocity time-series of a purely skewed wave is symmetrical about the vertical axis, but not about the horizontal. It is characterised by broad, low troughs and narrow, tall crests, but symmetrical front and rear faces. This wave contains a number of harmonics, which are all in phase with the fundamental. A purely asymmetric wave refers to one in which the velocity time-series is asymmetric about the vertical axis, but not the horizontal. The time-series will have a 'sawtooth' shape with gently sloping front faces and steep rear faces, but crests and troughs of equal amplitude. This wave also contains a number of harmonics, but each harmonic is shifted in phase with respect to the fundamental, i.e. the n^{th} harmonic is shifted by $(n-1)\frac{\pi}{2}$.

The flows in the swash-zone contain a great deal of negative asymmetry, leading to higher onshore than offshore accelerations, which is likely to have implications for the cross-shore sediment transport. Velocity skewness is also likely to be high in the swash-zone, and it will be shown here that low frequency negative skewness may contribute to offshore sediment transport. The importance of skewness to surf-zone sediment transport has been well established in previous studies. Indeed, many sediment transport models are based on various velocity moments relating to the velocity skewness (e.g. Nairn and Southgate, 1993; Russell and Huntley, 1999). It must also be borne in mind that the

velocity skewness and asymmetry are frequency dependent, and the interactions between harmonics in highly shoaled waves can be complicated. The bispectrum (Hasselman *et al*, 1963) is a useful tool for providing a visual and quantitative evaluation of these interactions. However, long, stationary time-series are required to obtain statistically reliable bispectral analysis (Elgar and Guza, 1985; Elgar and Sebert, 1989; Ruessink, 1998), and the number of degrees of freedom available from the data in the present study is somewhat limited.

Horn and Mason (1994) observed that 'bedload' transport tended to dominate the backwash, and 'suspended load' was more common on the uprush. In their study, bedload and suspended load were defined as sediment caught in a trap below and above 1cm. Therefore, a result of their study was that, in the swash-zone, sediment tends to move higher on the uprush than on the backwash. Although the instruments used in the present study cannot measure true bedload, the measurement of suspended sediment flux at various heights above the bed provide useful information regarding onshore and offshore transport mechanisms.

Whether the swash-zone is in an accreting or an eroding state will depend on the balance between competing processes which cause onshore or offshore transport. Quantification of the net onshore or offshore movement of sediment in the swash-zone is difficult, due to it being the small difference between two large and opposing quantities (Osborne and Rooker, 1998, 1999). The aims of this chapter are to identify two processes which contribute to this, namely the onshore transport associated with offshore to onshore velocity changes and turbulence on the uprush, mainly at incident time-scales; and the offshore transport associated with large, infragravity-frequency backwashes which start to suspend and advect sediment as the velocity reaches a threshold. The contribution of these processes to the onshore-offshore sediment transport balance, is examined using the calm and storm data bursts, and also the velocity data which was made available from Muriwai Beach, New Zealand (see section 7.4).

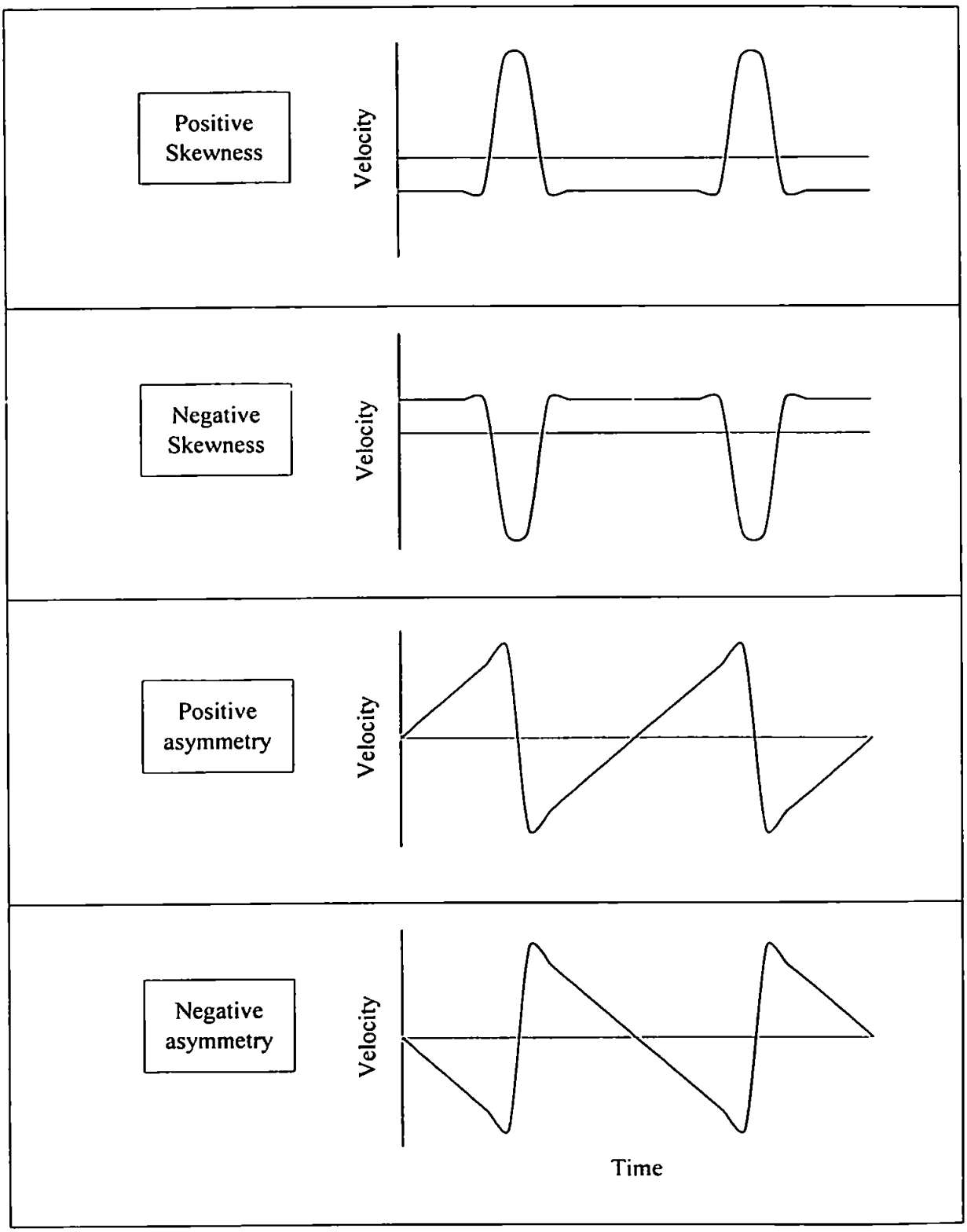

Figure 8.1: schematic illustration of skewed and asymmetric velocity time-series.

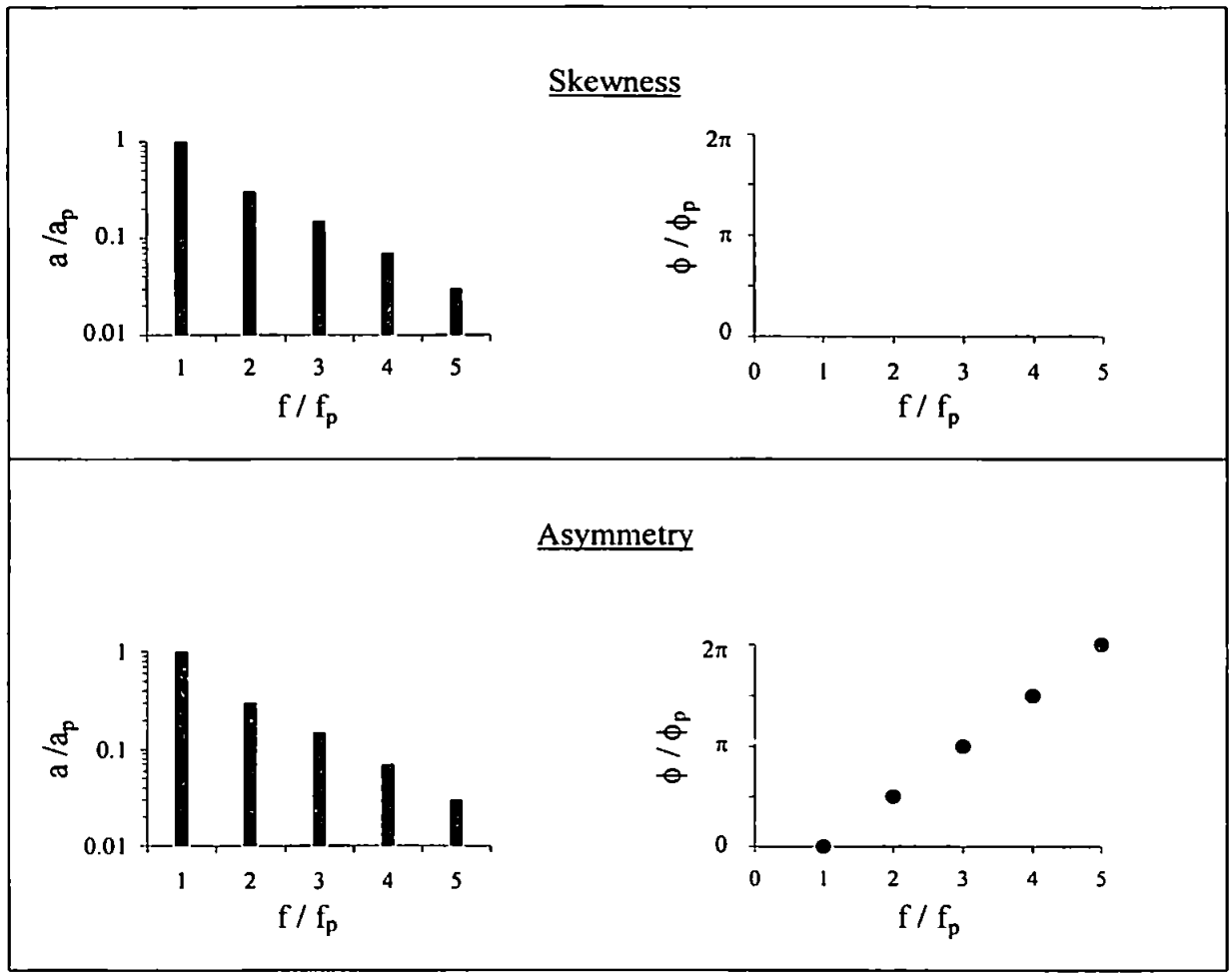

Figure 8.2: Schematic illustration of spectral composition and phase of skewed and asymmetric waves (adapted from Doering 1988). a = amplitude, ϕ = phase, f = frequency, and suffix p indicates primary (i.e. fundamental) component.

8.2 Onshore transport from negative asymmetry

8.2.1 Acceleration

A few studies in the past have attempted to relate not only the characteristics of cross-shore velocity, but also the acceleration, to suspended sediment transport. Hallermeier (1982) concluded, from a series of laboratory experiments involving sinusoidal flows that "a direct role of fluid acceleration in sand transport by oscillatory flow seems unequivocally to have been established". Hanes and Huntley (1986) measured cross-shore velocity and suspended sediment outside the surf-zone, and suggested that

fluid accelerations may have a large part to play in the suspension of sediment. King (1991) performed laboratory experiments using flows containing positive and negative sawtooth asymmetry, and found that sediment was more likely to be transported by the 'steep-fronted' waveform (negative asymmetry), than the 'steep-reared' one. Nielsen (1992) discusses the results of King (1991) in terms of boundary layer growth times. He suggests that, during times of high acceleration, the boundary layer has little time to grow, hence the 'free stream velocity' will be felt close to the bed, causing higher shear stresses, and hence a higher probability for sediment movement. In contrast, during times of steady flow or gentle acceleration, the boundary layer reaches a greater thickness, which means smaller near-bed velocities, and hence smaller shear stresses on the bed.

The cross-shore velocity in the swash-zone is strongly characterised by negative asymmetry, containing sharp offshore to onshore velocity transitions associated with the arrival of the swash-front at the measurement position. Visual observations indicate that a large amount of sediment is suspended at the front, not only from the passage of the front itself, but also from the turbulence caused by the interaction of the advancing front with the previous backwash. If Eulerian measurements of velocity and sediment concentration are obtained, then the passage of the front past the instruments, will result in the velocity going from a maximum negative to a maximum positive value, and the sediment concentration to suddenly rise. As the 'tail' of the front passes the instruments, the sediment which is settling out behind the front will be advected shorewards.

Time-series of cross-shore velocity, acceleration and SSC are shown in figure 8.3. The data are taken from the calm day, with both instruments measuring at 5cm above the bed. Acceleration was computed numerically from the velocity time-series, using a simple finite-difference scheme.

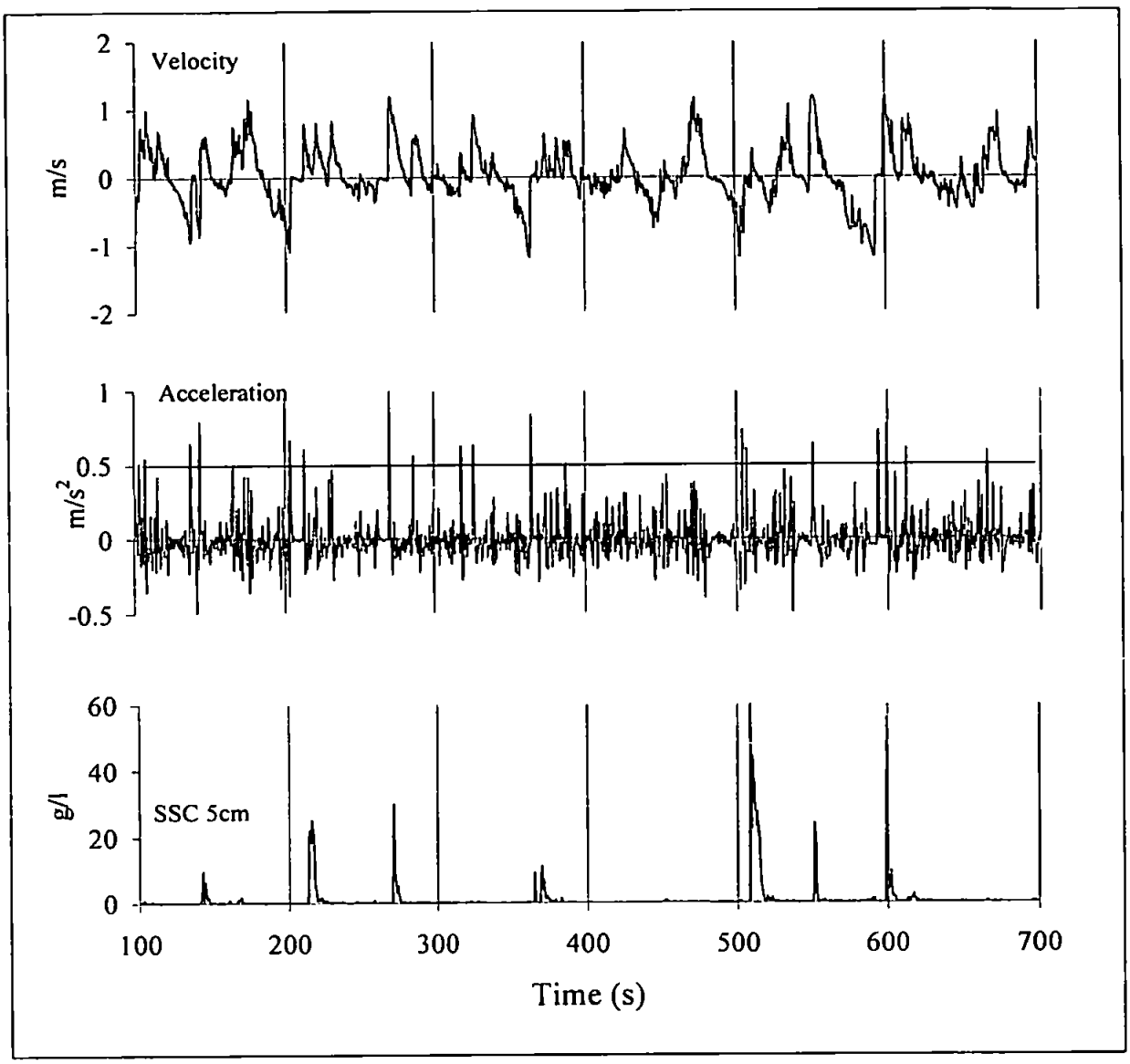

Figure 8.3: time-series of cross-shore velocity, acceleration and SSC. The horizontal line on the acceleration trace is an arbitrary threshold.

It can be seen from the velocity trace in figure 8.3 that the velocity contains a lot of negative asymmetry and the suspension events appear to coincide with the sharp acceleration associated with the sudden arrival of the swash-front at the instrument station. Inspection of the acceleration trace reveals that the sediment suspension events do indeed coincide with periods of high positive acceleration. An arbitrary threshold line has been drawn, showing that sediment appears to be suspended when the acceleration exceeds this threshold. Physically, this would mean that the rapid velocity change occurring at the

same time as the passage of the swash-front, must be of a certain magnitude before any suspended sediment is seen by the instruments.

The above observations are highlighted in figure 8.4, which shows only the values above the arbitrary threshold of $0.5ms^{-2}$ on the acceleration time-series.

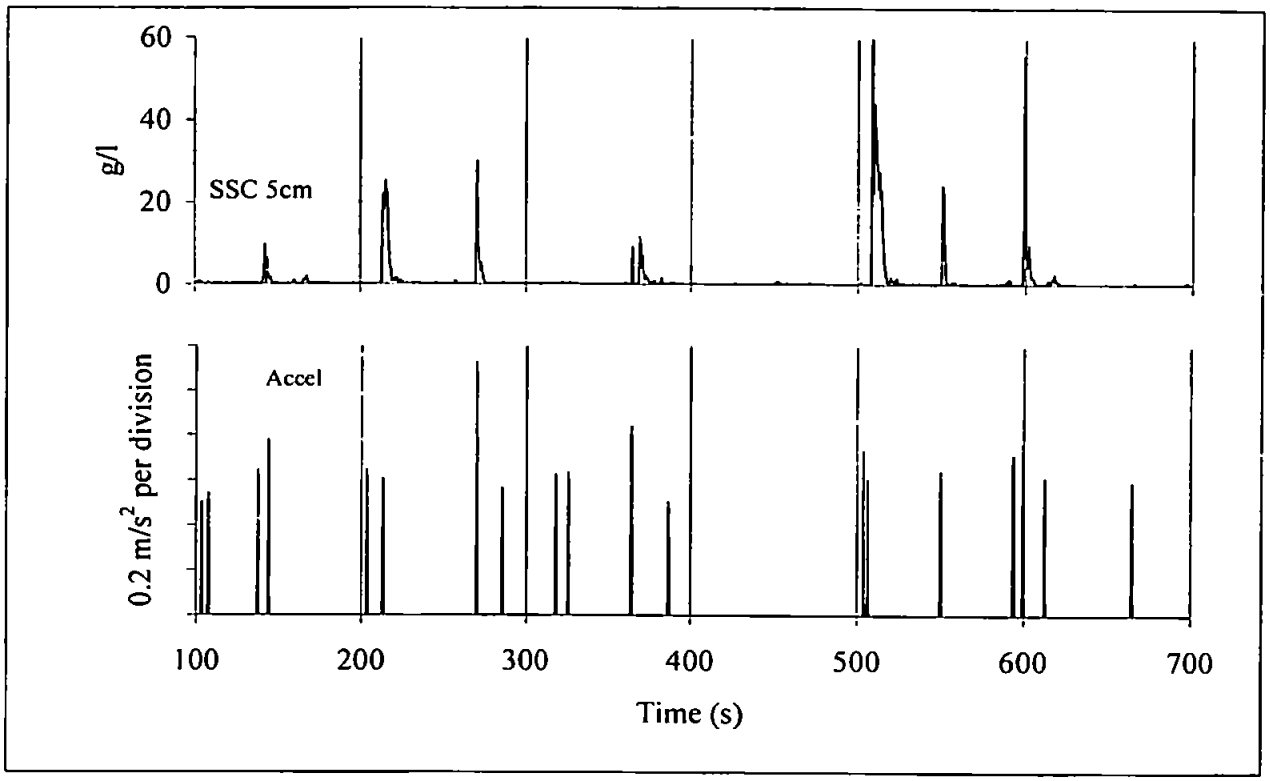

Figure 8.4: time-series of SSC at z = 5cm compared with acceleration above the arbitrary threshold of $0.5ms^{-2}$ only. Some correlation can be seen.

8.2.2 Turbulence in the swash-front

The swash-front contains a great deal of turbulence, which is a significant sediment suspension mechanism in itself (P. Neilsen, pers. comm., 1998). As this front passes the instrument site, a large onshore acceleration will be measured, but it is probably the turbulence which is making a larger contribution to the sediment suspension than the simple near-bottom flow acceleration like that observed by King (1991). Therefore, on the uprush, a link exists between acceleration and suspended sediment, but it is probably an indirect link, with turbulence in the swash-front providing the main suspension mechanism. Also, if the uprush meets with the previous backwash, there will be a larger

measured acceleration (due to the sudden flow reversal), but also greater turbulence from the interaction of the two opposing flows (see Chapter 10, on hydraulic jumps).

Some workers (e.g. Beach and Sternberg, 1996) have studied breaking wave turbulence, mainly with plunging breakers, but there have been few field measurements of the turbulence beneath an already-broken spilling wave.

Here, the velocity data made available from Muriwai Beach, (collected with a 3D ADV) is used to make a quantitative comparison of the turbulence in the uprush with the turbulence in the backwash.

Visual observations suggest that the uprush front has a lot of turbulence in it, and the water is moving in all directions, but the backwash is principally dominated by a smooth, shallow, offshore flow. On the uprush the 3D velocity field would contain considerable components in the y (longshore) and z (vertical) directions, whereas on the backwash the velocity field is much more dominated by flow in the x (cross-shore) direction. Hence, the uprush should contain more turbulence for a given cross-shore velocity than the backwash. This hypothesis is examined using a parameter derived from the ratio of the total velocity variance (reflecting the turbulence) and the cross-shore velocity. The average value of this parameter for all the uprushes in a time-series is then compared with the average value for all the backwashes.

The turbulent kinetic energy, TKE, may be computed using

$$TKE = \frac{1}{2}\rho\left(\overline{u'^2} + \overline{v'^2} + \overline{w'^2}\right) \tag{8.1}$$

where the overbar indicates time-averaging and ρ is the fluid density. Strictly speaking, TKE is an estimate of the total variance including wave motions and not just the turbulence (Stapleton, 1996; Osborne and Rooker, 1998, 1999). However, separation of the fluctuations due to wave motion and those due to turbulence is not straightforward (e.g. Soulsby and Humphery, 1989), and for the purposes of this exercise, all that is required is an estimation of the total fluid motion in all three directions, which can then be compared with the fluid motion in the cross-shore direction.

To obtain the time-averaged values of u^2, v^2 and w^2, the values derived from the original 10Hz velocity data were averaged over blocks of 0.5s, resulting in a 2Hz TKE time-series. This, together with the cross-shore velocity time-series, is shown in figure 8.5.

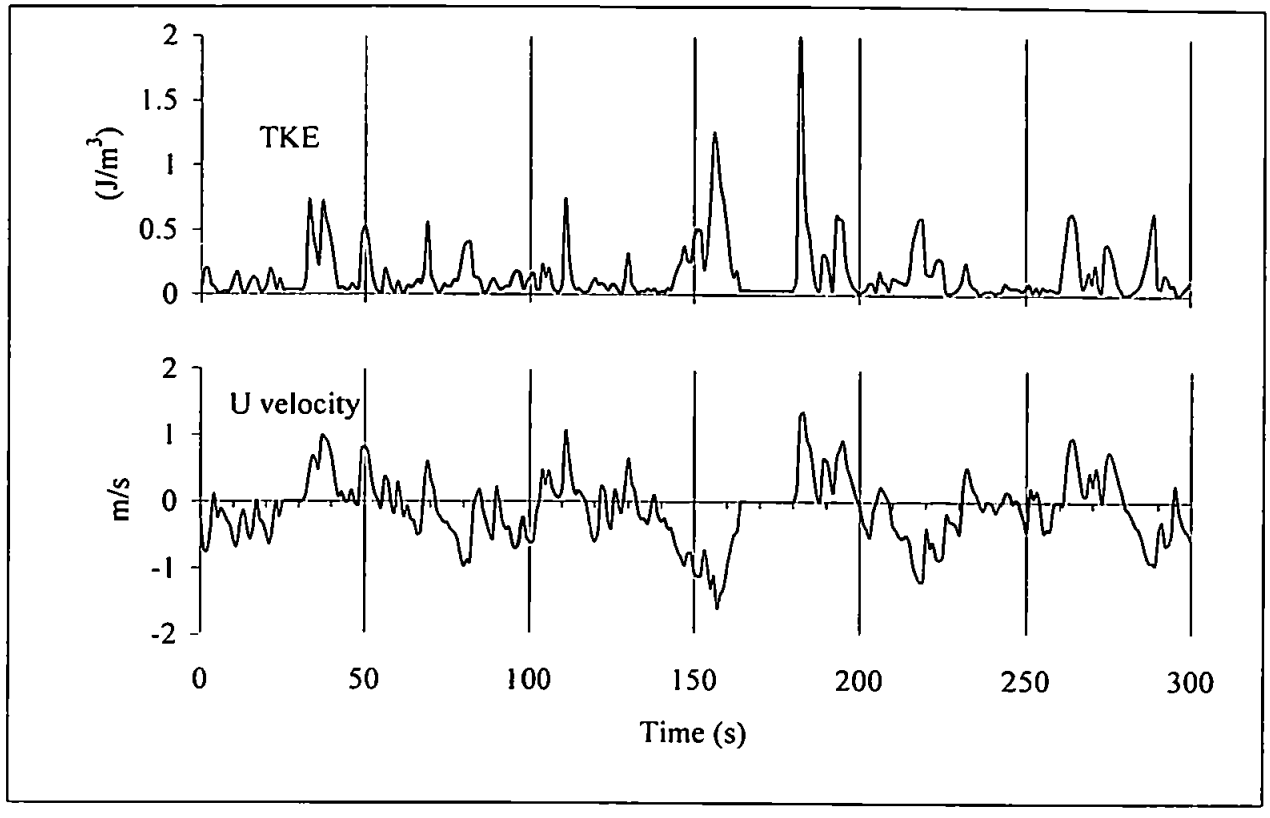

Figure 8.5: comparison of TKE (upper panel), and cross-shore velocity (lower panel) for the Muriwai data.

Initial inspection of figure 8.5 reveals that there are a number of occasions when large values of TKE are associated with uprush velocities, but corresponding or larger backwash velocities are accompanied by lower values of TKE. For example, compare t = 160s (large backwash velocity, small TKE) with t = 180s (similar uprush velocity, large TKE), illustrated in table 8.1. This suggests that the uprush might contain more turbulence than the backwash. An increase in u but a decrease in TKE also suggests that the TKE computations are not dominated by the cross-shore velocity.

Table 8.1: cross-shore velocity and TKE values.

	time (s)	u (ms^{-1})	TKE (Jm^{-3})
Backwash	160	-1.4	1.5
Uprush	180	1.3	2.0

To further investigate this hypothesis with some quantification, the average value of the ratio of TKE to velocity for all the uprushes (Ψ_u), was compared with that value for all the backwashes (Ψ_b), i.e.

$$\Psi_u = \overline{\left(\frac{TKE}{|u_u|}\right)} \tag{8.2}$$

and

$$\Psi_b = \overline{\left(\frac{TKE}{|u_b|}\right)} \tag{8.3}$$

where u_u and u_b are uprush and backwash velocities respectively. The time-series was filtered to include only onshore (offshore) velocities, to obtain the average of all the ratios for the uprush (backwash). Values of Ψ_u and Ψ_b were $\mathbf{0.81 Nsm^{-3}}$ and $\mathbf{0.49 Nsm^{-3}}$ respectively, further suggesting more turbulence in the uprush than the backwash.

8.3 Offshore transport from negative skewness

For offshore sediment transport in the swash-zone, one mechanism which is readily observed during high energy conditions is that associated with the larger-than-normal backwashes tending to occur at infragravity time scales. These reach greater velocities than the majority of backwashes, and they can be seen to start suspending and transporting sediment seawards as the velocity exceeds a threshold. On the velocity time-series the appearance of these backwashes would tend to show up as a negative skewness at infragravity frequencies.

Since beach erosion tends to occur during high energy conditions, then the processes causing offshore transport should become progressively more dominant as the sea state increases. Therefore, in high energy conditions, where the occurrence of these large backwashes is most noticeable on the time-series, there should be a corresponding increase in negative infragravity skewness.

In the storm time-series (see figure 8.6), examples can be seen of sediment suspension events uniquely associated with offshore velocities which have become large enough to exceed a threshold for suspension, e.g. at $t \approx 45s$ and 175s.

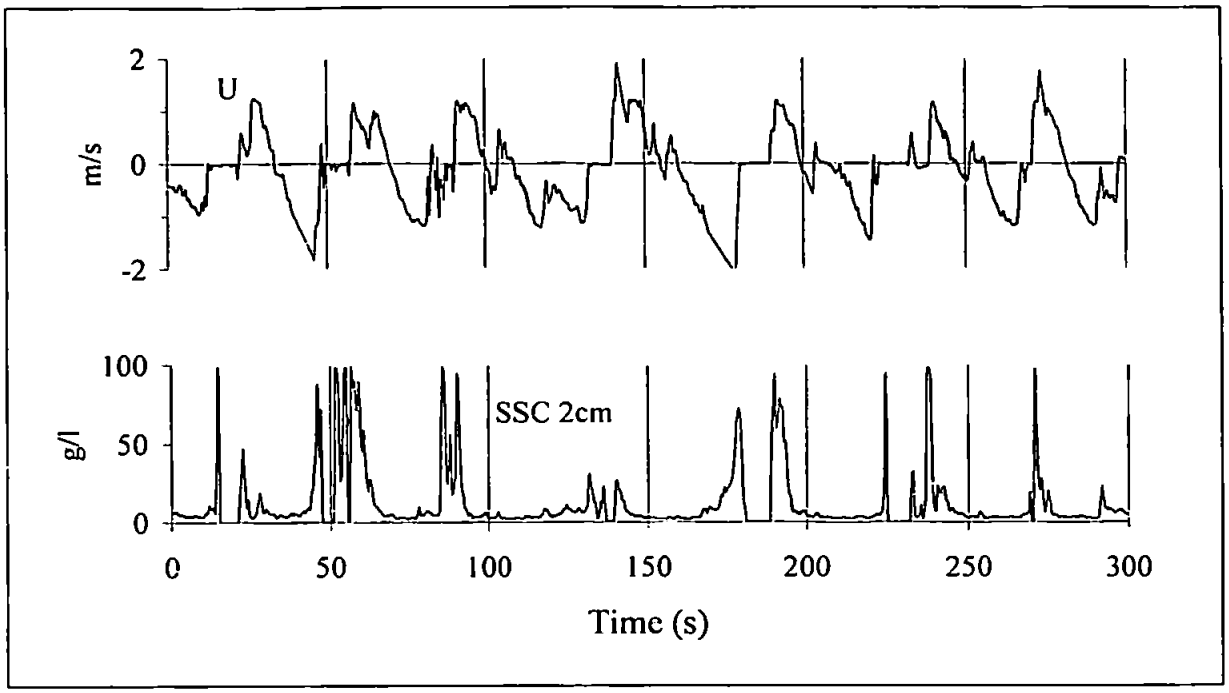

Figure 8.6: section of time series from storm data showing typical offshore transport events due to large backwashes at t ≈ 45 and 175s.

8.4 Quantification of skewness and asymmetry

8.4.1 Theory and results

The skewness (S) of the time-series may be quantified by using the normalised third moment of the time-averaged velocity, (e.g. Wells, 1967; Masuda and Kuo, 1981; Elgar, 1987; Elgar *et al*, 1988), i.e.

$$S = \frac{\langle u^3 \rangle}{\langle u^2 \rangle^{3/2}} \tag{8.4}$$

where u is the instantaneous velocity and the angle brackets denote time averaging.

A measure of the asymmetry (A) may be obtained from the skewness of the acceleration, therefore,

$$A = -\frac{\langle \varphi^3 \rangle}{\langle \varphi^2 \rangle^{3/2}} \tag{8.5}$$

where φ is the acceleration. Negative acceleration skewness is associated with positive velocity asymmetry, hence the minus sign (e.g. Doering, 1988). Figure 8.7 shows examples of hypothetical velocity time-series, providing a visual representation of the skewness and asymmetry quantities as computed from equations 8.4 and 8.5.

It must be pointed out that the magnitudes of skewness and asymmetry have no quantitative relation to sediment transport. Therefore, the potential transport due to skewness cannot be compared directly with that due to asymmetry. However, it does provide a useful method of comparing, say, the transport due to large backwashes (manifest in the time-series as negative infragravity skewness) on the calm day, with that on the storm day. Likewise, a comparison of the transport due to onshore acceleration (manifest as negative asymmetry) may also be made between the different days.

Total velocity skewness and asymmetry were calculated for the calm and storm data using this method, and also for the data obtained from Muriwai Beach, New Zealand. The three time-series were then filtered either side of 0.05Hz, and the skewness and asymmetry were calculated for the low and high frequency parts of the time-series. Results are shown in table 8.2, and a graphical representation is shown in figure 8.8.

Table 8.2: Skewness (S) and asymmetry (A) for calm and storm conditions. Values are dimensionless.

	Calm	Muriwai	Storm
S (total)	0.17	-0.63	-0.53
S (<0.05Hz)	0.04	-0.96	-0.81
S (>0.05Hz)	0.13	0.33	0.28
A (total)	-2.29	-1.58	-1.19
A (<0.05Hz)	-0.23	-0.36	-0.07
A (>0.05Hz)	-2.06	-1.22	-1.12

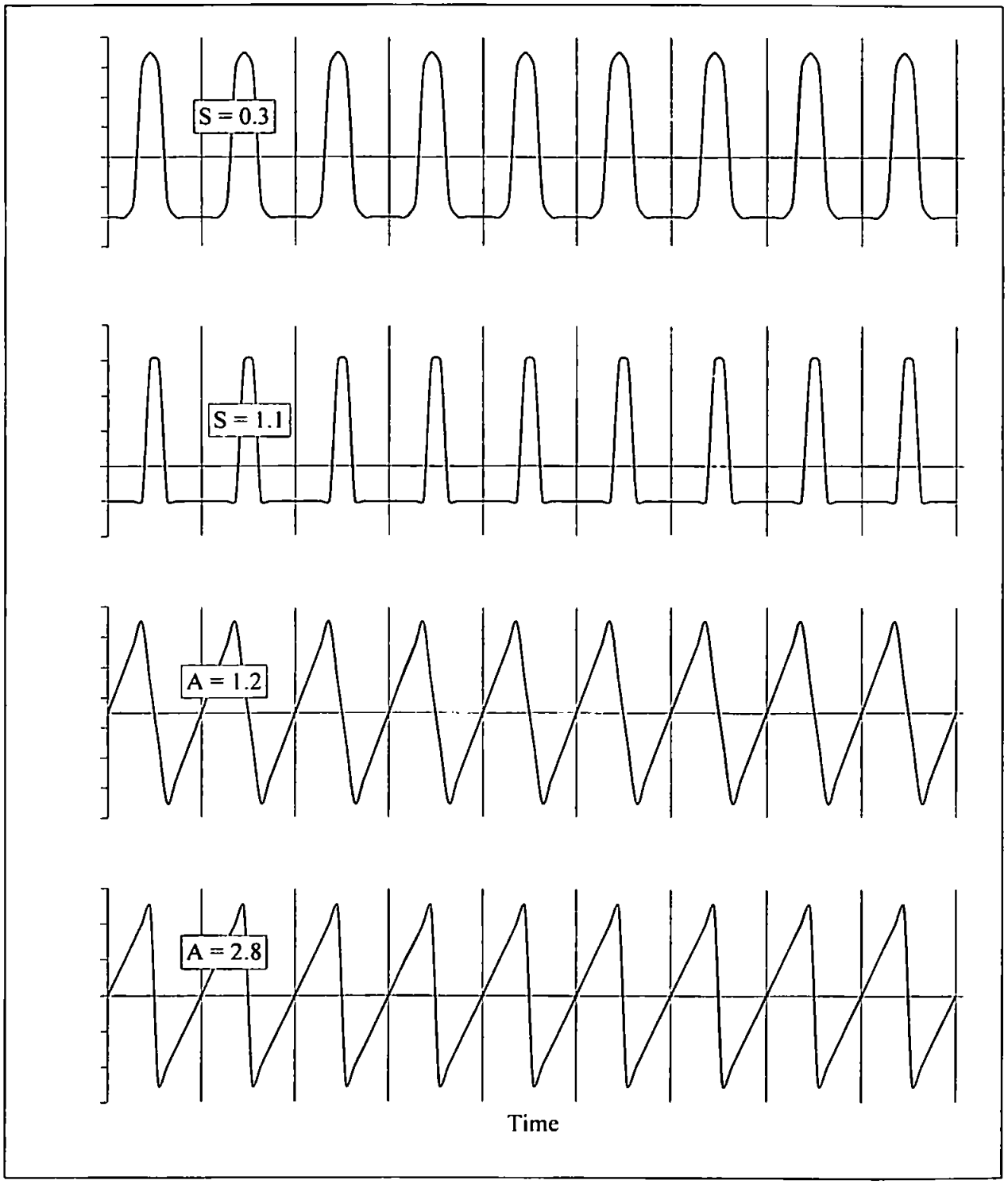

Figure 8.7: hypothetical skewed and asymmetric velocity time-series computed from equations 8.4 and 8.5.

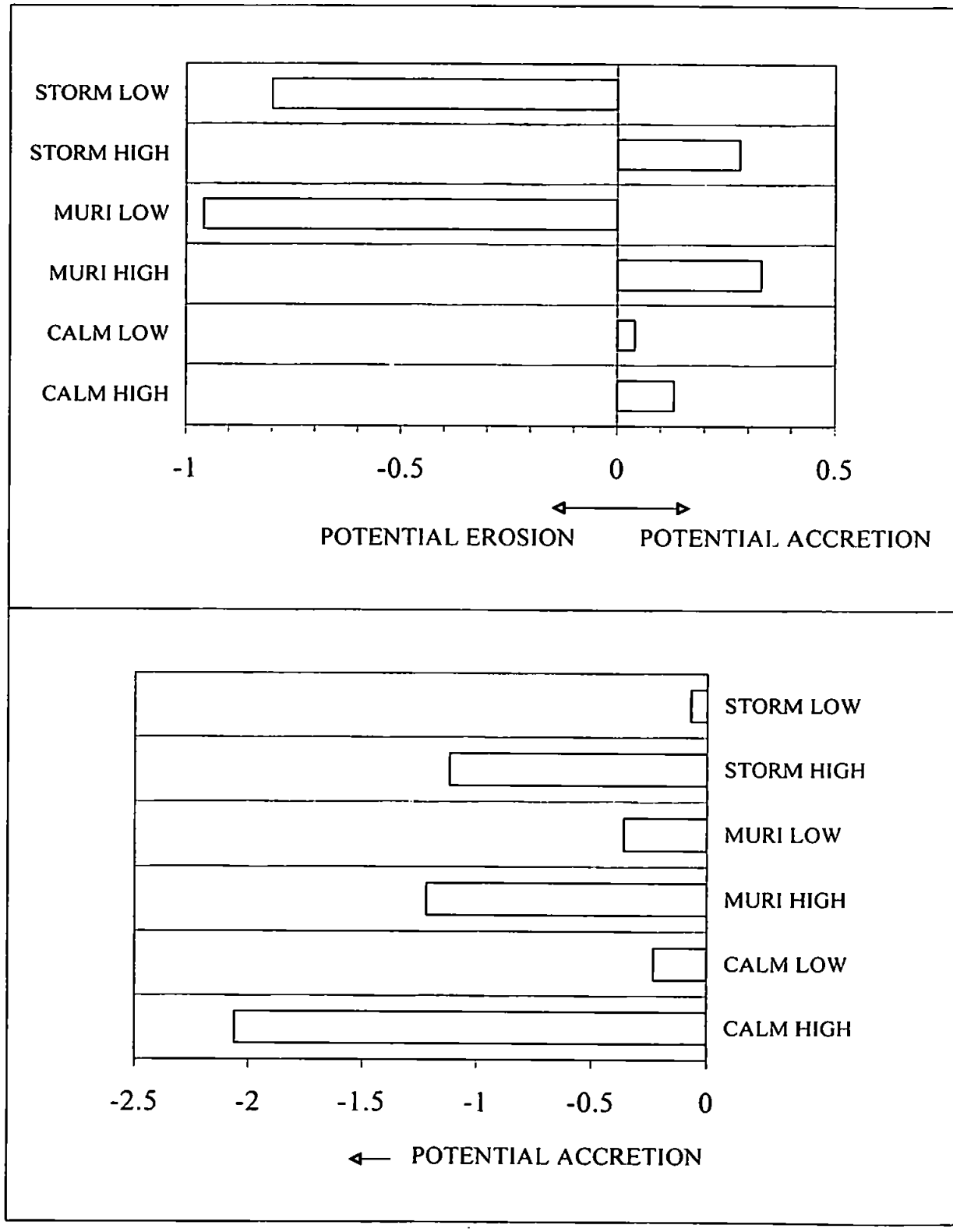

Figure 8.8: visual representation of skewness (top panel) and asymmetry (bottom panel) for calm and storm days, and the Muriwai data. 'Low' and 'high' refer to frequencies below and above 0.05Hz.

8.4.2 Calm-storm comparison

It can be seen that the total skewness is negative for the storm day, with a large negative contribution from the low frequency fluctuations, and a small positive high frequency contribution. This suggests the existence of a low frequency process which could increase the offshore transport in high energy conditions. The velocity field for the calm day is positively skewed at both high and low frequencies, suggesting a contribution to onshore transport by this mechanism during low energy conditions.

The asymmetry is negative for both calm and storm days, which is to be expected, since Eulerian velocity measurements in the swash-zone will always exhibit sudden onshore accelerations with the arrival of the swash-front. However, the negative asymmetry is larger on the calm day, principally at high frequencies, suggesting that, either the velocity changes are more sudden during the arrival of the swash-front, or the offshore accelerations during the rest of the swash cycle are more gradual. This suggests that this process is making a greater contribution to onshore transport in low energy conditions.

The increased occurrence of large backwashes whose velocity is likely to exceed some threshold can clearly be seen in the storm time series, and is confirmed by the large negative infragravity skewness calculated for the storm day. There was also about a three-fold increase in the infragravity-band energy, evident from the autospectra (section 7.2). The increase in negative infragravity skewness seems to coincide with an increase in infragravity-band energy, but the exact amount of skewness depends upon what happens during the shoaling process.

8.4.3 Muriwai-Perranporth comparison

The skewness and asymmetry for the Muriwai data appear to be very similar to the storm data, suggesting the transport to be more offshore-biased than expected, since the breaking wave height was at least 50% less than on the storm day.

In all three time-series presented here, the tidal height was such that the instruments were in the most landward position without actually drying out, i.e. in the most seaward part of the swash-zone. Since at Muriwai, the sensing volume of the current meter was placed 14 to 15cm above the bed, whereas at Perranporth it was 5 to 6cm above the bed, the average water depth must have been greater at Muriwai, i.e. the data is from a position further seaward than the Perranporth data. This might suggest inherent differences in the skewness and asymmetry.

To investigate this hypothesis, data from the cross-shore transect of measurements taken during the calm day, may be used. It must be borne in mind that that any variation of skewness and asymmetry with depth may, itself, be dependent on the prevailing conditions. Therefore only a rough idea may be obtained by using data from 'calm' conditions, only, where the infragravity skewness happened to be positive in the swash-zone.

The skewness and asymmetry were computed for the velocity time-series in the transect data burst, using equations 8.4 and 8.5. Results are shown in figure 8.9. The mean depth for each time-series is normalised by breaker depth.

It appears from figure 8.9 that, as the shoreline is approached from the break-point, (a) negative infragravity skewness becomes smaller, (b) positive incident skewness becomes smaller, (c) infragravity asymmetry remains fairly constant, and (d) negative incident asymmetry becomes larger.

The effect of 'moving' the Muriwai time-series further shoreward would be to make the infragravity skewness a smaller negative (offshore) value, and the incident asymmetry a larger negative (onshore) value. Therefore, the overall effect is to make the transport less biased towards the offshore, and therefore somewhere in between the two Perranporth days, which is correct if offshore transport is to increase with increasing overall energy.

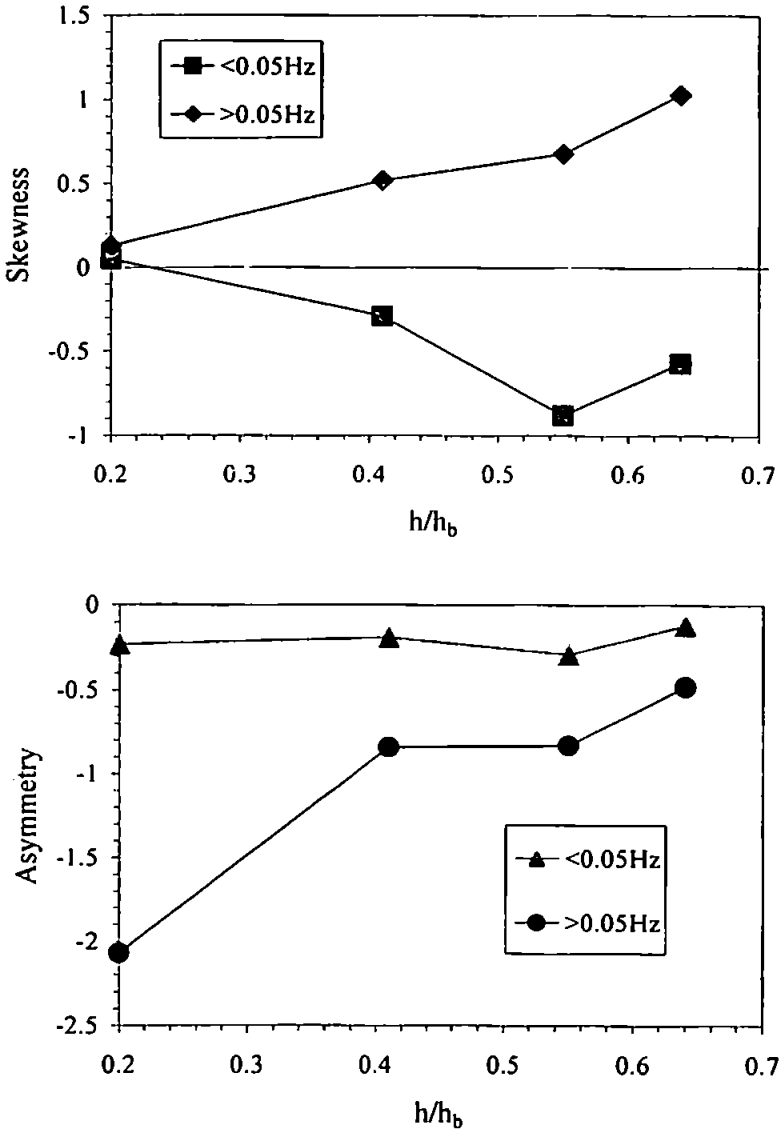

Figure 8.9: skewness (upper panel) and asymmetry (lower panel) over cross-shore transect.

8.4.4 Why is the infragravity skewness negative ?

It has been known for some time that infragravity skewness tends to be negative in the inner surf and swash-zones (e.g. Foote *et al*, 1994; Russell *et al*, 1996; Saulter *et al*, 1998; Russell and Huntley, 1999; and many others), but the exact processes which lead to the generation and interaction of harmonics to produce this negative skewness are still unclear. Ozanne (1998) hypothesised that one of the causes may be non-linear interactions between incident and reflected infragravity waves. Ozanne found that observed shoaling waves contained negative skewness near the shoreline, whereas those predicted by a Boussinesq model which did not take into account reflection, did not contain any negative skewness. However, Elgar *et al* (1997) found that triad interactions involving incident and reflected waves were far from resonance, therefore non-linear interactions were expected to be negligible.

To investigate whether the negative infragravity skewness might be related to reflection using some of the data obtained in the present study, the incoming and outgoing components of the velocity time-series were separated utilising the concurrent measurements of velocity and surface elevation. Guza *et al* (1984) proposed that the incoming and outgoing components of surface elevation could be separated by averaging the surface elevation expressed in terms of the velocity, with the measured surface elevation, i.e.

$$\eta_{in} = \frac{1}{2}\left(\eta + \sqrt{\frac{h}{g}}u\right) \tag{8.6}$$

$$\eta_{out} = \frac{1}{2}\left(\eta - \sqrt{\frac{h}{g}}u\right) \tag{8.7}$$

where η is instantaneous surface elevation (obtained by de-meaning the water depth), h is the time-averaged water depth, u is the instantaneous velocity and g is gravity. In simple terms, if u and η are out of phase (outgoing component), then η_{in} will be zero; likewise, if u and η are in phase (incoming component) the η_{out} will be zero. For a complete derivation of these equations using linear wave theory, see Miles (1997).

Similar expressions may be derived in terms of incoming and outgoing velocity components, i.e.

$$u_{in} = \frac{1}{2}\left(u + \sqrt{\frac{g}{h}}\eta\right) \tag{8.8}$$

$$u_{out} = \frac{1}{2}\left(u - \sqrt{\frac{g}{h}}\eta\right) \tag{8.9}$$

Using equation 8.8, the incoming component of the velocity time-series was computed for the storm data. The skewness for frequencies lower than 0.05Hz was then calculated using the techniques described above, for the incoming component only.

The result obtained for the infragravity skewness of the incoming wave only was **–0.21**. Comparing this with the **–0.81** previously obtained including both incoming and outgoing components, it can be seen that the skewness is still negative, but is greatly reduced by taking away the effect of reflection. Therefore, non-linear interactions between the incoming and reflected waves may have a part to play in making the infragravity skewness negative in the swash and inner surf-zones.

8.5 Measured sediment fluxes

By calculating the time-averaged sediment fluxes at different heights in the water-column, an insight may be gained into the potential effect of the transport mechanisms described in this study, particularly with regard to non-linearities in the velocity field.

As observed previously in the present study, sediment which is suspended on the backwash moves principally at low levels in the water-column, whereas on the uprush it is suspended to higher levels. This means that a backwash suspension event will tend to show a vertical gradient of SSC which increases towards the bed, whereas an uprush event might show a more vertically homogeneous profile of SSC. A comparison of a large backwash ($t \approx 178$s) followed by a large uprush event ($t \approx 188$s) is shown in the expanded time-series of figure 8.10, taken from the storm data. Here it can be seen that the vertical SSC gradient is much more pronounced on the backwash than on the uprush.

Since offshore transport appears to happen low in the water-column, then comparing vertical profiles of suspended sediment flux from high and low energy conditions should provide useful information on the increased dominance of offshore transport in high energy conditions.

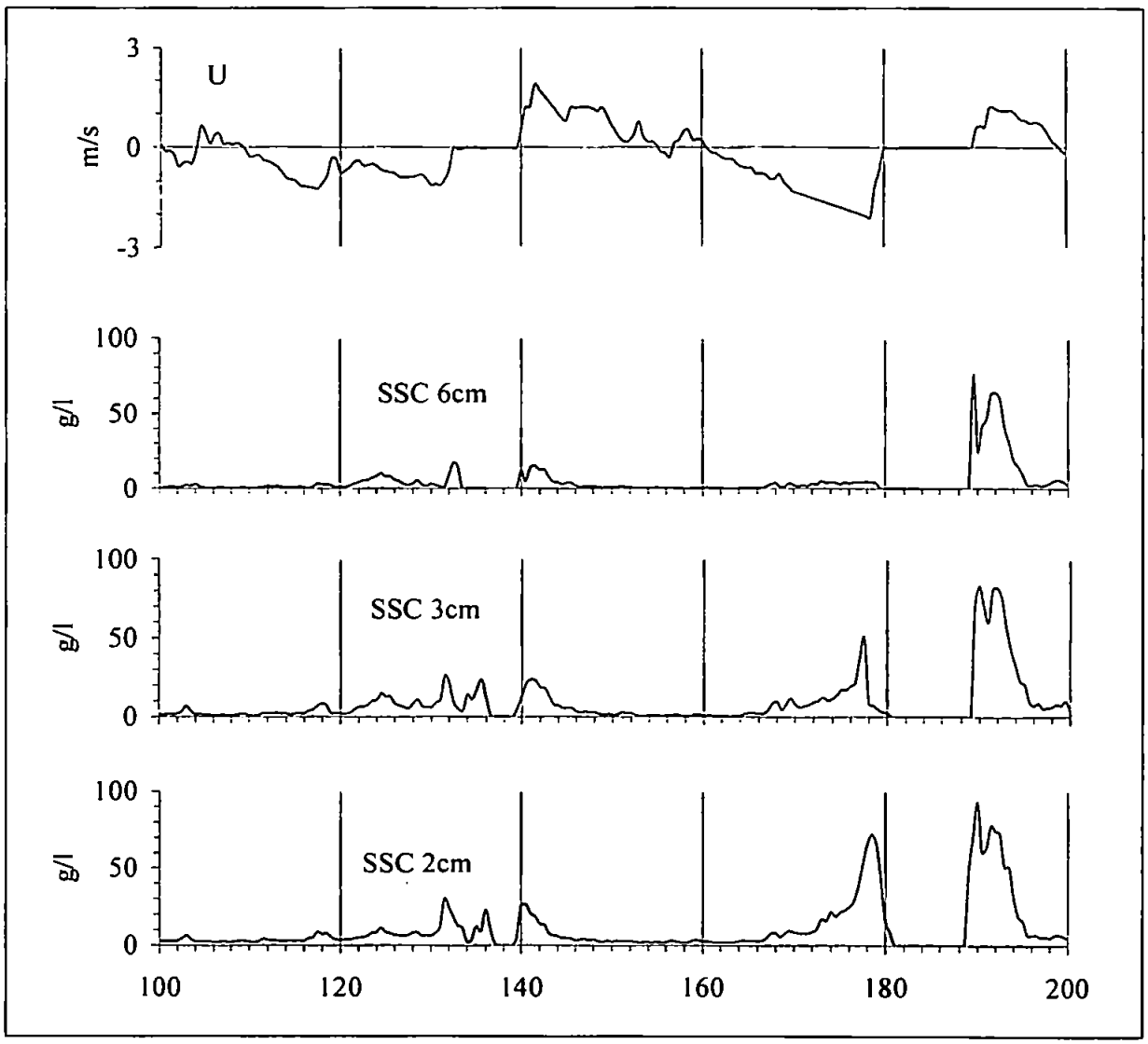

Figure 8.10: section of storm time-series showing backwash suspension event at t ≈ 178s and subsequent uprush event at t ≈ 188s. Sediment is suspended principally at low levels in the water-column on the backwash, but at all levels on the uprush.

The time-averaged net sediment fluxes for the calm and storm conditions were obtained by multiplying the velocity time-series with the SSC time-series, then averaging over time. Each instantaneous value of sediment flux will be zero unless both the velocity and concentration are non-zero at the same time (e.g. Huntley and Hanes, 1987). The sediment flux will then take the sign of the velocity. Note that, because there was only one current meter, situated at z = 5 to 6cm, then the velocity at this height had to be multiplied by the SSC at various different heights. The assumption has been made that the velocity is vertically constant between 1cm and 6cm. This can be justified to a certain extent if the formula of Jonsson (1966) is taken as a very rough estimate of boundary layer thickness (δ), i.e.

$$\delta = \frac{\pi}{2}\left(\frac{2\upsilon}{\omega}\right)^{\frac{1}{2}} \tag{8.10}$$

where $\upsilon \approx 10^{-6}$ m^2s^{-1} is the kinematic viscosity and $\omega = 2\pi / T$ where T is the wave period. With a maximum period of 100s (for infragravity waves), the boundary layer will still only be about 0.9cm thick using this formula. However, it must be stressed that choosing a formula for δ in the swash-zone is not straightforward, and there are many other formulae which give larger values (e.g. Sleath, 1970; Wilberg and Smith, 1983; Dyer, 1986; Sleath, 1987). The behaviour of the boundary layer is still very poorly understood, especially in difficult areas such as the swash-zone, and so calculation of its thickness is notoriously difficult (T. Aagaard, pers. comm., 1999).

The time-averaged onshore and time-averaged offshore fluxes for each day were also calculated, by averaging only positive or only negative fluxes from the time-series. Results for each height above the bed are shown in tables 8.3 and 8.4 together with the ratio of onshore to offshore flux. Note that the instrument heights were slightly different for the calm and storm days. Vertical profiles of net flux and onshore to offshore ratios are illustrated in figures 8.11 and 8.12 respectively.

Inspection of figure 8.11 shows that, for the calm day the flux is practically constant with height, although there is a slight decrease in onshore flux with height. In contrast, for the storm day there is a sharp increase in onshore flux with height, between z = 2cm and z = 3cm. At the heights measured, there appears to be no evidence of offshore flux.

From figure 8.12, the ratio of onshore to offshore transport appears to be lower for the storm day than for the calm day, at all levels in the water column. This suggests that, although the flux ratio is still positive (i.e. onshore dominated), the onshore dominance decreases as the energy increases from calm to storm conditions.

In figure 8.12 is also shown a hypothetical extrapolation of onshore/offshore transport ratios towards the bed. The lack of data at low levels means this cannot be confirmed quantitatively, but it does suggest that the transport might start to become offshore below about 1.5cm for the storm day and below about 0.5cm for the calm day.

Table 8.3: time-averaged suspended sediment fluxes for calm day ($kgm^{-2}s^{-1}$).

Height (cm)	Onshore	Offshore	Net flux	On/offshore ratio
10	0.15	0.04	0.11	3.75
5	0.23	0.07	0.16	3.28
2	0.46	0.18	0.28	2.56
1	1.02	0.73	0.29	1.39

Table 8.4: time-averaged suspended sediment fluxes for storm day ($kgm^{-2}s^{-1}$).

Height (cm)	Onshore	Offshore	Net flux	On/offshore ratio
11	3.22	1.12	2.1	2.88
6	3.63	1.56	2.07	2.32
3	4.41	2.45	1.96	1.79
2	4.07	3.12	0.95	1.29

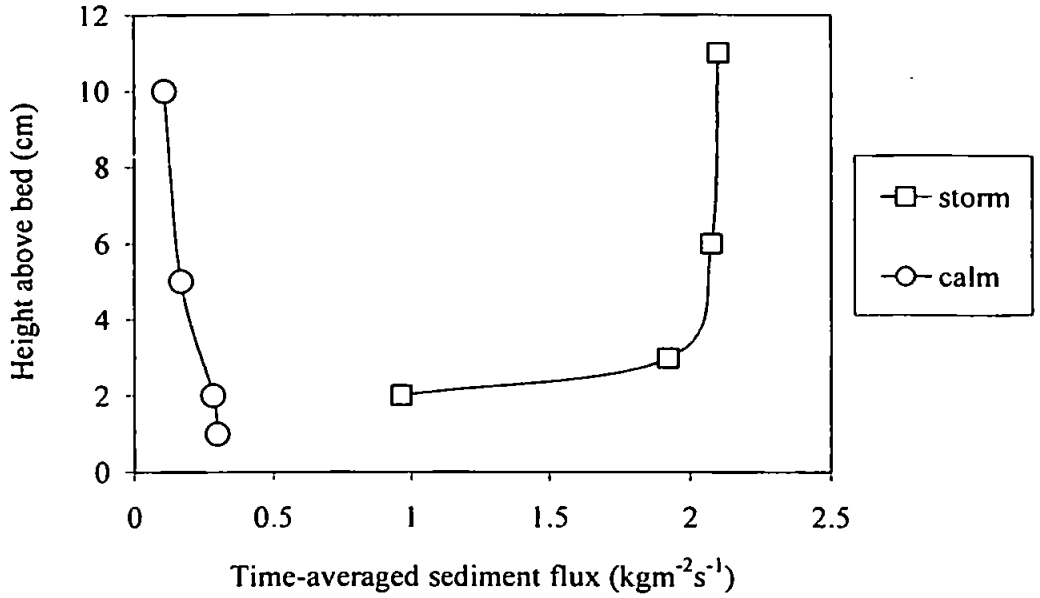

Figure 8.11: time-averaged net sediment fluxes as a function of height. Positive values represent onshore transport.

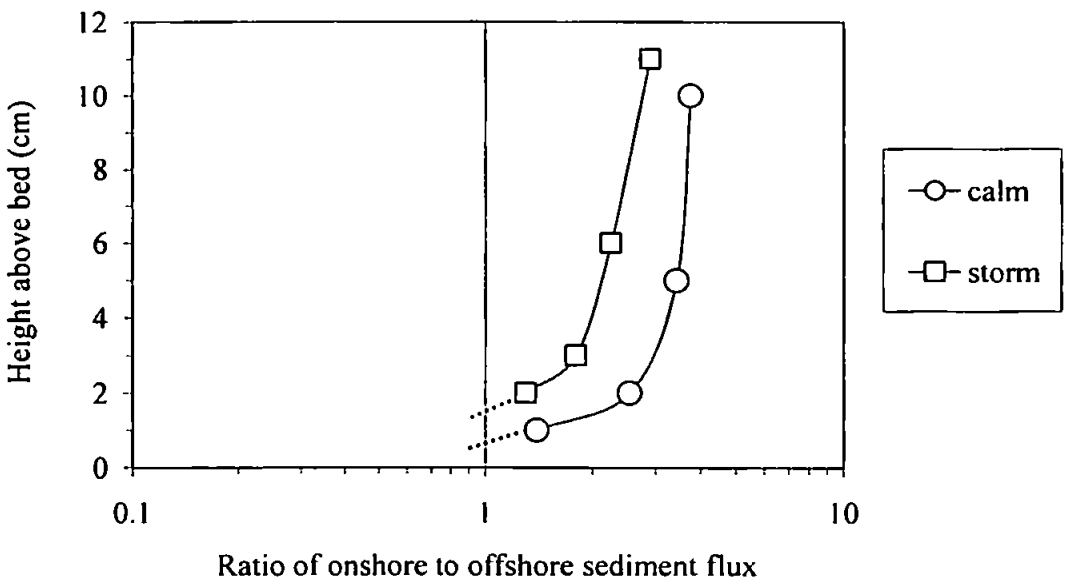

Figure 8.12: ratio of onshore to offshore time-average sediment fluxes as a function of height. The dotted lines indicate a possible extrapolation. Note the log scale.

8.6 Discussion

The results from this chapter identify two distinct processes which may contribute to erosion and accretion in the swash-zone. These are (a) the onshore transport from the offshore to onshore velocity transition and turbulence in the swash-front, and (b) the offshore transport from the thin, fast flowing, infragravity frequency backwashes. They are two totally different processes, and not simply reversals of each other.

The onshore transport associated with negative asymmetry, is probably almost entirely due to the turbulence in the swash-front, although some contribution is probably made by the near-bottom flow reversals themselves. Sharper offshore to onshore or larger zero to onshore transitions usually mean more turbulence, and so the two mechanisms are linked. It is easy to identify accelerations in the time-series and, without direct turbulence measurements, the existence of turbulence can be inferred by high accelerations in the time-series.

A direct comparison between the amount of swash-front turbulence in calm conditions with that in storm conditions would be a useful addition. Here only a confirmation that more turbulence exists in the uprush than the backwash, was able to be made. Note that the uprush/backwash turbulence comparison would probably be more convincing if the 3D velocity measurements were made closer to the bed (a greater difference would result between Ψ_u and Ψ_b). The fact that the current meter was dry for a large proportion of the backwash means that the times when the flow was most unidirectional were probably missed by these measurements.

The extra offshore transport due to the existence of large, infragravity frequency backwashes is shown to be a feature during storm conditions. These large backwashes are connected with negative infragravity skewness in the velocity field which seems to increase as conditions become more stormy. However, the link between a general increase in wave energy and an increase in negative offshore skewness is poorly understood. Suggestions have been made that non-linear triad interactions between the reflected and incoming infragravity wave may be a contributing factor, and some evidence exists, but it is still difficult to imagine how an increasing sea state would make these interactions change in such a way that they increased the negative skewness. Further study of this would require use of the bispectrum which, unfortunately, is beyond the scope of a study

such as the present one on a macrotidal beach, due to the large number of degrees of freedom required.

Velocity measurements in the 'true' swash-zone are difficult to obtain if the current meter is mounted too high above the bed, since it will be out of the water at important times during the uprush-backwash cycle. This is especially important when concurrent measurements of suspended sediment concentration are being made. Therefore, getting the current meter as close to the bed as possible is of paramount importance. At Perranporth, the electromagnetic current meter could not be mounted below z = 5cm due to interference effects from the bed, and at Muriwai it is believed that the sensing volume of the ADV was about 15cm from the bed. The calculated fluxes will only be non-zero if there is enough water to cover the current meter. Therefore some of the sediment movement low in the water column must have gone undetected by the instruments, and will not be included in the flux calculations. Visual observations suggest that a large proportion of the offshore sediment transport is at levels well below 5cm.

One is therefore led to speculate that if low-level measurements could be included, the net fluxes might turn out to be more offshore, although this cannot be confirmed until concurrent measurements of velocity and SSC are made at very low levels in the water column. The importance of low-level velocity measurements seems to have been somewhat neglected in comparison to SSC measurements. For example, Beach *et al* (1992) measured SSC down to z = 1.2cm, but their velocity measurements were made with an impeller current meter at z = 6cm; Osborne and Rooker (1998, 1999) employed an ADV to measure velocity, but this was mounted at z ≈ 5cm, (also, the ADV was pointing downwards, so that no velocity measurements could be made in water shallower than about 15cm).

Another point worth noting is that the true vertical flux gradient will depend upon the vertical velocity profile. It was shown that obtaining the thickness of the boundary layer in areas such as the swash-zone is not straightforward. It cannot therefore be stated that the measurements have definitely been taken above the boundary layer, which further highlights the need for co-located low-level velocity and SSC measurements. In the surf-zone, it has been shown that considerable errors may occur in flux calculations if velocity and SSC are not measured at the same height (Ogston and Sternberg, 1995).

It must also be borne in mind that sediment also moves along the bed itself, without actually being suspended into the water column (bedload). Hughes (1992) observed a kind of 'sand/water slurry' moving at high velocities on the backwash, and Masselink and Hughes (1998) have suggested that the sediment transport in the swash-zone be modelled

as sheet flow, rather than separating it into bedload and suspended load. To the author's knowledge an instrument capable of reliably and accurately measuring the sediment flux below 1cm has yet to be developed for field use.

The skewness and asymmetry computed for the Muriwai time-series suggests that the balance of onshore and offshore transport due to these processes was somewhere in between the two Perranporth days. There is no doubt that the Muriwai data lends considerable support to the conclusions drawn from the Perranporth data, although adjustments had to be made for the cross-shore position of the velocity measurements using a simple model, due to the fact that it was impossible to obtain measurements from the same cross-shore position.

8.7 Summary

The findings in this chapter may be summarised as follows:

- Inspection of time-series from the swash-zone has identified two possible mechanisms for accretion and erosion, namely (a) sediment suspension by the sudden offshore to onshore velocity transition and the turbulence in the swash-front, leading to subsequent onshore advection by the uprush, and (b) offshore transport due to low-frequency, fast flowing backwashes exceeding some threshold velocity.
- The above processes are linked to the prevailing wave conditions through the skewness and asymmetry of the velocity field. During low-energy conditions, negative incident asymmetry should dominate, favouring process (a), and contributing to possible accretion. During high-energy conditions, there should be a dominance of negative infragravity skewness, favouring process (b), and contributing to possible erosion. These processes are different from each other, and probably unique to the swash-zone.
- Quantification of low and high frequency skewness and asymmetry show increased negative infragravity skewness for the higher energy data implying potential contribution to erosion, and increased negative incident asymmetry for the lower energy conditions, implying potential contribution to accretion.
- A higher level of turbulence in the uprush than in the backwash suggests that swash-front turbulence is a major contributing factor in onshore sediment transport.

- The reason why negative infragravity skewness increases in higher energy conditions is poorly understood. However, there is some evidence that non-linear interactions between reflected and incoming infragravity waves may play a part.
- Calculation of vertical profiles of suspended sediment fluxes suggest that the net transport is onshore for both low and high energy conditions, but the ratio between onshore and offshore transport is decreasing for the high energy conditions. The net flux for the high energy conditions becomes less onshore with decreasing height.

This chapter of the thesis was based on *Suspended sediment transport processes in high energy swash* by T. Butt and P. Russell, accepted for publication in *Marine Geology*.

9. Infiltration-exfiltration

9.1 Introduction

One of the factors which may need to be taken into consideration for sediment transport in the swash-zone, is the vertical flow of water into and out of the bed, and its effect on sediment mobility. In the past, the effect of infiltration on sediment transport in the swash-zone has been assumed to be mainly connected with the percolation of water into the beach face, and hence the reduction of volume on the backwash (e.g. Grant, 1946; 1948; Emery and Gale, 1951; Duncan, 1964; Waddell, 1976). However, on fine to medium sand beaches, this mechanism is likely to be relatively unimportant compared with coarse sand or shingle.

It has more recently been hypothesised that fluidisation of the upper layer of sediment may occur due to rapid outflow of water from the beach face caused by sub-surface pressure forces acting vertically upwards on the backwash (Quick, 1991; Baird *et al*, 1996; Horn *et al*, 1998). On the uprush the water pressure will propagate rapidly into the upper layers of the sediment; then on flow reversal to backwash and subsequent reduction in swash depth, there will be a rapid decrease of pore-pressure, producing forces acting vertically upwards just below the surface. This may lead to rapid groundwater outflow and hence fluidisation. If the upper layers of sediment became fluidised then this might considerably increase the sediment transport since the fluidised layer would quickly become entrained by the seaward flow in the backwash.

This hypothesis was tested using a model by Baird *et al* (1996), who concluded that fluidisation may occur, especially in the latter stages of the backwash. Turner and Nielsen (1997) pointed out that rapid and relatively large upward fluctuations in the water table (simply a constant pressure surface) can be caused by minute amounts of downwards infiltration from swash uprush. Vertical flow magnitudes calculated from pore-pressure gradients measured in the field were two orders of magnitude too small for fluidisation. If the velocity of water-table rise had been (mistakenly) taken to be associated with upwards flow of water, then this would have easily exceeded the critical fluidising velocity.

Even if the upwards-directed pressure gradients are too small to produce fluidisation, they may still increase sediment transport on the backwash by reducing the effective weight of the sediment (i.e. 'destabilise' the bed). Conversely, downwards-

directed pressure gradients on the uprush will increase the effective weight of sediment (i.e, bed stabilisation), thereby decreasing the potential for sediment transport (Hughes *et al*, 1998; Nielsen, 1998). Therefore the net effect of the stabilisation-destabilisation process would be to bias the transport in the offshore direction.

Another mechanism which may have the opposite effect, is the altering of the thickness of the boundary layer due to vertical flow into and out of the beach face. This was investigated in the laboratory by Conley and Inman (1994), albeit outside the breakpoint. They confirmed that the thickness of the boundary layer is reduced by infiltration and increased by exfiltration, therefore making the near-bed velocity relatively greater during infiltration. The turbulent vortices during infiltration are maintained closer to the bed, thereby increasing the potential for sediment transport. During exfiltration the turbulent vortices are elevated further from the bed, effectively thickening the boundary layer and decreasing the potential for sediment transport. In the swash-zone, this process would tend to enhance uprush transport and decrease backwash transport, i.e. bias the net transport onshore. Schematic illustrations of the two processes above are shown in figures 9.1 and 9.2.

The balance between the two processes of bed stabilisation/destabilisation and boundary layer modification has been quantified by Nielsen (1998) and Turner and Masselink (1998; hereafter referred to as TM98), by defining a modified Shields parameter. On the uprush the numerator increases with decreasing w (upwards through-bed flow velocity), to account for the increased shear stress due to boundary layer thinning; and the denominator also increases with decreasing w, to account for the stabilisation brought about by infiltration. On the backwash, both the numerator and denominator decrease with increasing w to account for boundary layer thickening and destabilisation from exfiltration.

Nielsen (1998) hypothesised that quartz sands with a median grain size (d_{50}) of about 0.58mm are likely to be stabilised by infiltration (i.e. decreased transport on the uprush), whereas with larger grain sizes the boundary layer effects may start to become dominant, effectively increasing uprush transport.

The numerator of TM98, unlike Nielsen's, did not assume a linear relation between shear stress and infiltration velocity. They tested the modified Shields parameter using pore-pressure data from a beach with d_{50} = 0.5mm. Cross-shore velocities were obtained using a model. It was found that the effect of boundary layer modification appeared to dominate, with increased uprush transport and reduced backwash transport.

The purpose of this chapter is to examine some of the data collected as part of the present study, as a step towards improving the understanding of how infiltration-exfiltration influences the sediment transport in the swash-zone.

The question of whether fluidisation is likely to be an important factor is still under debate. Therefore a useful step is to investigate, using pore-pressure gradients, whether fluidisation was likely during the present study.

The apparently conflicting results of TM98 and Nielsen (1998) suggest that more study is required of the relative effects of the two processes which combine to cause a net onshore or offshore transport influence. The modified Shields parameter together with the measured velocities are used to assess which process was dominant during the present study. A representative swash event, obtained from ensembles of seven swash events from the mid-swash data, is examined in detail.

Finally, some sensitivity tests are performed, which attempt to identify the most important factors in determining which process will dominate under various different conditions. The equations derived contain some parameters (e.g. friction factor) which are difficult to estimate, and tests are done to assess the relative sensitivity of the results to changes in these parameters.

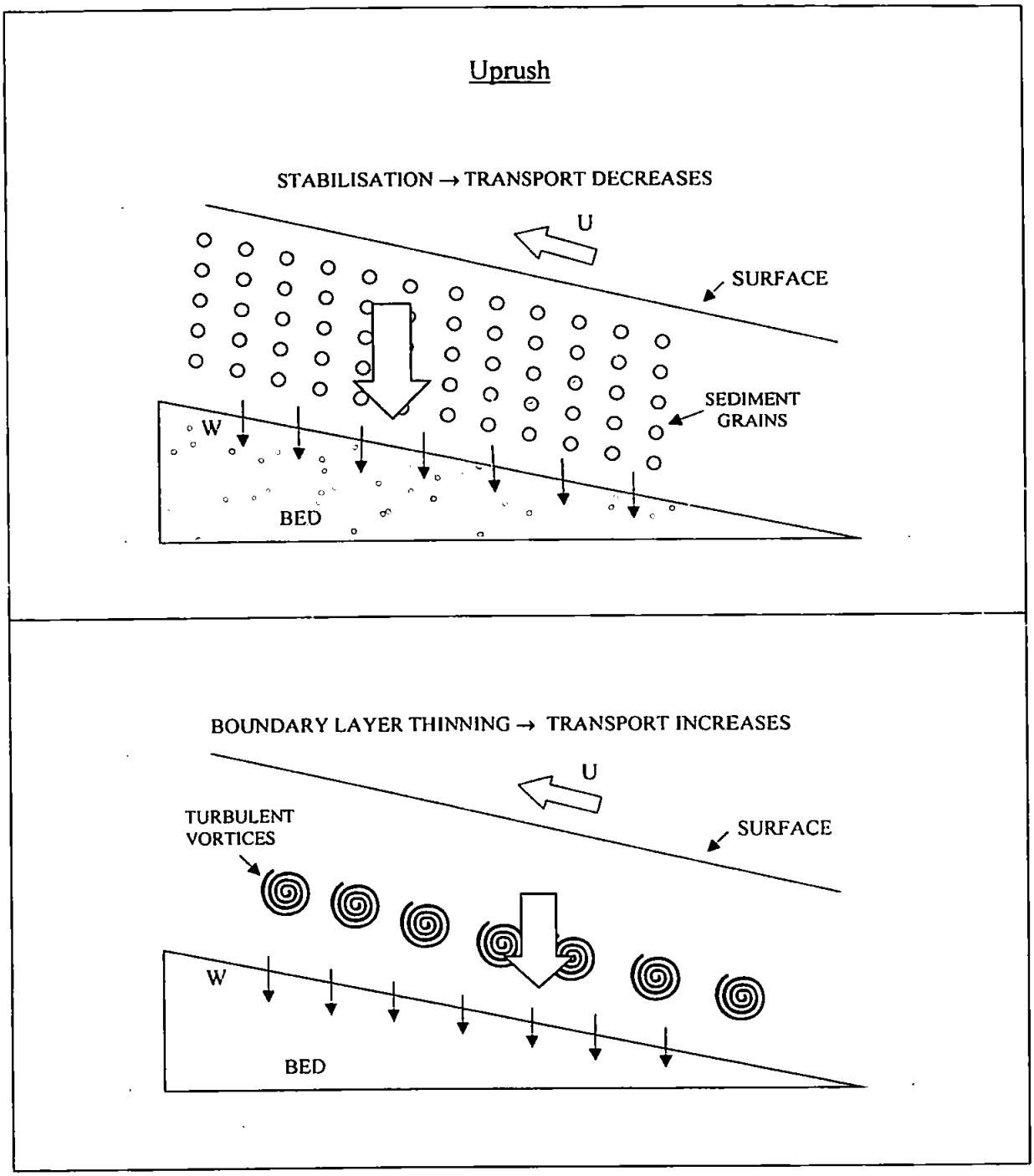

Figure 9.1: schematic representation of sediment stabilisation (top panel) and boundary layer thinning (bottom panel) due to infiltration on the uprush.

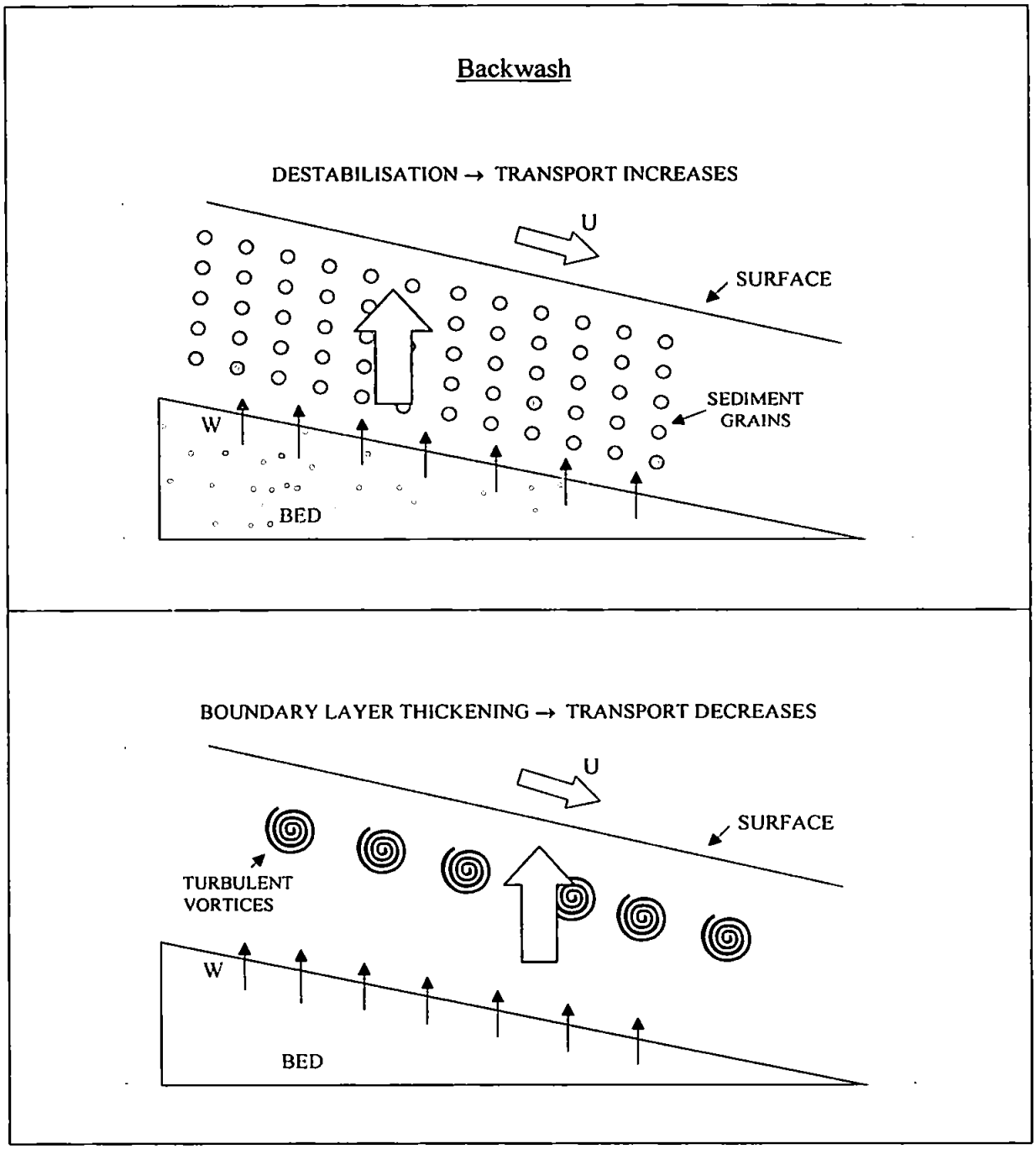

Figure 9.2: schematic representation of sediment destabilisation (top panel) and boundary layer thickening (bottom panel) due to exfiltration on the backwash.

9.2 Measurements

The measurements used for the analysis in this chapter were of cross-shore velocity at 5cm above the bed, water depth and sub-surface pore-pressure at distances of 2, 5, 9 and 13cm below the bed. Note that the pressure measurements presented are in hPa, where 1hPa is hydrostatically equivalent to 1cm head of water.

The data analysed in this chapter is from the mid-swash data burst, during moderately high energy conditions, with $H_b \approx 2.0$m and $T_s \approx 7$s. Since this chapter is more concerned with the characteristics of individual swash events rather than quantities averaged over the time-series, it was considered most appropriate to use data from the mid swash-zone, where the instruments were wetting and drying on almost every swash cycle.

9.3 Stabilisation-destabilisation and potential fluidisation

To determine the effective weight of surficial sediments due to the action of upwards or downwards directed pore-pressure gradients brought about by swash, the vertical balance of forces must be considered. The downward force per unit volume (F_g) due to gravity is given by

$$F_g = \rho_s g \tag{9.1}$$

where ρ_s is the sediment density and g is gravity. The total buoyancy force per unit volume (F_b) including any seepage force associated with infiltration or exfiltration is given by

$$F_b = \rho g\left(1 + 0.5\frac{w}{K}\right) \tag{9.2}$$

where ρ is the water density, w is the vertical fluid velocity in the bed (positive upwards), and K is the hydraulic conductivity [ms^{-1}]. The first term on the right hand side is the hydrostatic force and the second term is the seepage force. It has been suggested by Martin (1970), that the seepage force at the surface is about 50% of that within the bed, hence the factor of 0.5 in the second term.

Using Darcy's law, the buoyancy force per unit volume may also be given by the vertical pressure gradient, $\partial p/\partial z$, hence

$$\frac{\partial p}{\partial z} = -\rho g\left(1 + 0.5\frac{w}{K}\right)$$

i.e.
$$-\frac{\partial h}{\partial z} = \left(1 + 0.5\frac{w}{K}\right) \tag{9.3}$$

where h is the equivalent head of water corresponding to pressure p.

A downwards seepage force (i.e., infiltration) will cause the effective weight of the sediment to increase due to fluid drag, which will have a stabilising effect. Conversely, an upwards seepage force (i.e. exfiltration) will cause the sediment to become less stable. The stabilising (downwards) force per unit volume (F_{stab}) is given by $F_g - F_b$. Therefore, combining (9.1), (9.2) and (9.3)

$$F_{stab} = g\left(\rho_s + \rho\frac{\partial h}{\partial z}\right) \tag{9.4}$$

When $F_{stab} = 0$, the sediment becomes weightless, which leads to the possibility of bed fluidisation. Hence the condition for fluidisation is given by

$$s = -\frac{\partial h}{\partial z} \tag{9.5}$$

Where $s = \rho_s/\rho$ is the specific gravity of the sediment. If the water density is taken as 1025kgm^{-3} and the sediment density as 2650kgm^{-3} (for quartz) then fluidisation will occur if $(-\partial h/\partial z)$ exceeds about 2.6. If the downwards force is equal to gravity alone, i.e. the seepage force is zero, then $-\partial h/\partial z = 1$. So values of $-\partial h/\partial z$ below unity imply stabilisation of the bed, values above unity imply destabilisation, and values above 2.6 indicate the potential for bed fluidisation.

Figure 9.3 shows time-series of velocity, pore-pressure at four levels below the bed, and the pore-pressure gradient between the top and bottom sensors, taken from the mid-swash data burst. Each uprush-backwash cycle can clearly be seen, with the instruments submerging then emerging with each swash cycle.

Large, short duration, downwards-directed pore pressure gradients can be seen on the uprush, and longer duration upwards pressure gradients on the backwash. These pore-pressure gradients within the bed coincide with the variation in swash depth, which is the driving force for through-bed vertical flow. The values of $-\partial h/\partial z$ only reach about 1.2, so fluidisation is unlikely in this case.

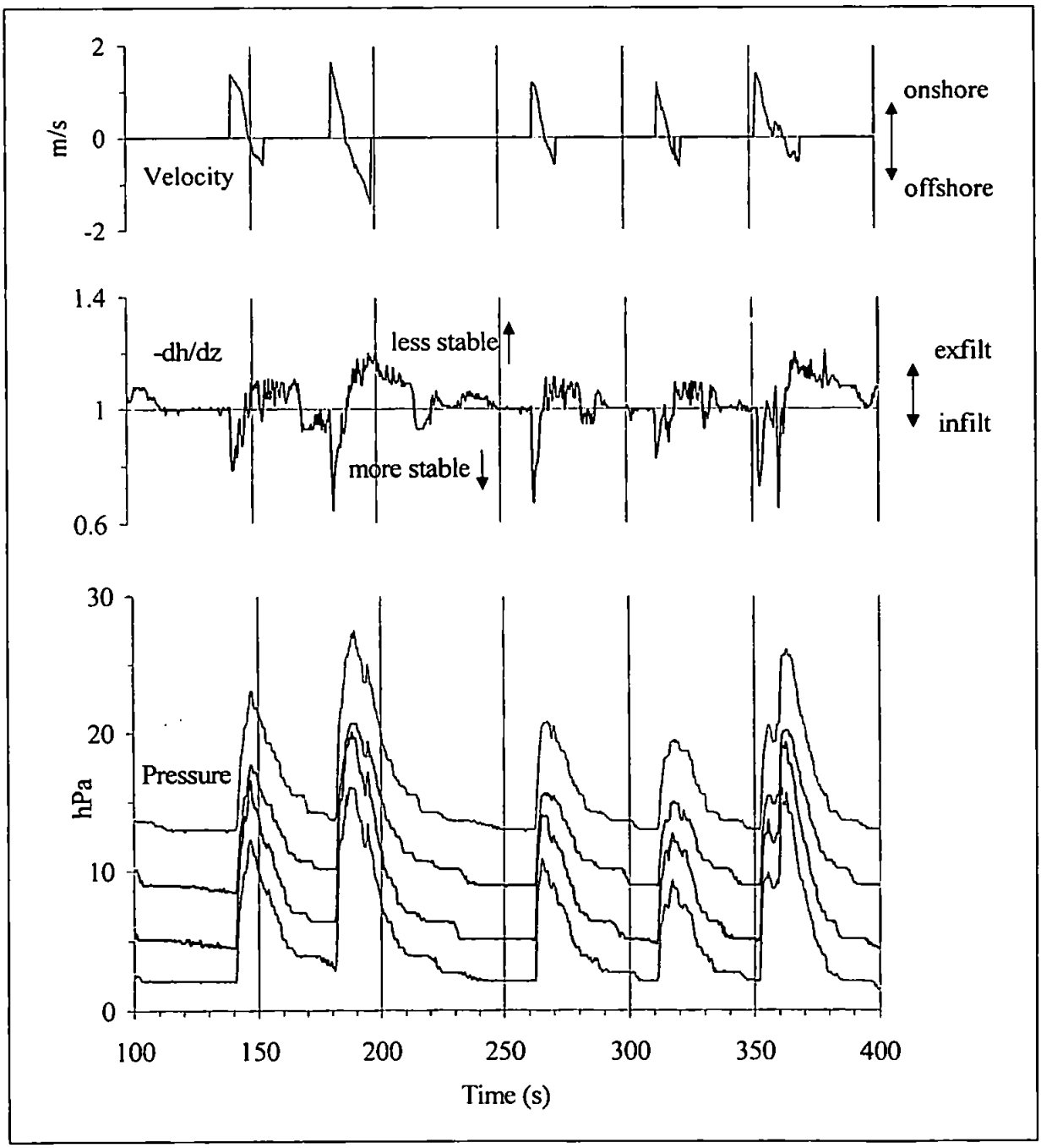

Figure 9.3. Representative time-series of cross-shore velocity (upper panel), vertical pore-pressure gradient (middle panel) and below-bed pore-pressures (lower panel), from mid-swash data. The lowest pressure trace corresponds to the transducer nearest the bed. Pressures are gauge, i.e. zero corresponds to atmospheric. 1hPa ≡ 1cm head of water.

9.4 Revised Shields parameters

The Shields parameter, θ (Shields, 1936) expresses the ratio between the disturbing and stabilising forces on sediment at the bed:

$$\theta = \frac{\tau}{\rho g d(s-1)} \tag{9.6}$$

where τ is the bed shear stress, ρ is the fluid density, d is the median grain size, and $s = \rho_s/\rho$ is the specific gravity of the sediment, where ρ_s is the sediment density. For the purposes of the present study, the denominator may be simplified to W, the immersed sediment weight per unit area. Hence, using the suffix '0' for the specific case of no through-bed flow,

$$\theta_0 = \frac{\tau_0}{W_0} \tag{9.7}$$

To quantify the effects of in-exfiltration, modifications to the numerator and denominator of this equation have recently been made by Nielsen (1998) and TM98, i.e.

$$\theta_w = \frac{\tau_w}{W_w} \tag{9.8}$$

where the suffix w means that this parameter contains extra terms to account for through-bed flow.

The two opposing effects of in-exfiltration may be quantified using (9.8). For example, on the uprush, when there is infiltration, the numerator will increase due to the thinning of the boundary layer but the denominator will also increase due to the extra stabilisation imparted on the sediment grains. On the backwash, when there is exfiltration, the numerator decreases due to the thickening of the boundary layer but denominator will also decrease due to destabilisation. Therefore, the Shields parameter will have a net increase or decrease according to the balance between the two opposing processes.

A simple and well-proven model for sediment transport (e.g. Meyer-Peter and Müller, 1948) is one in which the dimensionless sediment transport rate is proportional to

$\theta^{3/2}$, i.e. $Q \propto \theta^{3/2}$ where Q is the dimensionless transport. This reduces to a 'velocity-cubed' dependence analogous to the energetics approach (Bailard, 1981), and as applied in the surf-zone by Russell and Huntley (1999). Hence

$$Q_w = \left(\frac{\tau_w}{W_w}\right)^{\frac{3}{2}} \tag{9.9}$$

and

$$Q_0 = \left(\frac{\tau_0}{W_0}\right)^{\frac{3}{2}} \tag{9.10}$$

The difference between equations (9.9) and (9.10) will isolate that part of the dimensionless sediment transport due to in-exfiltration, and therefore give a simple indication of whether in-exfiltration effects are biasing the sediment transport one way or another:

$$Q_{infilt} = Q_w - Q_0 \tag{9.11}$$

i.e.

$$Q_{Infilt} = \frac{u}{|u|}\left[\left(\frac{\tau_w}{W_w}\right)^{\frac{3}{2}} - \left(\frac{\tau_0}{W_0}\right)^{\frac{3}{2}}\right] \tag{9.12}$$

The right-hand-side of (9.12) is multiplied by u/|u| to preserve the net direction of potential sediment transport. For example, if the total transport (including that due to in-exfiltration) is greater than the transport without in-exfiltration, the effect of Q_{infilt} will be to increase the sediment transport in the direction of the flow. If this happens during the uprush then the dominant process will be boundary layer thinning, but if it happens during the backwash, then the dominant process will be destabilisation. The four basic scenarios are illustrated in table 9.1.

Table 9.1: various solutions of equation (9.12).

u/|u|	Flow direction	Balance of terms inside bracket	Q_{infilt}	Dominant process
+1	onshore	term1 > term2	+ve (onshore)	boundary layer thinning
+1	onshore	term 1 < term2	-ve (offshore)	stabilisation
-1	offshore	term1 > term2	-ve (offshore)	destabilisation
-1	offshore	term1 < term2	+ve (onshore)	boundary layer thickening

9.5 Derivations of the modified Shields parameter

The immersed sediment weight per unit volume of the bed (W) may be adjusted for in-exfiltration by simply adding the weight loss or gain caused by seepage to the denominator of (9.6). (Note that the vertical velocity (w) is positive upwards):

$$W_w = \rho g d(s-1) - 0.5\rho g d\frac{w}{K}$$

i.e.
$$W_w = \rho g d\left(s - 1 - 0.5\frac{w}{K}\right) \tag{9.13}$$

To modify the numerator, Nielsen (1998) hypothesised a linear relation between shear stress (τ) and the relative vertical velocity (w/u). Based on this assumption, the following may be defined:

$$\tau_w = \tau_0\left(1 - \alpha\frac{w}{u}f'^{-1/2}\right) \tag{9.14}$$

where f' is a friction factor and α is an empirical constant.

TM98 have derived an alternative form for the modified numerator, which was based on the work by Mickley *et al* (1954), and Conley and Inman (1994). The numerator, unlike Nielsen's, does not assume a linear relation between shear stress and relative vertical velocity. The modified shear stress may be defined as follows:

$$\tau_w = \tau_0 \left(\frac{\Phi}{e^{\Phi} - 1} \right) \tag{9.15}$$

where

$$\Phi = \frac{c}{f'} \frac{w}{|u|} \tag{9.16}$$

where c is an empirical constant, which is about 2.0 for quasi-steady flow (Mickley *et al* 1954), and f′ is the friction factor.

Using the quadratic stress law, i.e.

$$\tau = 0.125 \rho f' u^2 \tag{9.17}$$

and equations (9.12) to (9.16), an expression for the relative sediment transport due to the effects of in-exfiltration (Q_{infilt}) is given by:

$$Q_{Infilt} = u^3 \left(\frac{f \left(1 - \alpha \frac{w}{u} f'^{-1/2} \right)}{8gd(s - 1 - 0.5w/K)} \right)^{\frac{3}{2}} - u^3 \left(\frac{f'}{8gd(s-1)} \right)^{\frac{3}{2}} \tag{9.18}$$

or

$$Q_{Infilt} = u^3 \left(\frac{f' \Phi / \left(e^{\Phi} - 1 \right)}{8gd(s - 1 - 0.5w/K)} \right)^{\frac{3}{2}} - u^3 \left(\frac{f'}{8gd(s-1)} \right)^{\frac{3}{2}} \tag{9.19}$$

Note that it is unnecessary to multiply the right hand side by u/|u| to preserve the direction of transport. This is clarified by taking u^3 outside the brackets.

9.6 Quantification of transport modification from in-exfiltration

Before equation (9.18) or (9.19) can be applied, the values of various parameters must be determined. For quartz sand in water, $s \approx 2.6$. With a knowledge of the hydraulic conductivity (K), a value for w may be obtained from (9.3). To obtain a value for K, the empirical formulation of Bear (1972) is used, i.e.

$$K = \left(\frac{\rho g}{\mu}\right)\frac{n^3}{(n-1)^2}\left(\frac{d^2}{180}\right) \tag{9.20}$$

where ρ is water density, $\mu \approx 10^{-3}$ Nsm^{-2} (Williams and Elder, 1989) is the dynamic viscosity, $n \approx 0.45$ is the porosity (Dyer, 1986) and $d = d_{50}$ the median grain size. For the grain size of 0.24mm in the present study, K is estimated to be of the order of 0.001 m/s.

The friction factor (f') is estimated using a formula for steady flow, since it is preferred to treat the flow in the swash-zone as quasi-steady (I. Turner, pers. comm., 1999), and the use of a formula for orbital flow (e.g. Swart, 1974; Wilson, 1989), is considered inappropriate (*c.f.* TM98; see also below).

The friction factor is often estimated by combining various basic equations relating to the boundary layer (e.g. Hughes, 1995). The von Karmen-Prantl equation ('law of the wall') gives the velocity profile in the boundary layer:

$$\frac{u(z)}{u_*} = \frac{1}{\kappa}\ln\left(\frac{z}{z_0}\right) \tag{9.21}$$

where u(z) is the velocity at height z above the bed; u_* is the friction velocity where $u_*^2 = \tau/\rho$; $\kappa \approx 0.4$ is the von Karman constant, and z_0 is the roughness length of the bed. If the depth-averaged velocity is assumed to occur where $z = h/e \approx 0.37h$, and the roughness length is approximately k/30 where h is the water depth and k is the Nikuradse effective bed roughness (van Rijn, 1993), then (9.21) may be written as

$$\frac{\bar{u}}{u_*} = 2.5\ln\left(11\frac{h}{k}\right) \tag{9.22}$$

Combining (9.17) with (9.22):

$$f' = 1.28\left(\ln\left(11\frac{h}{k}\right)\right)^{-2} \tag{9.23}$$

To obtain a value for k, it will be assumed that the bed is approximately flat, and any bedforms are negligible. Van Rijn (1982) reasoned that the grain roughness (k) presented to the flow is related to the grain size, and proposed

$$k \approx 6d_{50} \tag{9.24}$$

Therefore, for a particular grain size, the friction factor becomes a function of the water depth, i.e. it is time-dependent.

Equation (9.18) contains the empirical constant α for which a suitable value is presently unknown (P. Nielsen, pers. comm, 1998). The sensitivity of the equation to this parameter is quite low (the value of α was arbitrarily varied over three orders of magnitude and the average and maximum values of Q_{infilt} were only found to vary between 1.14% and 3.1% respectively). However, it is still preferred to use equation (9.19), whose numerator is able to take into account the possible non-linear relation between shear stress and velocity (Conley and Inman, 1994).

Figure 9.4 shows a representative section of the time-series of Q_{infilt} from the mid-swash data, calculated from (9.19). Also shown for comparison are the cross-shore velocity (u), upwards velocity (w), and the no through-bed flow equivalent transport (Q_0).

Both on the uprush and backwash, the effects of in-exfiltration appear to be biasing the potential sediment transport towards the offshore. This means that, on the uprush, the stabilising effect is dominating over boundary layer thinning, and on the backwash, destabilising is dominating over boundary layer thickening. This finding appears to contradict the results of TM98, which showed the opposite trend that modified boundary layer effects were dominant for the simulated swash cycle.

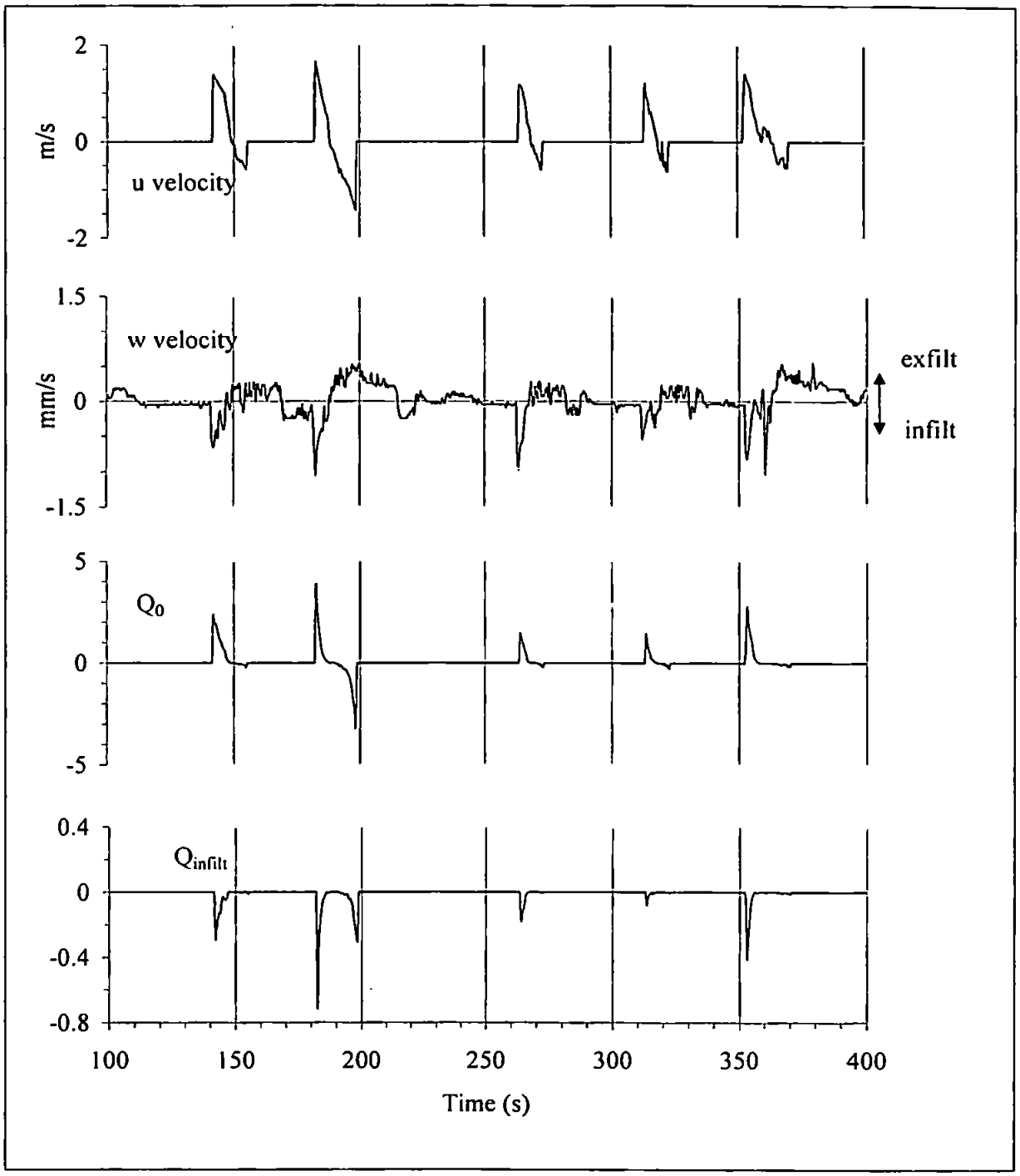

Figure 9.4: Representative time series of cross-shore velocity (positive onshore), vertical velocity (positive upwards), dimensionless sediment transport without in-exfiltration (Q_0) and dimensionless transport solely due to in-exfiltration effects (Q_{infilt}) calculated from equation (9.19).

To illustrate the effects of in-exfiltration over a single swash cycle, equation (9.19) was then computed using the ensembled swash events from the mid-swash data burst (the method of obtaining the ensembles was explained in section 7.5). A comparison of Q_0 and Q_w computed from the separate terms in (9.19), together with Q_{infilt} are shown over the ensembled swash cycle (see figure 9.5). Here, the decrease in transport on the uprush and the (smaller) increase in transport on the backwash can clearly be seen.

A useful exercise is to obtain the total dimensionless sediment transport over the uprush and backwash by integrating under the curves in figure 9.5, and then calculating the difference due to in-exfiltration. This provides useful insight to the net effect of in-exfiltration integrated over the entire swash cycle.

The total dimensionless sediment transported without taking in-exfiltration into account (I_0) is given by

For the uprush:
$$I_0(\text{uprush}) = \int_{t=0}^{t=0.5} (Q_0)dt \tag{9.25}$$

and for the backwash:
$$I_0(\text{backwash}) = \int_{t=0.5}^{t=1} (Q_0)dt \tag{9.26}$$

Taking in-exfiltration into account, the total sediment transported (I_w) is given by

For the uprush:
$$I_w(\text{uprush}) = \int_{t=0}^{t=0.5} (Q_w)dt \tag{9.27}$$

and for the backwash:
$$I_w(\text{backwash}) = \int_{t=0.5}^{t=1} (Q_w)dt \tag{9.28}$$

Since both the instantaneous transport and time are dimensionless, then I_0 and I_w have no physical units, and are used for comparison only. The most useful parameter here is the ratio between I_w and I_0 for the uprush, and the same ratio for the backwash. This gives an indication of the bulk effect of in-exfiltration over the uprush and over the

backwash. From the ensembled swash cycles, simple finite difference integration gives I_w/I_0 (uprush) = 0.895 and I_w/I_0 (backwash) = 1.045.

This means that, from the data collected in the present study, in-exfiltration is likely to decrease the total amount of sediment moved on the uprush by about 10.5%, and increase the total amount of sediment moved on the backwash by about 4.5%.

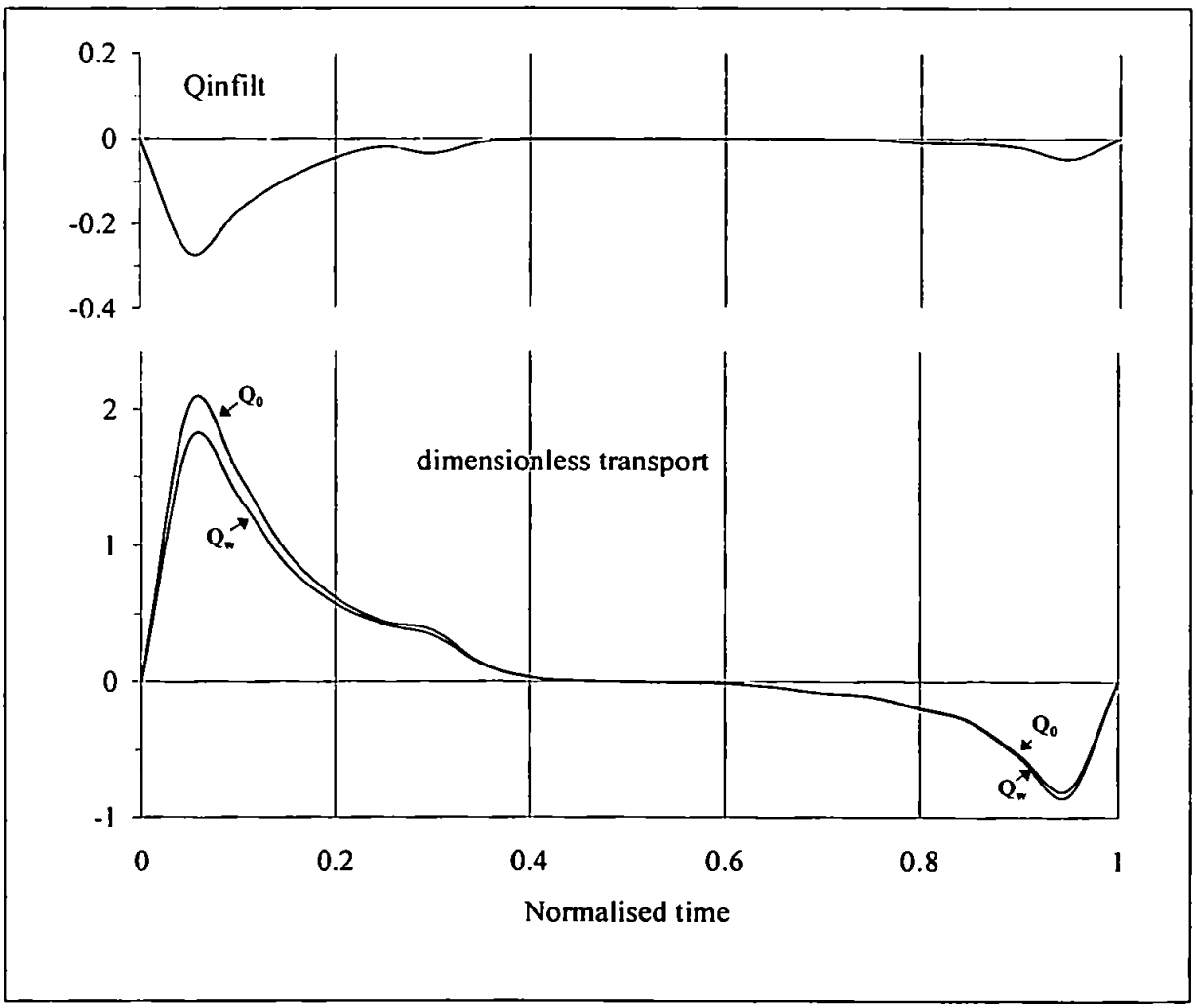

Figure 9.5: Comparison of transport with (Q_w) and without (Q_0) in-exfiltration over a single swash cycle, taken from the ensembles of swash cycles from the mid-swash data. Top panel (Q_{infilt}) is the transport solely due to the effects of in-exfiltration.

9.7 Sensitivity tests

The study of TM98 concluded that there was a dominance of boundary layer modification over stabilisation-destabilisation. As a result, they asserted that the role of infiltration-exfiltration in the swash-zone is generally to enhance uprush transport. This appears to conflict with the results of the present study. Potentially important differences in theoretical approach and experimental conditions between the two studies are:

- In the present study, the cross-shore velocity was measured at the field site. TM98 only measured sub-surface pore pressures: the cross-shore velocity was predicted using a model.
- The median grain size (d_{50}) at Perranporth was 0.24mm, whereas at Duck, USA (TM98), it was 0.5mm.
- TM98 used a friction factor calculation after Wilson (1989) which was originally designed for oscillatory flow. However, they acknowledge that the flows in the swash-zone are quasi-unidirectional since the constant (c) in the non-linear relation between τ and w/u is assumed to be 2.0 rather than 0.9 for oscillatory flow. In the present study, the friction factor was calculated from a formula for steady flow, and varied with water depth. The friction factor in TM98 was assumed to remain constant at 0.01.

It would therefore seem appropriate to examine the sensitivity of the calculations made in the present study, to various parameters. In other words, if certain parameters were allowed to vary, could the balance of transport due to in-exfiltration be made to change from offshore to onshore ?

An interesting exercise is to examine the dependency of grain size on the balance between the two processes. Nielsen (1998) suggested that boundary layer effects are only likely to dominate at grain sizes above about $d_{50} = 0.58$mm.

To assess the effect of grain size, the average value of Q_{infilt} over the whole mid-swash time-series, $\langle Q_{infilt} \rangle$, was calculated from equation (9.19), which was then repeated whilst varying the grain size from 0.1 to 1.0mm. Results are shown in figure 9.6. Where the curve crosses zero is the point where the balance goes from offshore to onshore.

Figure 9.6 shows that the direction of $\langle Q_{infilt} \rangle$ becomes more onshore with increasing grain size. This is in general accordance with nature, where coarser sediments are associated with beaches exhibiting steeper beachface gradients. The grain size at which the balance changes (the 'crossover' point, denoted here as d_{Q0}) is at about 0.55mm,

with a dominance of stabilisation-destabilisation below this value and a dominance of boundary layer effects above it. It can also be seen that around this area d_{Q0} is highly sensitive to errors or variations in the method of calculating Q_{infilt}. The other noteworthy point from figure 9.6 is that, below about d_{50} = 0.25mm, the offshore influence of infiltration-exfiltration increases much more sharply with decreasing grain size, indicating that the dominance of stabilisation-destabilisation is much more pronounced at smaller grain sizes.

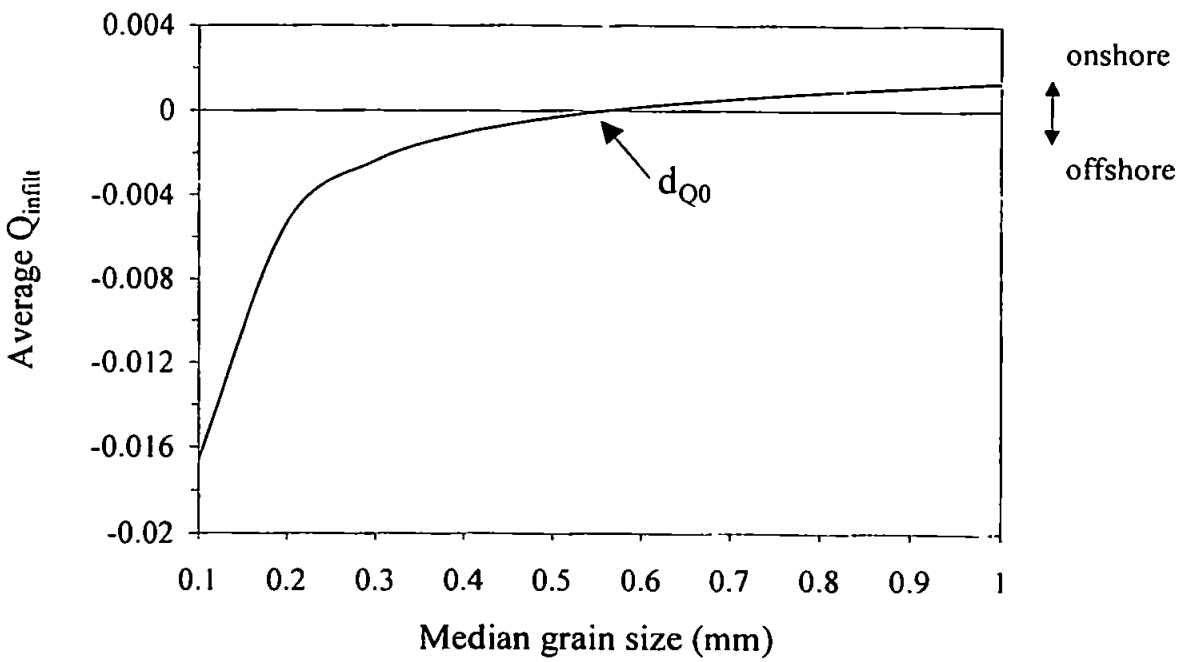

Figure 9.6: grain size dependency of the transport due to infiltration (Q_{infilt}), computed from equation (9.19) and averaged over the time-series. d_{Q0} is the point where (Q_{infilt}) goes from offshore to onshore.

The other two parameters which may be important, and which are not so straightforward to assess, are the friction factor (f') and the constant 'c' in equation 9.16.

The estimation of a friction factor is always a difficult task, especially for flows in the swash-zone which could be considered either quasi-steady or oscillatory, and in which the depth varies considerably. Some methods demand iterative techniques, and estimates

can vary over an order of magnitude. In TM98, f' was kept constant at 0.01, after using a formula for oscillatory flow following Masselink and Hughes (1998). In the present study it was considered more appropriate to use a formula for unidirectional flow, and the friction factor was not fixed but varied with water depth.

The constant 'c' relates to the non-linear relation between shear stress and infiltration (Conley and Inman 1994). Its value seems to be dependent upon whether or not the flow is considered oscillatory. In the present study the uprush and backwash are considered as two separate quasi-steady flows, and in considering the value of 'c', TM98 have also assumed the flow to be quasi-steady. However, along with Masselink and Hughes (1998) they have assumed the flow to be oscillatory when choosing a formula for f'.

It is therefore interesting to see how the balance between onshore and offshore transport might change if either f' or c are varied. This was accomplished by calculating a family of curves of $\langle Q_{infilt} \rangle$ v. d_{50} (similar to the one in figure 9.6) for a range of friction factors, and then calculating a further number of families of curves whilst allowing c to vary.

The result is a four-dimensional array which is somewhat difficult to visualise. Therefore it was decided to extract the value of d_{Q0} from each $\langle Q_{infilt} \rangle$ v. d_{50} curve, and plot this as a contour-plot in 'f'-c space'. This then gives an idea of how variation of f' and c affects the grain size at which the balance changes from offshore to onshore. Results are shown in figure 9.7. Each contour line has a unique $\langle Q_{infilt} \rangle$ v. d_{50} curve associated with it, with its own d_{Q0} value. Note that for the purpose of this sensitivity test, the friction factor is forced to various different values, although in the present study f' is dependent upon the depth, which changes with time.

It is instructive to focus on the region of figure 9.7 in the area around d_{Q0} = 0.24mm, i.e. d_{50} for the present study. If different methods were used in estimating f' and/or c, resulting in a point in f'-c space to the left hand side of the 0.24mm contour (i.e. $d_{Q0} < d_{50}$) then the balance would change to onshore, indicating a dominance of boundary layer effects over stabilisation-destabilisation.

It can also be seen that, around this region, the calculations are much more sensitive to f' than c. For the same values of f', using c = 0.9 (oscillatory flow) or c = 2.0 (steady flow) appears to make little difference. On the other hand, small changes in f' may tip the balance one way or the other. If f' had been assumed fixed in the present study, and the method of estimation had resulted in a value below about 0.0025, then the balance probably would have been onshore. Therefore, careful consideration of the method of

calculating the friction factor is important, if correct assessment of the direction of influence of in-exfiltration on the sediment transport is to be achieved.

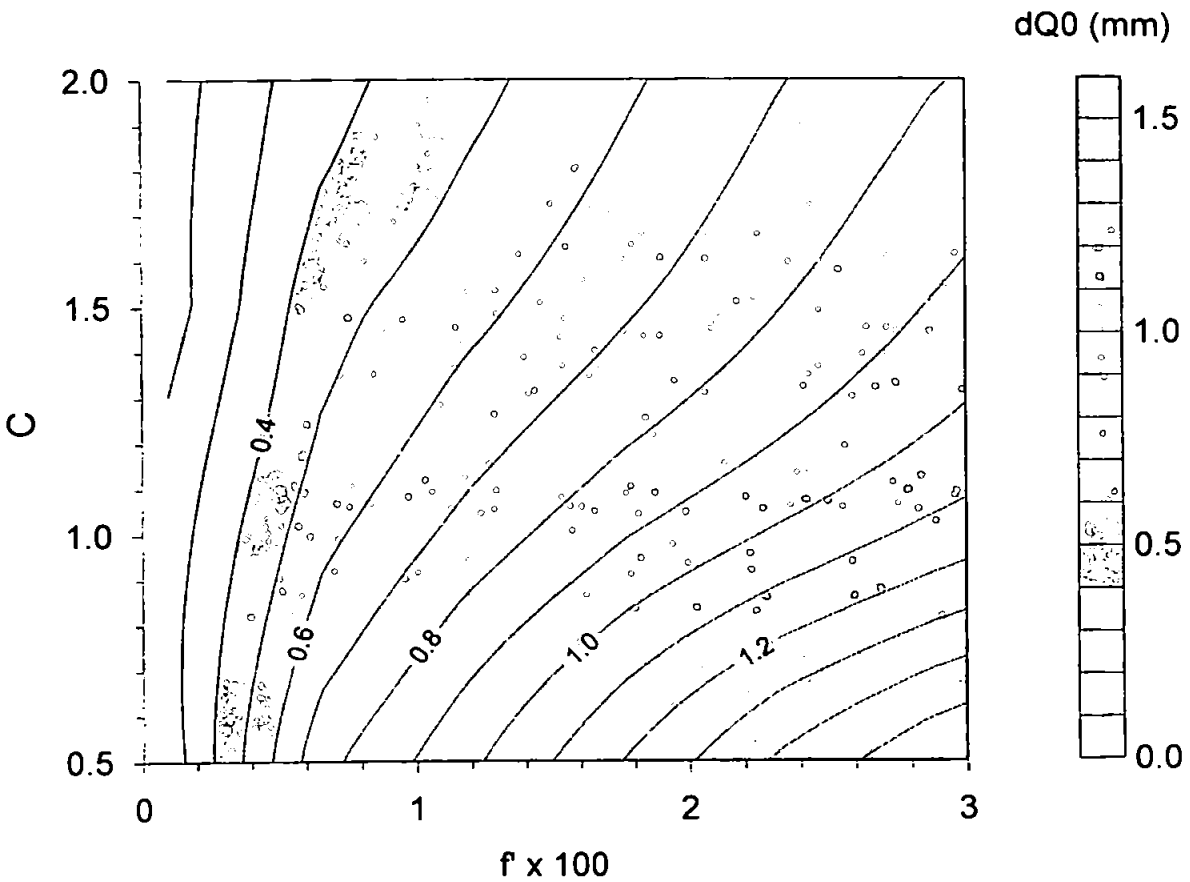

Figure 9.7: contours of the critical changeover value of grain size (d_{Q0}) for different values of friction factor and the constant 'c'.

Another important aspect to consider is the changing relative magnitudes of the two processes of effective sediment weight and boundary layer modification as a function of beachface grain size. To examine this, two dimensionless parameters may be defined (*c.f.* TM98):

τ_R is the shear stress with in-exfiltration relative to without in-exfiltration;

W_R is the effective weight with in-exfiltration relative to without in-exfiltration.

From (9.15):

$$\tau_R = \frac{\tau_w}{\tau_0} = \frac{\Phi}{e^{\Phi} - 1} \tag{9.29}$$

and from (9.6) and (9.13):

$$W_R = \frac{W_w}{W_0} = \frac{s - 1 - 0.5\,w/K}{s - 1}$$

i.e.

$$W_R = \frac{W_w}{W_0} = 1 - 0.5\frac{w}{K(s-1)} \tag{9.30}$$

By calculating τ_R and W_R for a range of different grain sizes, while keeping all the other parameters constant, an idea may be obtained of whether, when the grain size is changed, either the shear stress changes more than the effective weight or *vice-versa*.

To evaluate equations (9.29) and (9.30) over a range of grain sizes, values of |u| and w of $0.1ms^{-1}$ and $0.004ms^{-1}$ (Turner and Nielsen, 1997) have been used. Note that, in this case, since w has been chosen as positive (exfiltration), then through-bed flow will result in a simultaneous reduction of both shear stress and effective weight. Figure 9.8 shows a plot of W_R and τ_R against d_{50}. It can be seen that, at small grain sizes, W_R decreases rapidly with decreasing grain size, whereas the slope of τ_R remains fairly constant with grain size. This suggests that stabilisation-destabilisation has the greater influence on the characteristics of the $\langle Q_{infilt} \rangle$ v. d_{50} plot (figure 9.6).

To summarise the difference in sensitivity of the two processes to changes in grain size, the curves in figure 9.8 were split into two sections ($0.1mm < d_{50} < 0.3mm$ and $0.3mm < d_{50} < 1.0mm$) and each section was linearly regressed. The ratio of the slopes of the regression lines were then found for each section of the curves (see table 9.2). Above $d_{50} = 0.3mm$, effective weight has about 50% more sensitivity than shear stress to changes in grain size, and below $d_{50} = 0.3mm$, effective weight is fifteen times more sensitive than shear stress to changes in grain size. That is to say, if the grain size changes, then this will affect the stabilisation-destabilisation of the sediment more than it will affect the boundary layer modification.

In summary, if two different beaches are considered, then the difference in grain size will change the way in-exfiltration biases the sediment transport, primarily through the effective weight of the sediment. The grain size does not need to be very different for infiltration-exfiltration to bias the sediment transport onshore on one beach, but offshore

on another. Inspection of figure 9.7 reveals that if a fixed friction factor of 0.01 were used as in TM98, then the critical changeover point (d_{Q0}) would be 0.45mm. The grain size in TM98 was larger than this, confirming their findings of onshore transport dominance. The grain size in the present study was smaller than d_{Q0}, suggesting offshore dominance.

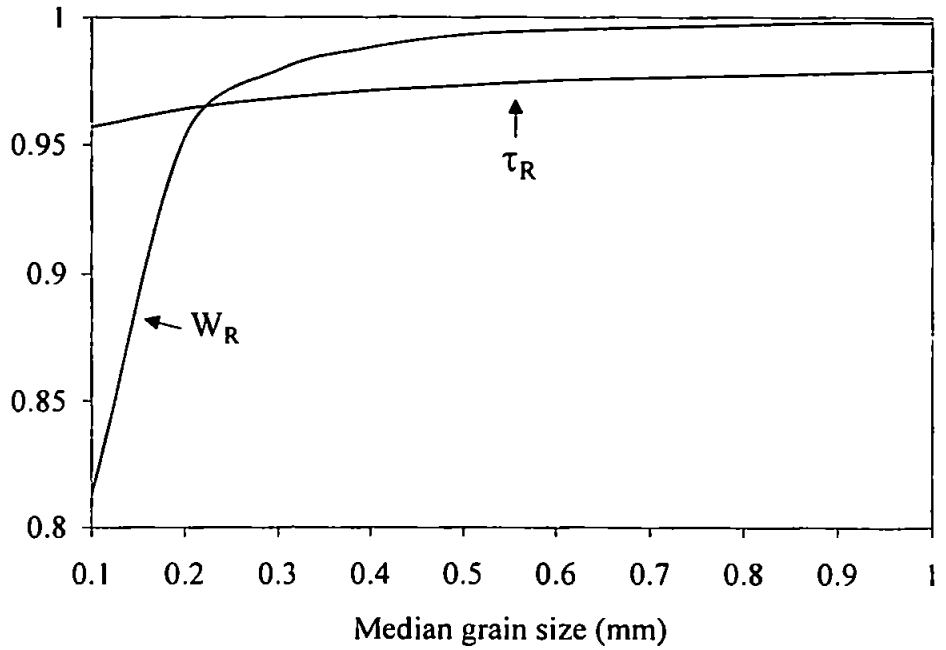

Figure 9.8: sensitivity to grain size of relative shear stress (τ_R) and relative effective weight (W_R).

Table 9.2: comparison of relative weight (W_R) and relative shear stress (τ_R) dependence on grain size, at different ranges of grain sizes.

d (mm)	W_R slope	τ_R slope	Ratio
0.1 < d < 0.3	0.831	0.055	15.1
0.3 < d < 1.0	0.023	0.015	1.53

Another very useful comparison is to see if changing offshore wave heights affect the influence of in-exfiltration on the sediment transport. Unfortunately, the sub-surface pore-pressures were unable to be measured in high and low energy conditions, so this comparison could not be made using the field data. However, as a simple test, the whole velocity time-series was multiplied by various factors, from 0.2 to 2.0 and the value of $\langle Q_{infilt} \rangle$, the time-averaged transport due to in-exfiltration, was re-computed using equation (9.19). Note that maximum velocities realistically expected in the swash-zone were about twice those measured (i.e. ~ $4ms^{-1}$).

Results (see figure 9.9) show that $\langle Q_{infilt} \rangle$ becomes increasingly negative with increasing velocity, implying that the influence of in-exfiltration on the sediment transport might become more offshore in higher energy conditions. Although only tentative, this provides a potential link between in-exfiltration and the other processes whose offshore influence increases with increasing sea-state. It also highlights the need for a more comprehensive set of measurements in high and low energy conditions.

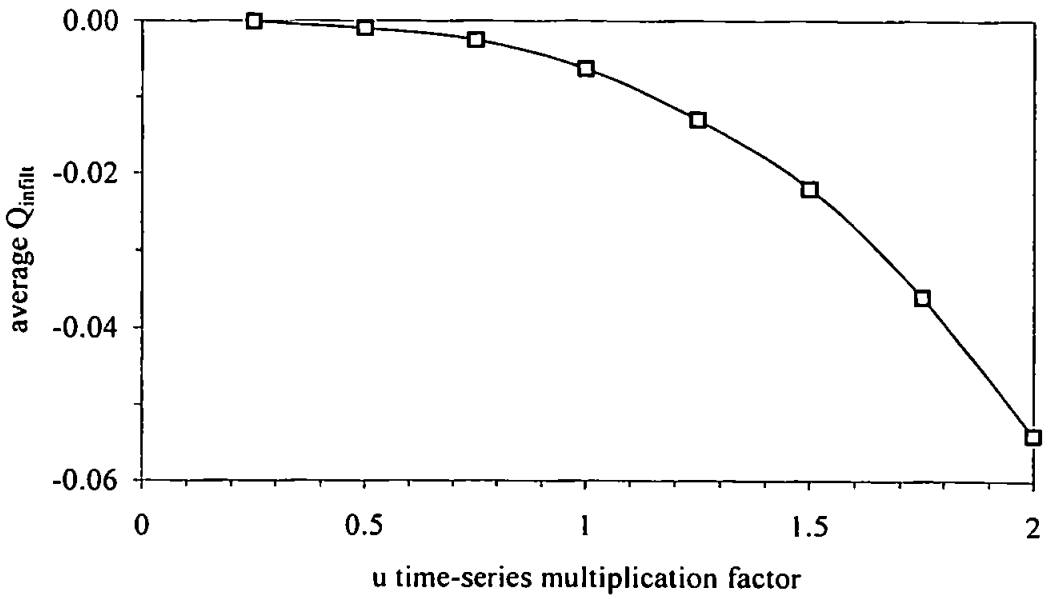

Figure 9.9: effect on $\langle Q_{infilt} \rangle$ of multiplying the velocity time-series by various factors.

9.8 Discussion

The principle finding in this chapter of the thesis is that there appears to be some critical grain size below which stabilisation-destabilisation effects dominate, causing in-exfiltration to bias the transport offshore, and above which modified boundary layer effects dominate, causing in-exfiltration to bias the transport onshore. The apparent conflict between the present study and that of TM98 is therefore explained by the fact that TM98 was undertaken on a significantly coarser beach.

Obtaining a value for the critical changeover point (d_{Q0}) is not straightforward, and it is sensitive to the method used when estimating various empirical constants, especially the friction factor. The value of d_{Q0} appears to lie somewhere between 0.45mm (using the methods of TM98) and 0.58mm (suggested by Nielsen, 1998). Other differences in approach may also be important, such as modelled (TM98) versus measured (present study) velocities, and linear (Nielsen, 1998) versus non-linear (present study and TM98) velocity-stress relationships.

It is clear that, if further studies are to be conducted to obtain a value for the critical changeover point, then methods must be standardised. Different experimental approaches and methods of estimating the various constants can make the results appear contradictory. The friction factor seems to be particularly important, and also one of the most difficult parameters to estimate.

A comprehensive analysis of friction factors for the uprush was performed by Hughes (1995), and it was suggested that the flow should be considered sheet flow (Wilson, 1988). The most appropriate formulation would therefore be

$$f' = 20 \ln\left(0.5 \frac{h}{\theta d}\right)^{-2} \tag{9.31}$$

Since the Shields parameter (θ) appears in this formula, which is in turn dependent on the friction factor, then iterative techniques would have to be used to solve it. Also, the work of Hughes (1995) was based upon a model of uprush following bore collapse on a steep beach, which is quite different from the conditions encountered in the present study.

As mentioned above, TM98 assume oscillatory flow when calculating f', but steady-flow when choosing a value for c. In the present study, quasi-steady flow is assumed for both. Oscillatory friction factor formulae (albeit different ones) were also

used by Hughes *et al* (1998), and Masselink and Hughes (1998), who acknowledge that equation 9.31 (above) might be more appropriate. Even if an oscillatory formula were used, it would be far from obvious which one to choose for the swash-zone (see Nielsen, 1992). More work, perhaps in the laboratory, is required to find out the nature of the boundary layer in the swash-zone, and the most appropriate way to estimate the friction factor.

For the present study, the relative effect of in-exfiltration over a single swash cycle was estimated to be a reduction of about 10% of the total sediment moved on the uprush and an increase of about 4.5% of the total sediment moved on the backwash. Although the direction is different from that in TM98 (due to grain size), in-exfiltration has more influence on the uprush than on the backwash in both studies. Inspection of the $-\partial h/\partial z$ time-series shows that the uprush is characterised by higher, more abrupt downward forces brought about by the sudden arrival of the swash-front at the measurement position, whereas the backwash is characterised by longer duration but lower magnitude upward forces. The difference in the nature of uprush and backwash flows is therefore further highlighted.

The magnitudes of in-exfiltration influence on the uprush and on the backwash were estimated by TM98 by comparing simulated peak transport rates. If this is done for the single swash cycle analysed here, an approximate 16% decrease in peak uprush transport and a 6% increase in backwash transport is found. TM98 obtained uprush increases of about 10% and backwash decreases of 5 to 10%, for a position in the mid swash-zone. They also suggested that the influence of in-exfiltration decreases with increasing distance up the beach-face.

Baird *et al* (1996) performed model simulations using the field data of Hughes (1992) to investigate the hypothesis that fluidisation of the bed might occur within the swash zone during the backwash. They concluded that, for one case out of five, fluidisation might be likely on the very last stages of the backwash. This was achieved by adjusting the assumed value of K to $0.0002 ms^{-1}$, about five times smaller than that obtained in the present study.

The estimation of K is, again, not straightforward and various empirical formulations are normally used, based on the grain size, porosity and sorting characteristics. In the present study, the formula of Bear (1972) was used, which is the most up to date formula suggested by Dominico and Schwartz (1998). Baird *et al* (1998)

found that, by using the older method of Krumbein and Monk (1942), values were an order of magnitude smaller than those carefully measured with permeameters. For the grain characteristics at Canford Cliffs, U.K (the field site used by Baird *et al*, 1998), estimation of K using the formula of Bear (1972) results in a value much nearer to that measured.

Therefore, it appears that fluidisation is of lesser importance, and no field evidence is available (including from the present study) to suggest that fluidisation occurs in the swash-zone. The fact is also highlighted that care must be taken in any estimation of K which is, along with the friction factor, another parameter notoriously difficult to estimate.

The result that the effects of in-exfiltration appear potentially to become more offshore with increasing cross-shore velocity (and hence higher energy conditions) must be taken tentatively because the variations in velocities were obtained simply by multiplying the whole time-series by fixed factors. With 'real' data, the characteristics of the velocity field could be very different, containing different non-linearities (see chapter 8) and would not simply be the same time-series 'grown' or 'shrunk'. However, this result does prove very useful in that it shows a link exists between the offshore wave field and the effects of in-exfiltration. It should be taken as an incentive to obtain more measurements of this kind, but comparing high and low energy conditions.

9.9 Summary

The findings in this chapter may be summarised as follows:

- Examination of time-series of sub-surface pore pressures has shown that upwards-directed pressure gradients on the backwash are not sufficient to cause fluidisation of the top layer of sediment, leading to enhanced offshore transport, as hypothesised by Baird *et al* (1996).
- A review of the theory has been presented concerning the two competing processes which may be important in altering the uprush and backwash transport through in-exfiltration, namely (a) stabilisation or destabilisation of the surface layers, and (b) boundary layer thickening or thinning. A modified Shields parameter has been derived with extra terms to take account of these processes, following the work of Nielsen (1998) and Turner and Masselink (1998).

- It was found that the net direction of Q_{infilt} was offshore for the data in the present study, i.e. uprush transport was inhibited and backwash transport enhanced by in-exfiltration, due to a dominance of stabilisation-destabilisation over boundary layer modification.
- By allowing the grain size to vary in the computations it was found that, above a particular critical grain size the effects of in-exfiltration changed from biasing the transport offshore to onshore, indicating a shift from a dominance of stabilisation-destabilisation to a dominance of boundary layer effects.
- The exact value of the critical grain size changeover point (d_{Q0}) is not straightforward to estimate, and it has been suggested that experimental methods and the method of estimating various constants be standardised before a reliable value of d_{Q0} can be found.
- Sensitivity tests on the friction factor (f') and the constant (c) in the shear-stress-velocity relationship have found that, although c is less sensitive, relatively small changes in the estimation of f' might change the direction of the apparent influence of in-exfiltration. A suitable formula for f' in the swash-zone has not yet been found.
- The net influence of in-exfiltration over a single swash cycle was to decrease the total sediment transported by about 10.5% on the uprush, and to increase the total sediment transported by about 4.5% on the backwash.
- Rough calculations have shown that the effects of in-exfiltration appear to become more offshore with increasing cross-shore velocity. This provides a tentative link between in-exfiltration and the offshore wave field.

This chapter of the thesis was based on *The influence of swash infiltration-exfiltration on beach face sediment transport: onshore or offshore?* by T. Butt, P. Russell and I. Turner, submitted for publication in *Coastal Engineering*.

10. Higher order processes

10.1 Introduction

Recent swash-zone field studies (Hughes *et al*, 1998; Osborne and Rooker, 1998, 1999) have acknowledged that the hydraulic jump is probably an important mechanism for transporting sediment in the swash-zone. The generation of hydraulic jumps and the resulting processes which contribute to sediment transport could be considered higher-order processes than those directly associated with the action of the fluid on the bed in the uprush and backwash, already identified previously in the thesis. Figure 10.1 shows a simplified example of how certain characteristics of the cross-shore velocity field can cause backwash transport to be modified in a number of ways. Higher order processes need lower order processes as pre-requisites, e.g. sediment cannot be advected from hydraulic jumps without the existence of large backwashes to produce the jumps in the first place. Likewise, sediment transport modification over a field of backwash ripples cannot take place without hydraulic jumps to produce the ripples.

Figure 10.1 only shows certain examples of swash-zone processes to illustrate the concept of higher order mechanisms. Other processes, e.g. those causing onshore transport, are not illustrated.

Observations as part of the present study have identified the existence of two types of hydraulic jump in the swash-zone. The first is a jump which occurs in the backwash itself when the flow reaches supercritical values, similar to a hydraulic jump occurring in any fast and shallow fluid flow whose Froude number exceeds unity. The second appears when the backwash flow is fast enough to interact with the next uprush bore such that its absolute velocity is reduced to zero. Little acknowledgement is given in the literature of the separate existence of these types of jump, probably due to the visual difficulty in differentiating between them.

The latter type of jump seems to locally suspend a great deal of sediment from the intense turbulence caused by the two interacting flows. Several workers have studied similar situations, but none has considered how sediment is suspended under hydraulic jumps in the swash-zone. For example, the vorticity generated in a bore-front has been investigated by considering the bore as a moving hydraulic jump (e.g. Madsen and Svenson, 1983; Svenson and Madson, 1984; Yeh, 1991). Digital particle velocimetry was

used by Hornung *et al* (1995) to observe the flow just downstream of a laboratory jump, who obtained an expression for the mean vorticity as a function of the Froude number. Shear stresses in a laboratory hydraulic jump were calculated by Veeramony and Svensen (1998), using a laser Döppler velocimeter (LDV), with the pretext of the jump being similar to a surf-zone roller.

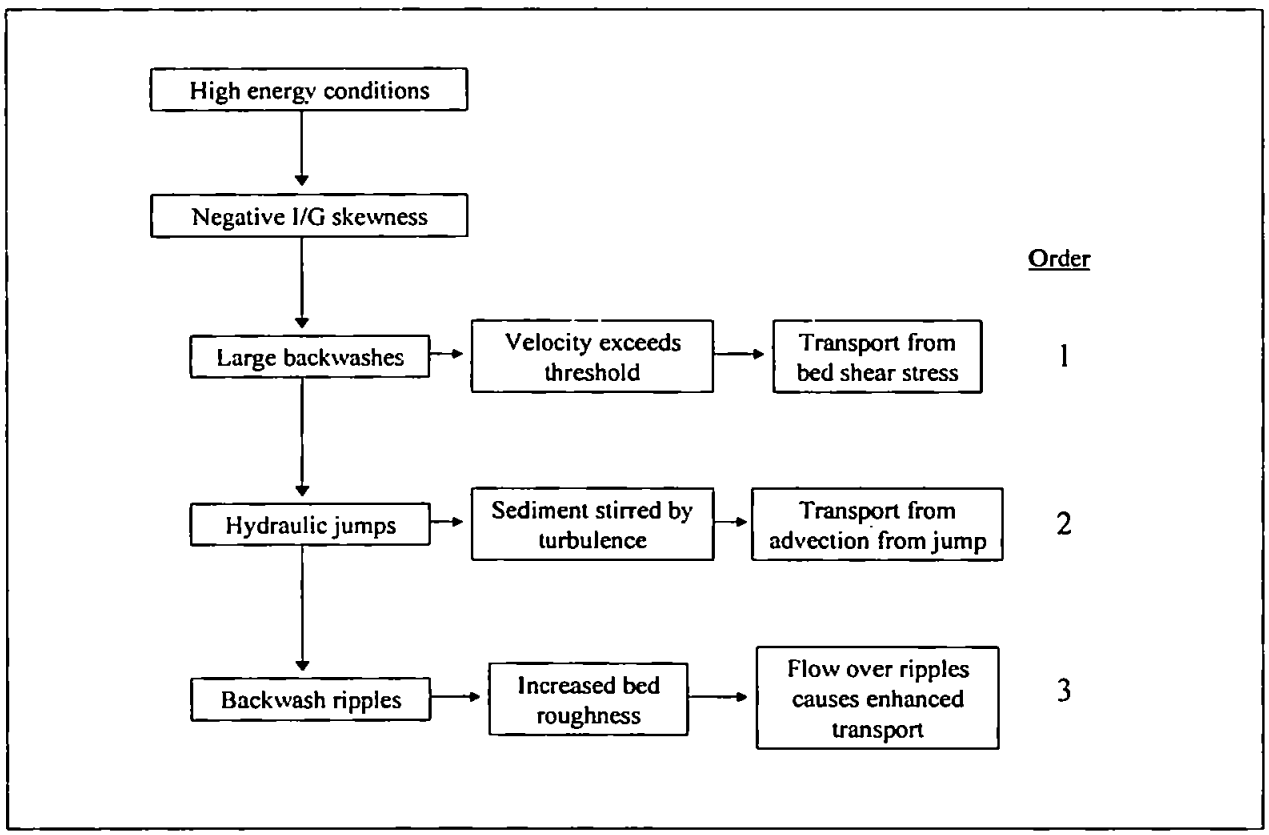

Figure 10.1: schematic representation of examples of different order sediment transport processes in the swash-zone.

A slightly different process resulting from uprush-backwash interaction has been studied by Matsunaga and Honji (1980, 1983) and Larson and Sunamara (1993). The vorticity produced by the interaction causes localised erosion, generating a step in the beach profile at the seaward extreme of the swash-zone. The formation of a 'beach-step' is normally confined to steep reflective beaches with plunging breakers, and was not observed in this study, but it does illustrate the fact that a great deal of turbulence is produced during uprush-backwash interaction.

Both types of jump can cause a secondary effect, namely the generation of a antidune ripple-field, which in turn may modify the sediment transport through increased bed roughness. Early observations of backwash ripples include those by van Straaten (1953), and Hayes (1972), and a comprehensive study was performed by Broome and Komar (1979). Interestingly, Broome and Komar performed their experiments on a high-energy dissipative beach, so their study can be considered a valuable early contribution to this kind of swash-zone work.

In the present study, it was observed that the formation of backwash ripples is more often caused by the type of jump produced in the backwash only, or by very weak uprush-backwash interaction, due to the higher likelihood of it being an 'undular' jump (Sellin, 1969), which favours the generation of a ripple field (see section 10.3.1). On the other hand, strong uprush-backwash interactions tended not to produce ripples, rather considerable onshore or offshore sediment advection from the jump itself.

This chapter is principally concerned with assessing the contribution of higher order processes involving hydraulic jumps, on the sediment transport in the swash-zone in high and low energy conditions.

The first section briefly reviews the Froude and Reynolds numbers, and compares different flow regimes in high and low energy conditions. The two types of hydraulic jump are then described in detail, followed by an assessment of the sediment advection from the hydraulic jump produced by uprush-backwash interaction. The mechanisms which form backwash ripples are then described, together with an assessment of the effect of backwash ripples on (backwash) sediment transport.

Briefly mentioned in the discussion is bore collapse, another process which may enhance uprush transport, and which appears to suspend sediment in a similar way to hydraulic jumps. As a sediment suspension mechanism on its own, this process is probably more important on steep beaches than on dissipative beaches (Hughes *et al*, 1997, 1998; Masselink and Hughes, 1998; Puleo, 1998).

10.2 Flow regimes

It has been suggested that, as the velocity increases and the depth decreases throughout the backwash, the flow will quickly go through a number of different regimes,

from laminar to turbulent and from subcritical to (possibly) supercritical (K.R. Dyer, pers. comm., 1998). The type of flow has important implications for modelling, and since this transition usually occurs in a very short time, this makes the backwash particularly difficult to describe.

In this section time-series of Froude and Reynolds numbers are computed for the calm and storm data, so that a simple comparison can be made of how the flow regimes change with the depth and velocity.

The Reynolds number (Re) is the ratio between the inertial forces and the viscous forces, and can be used to estimate whether the flow is laminar or turbulent. A Reynolds number may be defined for the backwash as follows

$$\mathrm{Re} = \frac{uh}{\nu} \tag{10.1}$$

where u is the velocity, h is the water depth and $\upsilon \approx 10^{-6} m^2 s^{-1}$ is the kinematic viscosity of the fluid. The flow may become turbulent if Re exceeds about 10^3.

The Froude number (Fr) is the ratio of the water velocity to the speed of a shallow-water wave:

$$\mathrm{Fr} = \frac{u}{\sqrt{gh}} \tag{10.2}$$

where u is the flow speed and h is the water depth. If Fr > 1, then the flow becomes supercritical and a hydraulic jump may occur. Different flow regimes are defined in figure 10.2 in terms of the critical Reynolds and Froude numbers.

Figures 10.3 and 10.4 show scatter plots of the depth and velocity from the calm and storm data, plotted onto the framework of figure 10.2. The plots show that, the majority of the time, the flow regime is turbulent and subcritical for both data sets, but the storm data shows a greater number of points in the turbulent supercritical sector.

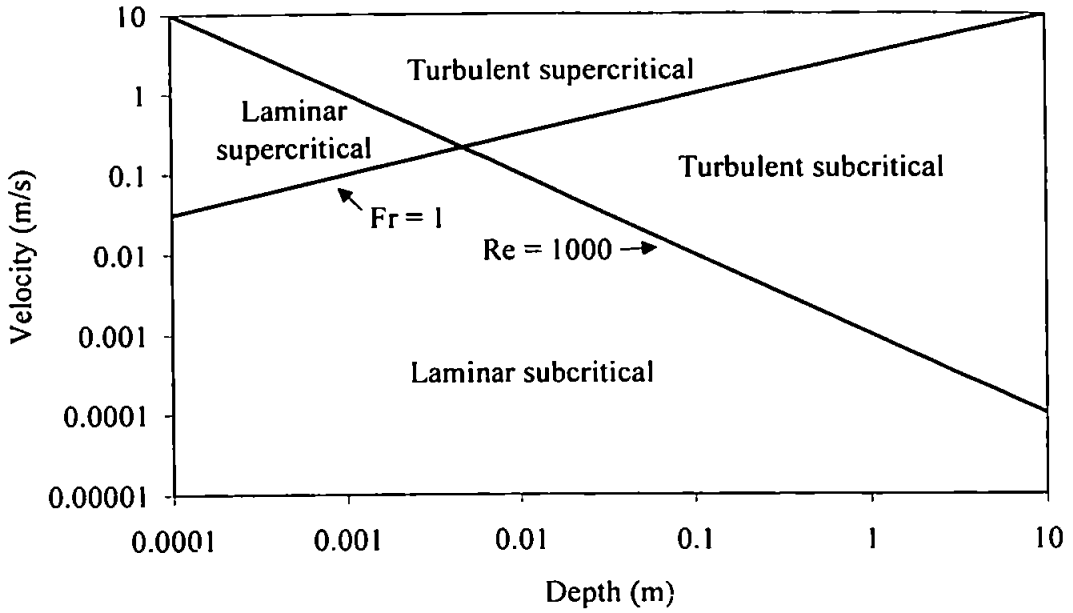

Figure 10.2: Flow regimes in terms of critical Reynolds and Froude numbers (adapted and corrected from Allen, 1985).

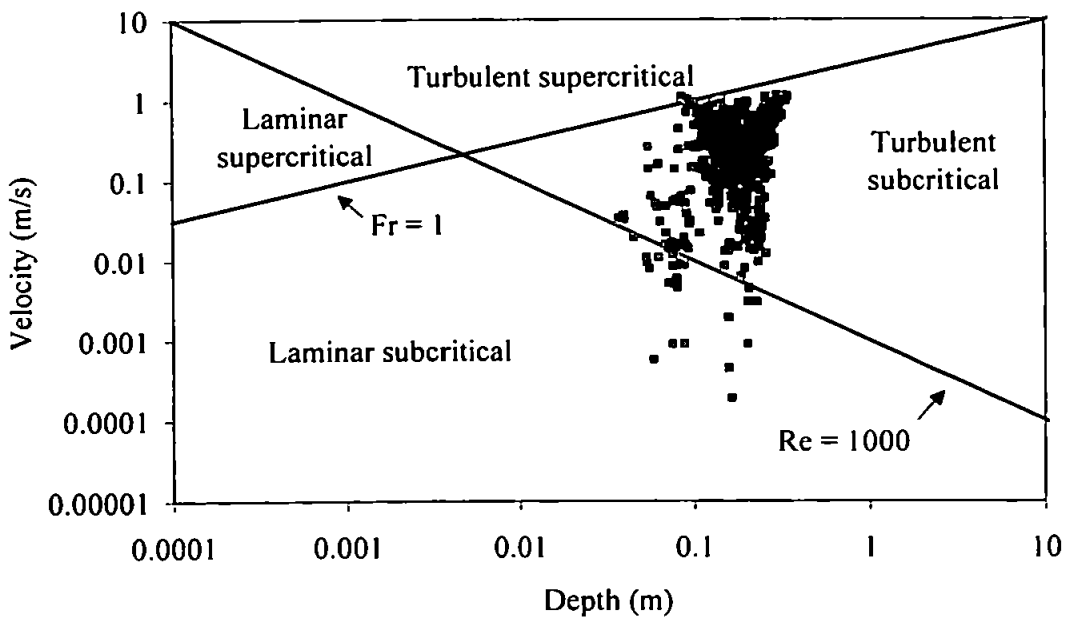

Figure 10.3: scatter plot of calm data onto flow regime diagram.

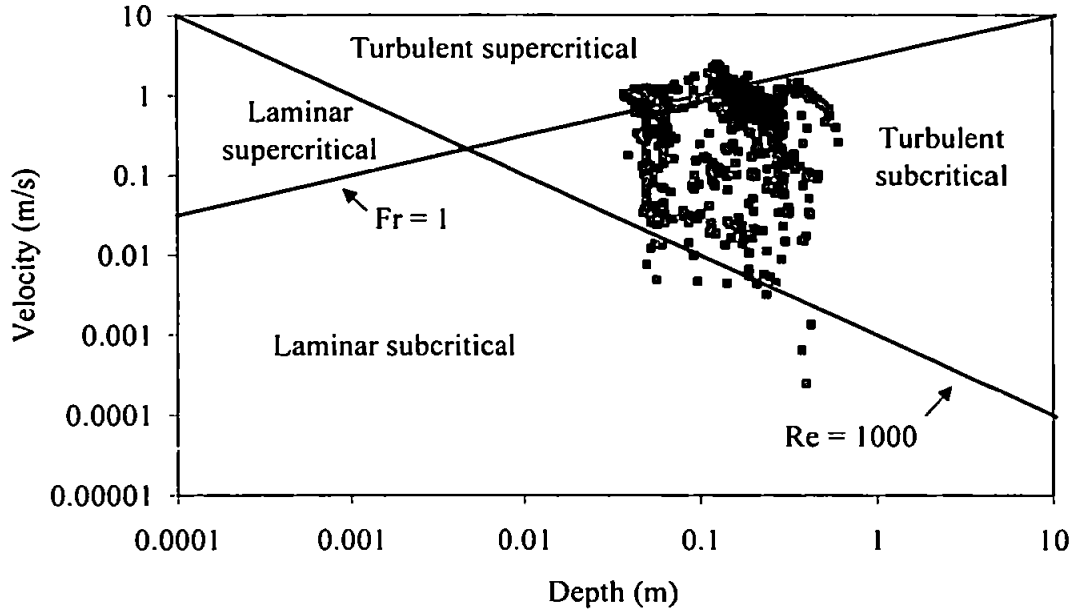

Figure 10.4: scatter plot of storm data onto flow regime diagram.

In figures 10.5 and 10.6 are plotted representative sections of the time-series of Reynolds and Froude numbers for the calm and storm data, together with the depth and velocity. Note that Re is plotted on a logarithmic scale.

It can be seen that the Reynolds number only drops to values lower than 10^3 when the velocity and/or depth are very near zero. For both the calm and storm data the Reynolds number is maintained well above 10^3 for the all the uprushes and backwashes, indicating turbulent flow beyond doubt. In the swash-zone the depth generally increases with decreasing velocity on the uprush, and *vice versa* on the backwash, keeping the Reynolds number fairly constant. Note that it was pointed out in section 7.2 that the phase relation between depth and velocity also appears to have some dependency on frequency.

The Froude number for the storm time-series is generally higher, with the number of occasions Fr > 1 being higher, indicating a higher number of chances for hydraulic jumps to occur. A few times during the storm time-series, mainly associated with large backwashes, the Froude number exceeded 2.

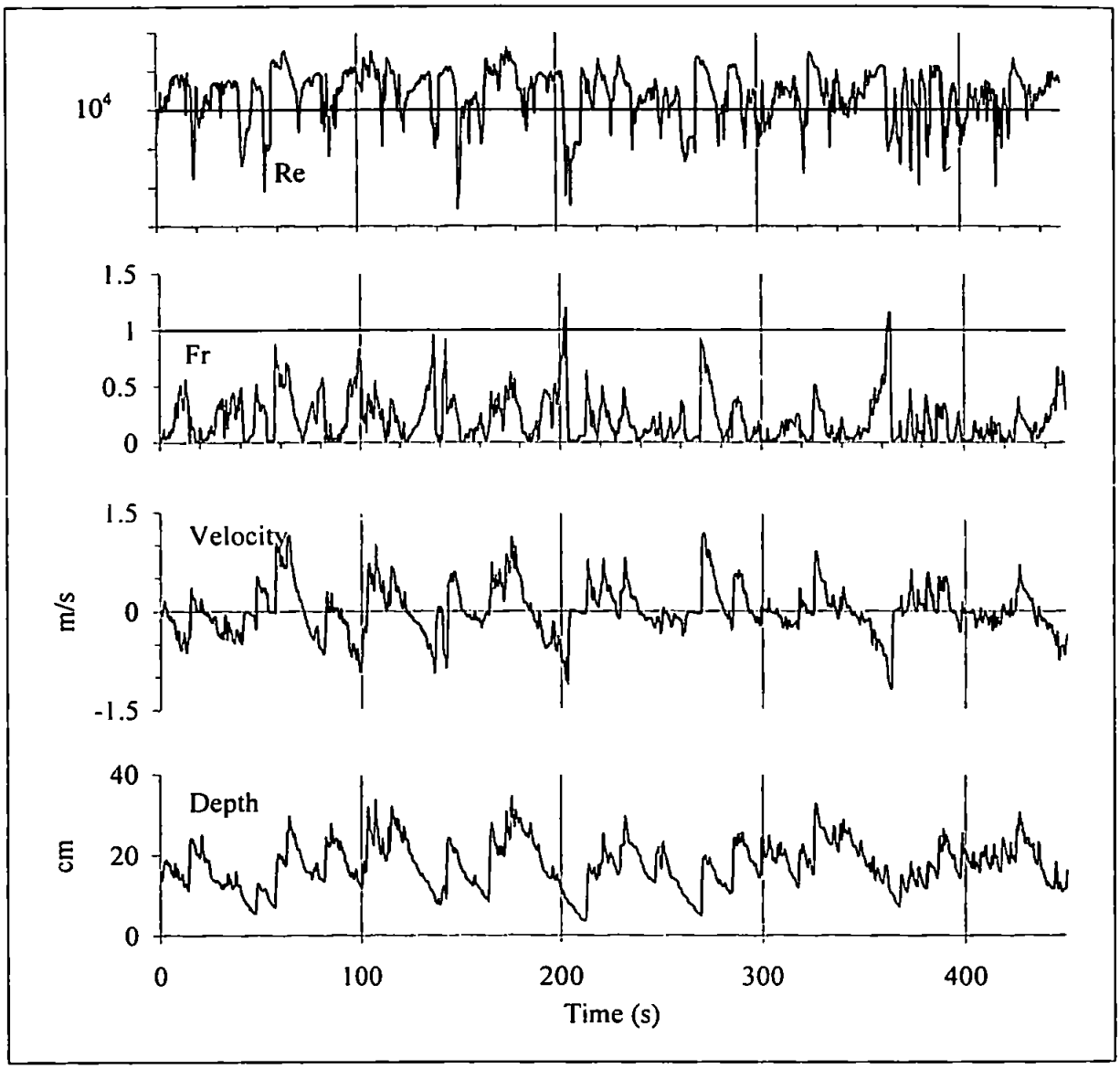

Figure 10.5: section of calm time-series of Froude and Reynolds numbers. (Scaling of Re is one decade per division).

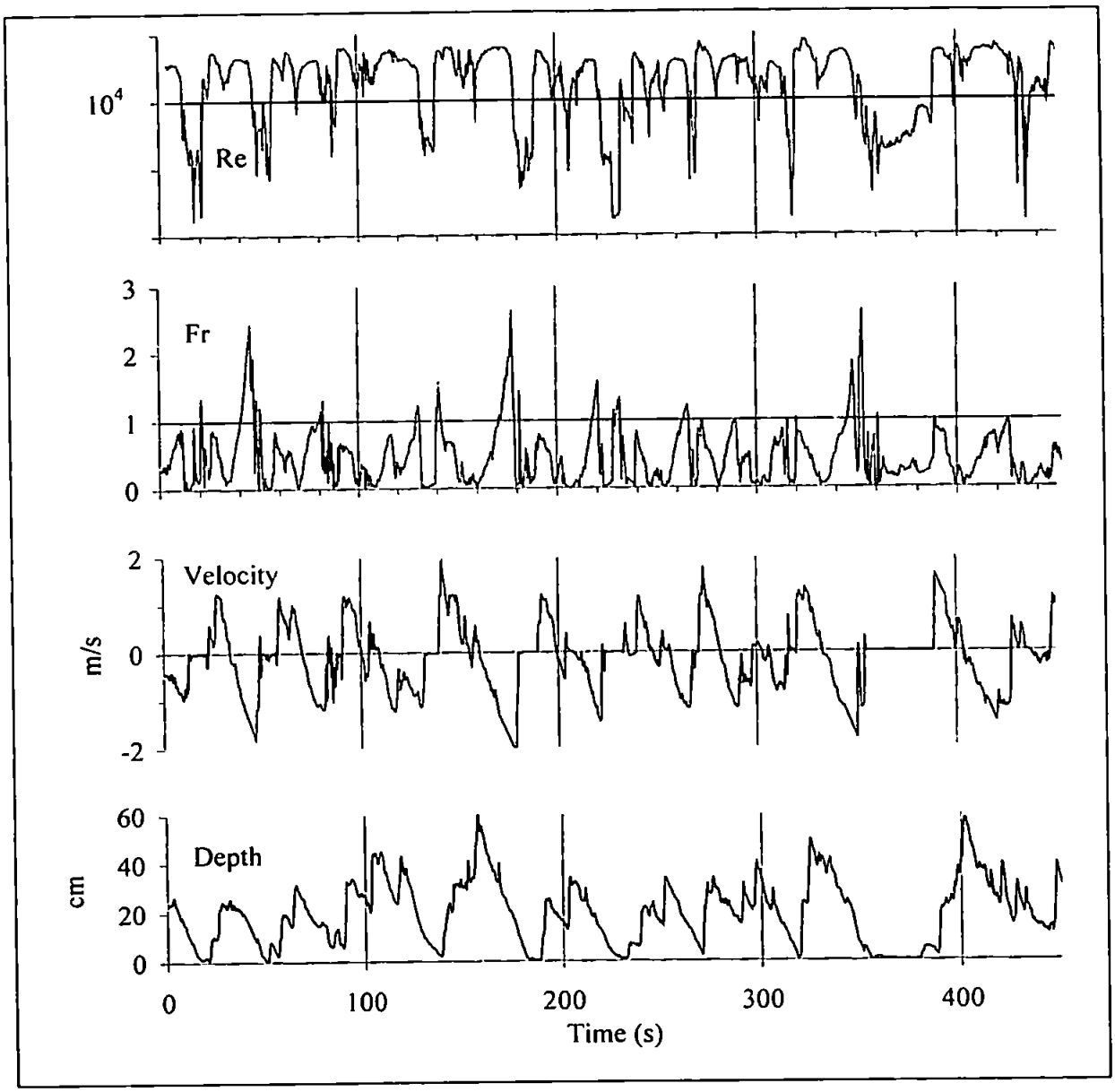

Figure 10.6: section of storm time-series of Froude and Reynolds numbers. (Scaling of Re is one decade per division).

10.3 Hydraulic jumps

10.3.1 Hydraulic jumps forming on backwash only

The first type of hydraulic jump found in the swash-zone is a similar process to that which occurs in many other natural situations where fast and shallow flows may occur. To allow a hydraulic jump to occur, the depth and velocity values on the backwash must be such that the flow becomes supercritical, which depends upon the Froude number (see above).

If Fr > 1, then a hydraulic jump may occur. For the flow to return to subcritical (Fr < 1) it must go through a depth change, where

$$\frac{h_1}{h_2} = \frac{u_2}{u_1} \tag{10.3}$$

where h_1 and u_1 are the depth and velocity on the upstream side of the jump, and h_2 and u_2 are the depth and velocity on the downstream side of the jump.

Depending on the value of the Froude number, the hydraulic jump itself may take on various forms (Sellin, 1969). The 'undular' jump consists of a group of waves extending downstream from the transition, and occurs when $1.0 < Fr < 2.0$. Froude numbers higher than this tend to cause breaking of the first wave in the group, resulting in a general loss of the grouping structure. It has been suggested by Broome and Komar (1979), that the jump formed in the backwash often tends to be the undular type, which rarely causes direct sediment transport modification. However, the secondary effect of the generation of a ripple-field is likely with this type of jump, and may cause enhanced sediment transport due to increased bed roughness (see below).

Inspection of the Froude number time-series for the calm and storm data reveals that Fr exceeds unity a number of times, especially at the end of the backwash, (e.g. at $t \approx$ 205s and 370s for the calm and $t \approx$ 45s, 185s and 350s, for the storm data). Table 10.1 shows the total number of backwashes during which the Froude number exceeded unity for each time-series. During the higher energy conditions the percentage of supercritical backwashes increases by a factor of more than three.

Table 10.1: Supercritical backwashes

	No. backwashes	No. supercritical backwashes	% supercritical backwashes
Calm	33	5	15 %
Storm	29	17	58 %

10.3.2 Hydraulic jumps forming due to uprush-backwash interaction

This type of jump is formed by the halting of the uprush by the previous backwash, causing the bore to temporarily become stationary relative to the bed. This increases local shear stress from extra turbulence caused by the interaction of the two flows, and hence enhances localised sediment suspension.

The formation of a stationary bore may be explained as follows. In the swash-zone, the backwash is effectively subducted under the next incoming uprush bore, with the bore propagating over the backwash. In this situation, it is convenient to consider the frame of reference as travelling seaward with the backwash. Therefore, if the celerity of the bore remains constant, and it is propagating over a seaward travelling frame of reference, then its velocity relative to the bed will be reduced. If the backwash velocity matches the bore celerity, then the bore will become stationary.

The possible existence of these types of jump may sometimes be seen on the time-series. In figure 10.7 is shown an expanded section of the depth, velocity and SSC (5cm) time-series from the calm data. At $t \approx 510$s there is a large sediment suspension event, after the backwash which occurred between $t \approx 490$ and 506s. This is accompanied by a sharp increase in depth which would normally indicate the arrival of the next uprush, but there is no sudden increase in velocity at this point. This might suggest some kind of mechanism which is suspending sediment *in-situ* without the water moving either onshore or offshore. These jumps were visually observed at the time of the field experiment, more details of which are given later.

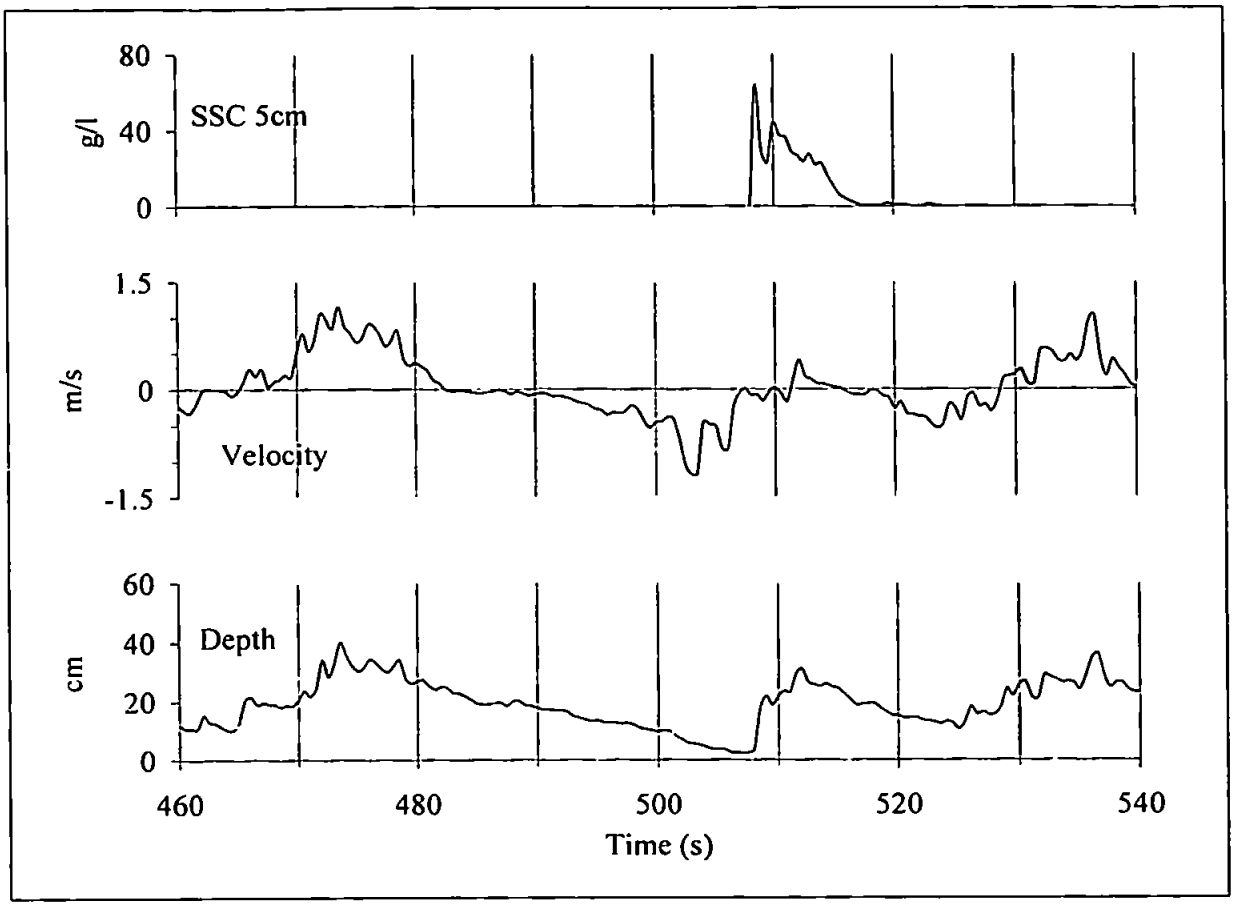

Figure 10.7: expanded time-series, showing the suspension event at $t \approx 510s$. The depth increases sharply even though the velocity remains close to zero.

It is useful to compare whether this type of jump is more likely to occur in high or low energy conditions, using the storm and calm data. In the above example, the jump happened to occur at the measurement location. Many more occurrences of hydraulic jumps would be missed by a single measuring station, so simply looking for phenomena like this in the time-series would be unreliable.

Therefore, a simple method would be to compare the relative likelihood of this type of jump to occur, using the following simple theory.

The absolute shoreward velocity of a bore (C_b) may be expressed in terms of the depth of water either side of the transition, in the same way as that of a tidal bore (e.g. Williams and Elder, 1996):

$$C_b = \sqrt{\frac{g}{2}\frac{h_2}{h_1}(h_1 + h_2)} - u_{bw} \tag{10.4}$$

where u_{bw} is the seaward velocity of the backwash, and h_1 and h_2 are the depth of water on the upstream and downstream side of the jump respectively. Hence the condition for a stationary bore to occur is given by $C_b = 0$, i.e.

$$\frac{u_{bw}}{\sqrt{\frac{g}{2}\frac{h_2}{h_1}(h_1 + h_2)}} = 1 \tag{10.5}$$

However, the problem with trying to apply this formula directly to the data collected in the present study, is that the depth of water either side of the hydraulic jump (h_1 and h_2) could not be measured simultaneously. Paradoxically, to measure h_1 and h_2 would have required *a priori* knowledge of whether or not the jump was stationary, which would eliminate the need for measurements of h_1 and h_2 in the first place.

Therefore to obtain a comparison of whether a stationary jump was likely to form using the calm and storm data, the following steps were taken. The depth time-series were first filtered to include only onshore values, then only offshore values, and the velocity time-series was likewise filtered to include only offshore values. In this way the time-averaged values of the uprush depth, backwash depth and backwash velocity over each time-series could be computed. The likelihood for a standing hydraulic jump to occur could then be expressed using a similar formula to equation (10.5), but with time-averaged values, i.e.

$$P_j = \frac{\langle u_{bw} \rangle}{\sqrt{\frac{g}{2}\frac{\langle h_u \rangle}{\langle h_{bw} \rangle}\left(\langle h_{bw} \rangle + \langle h_u \rangle\right)}} \tag{10.6}$$

where h_u is the uprush depth, h_{bw} is the backwash depth, and the angled brackets denote time-averaging. A high value of P_j indicates a high probability for standing jumps to occur during that data burst. Results are shown in table 10.2.

Table 10.2: relative likelihood of the occurrence of standing hydraulic jumps for calm and storm time-series.

	calm	storm	ratio
Mean uprush depth [m]	0.25	0.24	0.95
Mean backwash depth [m]	0.18	0.16	0.89
Mean backwash velocity [ms^{-1}]	0.24	0.54	2.25
P_j	**0.15**	**0.31**	**2.06**

The results in table 10.2 suggest that about twice as many jumps are likely to occur in the storm data, than in the calm data. The mean uprush and backwash depths do not show much difference, rather the backwash velocity appears to be the dominating factor. Therefore one of the major contributing factors for the formation of standing hydraulic jumps is a velocity time-series containing a considerable amount of high-velocity backwashes.

10.4 Sediment transport from uprush-backwash interaction

The hydraulic jump produced by uprush-backwash interaction is a mechanism which is able to suspend large amounts of sediment *in-situ*. The nature of this mechanism is highly transitory and its persistence is highly variable. To remain stationary, the condition has to be met that the backwash velocity is sufficient to halt the bore. If the backwash velocity exceeds that required for a stationary bore, then the jump will momentarily move seawards, continuing to suspend large amounts of sediment.

The hydrodynamic mechanisms which suspend the sediment, i.e. the vorticity generated just seaward of the jump, may be considered similar to those in a moving bore

(e.g. Peregrine and Svensen, 1978; Svensen *et al*, 1978). The longer this vorticity persists over the same section of the bed, the more sediment will be suspended.

Once the sediment has been stirred by this vorticity, it has the potential to subsequently be advected onshore or offshore, which requires some kind of onshore or offshore flow superimposed on the suspension mechanism. Osborne and Rooker (1999) observed that "high SSC close to the end of the backwash may lead to considerable advection of SSC into the inner surf zone and also to enhanced SSC during subsequent uprush events". Conceptual diagrams of scenarios where the advection is either onshore or offshore are shown in figures 10.8 and 10.9.

In cases where the advection is onshore, the slowing down of the uprush bore leads to the possibility for the next bore, which will be travelling faster relative to the bed, to catch up and overtake the first bore, advecting sediment shorewards. Whether or not the next bore is allowed to overtake the first seems to depend upon the time interval between the initiation of the standing jump and the arrival of the next bore (i.e. the period of the next wave). The shorter the period, the greater the chance of the next bore overtaking the standing jump, hence leading to onshore advection.

If the stationary jump is not overtaken by the next bore, then the sediment may be advected offshore, since the flow would be seawards both sides of the jump. Note that, in some cases, the backwash causes the first hydraulic jump to dissipate, and then goes on to halt the next incoming bore, effectively producing two hydraulic jumps within one backwash. A great deal of sediment is advected offshore in these cases.

Whether this process will contribute to enhanced uprush or backwash transport depends upon the number of standing jumps in the time-series which are overtaken by the next uprush (N_u), the number of standing jumps which are not overtaken by the next uprush (N_b), and the amount of sediment which is advected either onshore or offshore in each case (q_u and q_b). Therefore the bulk contribution to the sediment transport over the time-series (positive onshore) by this process can be given by

$$Q_j = N_u q_u - N_b q_b \qquad (10.7)$$

To evaluate this equation would require the measurement of SSC and velocity either side of the hydraulic jump, which could not be obtained as part of the present study and, as already mentioned, would be very difficult. To the author's knowledge there have

been no direct measurements of the flow characteristics in standing hydraulic jumps in the swash-zone of natural beaches, owing to the difficulty of instrument location due to the transient nature of the phenomenon. However, various contributing factors may be identified, and below is described a simple but useful experiment.

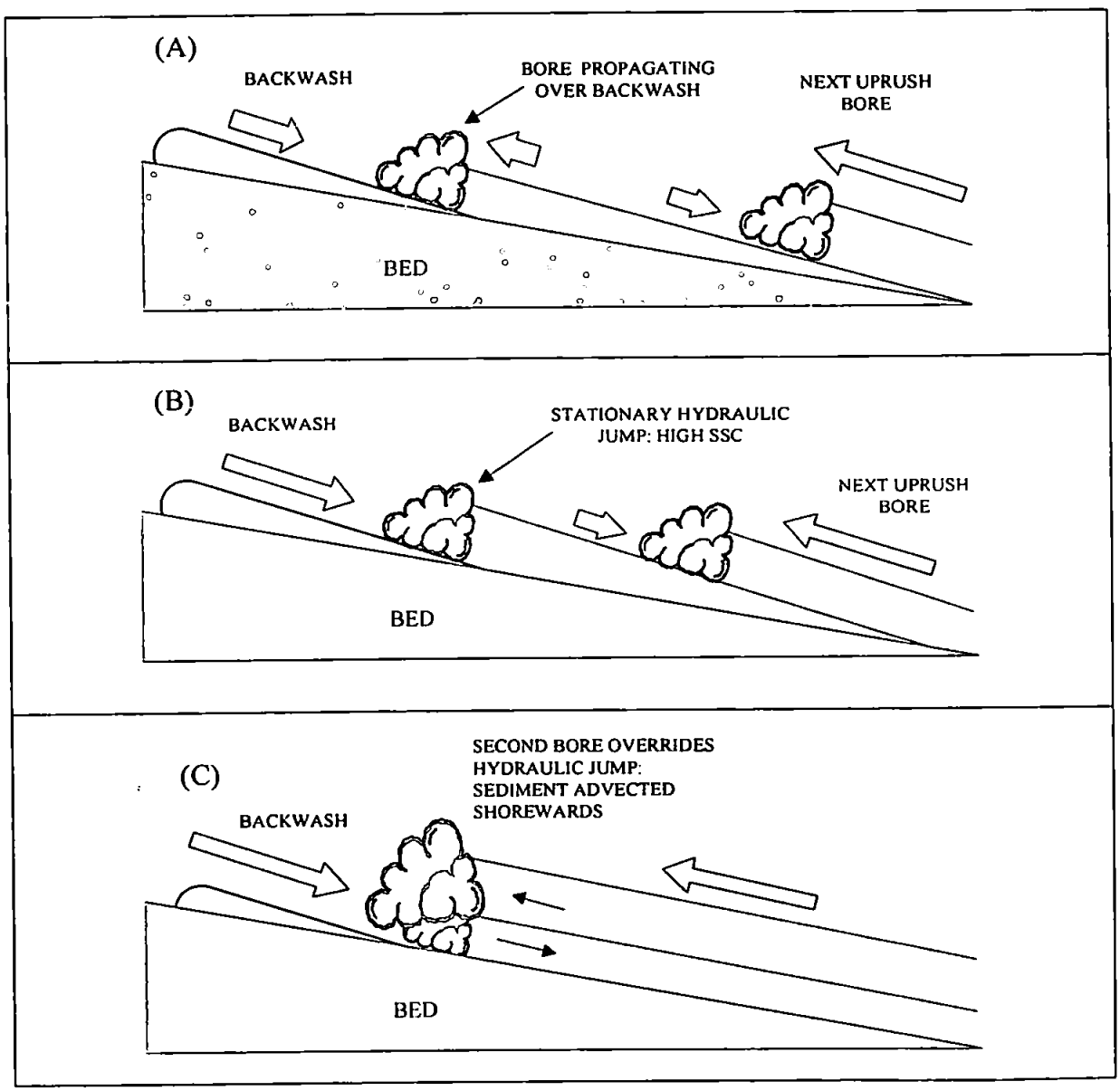

Figure 10.8: schematic representation of the formation of a stationary hydraulic jump by uprush-backwash interaction, and the subsequent onshore advection of sediment by the next uprush bore overriding the first. The arrows indicate velocity relative to the bed.

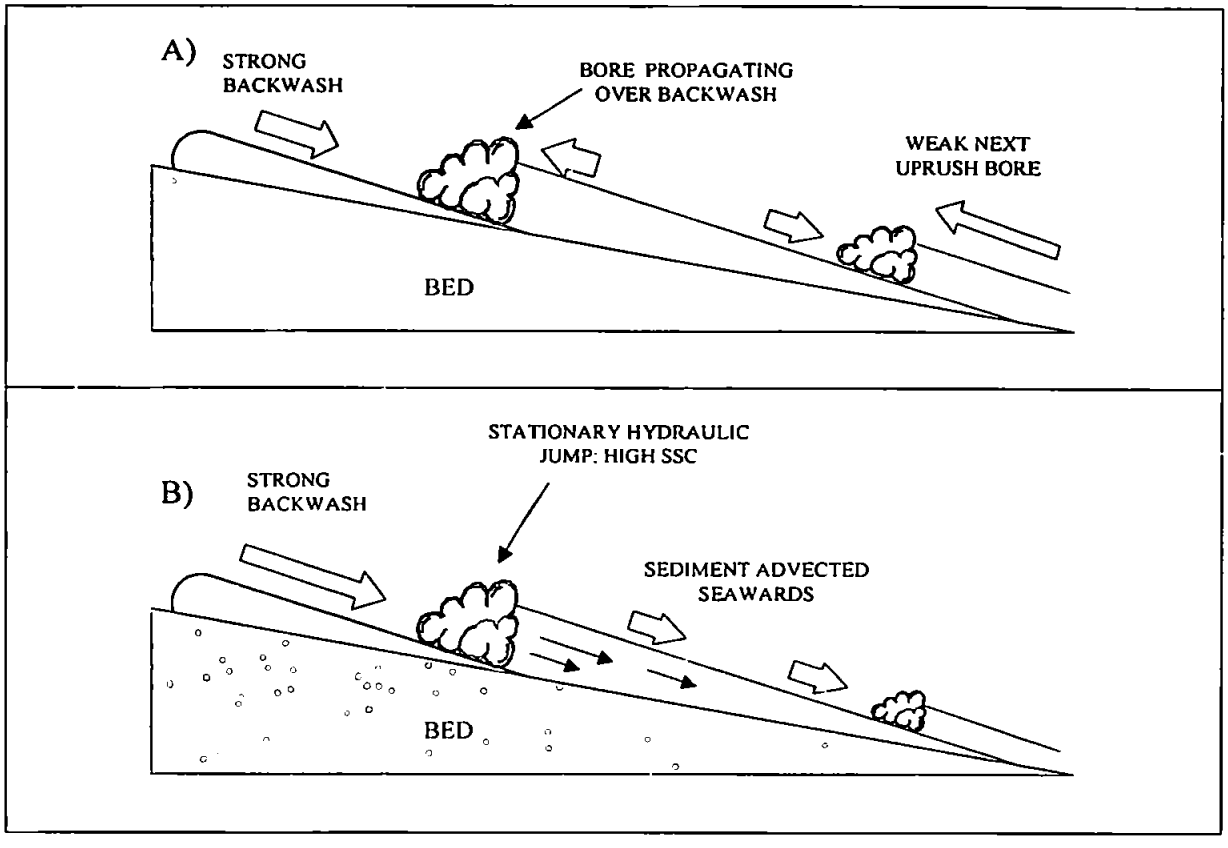

Figure 10.9: the formation of a stationary hydraulic jump by uprush-backwash interaction, and the subsequent offshore advection of sediment.

Visual observations of the characteristics of uprush-backwash hydraulic jumps were made at the time of the experiment, over a 2-hour period over high water on Tue 24 March and Fri 27 March, 1998. The objectives of these observations were to compare the number of hydraulic jumps occurring over the 2-hour period, and whether the sediment advection was either onshore or offshore in each case. As no field instrumentation is yet available to quantify the sediment advection from spatially and temporally transient phenomena such as hydraulic jumps, then simple visual observations had to be made. This was achieved by an observer carefully noting down the occurrence of each hydraulic jump, and the direction of sediment advection, during the 2-hour period.

Table 10.3 shows a comparison of the number of jumps observed over the 2-hour period during the high and low energy conditions, together with the theoretical probability for jumps to occur (P_j) computed from the storm and calm time series (above). The

number of observed jumps on the high energy day was about twice that on the low energy day, which agrees well with that predicted from the storm and calm data.

Table 10.4 shows the number of jumps where sediment advection was onshore (N_u) compared with the number where the advection was offshore (N_b) for the high and low energy conditions. The amount of sediment advected in each case (i.e. q_u and q_b in equation 10.7), was not measured, therefore an estimate of net onshore or offshore contribution to sediment transport could not be computed. However, a very rough idea of whether this process biases the transport onshore or offshore, in high and low energy conditions, may be made from $N_u - N_b$.

Table 10.3: total number of uprush-backwash jumps observed in high and low energy conditions. P_j is the theoretical likelihood of jumps occurring (see table 10.2).

	low energy	high energy	ratio
total jumps	45	91	**2.02**
P_j	0.15	0.31	**2.06**

Table 10.4: number of jumps with onshore or offshore advection.

	low energy	high energy
N_u	30	35
N_b	5	56
no advection	10	-
$N_u - N_b$	**25**	**-21**

From table 10.4, there appear to be more cases of onshore advection than offshore for the low energy conditions, and more cases of offshore than onshore for the high energy conditions. Although no information can be given about the net amount of sediment advected either way in each case, these results do suggest that high energy conditions mean some sort of contribution to offshore transport from this process.

10.5 Backwash ripples

A simple explanation for the initial formation of a backwash ripple field from a hydraulic jump can be given in terms of flow divergence and convergence. Broome and Komar (1979) used this principle to model the generation of backwash ripples, coupled with the mathematical description of an undular hydraulic jump (Peregrine, 1966).

If it is assumed that sediment transport is directly related to flow velocity, then spatially accelerating flow (divergence) will cause sediment erosion, and spatially decelerating flow (convergence) will cause sediment deposition. With an initially flat bed, continuity dictates that the flow beneath the troughs of the undular hydraulic jump will be faster than that beneath the peaks. This will lead to the convergence and divergence pattern as shown in figure 10.10 (a).

This will initially cause a bedform to develop which is 90^0 out of phase with the hydraulic jump. The flow conditions will then be slightly modified, giving the convergence and divergence patterns shown in figure 10.10 (b). Further erosion and deposition will eventually lead to the quasi-stable situation in figure 10.10 (c) where the bedform is in phase with the hydraulic jump, and the water depth is spatially constant.

This type of bedform, once fully established, will tend to migrate upstream due to lee side erosion and stoss side deposition (Dyer, 1986).

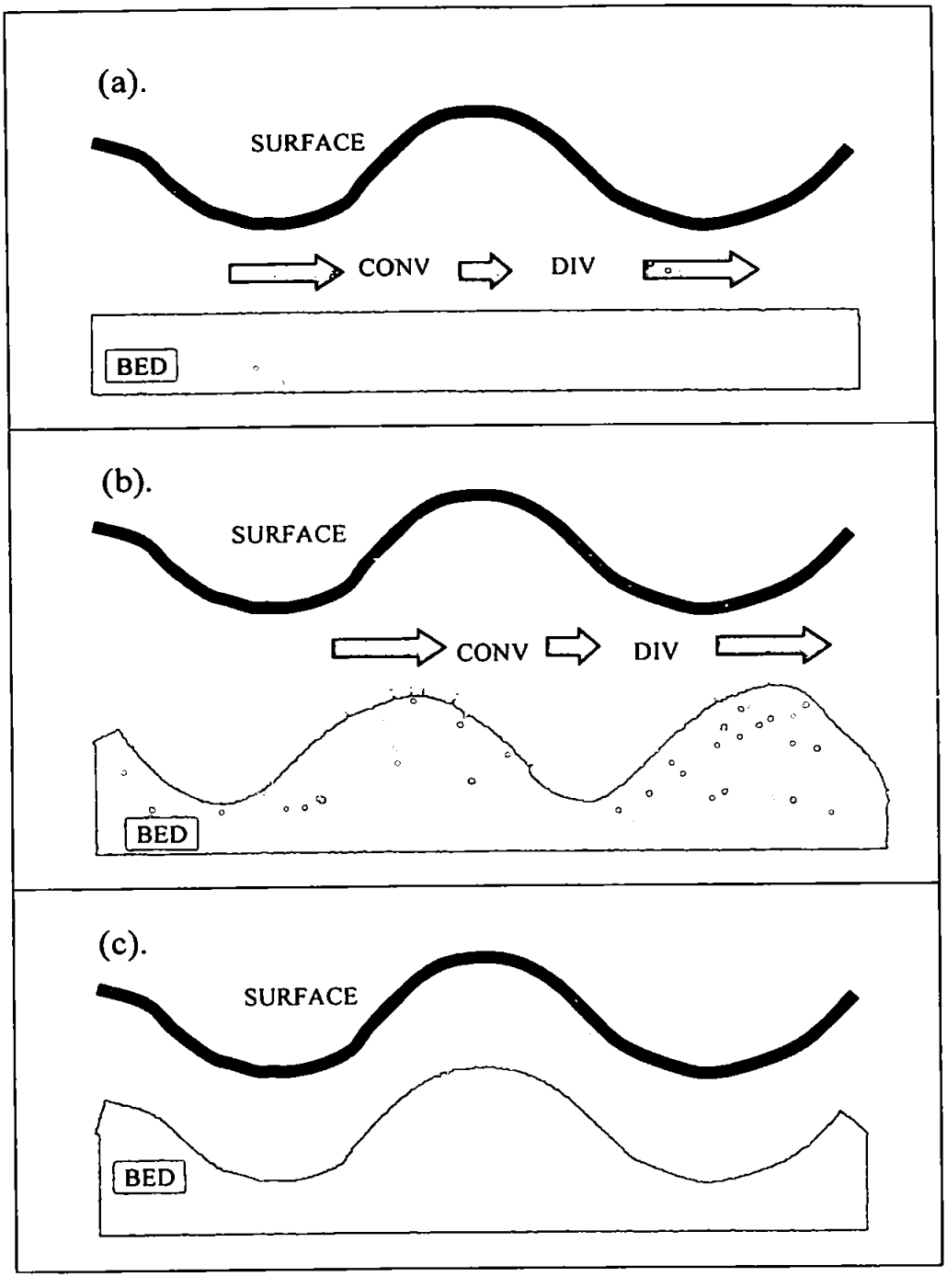

Figure 10.10: initial formation of a backwash ripple field from a hydraulic jump.

10.6 Increased sediment transport over backwash ripples

Once the backwash ripple field has been formed by the hydraulic jump, then any subsequent flow over this part of the bed will suspend more sediment than if the flow were over a flat bed, due to the increased roughness. To enable a comparison to be made between potential sediment transport with or without backwash ripples, a simple Shields-type sediment transport model may be used. The following work is based closely on that done in chapter 9 in connection with infiltration-exfiltration.

The Shields parameter, θ (Shields, 1936) was defined in section 9.4, i.e.

$$\theta = \frac{\tau}{\rho g d(s-1)} \tag{9.6}$$

where τ is the bed shear stress, ρ is the fluid density, $d = d_{50}$ is the median grain size and $s = \rho_s/\rho$ is the specific gravity of the sediment. Combining this with the quadratic stress law, i.e.

$$\tau = 0.125\rho f' u^2 \tag{9.17}$$

where u is the depth-averaged velocity and f' is a friction factor,

$$\theta = \frac{f' u^2}{8gd(s-1)} \tag{10.8}$$

Models basing the dimensionless sediment transport rate (Q) on a proportionality to $\theta^{3/2}$ appear to be most popular in the recent literature (see section 9.4), therefore

$$Q = \left[\frac{f' u^2}{8gd(s-1)}\right]^{\frac{3}{2}} \tag{10.9}$$

The sediment transport in the presence of a ripple field will be different from that over a flat bed, principally due to a change in the bed roughness which affects the friction factor. Therefore, the extra transport caused by the ripple field (Q_{rip}) may be defined as the

difference between the transport with ripples (Q_R) and the transport over a flat bed (Q_0), i.e.

$$Q_{rip} = Q_R - Q_0 \tag{10.10}$$

i.e. $$Q_{rip} = \left[\frac{f'_R u^2}{8gd(s-1)}\right]^{\frac{3}{2}} - \left[\frac{f'_0 u^2}{8gd(s-1)}\right]^{\frac{3}{2}} \tag{10.11}$$

where f'_R and f'_0 are friction factors with and without ripples respectively.

An expression for the friction factor was derived in section 9.6, based on various basic equations relating to the boundary layer, i.e.

$$f' = 1.28\left(\ln\left(11\frac{h}{k}\right)\right)^{-2} \tag{9.23}$$

where h is the instantaneous water depth and k is the Nikuradse effective bed roughness, which may be split into its grain and bedform components, k_g and k_R , i.e.

$$k = k_g + k_R \tag{10.12}$$

i.e. if the flow is over a flat bed then $k = k_g$, and if ripples exist then $k = k_g + k_R$, i.e.

$$f'_0 = 1.28\left(\ln\left(11\frac{h}{k_g}\right)\right)^{-2} \tag{12.13}$$

and $$f'_R = 1.28\left(\ln\left(11\frac{h}{k_g + k_R}\right)\right)^{-2} \tag{10.14}$$

The grain roughness (k_g) presented to the flow is approximately related to the grain size (Van Rijn, 1982), i.e.

$$k_g \approx 6d_{50} \tag{9.24}$$

Backwash ripples are characterised as having wavelengths larger than other types of ripples observable on beaches (Tanner, 1965). In the present study, average wavelengths were of the order of 50cm. To estimate k_R, a formula based on that suggested by van Rijn (1993) for k_R in the presence of dunes (whose wavelength are about an order of magnitude larger than the water depth) therefore seems the most appropriate, i.e.

$$k_R = 1.1\Delta\left(1 - \exp\left(\frac{-25\Delta}{\lambda}\right)\right) \tag{10.15}$$

where Δ and λ are the bedform height and length respectively.

Various other constants need to be determined before (10.11) can be evaluated. From the grain size analysis (section 4.1.5), d_{50} = 0.24mm. Average values for the ripple dimensions estimated at the field site are Δ = 1cm and λ = 50cm. Finally, s = 2.6 for quartz sand.

Figure 10.11 shows backwash time-series, taken from ensembles of the seven swash cycles in the mid-swash data (the method of obtaining the ensembles was outlined in section 7.5.2). The Froude number time series, computed from equation 10.2, shows that only at the end of the backwash ($t \approx 0.75$) does the flow become supercritical allowing the formation of hydraulic jumps in the backwash. Therefore, the only time during the backwash that enhanced transport is likely to occur would be between $t \approx 0.75$ and $t = 1$, when there is the possibility for hydraulic jumps, and therefore backwash ripples, to form.

Also shown are corresponding time-series of Q_R and Q_0, computed from the first and second terms in (10.11). If a hydraulic jump happens to form sometime after $t \approx 0.75$, then, from the difference between the Q_R and Q_0 maxima, the instantaneous transport has the possibility to increase up to a factor of 2.02 between the formation of the ripple field and its destruction.

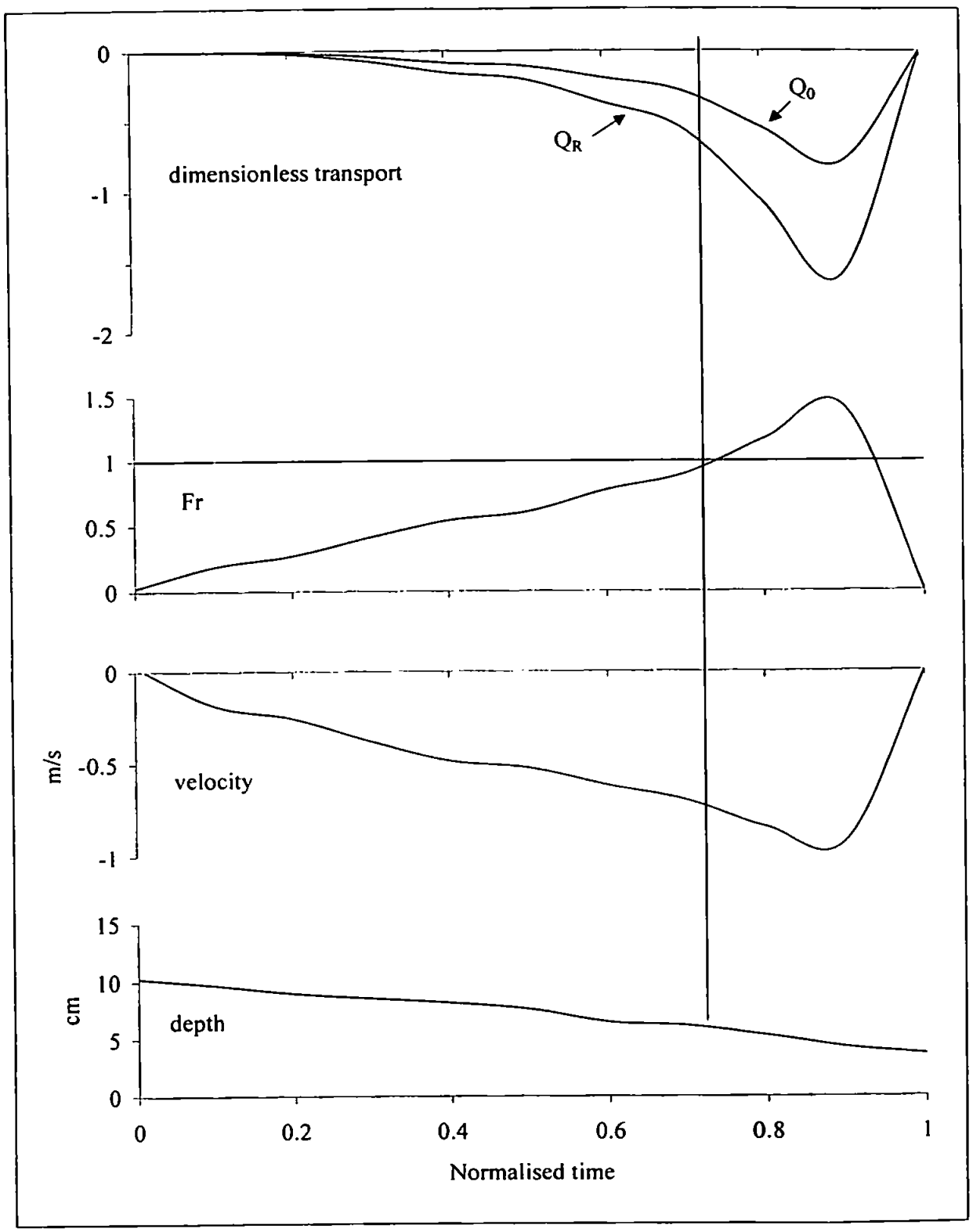

Figure 10.11: Ensembled backwash from mid-swash data including time-series of Fr, Q_0 and Q_R. The region to the right of the vertical line indicates when extra transport due to ripples is possible.

It cannot be known for certain exactly when during the time between t = 0.75 and t = 1, the ripple field will form, if indeed at all. However, the maximum offshore sediment transport modification would be made if the ripples were formed exactly at t = 0.75, and persisted until the end of the backwash.

Since the ripple field does not persist for the whole of the backwash, then it would be useful to compare the effect of the ripples on the total amount of sediment transported throughout the backwash. An estimate of the maximum effect ripples have on the amount of sediment transported during a single backwash, may be obtained by integrating the instantaneous transport.

The total sediment transported over the backwash without taking ripples into account (I_0) is given by

$$I_0 = \int_{t=0}^{t=1} (Q_0)dt \tag{10.16}$$

The total maximum sediment transported over the backwash taking into account backwash ripples, assuming they persist for the last quarter of the backwash (I_R) is given by

$$I_R = \int_{t=0}^{t=0.75} (Q_0)dt + \int_{t=0.75}^{t=1} (Q_R)dt \tag{10.17}$$

and the maximum extra amount of sediment transported over the backwash, due to effect of backwash ripples (I_{rip}) is given by

$$I_{rip} = \int_{t=0.75}^{t=1} (Q_R - Q_0)dt \tag{10.18}$$

Since both the instantaneous transport and time are dimensionless, then I_0 , I_R and I_{rip} have no physical units, and are used for comparison only. The most useful parameter here is the ratio between I_R and I_0 , which would give an idea of the bulk effect of the ripples over the full backwash. From the curves in figure 10.11, simple finite difference integration gives $I_R/I_0 = 1.64$.

This means that the maximum effect is to increase the amount of sediment moved during the whole backwash by 64%. This result refers to the sediment moved from a single point in the cross-shore transect. The ripple field will not exist over the full spatial extent of the swash-zone, (i.e. most of the flow will be over a flat bed), so to obtain a more realistic picture of the total effect over the swash-zone, this value should be reduced according to the relative width of the ripple field.

Observations as part of the present study indicate the ripple field to be anywhere between 2 and 4m wide (see also Broome and Komar, 1979), which was roughly about 10% of the width of the swash-zone on the storm day and 20% on the calm day, based on estimated average widths of the swash-zone (see section 4.2). In this respect, the ripples will have a reduced effect in higher energy conditions due to their smaller relative spatial effect. The value of I_{rip} will therefore be reduced by a factor of between 0.1 and 0.2, reducing the ratio I_R/I_0 to between 1.06 (storm) and 1.13 (calm).

To assess the effect of the ripple field on the amount of sand transported over a number of backwashes is more useful than over a single backwash. The effect of the ripples will be less if considered over a number of backwashes, since not every backwash was supercritical. A comparison of the total effect of the ripples over the 17-min. time-series of the calm and storm data bursts may be made taking into account the following factors:

- Out of all the backwashes in each data burst, only 15% were supercritical (allowing for the possibility of ripples to form) in the calm data and 58% in the storm data.
- The Fr and velocity time-series were carefully inspected to assess at what point in the backwash the flow went supercritical. This gave the maximum amount of time the flow could exist over ripples, assuming they are destroyed at the end of the backwash. Averaging over all the supercritical backwashes reveals that the flow was supercritical for the last 15% of the backwash in the calm data, and, for the last 37% in the storm data. The time-integrated transport modification over each backwash (I_{rip}) will roughly differ from that calculated above (for the mid-swash data) by a factor of 37/25 = 1.48 for the storm data, and 15/25 = 0.6 for the calm data.

Combining the factors above and applying them to the values of I_R/I_0 already calculated, it is found that the net effect of ripples over all the backwashes in each data burst is to increase the amount of sediment transported by 1.2% for the calm data and 5.5% for the storm data.

10.7 Discussion

In chapter 8 an argument was developed that negative infragravity skewness in the velocity field tends to make an offshore contribution to sediment transport through the action of increased offshore bed shear stress during large backwashes.

Based on the observations in this chapter, it also appears that the occurrence of large, high-velocity backwashes is an important factor for obtaining hydraulic jumps in the swash-zone. These backwashes not only increase the chances of jumps occurring by being supercritical, but also favour the subsequent advection of sediment offshore from the jump. This suggests that a time-series of cross-shore velocity containing negative skewness will tend to favour offshore-directed sediment transport not only by increasing the number of hydraulic jumps possible, but also by making the subsequent advection from these jumps offshore. The hypothesis in chapter 8 is therefore augmented by the findings here.

The balance between the number of hydraulic jumps from which the advection was either offshore or onshore was onshore biased for the calm data and offshore biased for the storm data. This is not stating that the overall transport due to advection from these jumps was offshore on the storm day, since no information is available on the quantity of sediment moved from each jump. Therefore these results must be taken tentatively, and only as a rough approximation.

The analysis concerning backwash ripples suggests that, although the overall effect on the sediment transport is small, offshore transport is increased through this process in high energy conditions. However, the analysis was principally concerned with backwash transport, and no consideration was given to the possible increased uprush transport due to this mechanism. Observations suggest that the ripples did not tend to survive the uprush and were probably destroyed a very short time after the arrival of the swash-front, due to the intense turbulence (*c.f.* Osborne and Rooker, 1999). The suspension of sediment by turbulent vortices produced in situations more complex than simple unidirectional or oscillating flow is much more difficult to quantify, and would require a large backup of laboratory experiments like those of Veeramony and Svendsen (1998).

Another phenomenon which may be observed as a possible sediment transport mechanism in the swash-zone is bore-collapse. This will tend to transport sediment

onshore and is considered an important mechanism on steep beaches (e.g. Hughes, 1995). A schematic illustration of bore-collapse is shown in figure 10.12.

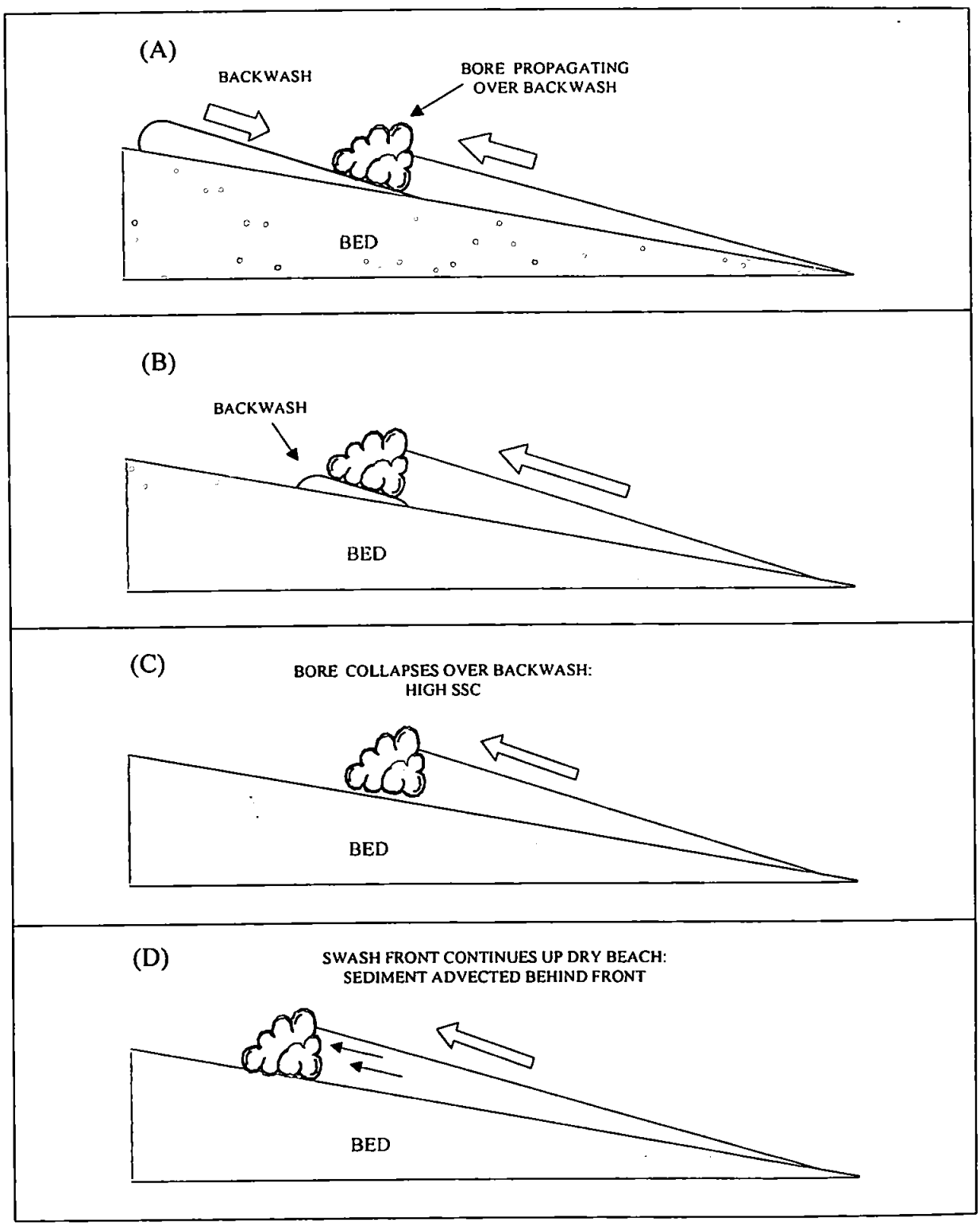

Figure 10.12: Schematic representation of bore collapse.

In dissipative conditions with a saturated or mostly saturated incident wave-field, this feature appears to be a relatively weak sediment suspension mechanism. By the time the swash-front reaches the stage where it begins to propagate over a 'dry' beach (i.e. the backwash has disappeared), it has often weakened so that any extra sediment suspended at this point is negligible.

10.8 Summary

The findings in this chapter may be summarised as follows:

- Sediment transport processes involving hydraulic jumps may be termed 'higher order' processes, since they require prerequisites which, themselves, are sediment transport processes.
- Two types of hydraulic jump may be observed in the swash-zone: the jump produced in the backwash itself by supercritical flows, and the jump caused at the interaction between uprush and backwash.
- The flow is supercritical on more occasions for the storm data than for the calm, with the Froude number exceeding 2 a number of times on the storm day. There were about three times as many supercritical backwashes for the storm data than for the calm.
- Based on simple theory, hydraulic jumps caused by uprush-backwash interaction appear to be about twice as likely to occur in the storm than the calm data. This is backed up by visual observations.
- The balance between the number of jumps from which sediment was advected onshore and number from which it was advected offshore, is weighted towards the onshore for the low energy data and the offshore for the high energy data (i.e. the number of onshore advections minus the number of offshore advections was 25 for the low energy data and –21 for the high energy data). It is not known how much sediment was advected each time, so this result must be taken tentatively.
- When considered over the relative spatial and temporal extent of the swash-zone, and considering that ripples are not produced on every backwash, the total sediment moved over all the backwashes in the 17-min. data burst is increased by approximately 1% (calm) and 5% (storm) due to the existence of backwash ripples.

- The presence of negative infragravity skewness in the cross-shore velocity time-series seems to be a key factor, which will also lead to higher order sediment transport processes tending to bias the transport towards the offshore in high energy conditions.

11. General discussion

11.1 Introduction

The underlying theme of the work presented in this thesis has been to improve the understanding of sediment transport in the swash-zone by identifying the important physical processes which transport the sediment in this area. This chapter puts into context the most important findings of the thesis, which have identified various mechanisms, attempted to quantify their importance and suggested which way (onshore or offshore) the influence of each process might bias the transport under certain conditions.

A summary table of the mechanisms identified is first presented, together with general comments about each process, and how it might be parameterised for eventual inclusion into some morphological model. Then a simplified schematic illustration of how these processes might be connected together is offered in the form of a flow diagram. Next, the results of the study as a whole are put into context with some of the fundamental observations made of shoreline morphology, including a discussion on a possible quasi-universal transport function applicable in the swash-zone. Lastly, a brief consideration of errors is made and suggestions for future continuations of this work are given.

11.2 Summary of the most important processes identified

Table 11.1 shows a summary of the processes identified as part of the present study. The accuracy of the results of the present study is not high enough to reliably quantify the relative importance of all the processes. However, results suggest that non-linearities in the velocity field are probably the most important, followed by advection from a hydraulic jump. Processes which involve turbulent vortices as sediment stirring mechanisms, followed by some flow which advects the sediment one way or another, seem to be the most important.

The potential influence of in-exfiltration was to alter the dimensionless sediment transport over a swash cycle by 10.5% or less, and the potential influence of backwash ripples over a 17-min. time series was to alter the dimensionless transport by less than 5%. Therefore, these processes are considered of lower importance

The second column in the table shows the estimated relative importance of each process. The third column shows whether each process is either first, second or third order, as explained in section 10.1. Whether the net transport due to each process will be onshore or offshore depends upon the balance between the 'sub-processes' shown in the fourth column. The net direction is shown in the fifth column.

Table 11.1: summary of processes

Process	Importance	Order	Sub-process	Direction
Nonlinearities in velocity field	1st	1st	Swash-front turbulence	Onshore
			Large backwashes	Offshore
Hydraulic jumps	2nd	2nd	Onshore advection	Onshore
			Offshore advection	Offshore
Infiltration-exfiltration	3rd	1st	Boundary layer modification	Depends on grain size (see text)
			Stabilisation-destabilisation	
Backwash ripples	4th	3rd	Ripples present during uprush	Onshore*
			Ripples present during backwash	Offshore

*unlikely

Nonlinearities in the velocity field appear to be the most fundamental of the processes discussed here. Uprush transport is principally caused by turbulence in the swash-front stirring the sediment beneath the front, and then the uprush flow itself advecting the sediment onshore. Rapid near-bed flow reversal at the start of the uprush may also have a direct influence as suggested by King (1991). Backwash transport is caused by offshore-directed bed shear-stress reaching a high enough level to start moving sediment. High velocity backwashes occurring at infragravity time scales are more likely to exceed this threshold, therefore more offshore transport is likely in a time-series

containing more of these large backwashes. Note that the above principles still apply to transport below the levels measured.

The existence of both the above sub-processes can be inferred from negative asymmetry and negative skewness in the time-series respectively, which may be quantified using simple third-order velocity moments.

As a step towards parameterising this process for inclusion into a morphodynamic model, the skewness and asymmetry in the swash-zone must be somehow linked with the characteristics of the offshore wave field. The non-linear interactions which occur through shoaling and breaking would have to be taken into account. Then, from the predicted frequency-dependent skewness and asymmetry in the swash-zone, an estimate would have to be made of the effect on sediment transport. Various workers have already considered non-linear interactions in models of shoaling and breaking waves (e.g. Schäffer *et al*, 1993; Madsen *et al*, 1994, 1997; Wei *et al*, 1995, and many others), but it has been pointed out in the present study (section 8.4) that negative infragravity skewness in the swash-zone is still poorly understood.

Infiltration-exfiltration and its two sub-processes, namely stabilisation-destabilisation and boundary layer modification, compete against each other to result in a net onshore or offshore transport bias. Whether the net transport bias is onshore or offshore appears to depend principally on grain size, with a change from offshore to onshore bias as the grain size exceeds a certain value. The traditional hypothesis that percolation reduces backwash volume and therefore increases onshore transport (e.g. Grant, 1946, 1948), is more applicable to beaches with much larger grain sizes than those studied here (typically coarse sand or shingle). There might be another, larger, critical grain size whereby the onshore influence due to the dominance of boundary layer modification over stabilisation-destabilisation becomes less important than the onshore influence due to percolation. This would have to be investigated with a series of field (and possibly laboratory) experiments using a wide range of grain sizes.

A tentative link has been found between in-exfiltration and the other important processes outlined here, namely that the transport influence due to this process appears potentially to become more offshore in higher energy conditions. Since the sub-surface pore-pressures were not measured in a variety of different conditions, the cross-shore velocities had to be varied arbitrarily. Without this link, the effects of this process would only depend upon the more 'static' characteristics of the system (e.g. grain size). No work appears to have been done so far on examining its effect under different conditions (e.g. high/low energy, or incident/infragravity dominated).

This process has already been partly parameterised by adding extra terms to a Shields parameter to account for the competing sub-processes. Terms such as these, which encompass parameters such as grain characteristics and vertical through-bed velocity could be incorporated into a morphodynamic model.

The second order process of advection from hydraulic jumps is responsible for suspending large amounts of sediment *in-situ*, and probably also advecting a great deal of sediment onshore or offshore. However, extremely little work has been done on this, and suitable measurement techniques have not been developed yet to quantify the sediment movement in each direction away from the jump. This is due to the transient nature of the jump, and the fact that it is impossible to know whereabouts it might appear with enough certainty to deploy instrumentation. In the present study, the probability of occurrence of these jumps was estimated from the data to be higher in high energy conditions than in low energy conditions.

The hydraulic jump is a second order process because large backwashes (which themselves cause offshore sediment transport) are required before the jump can exist. Moreover, if the swash-zone velocity field contains a lot of negative skewness then the subsequent advection from the jump will more likely be offshore than onshore.

Since the likelihood for occurrence of a jump is linked to the backwash velocity, and therefore to the negative skewness in the velocity field, then parameterisation of this process for inclusion into a model would somehow need to include this link.

Increased bed roughness due to backwash ripples could be termed a third order process because the existence of a hydraulic jump (a second order process) is necessary before backwash ripples can form. Only then do the ripples alter the bed roughness which modifies the sediment transport over that part of the bed.

The possible existence of backwash ripples is linked to the formation of hydraulic jumps probably only on the backwash rather than during uprush-backwash interaction, because the intense turbulence at the swash-front will tend to wipe out the ripples fairly quickly (Osborne and Rooker, 1999). Calculations showed that ripples were only likely to form within the last 25% of the duration of the backwash and, when integrated over the whole time-series, the overall effect on the dimensionless sediment transport was likely to be small (between 1% and 5%).

11.3 Interconnectedness of processes

The flow diagram in figure 11.1 shows a simplified schematic representation of how the processes might be connected. The diagram is not meant to be a complete representation of a morphodynamic model.

It can be seen that negative infragravity skewness in the velocity field, leading to high-velocity backwashes is a very important component. It is not only associated with enhanced offshore transport through increased bed shear stress due to the backwash itself, but also feeds through to higher order processes. For example, a time-series containing negative infragravity skewness will tend to increase the likelihood of the formation of hydraulic jumps, and also increase the chances that the advection from these jumps will be offshore. It cannot be said whether infiltration-exfiltration is affected by negative infragravity skewness, but arbitrarily increasing the cross-shore velocity values in the time-series has suggested that higher energy conditions might mean an increasing offshore contribution by this process.

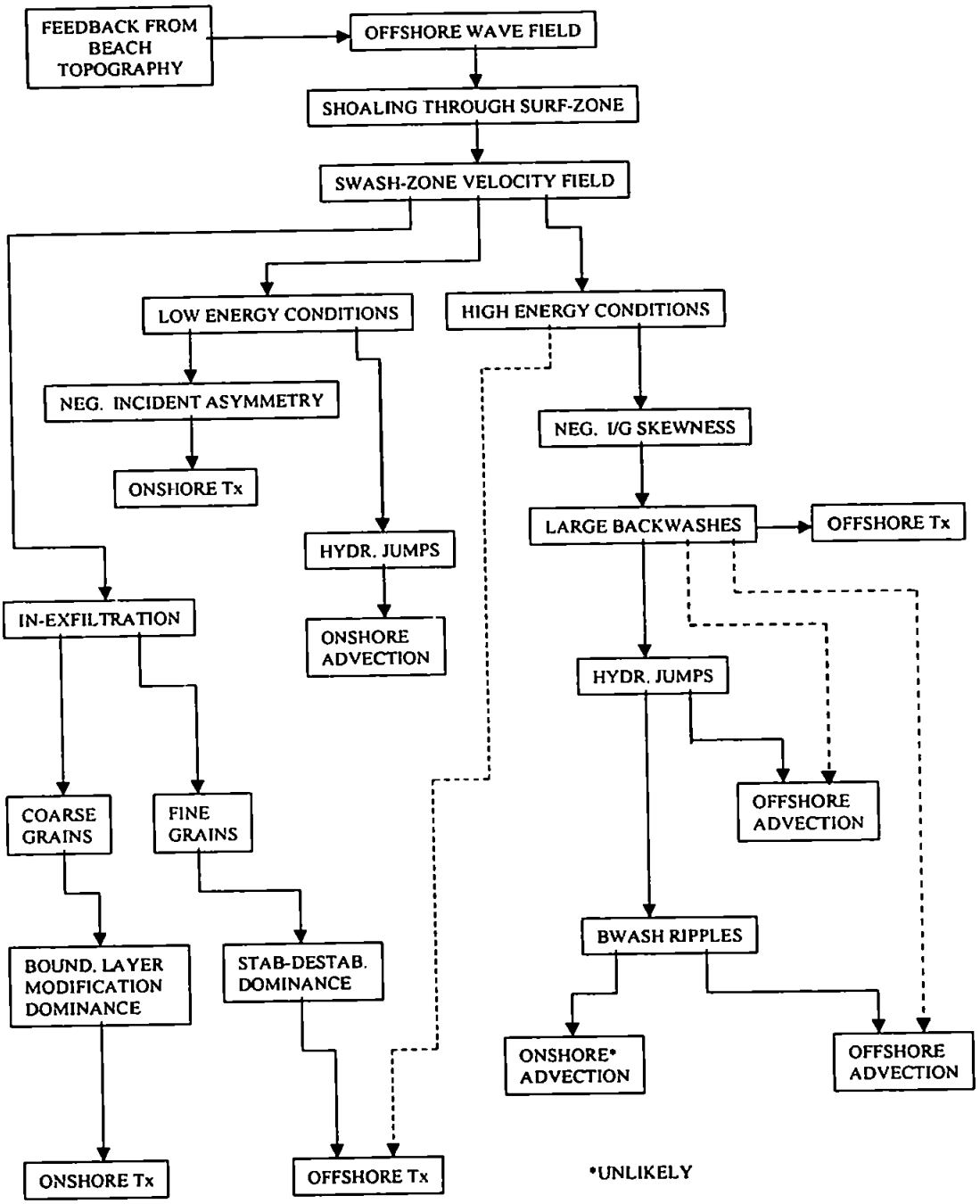

Figure 11.1: simplified schematic representation of the links between processes. 'Tx' means 'transport', i.e. a contribution to the sediment transport in the stated direction. Advection also implies transport. The dashed lines mean additional connections between processes.

11.4 General comments based on overall results

Two of the most fundamental aspects of shoreline morphology which have been observed for many years are (a) that beach erosion tends to occur during high energy conditions (e.g. Shepard, 1950; Bascom, 1954), and (b) that beaches with finer grains tend to be flatter than beaches with coarser grains. The latter has traditionally been associated with decreased backwash transport due to percolation on the backwash on coarse sand or shingle beaches (e.g. Grant, 1946, 1948).

These two basic observations have been confirmed in the swash-zone from the overall results of the present study. It appears that, in the swash-zone, the sediment transport is likely to be more offshore on finer grained beaches in high energy conditions, than on coarser grained beaches in low energy conditions. The checking of results for intuitive correctness or against visual observations must not be overlooked. Most scientific research originally stems from the most basic of observations; results which contradict observations made in nature must be taken as questionable.

The importance of infragravity waves and the general observation that they tend to grow shoreward (e.g. Guza and Thornton, 1985) has been further elucidated in the present study by identifying important swash-zone sediment transport processes associated with negative infragravity skewness. Infragravity energy, and negative infragravity skewness in the swash-zone, appear to be of central importance to the mechanisms which cause offshore transport in high energy conditions. The link between this negative skewness and the offshore wave conditions is still poorly understood, probably because its importance has not been previously acknowledged. The findings in the present study indicate that it should be investigated further if this link is to be better understood.

The initial motivation for this research emerged from the 'shape function' studies of Foote *et al* (1994), Russell *et al* (1996), Fisher and O'Hare (1997, 1998) and Russell and Huntley (1999). To produce realistic beach profiles in this model, the sediment transport in the swash-zone had to be assumed to be onshore, even though no data was available to back this up. The velocity data from these studies was obtained from current meters mounted at single heights of approximately 10cm above the bed. The method used assumes that the depth-integrated sediment flux is adequately obtained from velocity measurements at a single point just above the wave boundary layer.

If the sediment flux values obtained in the present study were not hypothetically extrapolated to the bed (see section 8.5) and the flux at, say, z = 10cm were taken as representative of the depth integrated transport, then the net transport would, indeed,

appear onshore in the swash-zone, even in high energy conditions. However, care must be taken when measurements at a single height in the water-column are taken as representative of the sediment transport at all heights, especially in the swash-zone. Findings from the present study suggest that a large proportion of the offshore directed transport is at levels below z = 5cm. Velocity measurements below this level are required before the whole swash cycle can be captured, and more realistic representations of the depth-integrated transport can be made.

11.5 Error sources

A brief consideration of errors is necessary as part of the present study. It has already been stressed that, since the present study is more concerned with temporal changes in the measured parameters than with their absolute values, then a higher level of uncertainty in the measured values can be tolerated. However, it is useful to identify potential sources of error, to assess whether measurement and calculation inaccuracies might propagate through and cause a large amount of uncertainty in the overall findings.

The principal sources of error which might directly affect the conclusions made about the processes are listed below in order of priority. Note that, using simple propagation of errors formulae (e.g. Taylor, 1982), it may be shown that the error associated with a time-averaged value, may be significantly smaller than that associated with each individual measurement, provided the individual errors are uncorrelated. Therefore, in many cases, errors associated with parameters derived from, say, time-averaged velocity, will be small.

1) Accuracy of the velocity obtained from the electromagnetic current meters, which appears to be around 10% for both steady and oscillatory flows (see section 3.3.3). The important result that offshore transport may be related to negative infragravity skewness relies on calculations of the third moment of the velocity.
2) Accuracy of the miniature optical backscatter sensors. This is not as important as the EMCM accuracy because (a) the SSC is not used in as many of the calculations and (b) no higher order moments are calculated from the SSC.
3) Estimation of the various 'constants' in some of the formulae. The values of these parameters will vary according to the method used to estimate them and, for the swash-zone, a standard method of estimating some of these parameters has not yet been established (e.g. friction factor). This was covered comprehensively in section 9.7 on

infiltration-exfiltration. One of the most important results from the infiltration calculations was that there is a particular critical grain size, above which the transport influence due to this process changes from offshore to onshore. It was acknowledged that the exact value of this grain size is difficult to determine, due to the various different methods in estimating the constants. However, the conclusions that (a) this value exists, and (b) that the transport influence is offshore below it and onshore above it, are still valid if the variations in these constants are considered.

4) Confidence limits in the spectral estimates. The method used to estimate the various spectra (explained in section 5.3) will always have errors associated with it for finite time-series. This principally affects whether a peak on the spectrum is considered 'real' or not. For example, if the confidence limits are taken into consideration the visible peak in the velocity and surface elevation spectra at the first harmonic of the main infragravity peak, is somewhat questionable. This result is of lesser importance than those directly relating to specific sediment transport processes. However, its identification, although tentative, is useful, and it does suggest that there is relatively little energy in the higher harmonics (B. Ruessink, pers. comm., 1999). To further investigate the potential significance of this peak and the generation of nonlinearities through shoaling would require more data, and the use of the bispectrum which, as already pointed out, is impractical in the present study.

11.6 Suggested further work

Throughout the present study many potentially important aspects of sediment transport in the swash-zone have been identified, but have been unable to be studied in greater detail, mainly due to lack of suitable equipment and measurement techniques. The following is a list of the most important points which require further study.

- Recent swash-zone studies in high energy dissipative conditions (e.g. Beach and Sternberg, 1991; Osborne and Rooker, 1998, 1999) have used current meters which have only been able to function at a minimum height above the bed of at least 5cm, whereas SSC has been measured at virtually bed level (e.g. Puleo, 1998). The measurement of cross-shore velocity is vital at low levels because (a) most of the backwash flow takes place below 5cm, so much of the swash cycle has been missed so far in current measurements; and (b) to compute sediment fluxes requires both velocity

and SSC to be measured at the same height (Ogston and Sternberg, 1995). Therefore a useful and logical further step to the present study would be to develop an array of unobtrusive current meters which can measure velocity down to bed level.

- The importance of turbulence in the uprush as an onshore sediment suspension mechanism has been highlighted in the present study, through three-dimensional velocity data obtained from another, similar, experiment. More extensive 3D velocity measurements need to be made using ADVs, to further quantify the importance of turbulence in the swash-zone.

- The array of MOBS sensors developed as part of the present study turned out to be highly successful at measuring SSC at heights of between 1 and 10cm above the bed. It is envisaged that this instrument be developed further, and several be built using higher quality optical sensors. The new instruments would have a greater number of sensors in a vertical array (say 10), and would operate down to, and below, the bed (*c.f.* Puleo, 1998). In this way, an idea of instantaneous bed level could also be obtained.

- It has been shown as part of the present study that (a) grain size is a vital factor in deciding whether the contribution of sediment transport due to in-exfiltration is onshore or offshore, and (b) that the transport due to in-exfiltration might change according to offshore wave conditions. It would therefore be useful to obtain measurements of sub-surface pore-pressure concurrent with velocity and SSC, on more than one beach, and during a range of different conditions.

- The hydraulic jump as a significant swash-zone sediment suspension process has been confirmed from the simple tests performed in the present study. However, the quantification of suspended sediment advected from one of these jumps has not been done. To obtain any measurements close to a jump is extremely difficult due to its transient nature in space and time. Therefore a challenging, but very important, step in the study of swash-zone processes would be to develop some (possibly remote sensing) method of measuring the SSC and flow velocity near to a hydraulic jump.

- The present study has concentrated on obtaining measurements from a dissipative site, since there was a particular lack of data from this type of beach. However, so far, no swash-zone experiments (including the present study) have been able to provide a

direct comparison between the kinds of measurements obtained here, but on two beaches with different slopes. If the same set of measurements could be obtained on both beaches, using the same instrumentation, in conditions ranging from low to high energy, then an insight could be gained into the relative importance of various processes on each type of beach. For example, it might be found that hydraulic jumps are more important on dissipative beaches, but the similar process of bore-collapse, which tends to lead to onshore advection of sediment (G. Masselink, pers. comm., 1999), is probably likely to be more important on steep beaches.

- The importance of negative infragravity skewness in the swash-zone has been highlighted in the present study and, although its existence has been acknowledged, the reason it becomes negative close to the shoreline is poorly understood. More comprehensive field studies of the frequency-dependent shoaling transformations of waves, up to the shoreline, is required to find out the source of this negative skewness. This kind of study would need to be undertaken on a beach other than a macrotidal one, since long stationary time-series are required to allow reliable bispectral analysis to be performed (see section 8.1).

12. Conclusions

From a comprehensive review of the literature, the following gaps in the knowledge of sediment transport in the swash-zone, were found:

(a) there has been a general lack of field data from high energy conditions on dissipative beaches;

(b) the importance of higher-order velocity moments to sediment transport had been well established in the surf-zone, but this had not been extended to the swash-zone;

(c) concurrent measurements of velocity and sub-surface pore pressure had not been made, which is an important requirement for studying the effects of infiltration-exfiltration;

(d) the existence of hydraulic jumps as important sediment suspending mechanisms on dissipative beaches has been little more than acknowledged in the literature.

From Perranporth Beach, UK, a highly dissipative site, concurrent measurements of velocity, water depth, sub-surface pore-pressure and suspended sediment concentration (SSC) were successfully obtained, in low and high energy conditions. To measure SSC, an array of miniature optical backscatter sensors were developed, which turned out to be highly successful and appropriate for use in future studies. The bodies of all the instruments were successfully mounted below the bed with just the transducer heads protruding, thus causing negligible scour and flow redirection, and avoiding the use of bulky and expensive mounting equipment.

The wave field was found to be infragravity dominated in the swash-zone in both high ($H_s \approx 2.2$m) and low ($H_s \approx 0.8$m) energy conditions. Infragravity energy increased towards the shore, with the ratio between low frequency ($f < 0.05$Hz) and high frequency ($f > 0.05$Hz) variance increasing from about 0.6 at the most seaward ($h/h_b = 0.64$) location to about 2.3 at the most shoreward ($h/h_b = 0.2$) location, for both velocity and surface elevation in low energy conditions. Low (high) frequency variance in the swash-zone increased by a factor of about 3.5 (2.3) from low to high energy conditions, suggesting a greater infragravity dominance in higher energy conditions.

The velocity-SSC co-spectrum was shown to be infragravity dominated in the swash-zone. SSC at z = 1cm increased by a factor of about 5 from the inner surf-zone to

the swash-zone. Suspended sediment fluxes at z = 5 to 6cm increased by a factor of about 2 from low to high energy conditions.

Inspection of a single swash cycle highlighted important velocity-SSC phase differences. It was suggested that these be associated with sediment stirring mechanisms not directly related to the velocity, such as turbulence and hydraulic jumps, at the start and end of the swash cycle, thus confirming the potential importance of these mechanisms.

Large high-velocity backwashes at infragravity frequencies were shown to be important mechanisms for transporting sediment offshore. These were manifest in the velocity time-series as negative infragravity skewness, probably caused by non-linear interactions through shoaling and reflection. Low frequency ($f < 0.05$Hz) skewnesses, calculated from third-order velocity moments, were 0.04 and –0.81 for low and high energy conditions respectively, suggesting increased backwash transport in high energy conditions.

Turbulence calculations using 3D velocities obtained from a similar experiment at Muriwai Beach, New Zealand, with infragravity-dominated conditions and $H_s \approx 1.5$m, showed TKE/velocity ratios about 1.65 times as high for the uprush than for the backwash, suggesting higher levels of turbulence in the uprush than in the backwash.

Turbulence and sudden flow reversal, manifest in the velocity time-series as high frequency negative asymmetry, were shown to be important mechanisms for onshore transport. The high frequency negative asymmetry at Perranporth was larger for the low energy data by a factor of 1.8, suggesting that these processes have a greater relative importance in lower energy conditions.

Skewness and asymmetry calculations for the Muriwai data showed results consistent with those of the present study, with depth-normalised values between those of the low and high energy Perranporth values, further confirming the suggestion that backwash transport increases with increasing offshore wave height.

The influence of infiltration-exfiltration was examined using the measurements of velocity and sub-surface pore pressure, and a modified Shields parameter, which quantifies the balance between boundary layer modification and stabilisation-destabilisation. This resulted in the dimensionless transport due to in-exfiltration, integrated over a swash cycle, decreasing by 10.5% on the uprush and increasing by 4.5% on the backwash (i.e. an offshore influence due to a dominance of stabilisation-destabilisation over boundary layer modification).

Sensitivity tests showed that there is a critical grain size above which the transport bias due to in-exfiltration changes from offshore to onshore (in accordance with the widely observed occurrence of steeper equilibrium profiles on coarser grained beaches). The critical grain size occurred at $d_{50} \approx 0.55$mm for the present study, but was shown to be highly sensitive to the method used to estimate certain empirically-derived parameters, such as friction factor, hydraulic conductivity and a constant used in the relationship between shear stress and velocity.

To investigate if changing offshore wave heights are likely to affect the influence of in-exfiltration on the sediment transport, the cross-shore velocity time-series was multiplied by various factors from 0.2 to 2.0. It was tentatively concluded that the influence of in-exfiltration becomes more offshore with increasing velocity.

Hydraulic jumps caused by uprush-backwash interaction were found to be about 2.1 times as likely to occur during the higher energy conditions than during the lower energy conditions. During the high energy conditions, sediment was observed to be advected offshore from 21 more jumps than it was advected onshore, and during the low energy conditions, sediment was advected onshore from 25 more jumps than it was advected offshore, during a 2-hour period. This suggested that backwash transport associated with hydraulic jumps is higher during high energy conditions.

Backwash ripples were found to be relatively unimportant, since their existence is spatially and temporally limited. Over a 17-min. time-series the potential influence of backwash ripples on the sediment transport was between about 1% (low energy conditions) and 5% (high energy conditions).

Negative infragravity skewness in the velocity field, leading to high velocity, low frequency backwashes, appears to be a key factor in influencing the transport towards the offshore. These backwashes not only directly cause increased backwash transport through bed stress, but also increase the chances of sediment stirring and subsequent offshore advection, from hydraulic jumps. Since negative infragravity skewness appears to be higher in high energy conditions, then this provides a tentative link between high energy conditions and potential shoreline erosion.

The common observation that beaches with fine grains more readily erode and beaches with coarse grains more readily accrete has been backed up by field measurements and simple modelling. More evidence has also been presented that onshore transport

occurs during low energy conditions and offshore transport during high energy conditions on dissipative beaches.

References

Aagaard, T. and Holm, J. 1989. Digitisation of wave runup using video records. *J. Coastal Research* **5**: 547-551.

Allen, J. R. 1985. *Principles of Physical Sedimentology.* George Allen and Unwin, London. 400pp.

Amein, M. 1966. A method for determining the behaviour of long-waves climbing a sloping beach. *J. Geophysical Research* **71**: 401-410.

Aubrey, D. G. 1989. Measuring surf-zone dynamics: (c) Measurement errors for electromagnetic current meters. In: Seymour, R. J. *Nearshore sediment transport.* Plenum Press, N.Y. pp67-78.

Aubrey, D. G. and Trowbridge, J. 1985. Kinematic and dynamic estimates from electromagnetic current meter data. *J. Geophysical Research* **90**: 9137-9146.

Aubrey, D. G., Spencer, W. and Trowbridge, J. 1984. Dynamic response of electromagnetic current meters. *Woods Hole Oceanographic Institution Technical Report* 84-20. 150pp.

Bagnold, R. A. 1956. The flow of cohesionless grains in fluids. *Phil. Trans. Roy. Soc. Lon*: **964**(249): 235-297.

Bagnold, R. A. 1963. Mechanics of marine sedimentation. In: M. N. Hill: *The Sea, 3.* Wiley Interscience, N.Y. pp507-528.

Bagnold, R. A. 1966. An approach to the sediment transport problem from general physics. *U.S. Geological Survey Professional Paper 422-1.* 37pp

Bailard, J. A. 1981. An energetics total load sediment transport model for a plane sloping beach. *J. Geophysical Research* **86**: 10938-10954.

Baird, A. J. and Horn, D. 1996. Monitoring and modelling groundwater behaviour in sandy beaches. *J. Coastal Research* **12**: 630-640.

Baird, A. J., Horn, D. and Mason, T. 1996. Mechanisms of beach ground-water and swash interaction. *25th Internatonal Conference Coastal Engineering.* ASCE. pp4120-4133.

Baird, A. J., Mason, T. and Horn, D. 1998. Validation of a Boussinesq model of beach ground water behaviour. *Marine Geology* **148**: 55-69.

Baldock, T. and Holmes, P. 1996. Pressure gradients within sediment beds. *Proc. 25th Internatonal Conference Coastal Engineering.* ASCE. pp4161-4173.

Baldock, T., Holmes, P. and Horn, D. 1997. Low frequency swash motion induced by wave grouping. *Coastal Engineering* **32**: 197-222.

Barber, N. F. and Ursell, F. 1948. The generation and propagation of ocean waves and swell. *Philos. Trans. Royal Soc. London.* **240**: 527-560.

Bascom, W. H. 1954. Characteristics of natural beaches. *Proc. 4th International Conference Coastal Engineering.* ASCE. pp163-180.

Battjes, J. A. 1974. Computation of set-up, longshore currents, run-up and overtopping due to wind-generated waves. *Delft Univ. Tech., Dep. Civil Eng. Comm. on Hydr. Report 74-2.*

Battjes, J. A. and Stive, M. 1985. Calibration and verification of a dissipative model for random breaking waves. *J. Geophysical Research* **90**: 9159-9167.

Beach, R.A. and Sternberg, R. 1988. Suspended sediment in the surf zone: response to cross-shore infragravity motion. *Marine Geology* **80**: 61-79.

Beach, R. A. and Sternberg, R. 1991. Infragravity-driven suspended sediment transport in the swash, inner and outer surf zone. *Proc. Coastal Sediments '91.* ASCE. pp114-128.

Beach, R. A. and Sternberg, R. 1996. Suspended sediment transport in the surf-zone: response to breaking waves. *Continental Shelf Research* **16**: 1989-2003.

Beach, R. A., Sternberg, R. and Johnson, R. 1992. A fiber optic sensor for monitoring suspended sediment. *Marine Geology* **103**: 513-520.

Bear, J. 1972. *Dynamics of Fluids in Porous Media.* American Elsevier, New York. 764pp.

Black, K. P. and Rosenberg, M. 1991. Suspended load at three time scales. *Proc. Coastal Sediments '91.* ASCE. pp313-327.

Bowen, A. J., D. Inman and Simmons, V. 1968. Wave set-down and set-up. *J. Geophysical Research* **73**: 2569-2577.

Bradshaw, M. P. 1980. Topographic control of run-up variability. *Proc. 17th Internatonal Conference Coastal Engineering.* ASCE. pp1091-1105.

Bradshaw, M. P. 1982. Bores and swash on natural beaches. *Coastal Studies Unit Technical Report 82/4.* University of Sydney. 107pp

Brøker-Hedegaard, I., Roelvink, J., Southgate, H., Pechón, P., Nicholson J. and Hamm, L. 1992. Intercomparison of coastal profile models. *Proc. 23rd Internatonal Conference Coastal Engineering.* ASCE. pp2108-2121.

Broome, R. and Komar, P. 1979. Undular hydraulic jumps and the formation of backwash ripples on beaches. *Sedimentology* **26**: 543-559.

Christie, M. 1997. *The* in situ *Erosion of Intertidal Muds.* Ph.D thesis. University of Plymouth. 219pp

Christie, M. and Dyer, K. 1998. Measurements of the turbid tidal edge over the Skeffling mudflats. In Black, K (ed): *Sediment Processes in the Intertidal Zone.* Special publication 139, Geological Society, London. 409pp.

Conley, D. C. and Inman, D. 1994. Ventilated oscillatory boundary layers. *J. Fluid mechanics* **273**: 261-284.

Cowell, P. J. and Thom, B. 1995. Morphodynamics of coastal evolution. In: Carter, R. and Woodruffe, C. *Coastal Evolution.* Cambridge University Press, Cambridge. 517pp.

D & A Instruments. 1991. *Optical Backscatterance Turbidity Monitor Instruction Manual.* Washington D.C. 20007, USA.

Dally, W. R. and Dean, R. 1986. Transformation of random breaking waves on surf beat. *Proc. 20th Internatonal Conference Coastal Engineering.* ASCE. pp109-123.

Darbyshire, J. 1952. The generation of waves by wind. *Proc. Roy. Soc. Lon.* **215**: 299-328.

Davidson, M. A., Russell, P., Davidson, M., Huntley, D. and Hardisty, J. 1993. Tidal asymmetry in suspended sand transport on a macrotidal intermediate beach. *Marine Geology* **110**: 333-353.

Davidson, M. A., Huntley, D., Holman, R. and George, K. 1998. The evaluation of large scale (km) intertidal beach morphology on a macrotidal beach using video images. *Proc. Coastal Dynamics '97.* ASCE. pp385-394.

Doering, J. C. 1988. *Wave-Wave Interactions in the Nearshore.* PhD thesis. Dept. Oceanography, Dalhousie University, Canada. 139pp.

Doering, J. C. and Bowen, A. 1987. Skewness in the nearshore: A comparison of estimates from Marsh-McBirney current meters and colocated pressure sensors. *J. Geophysical Research* **80**: 2997-3012.

Domenico, P. A. and Schwartz, W. 1998. *Physical and Chemical Hydrology.* 2nd. ed. Wiley. 506pp.

Downing, J. P., 1984. Suspended sand transport on a dissipative beach. *Proc. 19th Internatonal Conference Coastal Engineering.* ASCE. pp1765-1781.

Downing, J. P. and Beach, R. 1989. Laboratory apparatus for calibrating optical suspended solids sensors. *Marine Geology* **86**: 243-249.

Downing, J. P., Sternberg, R. and Lister, C. 1981. New instrumentation for the investigation of sediment suspension processes in the shallow marine environment. *Marine Geology* **42**: 19-34.

Duncan, J. R. 1964. The effects of water table and tide cycle on swash-backwash sediment distribution and beach profile development. *Marine Geology* **2**: 168-187.

Dyer, K. R. 1986. *Coastal and Estuarine Sediment Dynamics.* Wiley. 324pp.

Elgar, S. 1987. Relationships involving third moments and bispectra of a harmonic process. *IEEE Trans. Acoust. Speech and Signal Processing* **12**: 1725-1726.

Elgar, S, and Guza, R. 1985. Observations of bispectra of shoaling surface gravity waves. *J. Fluid Mechanics* **161**: 425-448.

Elgar, S. and Sebert, G. 1989. Statistics of bicoherence and biphase. *J. Geophysical Research* **94**: 10993-10998.

Elgar, S, Guza, R., and Freilich, M. 1988. Eulerian measurements of horizontal accelerations in shoaling gravity waves. *J. Geophysical Research* **93**: 9261-9269.

Elgar, S., Herbers, T., Okihiro, M., Oltman-Shay, J., and Guza, R. 1992. Observations of infragravity waves. *J. Geophysical Research* **97**: 15573-15577.

Elgar, S., Guza, R., Raubenheimer, B., Herbers, T., and Gallagher, E. 1997. Spectral evolution of shoaling and breaking waves on a barred beach. *J. Geophysical Research* **102**: 15797-15805.

Emery, K. O. and Gale, J. F. 1951. Swash and swash marks. *Trans. Am. Geophys. Union* **32**: 31-36.

Emery, W. J. and Thomson, R. 1997. *Data Analysis Methods in Physical Oceanography.* Elsevier. 383pp.

Ericksen, N., J. 1970. Measurement of tide induced changes to water table profiles in coarse and fine sand beaches along Pegasus Bay, Canterbury. *Earth Sciences Journal* **4**: 24-31.

Fisher, P. R. and O'Hare, T. 1997. Modelling sand transport and profile evolution on macrotidal beaches. *Proc. 25th International Conference Coastal Engineering.* ASCE. pp2994-3005.

Fisher, P. R. and O'Hare, T. 1998. Morphological effect of spring-neap tidal variations on macrotidal beaches. *Proc. Coastal Dynamics '97.* ASCE. pp476-485.

Folk, R. L. 1966. A review of grain size parameters. *Sedimentology* **6**: 73-93.

Folk, R. L. and Ward, W. 1957. Brazos River Bar: a study in the significance of grain size parameters. *J. Sedimentary Petrology* **27**: 3-26.

Foote, Y., Huntley, D., O'Hare, T. 1994. Sand transport on macrotidal beaches. *Proc. Euromech 310 Colloquiem (Le Havre).* pp360-374.

Freeman, J. C. and LeMehaute, B. 1964. Wave breakers on a beach and surges on a dry bed. *J. of the Hydraulics Division*, A.S.C.E., HY2, 187-216.

Freilich, M. H. and Guza, R. 1984. Nonlinear effects on shoaling surface gravity waves. *Philos. Trans. Royal Soc. London, Ser. A.* **311**: 1-41.

Friedman, G. M. 1961. Distribution between dune, beach and river sands from textural characteristics. *J. Sedimentary Petrology* **31**: 514-529.

Gordon, H. R., Smith, R, and Zaneveld, J. 1984. Introduction to Ocean Optics. *Soc. Photo-Opt Instrum. Eng.* **89**:1-41

Gourlay, M. R. 1992. Wave set-up, wave run-up and beach water table: interaction between surf zone hydraulics and groundwater hydraulics. *Coastal Engineering* **17**: 93-144.

Grant, U. S. 1946. Effects of ground water table on beach erosion. *Bulletin of the Geological Society of America* **57**: 1252-1264.

Grant, U. S. 1948. Influence of the water table on beach aggradation and degradation. *J. Marine research* **7**: 655-660.

Green, M. O. and Boon, J. 1993. The measurement of constituent concentrations in nonhomogeneous sediment suspensions using optical backscatter sensors. *Marine Geology* **110**: 73-81.

Greenwood, B., Osborne, P., Bowen, A., Hazen D., and Hay, A. 1990. Nearshore sediment flux and bottom boundary dynamics. The Canadian Coastal Sediment Transport Program, C-COAST. *Proc. 22nd Internatonal Conference Coastal Engineering.* ASCE. pp1983-1996.

Guza, R. T. and Inman, D. 1975. Edge waves and beach cusps. *J. Geophysical Research* **80**: 2997-3012.

Guza, R. T. and Thornton, E. 1981. Wave set-up on a natural beach. *J. Geophysical Research* **86**: 4133-4137.

Guza, R. T. and Thornton, E. 1982. Swash oscillations on a natural beach. *J. Geophysical Research* **87**: 483-491.

Guza, R. T. and Thornton., E. 1985. Observations of surf-beat. *J. Geophysical Research* **90**: 3161-3172.

Guza, R. T., Thornton, E. and Holman, R. 1984. Swash on steep and shallow beaches. *Proc. 19th Internatonal Conference Coastal Engineering.* ASCE. pp708-723.

Guza, R. T., Clifton, M. and Rezvani., F. 1988. Field intercomparisons of electromagnetic current meters. *J. Geophysical Research* **93**: 9302-9314.

Hallermeier, R. 1982. Oscillatory bedload transport: Data review and simple formulation. *Continental Shelf Research* **1**: 159-190.

Hanes, D. M. and Huntley, D. 1986. Continuous measurements of suspended sand concentration in a wave-dominated nearshore environment. *Continental Shelf Research* **6**: 585-596.

Hardisty, J. 1991. Bedload transport under low frequency waves. *Proc. Coastal Sediments '91.* ASCE. pp726-733

Hardisty, J., Collier J. and Hamilton, D. 1984. A calibration of the Bagnold beach equation. *Marine Geology* **61**: 95-101.

Harrison, W. 1971. Groundwater flow in a sandy tidal beach: 1. One-dimensional finite element analysis. *Water Resources Res* **7**: 1313-1322.

Hasselman, K., Munk, W. and McDonald, G. 1963. Bispectra of ocean waves. in: *Time Series Analysis*, M. Rosenblatt (ed). Wiley, New York. pp125-139.

Hayes, M. O. 1972. Forms of sediment accumulation in the beach zone. In: Meyer, R. E. *Waves on Beaches.* Academic Press, New York. pp297-356.

Heathershaw, A. D. and Thorne, P. 1985. Sea-bed noises real role of turbulent bursting phenomenon in sediment transport by tidal currents. *Nature* **316**: 339-342.

Hegge, B. and Masselink. G. 1991. Groundwater table responses to wave runup: an experimental study from Western Australia. *J. Coastal Research* 7: 623-634.

Herbers, T. H., Elgar, S., and Guza, R. 1994. Infragravity-frequency (0.005-0.05Hz) motions on the shelf. Part 1: Forced waves. *J. Physical Oceanography* **24**: 917-927.

Hibberd, S. and Peregrine, D. 1979. Surf and run-up on a beach: a uniform bore. *J. Fluid Mechanics* **95**: 323-345

Ho, D.V., Meyer R. and Shen, M. 1962. Climb of a bore on a beach: Part 1, uniform beach slope. *J. Fluid Mechanics* **14**: 305-318.

Holland, K. T. 1995. *Foreshore Dynamics: Swash Motions and Topographic Interactions on Natural Beaches.* PhD thesis. Oregon State Univ., USA. 119pp.

Holland, K. T. and Holman, R. 1997. Runup kinematics on a natural beach. *J. Coastal Research* **13**: 81-87.

Holland, K. T., Raubenheimer, B., Guza, R. and Holman, R. 1995. Runup kinematics on a natural beach. *J. Geophysical Research* **100**: 4985-4993.

Holland, K. T., Sallenger, A., Raubenheimer, B. and Elgar, S. 1998. Swash-zone morphodynamics and sediment transport processes. *Proc. 26th Internatonal Conference Coastal Engineering.* ASCE. pp2799-2811.

Holman, R. A. 1981. Infragravity energy in the surf-zone. *J. Geophysical Research* **87**: 6442-6450.

Holman, R. A. 1983. Edge waves and the configuration of the shoreline. In: *CRC Handbook of Coastal Processes and Erosion.* CRC Press Inc. Boca Raton, Florida. pp21-33

Holman, R. A. 1986. Extreme value statistics for wave run-up on a natural beach. *Coastal Engineering* **9**: 527-544.

Holman, R. A. and Bowen, A. 1984. Longshore structure of infragravity motions. *J. Geophysical Research* **89**: 6446-6452.

Holman, R. A. and Guza, R. 1984. Measuring runup on a natural beach. *Coastal Engineering* **8**: 129-140.

Holman, R. A. and Sallenger, A. 1985. Setup and swash on a natural beach. *J. Geophysical Research* **90**: 945-953.

Horn, D. P. 1997. Beach research in the 1990s. *Progress in Physical Geography* **21**: 454-470.

Horn, D. P. and Mason. T. 1994. Swash zone sediment transport modes. *Marine Geology* **120**: 309-325.

Horn, D. P., Baldock, T. Baird, A. and Mason. T. 1998. Field measurements of swash induced pressure gradients within a sandy beach. *Proc. 26th Internatonal Conference Coastal Engineering.* ASCE. pp2812-2825.

Hornung, H. G., Willert, C. and Turner, S. 1995. The flow field downstream of a hydraulic jump. *J. Fluid Mechanics.* **287**: 299-316.

Howd, P. A. and Holman, R. 1984. Beach foreshore response to long period waves. *Proc. 19th Internatonal Conference Coastal Engineering.* ASCE. pp1968-1982.

Hughes, M. G. 1992. Application of a non-linear shallow water theory to swash following bore collapse on a sandy beach. *J. Coastal Research* **8**: 562-578.

Hughes, M. G. 1995. Friction factors for wave uprush. *J. Coastal Research* **11**: 1089-1098.

Hughes, M. G., Masselink, G. and Brander, R. 1997. Flow velocity and sediment transport in the swash-zone of a steep beach. *Marine Geology* **138**: 91-103.

Hughes, M. G., Masselink, G., Hanslow, D. and Mitchell, D. 1998. Towards a better understanding of swash-zone sediment transport. *Proc. Coastal Dynamics '97.* ASCE. pp804-813.

Huntley, D. A. 1976. Long period waves on a natural beach. *J. Geophysical Research* **81**: 6441-6449.

Huntley, D. A. and Bowen, A. 1973. Field observations of edge waves *Nature* **243**: 160-161.

Huntley, D. A. and Hanes, D. 1987. Direct measurements of suspended sediment transport. *Proc. Coastal Sediments '87.* ASCE. pp723-737.

Huntley, D. A., Guza R., and Bowen, A. 1977. A universal form for shoreline runup spectra? *J. Geophysical Research* **82**: 2577-2581.

Huntley, D. A., Guza R., and Thornton, E. 1981. Field observations of surf-beat, 1: Progressive edge waves. *J. Geophysical Research* **83**: 1913-1920.

Huntley, D. A., Davidson, M., Russell, P., Foote Y., and Hardisty, J. 1993. Long waves and sediment movement on beaches: recent observations and implications for modelling. *J. Coastal Research Special Issue* **15**: 215-229.

Jaffe, B., Sternberg, R. and Sallenger, A. 1984. The role of suspended sediment in shore normal beach profile change. *Proc. 19th Internatonal Conference Coastal Engineering.* ASCE. pp1983-1996.

Jaffe, B. E., Rubin, D. and Sallenger, A. 1994. How much velocity information is necessary to predict sediment suspension in the surf zone? *Proc. 24th Internatonal Conference Coastal Engineering.* ASCE. pp776-790.

Jagger, K. A. and Hardisty, J. 1991. Higher frequency acoustic measurements of coarse bedload transport. *Proc. Coastal Sediments '91.* ASCE. pp2187-2198.

Jenkins, G. M. and Watts, D. 1968. *Spectral Analysis and its Applications.* Holden-Day, San Francisco. 525pp.

Johnson, B. D. and Kobayashi, N. 1998. Nonlinear time-averaged model in surf and swash zones. *Proc. 26th Internatonal Conference Coastal Engineering.* ASCE. pp2785-2798.

Jonsson, I. G. 1966. Wave boundary layers and friction factors. *Proc. 10th Internatonal Conference Coastal Engineering.* ASCE. pp127-148.

Kawata, Y., Yoshioka, H. and Tsuchiya, Y. 1990. The *in-situ* measurements of sediment transport and bottom topography changes. *Proc. 22nd Internatonal Conference Coastal Engineering.* ASCE. pp2332-2345.

Kineke, G. and Sternberg, R. 1992. Measurements of high concentration suspended sediment using the optical backscatterance sensor. *Marine Geology* **108**: 253-258.

King, D. B. 1991. *Studies in Oscillatory Flow Bedload Sediment Transport.* PhD thesis, University of California, San Diego. 183pp.

Kobayashi, N. and Karjadi, E. 1994. Swash dynamics under obliquely incident waves. *Proc. 24th Internatonal Conference Coastal Engineering.* ASCE. pp2155-2168.

Kobayashi, N. and Karjadi, E. 1996. Obliquely incident irregular waves in surf and swash-zone. *J. Geophysical Research* **101**: 6527-6542.

Kobayashi, N., Otta, A. and Roy, I. 1987. Wave reflection and run-up on rough slopes. *J. Waterway, Port, Coastal and Ocean Division ASCE.* **113**: 282-298.

Kobayashi, N., DeSilva, G. and Watson, K. 1989. Wave transformation and swash oscillation on gentle and steep slopes. *J. Geophysical Research* **94**: 951-966.

Kobayashi, N., Cox, D. and Wurjanto, A. 1990. Irregular wave reflection and run-up on rough, impermeable slopes. *J. Waterway, Port, Coastal and Ocean Division ASCE.* **116**: 708-728.

Kobayashi, N., Orzech, M., Johnson, B. and Herrman, M. 1997. Probability modelling of surf zone and swash dynamics. *Proc. Waves '97. ASCE.* pp107-121.

Kobayashi, N., Herrman, M., Johnson, B. and Orzech, M. 1998. Probabalistic distribution of surface elevation in the surf and swash-zones. *J. Waterway, Port, Coastal and Ocean Division ASCE.* **124**: 102-113.

Kraus, N. C., Lohrmann, A., and Cabrera, R. 1994. New acoustic meter for measuring 2D laboratory flows. *J. Hydraulic Engineering* **120**: 406-412.

Krumbein, W. C. 1934. Size frequency distributions of sediments. *J. Sedimentary Petrology* **4**: 65-77.

Krumbein, W. C., and Monk, G. 1942. Permeability as a function of the size parameters of unconsolidated sand. *Trans Am. Institute of Mining and Metallurgical Engineering*: **151**: 153-163.

Larson, M. and Sunamara, T. 1993. Laboratory experiment on flow characteristics at a beach step. *J. Sedimentary Petrology* **63**: 495-500.

Lewandowski, A. and Zeidler, R. 1978. Watertable overheight due to wave runup on a sandy beach. *Proc. 16th International Conference Coastal Engineering.* ASCE. pp2015-2065.

Li, L., Barry, D., Parlange, J. and Pattiaratchi. C. 1997. Beach watertable fluctuations due to wave run-up: Capillarity effects. *Water Resources. Res.* **35**: 935-945.

Longuet-Higgins, M. S. 1970. Longshore currents generated by obliquely incident sea waves. *J. Geophysical Research* **75**: 6778-6789.

Longuet-Higgins, M. S. 1986. Eularian and Lagrangian aspects of surface waves. *J. Fluid Mechanics* **173**: 683-707.

Longuet-Higgins, M. S. and Stewart, R. 1964. Radiation stress in water waves: a physical discussion with applications. *Deep Sea Res. Ocean. Abstr.* **11**: 529-562.

Ludwig, K. A., and Hanes, D. 1990. A laboratory evaluation of optical backscatterance suspended solids sensors exposed to sand-mud mixtures. *Marine Geology* **94**: 173-179.

Madsen, P. A. and Svendsen, I. 1983. Turbulent bores and hydraulic jump. *J. Fluid Mechanics* **129**: 1-25.

Madsen, P. A., Sørensen, O., and Schäffer, H. 1994. Time domain modelling of wave breaking, run-up and surf-beats. *Proc. 24th International Conference Coastal Engineering.* ASCE. pp399-411.

Madsen, P. A., Sørensen, O., and Schäffer, H. 1997. Surf zone dynamics simulated by a Boussinesq type model. Part II: Surf beat and swash oscillations for wave groups and irregular waves. *Coastal Engineering* **32**: 289-319.

Martin, C. S. 1970. Effect of a porous bed on incipient sediment motion. *Water Resources Res.* **6**: 1162-1174

Mase, H. 1988. Spectral characteristics of random wave run-up. *Coastal Engineering* **12**: 175-189.

Masselink, G. 1995. Group bound long waves as a source of infragravity energy in the surf-zone. *Continental Shelf Research* **15**: 1525-1547.

Masselink, G., and Hughes, M. 1998. Field investigation of sediment transport in the swash-zone. *Continental Shelf Research* **18**: 1179-1199.

Masuda, A. and Kuo, Y. A note on the imaginary part of the bispectra. *Deep Sea Res.* **A28**: 213-222.

Matsunaga, N. and Honji, H. 1980. The backwash vortex. *J. Fluid Mechanics* **99**: 813-815.

Matsunaga, N. and Honji, H. 1983. The steady and unsteady backwash vortices. *J. Fluid Mechanics* **135**: 189-197.

Meadows, G. A., Shuchman, R. and Lyden, J. 1982. Analysis of remotely sensed long-period wave motions. *J. Geophysical Res.* **87**: 5731-5740.

Meyer-Peter, E. and Müller, R. 1948. Formulas for bed-load transport. *Proceedings of the 2nd Congress of the International Association for Hydraulics Structures Research,* Stockholm. pp39-64.

Miche, R. 1951. Le pouvoir réfléchissant des ouvrages maritimes exposés à l'action de la houle. *Ann. Ponts Chaussees* **121**: 285-319.

Mickley, H. S., Ross, R., Squyers, A., and Stewart, W. 1954. Heat, mass and momentum transfer over a flat plate with blowing. *Tech. Note 4017.* Nat. Adv. Comm. Aeronaut., Washington. 149pp.

Miles, J. R. 1997. *Enhanced sediment transport near seawalls and reflective beaches.* PhD Thesis. University of Plymouth, U. K. 192pp.

Millard, N. W. 1976. Noise generated by moving sediments. *Proc. Conf. on Recent Developments in Underwater Acoustics.* AUWE, Portland, UK, paper 3.5.

Mizuguchi, M. 1984. Swash on a natural beach. *Proc. 19th International Conference Coastal Engineering.* ASCE. pp678-694.

Munk, W. H. 1949. Surf beats. *E.O.S. Trans. A.G.U. 30*: pp849-854.

Nairn, R. B. and Southgate, H. 1993. Deterministic profile modelling of nearshore processes, part 2: Sediment transport and beach profile development. *Coastal Engineering* **19**: 57-96.

Nielsen, P. 1990. Tidal dynamics of the water table in beaches. *Water Resources research* **26**: 2127-2134.

Nielsen, P. 1992. *Coastal Bottom Boundary Layers and Sediment Transport.* Advanced Series on Ocean Engineering, Vol. 4. World Scientific, Singapore. 324pp.

Nielsen, P. 1998. Coastal groundwater dynamics. *Proc. Coastal Dynamics '97.* ASCE. pp546-555.

Nielsen, P., and Kang, H. 1995. Groundwater dynamics in beaches and coastal barriers. *Proc. Coastal Dynamics '95.* ASCE. pp521-532.

Neilsen, P., Davis, G., Winterbourne, J. and Elais, G. 1988. Wave setup and the watertable in sandy beaches. *Public Works Dept. Coastal Branch, New South Wales, Technical Memorandum* **88/1**. 132pp.

Ogston, A. S. and Sternberg, R. 1995. On the importance of nearbed sediment flux measurements for estimating sediment transport in the surf zone. *Continental Shelf Research* **15**: 1515-1524.

Oltman-shay, J. and Guza, R. 1987. Infragravity edge wave observations on two California beaches. *J. Physical Oceanography* **17**: 644-663.

Oppenheim, A. V. and Schafer, R. 1975. *Digital Signal Processing.* Prentice Hall International, London. 585pp.

Osborne, P. D. and Rooker. G. 1998. Surf zone and swash zone sediment dynamics on high energy beaches: West Aukland, New Zealand. *Proc. Coastal Dynamics '97.* ASCE. pp814-823.

Osborne, P. D. and Rooker. G. 1999. Sand re-suspension events in a high-energy infragravity swash zone. *J. Coastal Research* **15**:74-86.

Ozanne, F. 1998. *Performance of a Boussinesq Model for Shoaling and Breaking Waves.* PhD thesis. University of Plymouth, UK. 162pp.

Packwood, A. R. 1983. The influence of beach porosity on wave uprush and backwash. *Coastal Engineering* **15**: 313-332.

Peregrine, D. H. 1966. Calculations on the development of an undular bore. *J. Fluid mechanics* **25**: 321-330.

Peregrine D. H. 1990. Theory versus measurements. In: Torum, A. and Gudmestad, O. (eds). *Water Wave Kinematics.* Kluwer Acad. Publ. pp17-20.

Peregrine, D. H. and Svendsen, I. 1978. Turbulent bores and hydraulic jump. *J. Fluid mechanics* **129**: 1-25.

Puleo, J. A. 1998. *Swash Zone Sediment Suspension and Transport.* MSc thesis. Oregon State University, USA. 91pp.

Quick, M. C. 1991. Onshore-offshore sediment transport on beaches. *Coastal Engineering* **15**: 313-332.

R.S. Components. 1997. Data sheet 232-2447. *Reflective and Slotted Opto Switches 2601.* Issued March 1997.

Raubenheimer, B. and Guza. R. 1996. Observations and predictions of run-up. *J. Geophysical Res.* **101**: 25575-25587.

Raubenheimer, B., Guza, R., Elgar S. and Kobayashi, N. 1995. Swash on a gently sloping beach. *J. Geophysical Res.* **100**: 8751-8760.

Ribberink, J. and Al-Salem, A. 1990. Bed forms, sediment concentrations and and sediment transport in simulated wave conditions. *Proc. 22nd International Conference Coastal Engineering.* ASCE. pp2318-2331.

Ribberink, J. and Al-Salem, A. 1992. Time-dependent sediment transport phenomena in oscillatory boundary layer flow under sheet-flow conditions. *Delft Hydraulics Report H840.20 part VI (Kustgenese / MaST).*

Ribberink, J. and Al-Salem, A. 1994. Sediment transport in oscillatory boundary layers in cases of rippled beds and sheet flow. *J. Geophysical Research* **94**: 12707-12727.

Ribberink, J. S. and Al-Salem, A. 1995. Sheet-flow and suspension of sand in oscillatory boundary layers. *Coastal Engineering* **25**: 205-225.

Ruessink, B.G. 1998. *Infragravity Waves in a Dissipative Multiple Bar System.* PhD Thesis. Netherlands Geographical Studies. 245pp.

Ruessink, B.G., Kleinhans, M., and P. van den Beukel. 1998. Observations of swash under highly dissipative conditions. *J. Geophysical Research* **103**: 3111-3118.

Russell, P. E. 1993. Mechanisms for beach erosion during storms. *Continental Shelf Res.* **13**: 1243-1266.

Russell, P. E. and Huntley, D. 1999. A cross-shore sediment transport 'shape function' for high energy beaches. *J. Coastal Research* **15**:198-205

Russell, P. E., Davidson, M., Huntley, D., Cramp, A., Hardisty J., and Lloyd, G. 1991. The British Beach and Nearshore Dynamics (B-BAND) Programme. *Proc. Coastal Sediments '91.* ASCE. pp371-384.

Russell, P. E., Foote Y. and Huntley, D. 1996. An energetics approach to sand transport on beaches. *Proc. Coastal Dynamics '95.* ASCE. pp829-840.

Sallenger, A. H. and Holman, R. 1987. Infragravity waves over a natural barred profile. *J. Geophysical Res.* **92**: 9531-9540.

Saulter, A. N., O'Hare, T. and Russell, P. 1998. Analysis of infragravity wave-driven sediment transport on macrotidal beaches. *Proc. Coastal Dynamics '97.* ASCE. pp1033-1042.

Sasaki, T. and Horikawa, K. 1978. Observation of nearshore current and edge waves. *Proc. 16th International Conference Coastal Engineering.* ASCE. pp791-809.

Sellin, R. H. 1969. *Flow in Channels.* Macmillan, London. 149pp.

Schäffer, H. A., Madsen, P., and Deigaard, R. 1993. A Boussinesq model for wave breaking in shallow water. *Coastal Engineering* **20**: 185-202.

Shen, M. C. and Meyer, R. 1963. Climb of a bore on a beach: part 3, run-up. *J. Fluid Mechanics.* **16**: 113-125.

Shepard, F. P. 1950. Beach cycles in Southern California. *Beach Erosion Board Tech. Memo* **20**. U.S. Army Corps of Engineers. 26pp.

Shields, A. 1936. Anwendung der Aehnlichkeitsmechanik und Turbulenzforschung auf die Geschiebebewegung. *Mitt Preuss Versuchsanstalt für Wasserbau und Schiffbau, No.26,* Berlin.

Sleath, J. F. 1970. Velocity measurements close to the bed in a wave tank. *J. Fluid Mechanics* **42**: 111-123.

Sleath, J. F. 1987. Turbulent oscillatory flow over rough beds. *J. Fluid Mechanics* **182**: 369-409.

Sonu, C. J., Pettigrew, N. and Fredericks, R. 1974. Measurement of swash profile and orbital motion on the beach. *Proc. Ocean Wave Measurement and Analysis Conference.* pp621-638.

Soulsby, R. L. and Humphery, J. 1989. Field observations of wave-current interaction at the sea bed. *Proc. NATO Advanced Research Workshop on Water Wave Kinematics.* Kluwer Academic. Publ., Dordrecht. pp189-266.

Southgate, H. N., and Capobianco, M. 1998. The role of chronology in long-term morphodynamics. Theory, practice and evidence. *Proc. Coastal Dynamics '97.* ASCE.

Stapleton, K. R. 1996. *Wave and Current Interaction in the Nearshore.* PhD thesis. University of Plymouth, UK. 126pp

Sternberg, R. W., Shi, N. and Downing, J. 1984. Field investigations of suspended sediment transport in the nearshore zone. *Proc. 19th Internatonal Conference Coastal Engineering.* ASCE. pp1782-1798.

Strahler, A. N. 1966. Tidal cycle of changes in an equilibrium beach, Sandy Hook, New Jersey. *J. Geology* **74**: 247-268.

Suhayda, J. N. 1972. *Experimental study of the shoaling transformation of waves on a sloping bottom.* PhD thesis. Scripps Institute of Oceanography, USA.

Suhayda, J. N. 1974. Standing waves on beaches. *J. Geophysical Research* **79**: 3065-3071.

Sunamara, T. 1984. Onshore-offshore sediment transport rate in the swash zone of laboratory beaches. *Coastal Engineering Japan.* **27**: 205-212.

Sutherland, A. J. 1967. Proposed method for sediment entrainment by turbulent flows. *J. Geophysical Research* **72**: 6183-6194.

Svendsen, I. A. and Madsen, P. 1984. A turbulent bore on a beach. *J. Fluid Mechanics.* **148**: 73-96.

Svendsen, I. A., Madsen, P., and Hansen, J. 1978. Wave characteristics in the surf-zone. *Proc. 16th Internatonal Conference Coastal Engineering.* ASCE. pp520-539.

Swart, D. H. 1974. A schematization of onshore-offshore transport. *Delft Hydraulics Lab. Publ. No 131.*

Symonds, G., Huntley, D. and Bowen, A. 1982. Two-dimensional surf-beat: long wave generation by a time-varying breakpoint. *J. Geophysical Research* **87**: 492-498.

Tanner, W. F. 1965. High-index ripple marks in the swash-zone. *J. Sedimentary Petrology* **35**: 968-983.

Taylor, J. 1982. *An Introduction to Error Analysis: The Study of Uncertainties in Physical Measurements.* University Science Books. 270pp.

Thompson, R. 1979. Coherence significant levels. *J. Atmospheric Sciences* **36**: 2020-2021.

Thorne, P. D. 1985. The measurement of acoustic noise generated by moving artificial sediments. *J. Acoustic Soc. Am.* **78**: 1013-1023.

Thorne, P. D. 1986. Laboratory and marine measurements on the acoustic detection of sediment transport. *J. Acoustic Soc. Am.* **80**: 899-910.

Thorne, P. D., Salkield, A. and Marks, A. 1983. Application of acoustic techniques in sediment transport research. *Inst. of Acoustic, Proc. of the Conf. on Acoustics and the Seabed.* Bath University, UK., pp395-402.

Thorne, P. D., Heathershaw, A. and Triano, L. 1984. Acoustic detection of seabed gravel movement in turbulent tidal currents. *Marine Geology* **54**: 43-48.

Thorne, P. D., Williams, J. and Heathershaw, A. 1989. *In-situ* measurements of marine gravel threshold and transport. *Sedimentology* **36**: 61-74.

Thornton, E. and Abdelrahman, S. 1991. Sediment transport in the swash zone due to obliquely incident wind-waves modulated by infragravity waves. *Proc. Coastal Sediments '91.* ASCE. pp100-113.

Tucker, M. J. 1950. Surf beats: Sea waves of 1 to 5 min. period. *Proc. Roy. Soc.* **A:202**: 565-571.

Turner, I. L. 1993(a). The total water content of sandy beaches. *J. Geophysical Research* **15**: 11-26.

Turner, I. L. 1993(b). Water table outcropping on macro-tidal beaches: a simulation model. *Marine Geology* **115**: 227-238.

Turner, I. L. 1995. Simulating the influence of groundwater seepage on sediment transported by the sweep of the swash zone across macro-tidal beaches. *Marine Geology* **125**: 153-174.

Turner, I. L. 1998. Monitoring groundwater dynamics in the littoral zone at seasonal, storm, tide and swash frequencies. *Coastal Engineering* **35**: 1-16.

Turner, I. L. and Nielsen, P. 1997. Rapid water table fluctuations within the beach face: Implications for swash-zone sediment mobility? *Coastal Engineering* **32**: 45-59

Turner, I. L. and Masselink, G. 1998. Swash infiltration-exfiltration and sediment transport. *J. Geophysical Research* **103**: 30813-30824.

Turner, I. L., Coates, B. and Acworth, R. 1997. Tides, waves and the super-elevation of groundwater at the coast. *J. Coastal Research* **13**: 46-60.

van Hardenberg, B., Hay, A., Sheng, Y., and Bowen, A. J. 1991. Field measurements of the vertical structure of suspended sediment. *Proc. Coastal Sediments '91.* ASCE. pp300-312.

van Rijn, L. C. 1982. Equivalent roughness of alluvial bed. *J. of the Hydraulics Division.* ASCE. No. HY10.

van Rijn, L. C. 1993. *Principles of Sediment Transport in Rivers, Estuaries and Coastal Seas.* Aqua Publications, The Netherlands. 584pp.

van Straaten, L. M. 1953. Rhythmic patterns on Dutch North Sea beaches. *Geologie Mijnb* **15**: 31- 43

Veeramony, J. and Svendsen, I. 1998. Analysis of the roller in hydraulic jumps. *Proc. Coastal Dynamics '97.* ASCE. pp305-314.

Voulgaris, G. and Trowbridge, J. 1998. Laboratory evaluation of the acoustic döppler velocimeter for turbulence measurements. *J. Ocean and Atmospheric Technology.* **8**: 272-289.

Waddell, E. 1973. Dynamics of swash and implication to beach response. *Coastal Studies Institute Technical Report 139.* Louisiana State Univ. 49pp.

Waddell, E. 1976. Swash-groundwater-beach profile interactions. In: R. A. Davis and R. L. Etherington (eds): *Beach and Nearshore Sedimentation. SEPM Special Publication* **24**: 115-125.

Waddell, E. 1980. Wave forcing of beach groundwater. *Proc. 17th Internatonal Conference Coastal Engineering.* ASCE. pp1436-1452.

Wei, G., Kirby, J., Grilli, S. and Subramanya, R. 1995. A fully non-linear Boussinesq model for surface waves, part 1, highly non-linear unsteady waves. *J. Fluid Mechanics* **294**: 71-92.

Welch, P. D. 1967. The use of fast Fourier transform for the estimation of power spectra: a method based on time averaging over short modified periodograms. *IEEE Trans. Audio Electroacoustics.* AU-15. pp70-73.

Wells, D. R. 1967. Beach equilibrium and second-order wave theory. *J. Geophysical Research* **72**: 497-504.

Wentworth, C. K. 1922. A scale of grade and class terms for clastic sediments. *J. Geology* **30**: 377-392.

Werner, B. T. and Fink, T. 1993. Beach cusps as self-organised patterns. *Science* **260**: 968-970.

Wilberg, P. and Smith, J. 1983. A comparison of field data and theoretical models for wave-current interactions at the bed on the continental shelf. *Continental Shelf Research* **2**: 147-162.

Williams, J. M., and Elder, S. 1996. *Fluid Physics for Oceanographers and Physicists.* (2nd ed.) Butterworth-Heinemann, Oxford. 395pp.

Wilson, K. C. 1987. Analysis of bed-load motion at high shear stress. *Coastal Engineering* **12**: 97-103.

Wilson, K. C. 1988. Frictional behaviour of sheet-flow. *Progress Report 67, Institute of Hydrodynamic and Hydraulic Engineering.* Tech. Univ. Denmark. pp11-22.

Wilson, K. C. 1989. Friction of wave induced sheet-flow. *J. Hydraulic Engineering* **113**: 371-379.

Wilson, K. C., Anderson, J. and Shaw, J. 1995. Effects of wave asymmetry on sheet-flow. *Coastal Engineering* **25**: 191-204.

Wright, L. D. and Thom, B. G. 1977. Coastal depositional landforms: a morphodynamic approach. *Progress in Physical Oceanography* **1**: 412-459.

Wright. L. D., and Short, A. 1984. Morphodynamic variability of surf zones and beaches: a synthesis. *Marine Geology* **56**: 93-118.

Yalin, M. S. and Karahan, E. 1979. Inception of sediment transport. *J. Pipelines* **4**: 171-176.

Yeh, H, H. 1991. Vorticity generation mechanisms in bores. *Proc. Royal Soc. London A.* **432**: 215-231.

Yu, Z. H., Niemeyer, H. and Bakker, W. 1990. Site investigation on sand concentration in the sheetflow layer. *Proc. 22nd Internatonal Conference Coastal Engineering.* ASCE. pp2361-2371.